Analysis of the spectra of isotopically substituted water vapour

Mizuho Tanaka

Thesis submitted for the Degree of Doctor of Philosophy

UNIVERSITY
COLLEGE LONDON

January 2005

ProQuest LLC
789 East Eisenhower Parkway
P.O. Box 1346
Ann Arbor, MI 48106-1346

Abstract

The spectrum of water vapour is widely studied due to its significance in many areas of science. Isotopically substituted water vapour such as $H_2{}^{17}O$ and $H_2{}^{18}O$ are known to contribute significantly to the absorption of solar radiation in the Earth's atmosphere, yet they have been less extensively studied.

Recent advances in the variational nuclear motion calculations, high quality potential energy surfaces (PES) and dipole moment surfaces (DMS) allow us to accurately calculate the energy levels and spectra of water vapour. Using the DVR3D program suite developed at UCL, the energy levels of D_2O have been calculated in order to analyse the spectrum by the D_2O laser. The calculated band origins of D_2O is given in this thesis.

New linelists for $H_2{}^{17}O$ and $H_2{}^{18}O$ are also generated using the DVR program suite. Using these linelists, several experimental spectra of isotopically substituted water vapour have been studied. We analysed the $H_2{}^{17}O$ and $H_2{}^{18}O$ spectra measured by Fourier transform spectrometer at Kitt Peak National Solar Observatory (AZ, USA). Both spectra lie in $3\nu + \delta$ and 4ν polyad region where currently no data is publicly available. We also analysed the the $H_2{}^{17}O$ and $H_2{}^{18}O$ spectra in 5ν polyad region recorded by cavity ring-down spectroscopy at the Vrije Universiteit (Amsterdam, the Netherlands). The wavenumber region analysed in this work is the highest to date for both water isotopologues. The results of analyses are presented in this thesis.

Contents

List of Figures

List of Tables

Acknowledgements

I would like to thank my supervisor Jonathan Tennyson for his continuous guidance and support, without him this work would not have been possible. I thank my collaborators, Maarten Sneep, Wim Ubachs and Jim Brault for providing me with the experimental data. I also thank Olga Naumenko for helpful discussions and for providing her assignments of the spectra.

I thank Roman Tolchenov, Oleg Polyansky and Nikolai Zobov for useful discussions.

My special thanks go to Jimena Gorfinkiel and Natalia Vinci for keeping me alive during the stressful days and Jayesh Ramanlal for his countless helps. And I also thank my ex and current office mates.

Finally, I would like to thank my family and Anthony for their supports throughout my PhD study.

Chapter 1

Introduction

As we all know, water is essential for life. We drink, wash and cook with it – without water our lives simply cannot continue. It has a high abundance in the universe, in fact it is believed to be the third most abundant molecule after hydrogen and carbon monoxide. Water vapour is the most important greenhouse gas [1] and provides some 30 K of heating to the Earth through the greenhouse effect [2].

For decades water has been studied extensively in many different fields of science. In astronomy, water studies have helped to further our understanding of the interstellar medium [3], cool stars [4] and sunspots [5]. In combustion science, where water is the primary product of burning hydrocarbons, water data is used for modelling fumes and exhausts [6]. This has resulted in methods for the early detection of forest fires [7] and for tracking ships, aeroplanes *etc.* by analysing the hot water emissions from their exhaust fumes [8]. Such demands have meant that the need for accurate spectroscopic knowledge of water is increasing and will continue to do so in the future.

1.1 Atmospheric Modelling and The Databases

Water plays an important role in atmospheric science. Currently, most models of the Earth's atmosphere underestimate the solar energy absorbed in the atmosphere by 15 – 30 Wm^{-2} [9–12] out of 324 Wm^{-2} global average incoming solar energy. Various suggestions have been made for the causes of this discrepancy. Water vapour is considered to be the prime suspect for this

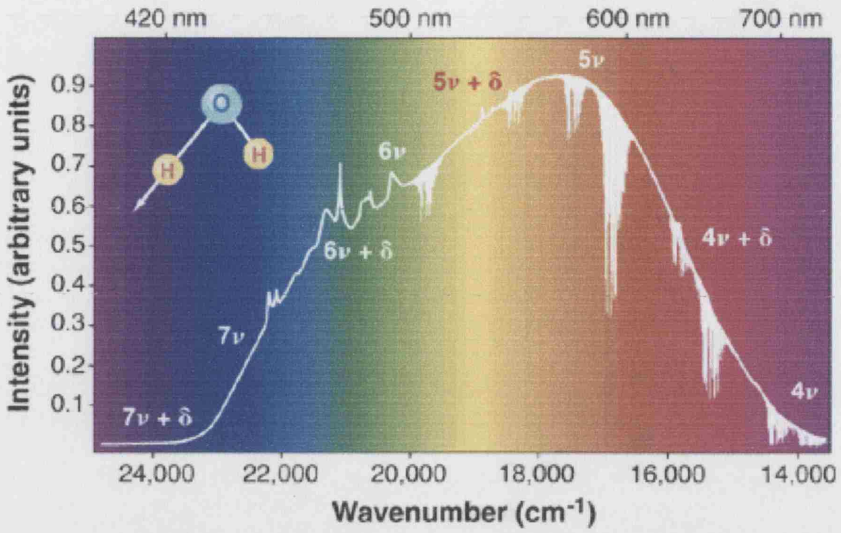

Figure 1.1: The absorption spectrum of $H_2{}^{16}O$ in the visible region, recorded with a high-resolution Fourier transform spectrometer and a long-path absorption cell. The background distribution of the spectrum is by the light source used for the measurement (not the actual solar radiation). The image was taken from reference [15]

"missing absorption problem", although it already accounts for about 70 % of absorption of incoming solar radiation in the Earth's atmosphere [13]. Weak lines of water unobserved in the laboratory in the near-infrared and visible regions are considered to be one of the causes [14]. It is estimated the unaccounted weak water lines in the near infrared and visible regions contribute more than 10 % additional opacity [14]. Weak lines of water vapour in this region are particularly important as the solar photon flux peaks at around 630 nm (yellow-red region) [15]. Figure 1.1 illustrates the water absorption spectrum in the visible region. In the figure, the yellow-red region of the visible spectrum is dominated by a cluster of weak absorption lines denoted as $5\nu + \delta$. Until recently, the weak lines in this region were not properly characterised due to experimental and theoretical difficulties.

The measurement of weak water lines in a laboratory is a difficult task since the weak absorption lines are observed only when long pathlengths are used. For solar radiation, the long pathlengths are naturally achieved in the Earth's atmosphere but it is difficult to recreate this in the confines of a laboratory. The laser based experiments such as cavity ring-down spectroscopy [16], intracavity absorption spectroscopy [17] and frequency modulation spectroscopy [18] are the most sensitive techniques to detect weak absorption by water. Another

commonly used technique is the high-resolution Fourier transform spectrometry coupled with a White-type multipass absorption cell to create a long pathlength. Using this technique, several researchers [19–22] successfully identified many of the previously unobserved weak lines in the near-infrared and visible regions.

Another possible cause of discrepancy is the unaccounted absorption by trace isotopologues of water, such as $H_2{}^{17}O$, $H_2{}^{18}O$ and HDO. Table 1.1 shows the natural abundance of water. The second most abundant water isotopologue $H_2{}^{18}O$ is thought to be the fifth biggest absorber in the Earth's atmosphere, yet the current available experimental data is very limited compared to $H_2{}^{16}O$. The spectra of natural abundance water contain some strong transitions by water isotopologues, usually dominated by $H_2{}^{18}O$. Schermaul *et al.* [21], for example, found 42 transitions due to $H_2{}^{18}O$ and 6 due to $H_2{}^{17}O$ in their analysis of the natural abundance water spectrum in the region of 13200 – 15000 cm^{-1} (near-infrared to red region). This is not the best way to study those less abundant water isotopologues, however. In 1980, Chevillard *et al.* [23–25] recorded the spectra of isotopically enhanced $H_2{}^{18}O$ and $H_2{}^{17}O$ using a Fourier transform spectrometer for a wide range of wavenumbers. The far-infrared region of both spectra has been studied in the past [23–32] but the near-infrared and visible portions of their spectra have been unanalysed for more than 20 years, partly due to a lack of adequate theoretical models needed in the analysis of these spectra. Fortunately, recent advances in computer and theoretical methods now allow us to study those spectra to improve the data of trace isotopologues of water. In this thesis, the above mentioned spectra of $H_2{}^{18}O$ and $H_2{}^{17}O$ in the near-infrared and visible region are analysed. The success of this study has stimulated the recording of further spectra of isotopically enhanced samples. The spectra of $H_2{}^{18}O$ and $H_2{}^{17}O$ in the visible (red) region were recorded for us by W. Ubachs' group (Vrije Universiteit) in Amsterdam using cavity ring-down spectroscopy. The spectra lie near the peak of the solar spectrum and contain the highest wavenumber to be studied to date for these isotopologues. The analysis of these spectra are presented in this thesis.

The spectroscopic information on atmospheric molecules is compiled in databases which can be used in model calculations. The widely used databases for atmospheric modelling are HITRAN (High-resolution Transmission Molecular Absorption Database) [33] and GEISA (Gestion et Etude des Informations Spectroscopiques Atmosphériques) [34]. The databases contain the line positions, intensities and line parameters such as air and self broadening co-

Table 1.1: Natural abundance of water used in the HITRAN database [33]. Isotopic abundances are given as mole fractions in percents (%). These abundances are used throughout this thesis.

$H_2{}^{16}O$	$H_2{}^{18}O$	$H_2{}^{17}O$	$HD^{16}O$	$HD^{18}O$	$HD^{17}O$
0.997317	0.00199983	0.000372	0.00031069	0.000000623	0.000000116

efficients that are important for atmospheric modelling. HITRAN, for example, contains over 1 080 000 spectral lines for 36 different molecules [35] and is regularly updated. This well-used database provides valuable information on the spectroscopic properties of molecules, but it is known many of the transition intensities are unfortunately not very accurate. Belmiloud *et al.* [36] recently showed the systematic underestimation of intensities of strong water lines in the near-infrared and red region compiled in HITRAN96 [37] and those corrected by Giver *et al.* [38]. The current version of HITRAN (HITRAN2000) [33] contains some revised intensities of water but many problems still remain. The incorrect transition intensities listed in the databases are considered to be another contributor to the "missing absorption problem" in the calculated atmospheric models.

Recently, several independent groups constructed new databases for water vapour in an attempt to improve the quality of water data. Schermaul *et al.* [39, 40] measured the water vapour spectrum in the spectral range 8600 – 15000 cm^{-1} with a high-resolution Fourier transform spectrometer under the auspices of the European Space Agency (ESA). The results of new experimental measurements combined with the theoretically calculated lines are compiled in the ESA-WVR (Water Vapour Red) linelist [41]. The theoretical lines from variational nuclear motion calculations [42] are included to compensate for the very weak lines which are not observed experimentally. Although this approach provides a complete list for the near-infrared and visible region, the accuracy of the theoretical lines is still debatable, especially for the intensities [43]. Coheur *et al.* [20] constructed a so-called "Brussels linelist" [44] in the range of 13000 – 26000 cm^{-1} from the previous measurements with the high-resolution Fourier transform spectrometer [19, 45]. The lower limit of spectral range covered in the linelist was later stretched to 9250 cm^{-1} [46]. This linelist only contains the results of their new measurements. More recently, spectra of pure water vapour were recorded by a collaboration of University College London and Imperial College (UCL-IC). The new Fourier transform spectra, measured

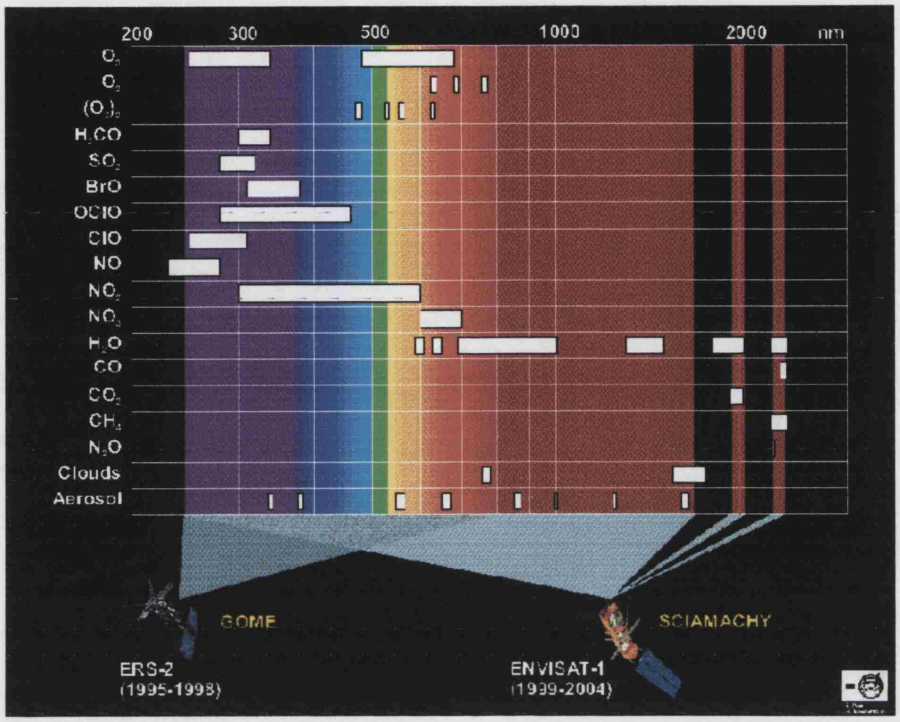

Figure 1.2: The spectral range covered by GOME and SCIAMACHY. White strips show the spectral regions where each molecule can be detected. The image was taken from the ESA website (http://envisat.esa.int/instruments/sciamachy).

with the same instrument as for the ESA-WVR, cover the range of 6500 – 16400 cm^{-1}. So far, detailed analysis of these spectra have been undertaken in the ranges 13200 –15000 cm^{-1} [21] and 11787 – 13554 cm^{-1} [22]. The higher wavenumber region (15000 – 16400 cm^{-1}) is currently being analysed by R. Tolchenov (UCL) and co-workers (private communication). These spectra were found to contain a large number of previously unobserved weak lines and the thorough analysis of these spectra can provide an improved view of water absorption in the near-infrared and visible region.

The water data – such as line positions, absolute intensities and line broadening parameters – is very important for the retrieval of water vapour densities from the satellite-borne spectrometers such as the European Space Agency's Global Ozone Monitoring Experiment (GOME) on ERS-2 satellite [47] and the Scanning Imaging Absorption Spectrometer for Atmospheric Chartography (SCIAMACHY) on ENVISAT-1 satellite [48]. Figure 1.2 shows the spectral range covered by the two spectrometers. GOME covers the ultraviolet and visible range whereas SCIAMACHY covers a much wider range including the far-infrared region. The retrieval of

water vapour from these instruments has been demonstrated in several papers [49–51]. Maurellis *et al* [51] interestingly compared the retrieval simulations for GOME and SCIAMACHY based on four different data sources: UCL-IC, Brussels, ESA-WVR and HITRAN (1996 and 2000). In this study, disparity in the results suggests that these databases are still incomplete.

Another use of the water data for analysis of satellite-borne spectra is to eliminate the contaminations by water vapour. Because water predominantly absorbs solar radiation in a very wide spectral range, satellite-borne spectra are heavily contaminated by water and the retrievals of other atmospheric species are virtually impossible unless the water lines are effectively eliminated. Construction of the ESA-WVR linelist was indeed funded by ESA for this very reason.

1.2 Overview of Theoretical Calculation

Experimentally observed transitions of water need to be assigned in order to be used for atmospheric modelling and other purposes as this yields their temperature dependence. Assignment is a procedure which attributes quantum numbers for lower and upper levels in a transition. In this work, the quantum numbers required are those for vibration and rotation. Water spectra are very rich and complicated with many transitions, therefore we need highly accurate theoretical predictions of the spectra for making assignments. Calculated theoretical spectra are useful not only for making assignments but also for predicting unobserved transitions, if such predictions are sufficiently accurate.

A starting point for calculating water spectra is the Born-Oppenheimer (BO) approximation [52] which separates the electronic and nuclear motion. The approximation is based on the assumption that the light electrons instantaneously adjust their positions with respect to the movements of heavy nuclei. The nuclear motion can be further separated into vibrational and rotational motion by assuming the rigid rotor approximation for rotations and harmonic approximation for vibrations. In this crude approximation of nuclear motion the interactions between the vibrational and rotational motion, called Coriolis coupling, are ignored although it is important in the case of water. Within these simple models, the vibrational wavefunctions are the product of harmonic oscillators and the rotational wavefunctions are the solutions to the rigid rotor model. These models, however, do not accurately represent the motions of nuclei

but are widely used for the labelling schemes of transitions.

Traditionally, this harmonic oscillator-rigid rotor model is improved by the perturbation theory. The commonly used Hamiltonian in perturbation theory is due to Watson [53, 54] based on the Eckart conditions [55], which maximise the separation between the vibrational and rotational motion of molecules. In this Hamiltonian, the harmonic oscillator-rigid rotor model is used as a zeroth order and a perturbation expansion is made by including the correction terms such as Coriolis coupling, centrifugal distortion, anharmonic potential *etc.* The constants related to these added terms are often derived by fitting to the experimental energy levels. Perturbation methods have been widely used in vibration-rotation calculations of many molecules, however for water the perturbation expansion is known to diverge at J as low as 7 [56]. It is now well known that the perturbation methods are not the best choice for high accuracy water calculations for the following reasons. Firstly, the vibration is assumed to be small in amplitude, which is clearly not the case for light molecules like water. Secondly, the methods break down when water reaches linearity since the Hamiltonian is different for bent and linear molecules [53]. And thirdly, the rotational expansions diverge at low J.

In recent years, variational methods have become a popular choice for high accuracy calculations of water. The methods are based on the variational principle proposed by Rayleigh and Ritz [57, 58] and solve for the exact nuclear kinetic energy operators within the BO approximation. In this approach, the energy levels are obtained by diagonalising the Hamiltonian matrix constructed by sets of basis functions for rotational and vibrational motion. The finite basis representation (FBR) uses a finite series of basis functions to construct a Hamiltonian matrix. This method gives accurate predictions of low-lying states, however it is less suitable for the high-lying states as a large number of functions are required to be converged. Alternatively, the discrete variable representation (DVR) [59–61] can be used to transform the FBR Hamiltonian matrix to a grid of internal coordinates determined by the appropriate Gaussian quadrature scheme for each basis function. In the DVR method, the final Hamiltonian matrix can be very compact with a high density of information. The variational methods are computationally demanding and expensive but the recent advances in computers made this type of calculation almost routine.

Within the BO approximation, the solutions to the electronic motion problem are treated

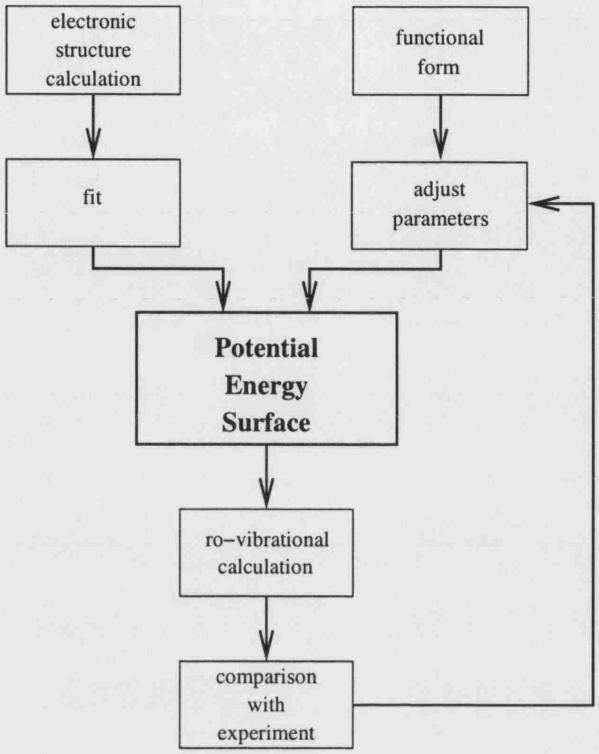

Figure 1.3: Schematic diagram showing how potential energy surfaces are constructed. The left hand side shows the *ab initio* calculation and the right hand side shows the purely empirical form. The figure was taken from the reference [62].

as the potential upon which nuclei move. The accuracy of potential energy surface (PES) is the dominant feature which determines the accuracy of overall calculation. Therefore electronic structure calculations of water have been the centre of considerable attention by quantum chemists for many years. There are three types of PES currently available: empirical, *ab initio* and semi-empirical. An empirical PES is determined firstly by guessing a suitable potential function. This function is used to calculate the vibration-rotation energy levels which are then compared with the known experimental levels. The parameters in the potential function are adjusted and the procedure is iterated until the calculations reproduce the experimental levels.

An *ab initio* PES for water is calculated by solving the electronic Schrödinger equation for a series of molecular geometries, i.e. different bond lengths and bond angle, to define the electronic energy at a grid of points [42, 63, 64]. These points are then interpolated analytically between the points to form a surface. This is usually done by least-squares fitting to the parametrised potential function. Figure 1.3 summarises the construction of an *ab initio* and an

empirical surface. *Ab initio* PESs usually give significantly larger errors compared to empirical surfaces. For example, the empirical PES by Polyansky *et al.* [65] gives a standard deviation of 0.25 cm^{-1}, whereas the *ab initio* PES by Partridge and Schwenke [42] has a typical errors of a few cm^{-1}. However, it is known that the accuracy of *ab initio* surfaces can be dramatically improved by making some empirical adjustments. The adjustments are usually made by fitting the *ab initio* potential to the experimental energy levels. Such empirically adjusted surfaces are called semi-empirical PESs in this thesis. A semi-empirical PES by Shirin *et al.* [66], which is currently the most accurate surface available, was extensively fitted to experimental levels lying up to 25 000 cm^{-1} above the ground state. It gives a standard deviation of 0.10 cm^{-1}.

The corrections arising from the breakdown of the BO approximation and the relativistic and quantum electrodynamic effects are not negligible for achieving spectroscopic accuracy [67]. The electron-nucleus interaction terms neglected in the BO approximation need to be evaluated as they can contribute considerably to the final outcomes. There are two types of corrections to the BO approximation: adiabatic and non-adiabatic correction. The adiabatic correction, often called the Born-Oppenheimer diagonal correction (BODC), is the energies obtained from the nuclear kinetic energy operator acting on the ground state electronic wavefunction. This correction is relatively easy to evaluate [68] but for water its effect is much smaller than the non-adiabatic correction, which is the difference between the full correction and the adiabatic correction. The non-adiabatic correction is more difficult to evaluate since we need to consider the interactions between the electronic ground states and all possible excited states. Zobov *et al.* [68] showed that this correction could be, at least partly, compensated by using the hydrogen mass exactly half way between the nuclear and atomic masses. The first *ab initio* calculation of non-adiabatic correction was recently carried out by Schwenke [67] based on the effective Hamiltonian developed by Bunker and Moss [69].

The relativistic effects occur due to the non-relativistic approach employed for construction a water PES. The full relativistic treatment for electronic calculation exists [70] but the non-relativistic approach is preferred by many people for its simplicity. However, the resulting errors arising from the non-relativistic approach are non-negligible in the vibration-rotation calculations of water. The relativistic corrections to the water PES have been investigated [71–76] and their substantial influence to the vibration-rotation energy levels of water is confirmed.

For the calculation of spectral intensities, we need to have a dipole moment surface (DMS). DMS provides the first moment of charge distribution in an analytic form similar to PES. However, constructing an accurate DMS can be difficult. *Ab initio* calculations of DMS do not obey the variational principle and converge differently from the electronic energies. This means that different dipole moments can be obtained from the *ab initio* calculations, which give similar electronic energies [77–79]. Empirical DMSs can be unreliable because the fit is made to experimental intensities which are very difficult to measure in high accuracy. Indeed, Lynas-Gray *et al.* [80] showed that for water, *ab initio* DMSs are more accurate than empirically fitted ones. Callegari *et al.* [43] recently developed an interesting method for testing the reliability of DMSs without measuring line intensities. Their results suggest that there is still a room for improvement for DMSs to produce accurate intensities.

1.3 Layout of the Thesis

This thesis is organised as follows. In chapter 2, the theories and methods relating to the water spectra calculations are introduced and the definitions of commonly used notations are also presented. The aim of this chapter is to give a basic knowledge required for the theoretical calculations of water.

In chapter 3, two widely used experimental techniques for measuring water spectra – Fourier transform spectrometry (FTS) and cavity ring-down spectroscopy (CRDS) – are discussed. The advantages and disadvantages of these two techniques are considered in section 3.3. A description of the previous experimental work on vibration-rotation spectra of $H_2{}^{18}O$ and $H_2{}^{17}O$ are also included in this chapter.

In chapter 4, the calculation of D_2O energy levels up to $J = 12$ using the DVR3D program suite developed at UCL [59], is presented. The purpose of this calculation was to familiarise myself with the program suite and to provide theoretical energy levels to analysed the spectrum recorded in the D_2O laser experiment [82]. Details of the calculation can be found in section 4.1.

In chapter 5, the generation of theoretical linelists for $H_2{}^{18}O$ and $H_2{}^{17}O$ is described. The new linelists are generated using the DVR3D program suite [59] for the purpose of assigning

experimental spectra of water isotopologues. The most difficult part of linelist generation is labelling the levels correctly. The labelling scheme used in this work can be found in subsection 5.1.3.

In chapter 6, the Fourier transform spectra of $H_2{}^{18}O$ and $H_2{}^{17}O$ are analysed and the results are presented. The spectra lie in the $3\nu + \delta$ and 4ν polyads region and are not included in HITRAN2000. The method used to assign spectra is discussed in detail in section 6.2.

In chapter 7, analysis of cavity ring-down spectra of $H_2{}^{18}O$ and $H_2{}^{17}O$ is presented. The spectra cover the 5ν polyad region, which is the highest wavenumber range studied to date for these isotopologues. The assignment results of these spectra are presented in the chapter.

In chapter 8, the summaries and discussions of the work are given. Possible future studies are also discussed.

This work is aimed to provide spectroscopic information of trace water isotopologues – $H_2{}^{17}O$ and $H_2{}^{18}O$ – which have been studied less extensively than $H_2{}^{16}O$. The experimental linelists of $H_2{}^{17}O$ and $H_2{}^{18}O$ in the near-infrared and visible regions presented in this thesis can be used to simulate absorption by these trace isotopologs in the Earth's atmosphere. The data obtained in this work should be compiled in the molecular databases and used to improve the quality of the models of the Earth's atmosphere.

Chapter 2

Calculating the Spectra of Water – Theoretical Background

The time-independent Schrödinger equation:

$$\hat{H}\Psi = E\Psi \tag{2.1}$$

is the most fundamental equation behind the theory of molecular spectroscopy. However, for molecules with two or more interacting particles, such as water, there are no exact solutions to this equation. In this chapter, the approximation to this equation and the methods to calculate the spectra of water will be presented.

2.1 The Born-Oppenheimer approximation

Consider a system with N nuclei of mass M_I, charge Z_I, coordinates $\mathbf{R}_I$ ($I = 1, 2, ...N$) and n electrons of mass m_e, charge $-e$, coordinates $\mathbf{r}_i$ ($i = 1, 2, ...n$). The Hamiltonian of this system can be written as:

$$\hat{H} = -\sum_{I=1}^{N} \frac{\hbar^2}{2M_I}\nabla_I^2 - \sum_{i=1}^{n} \frac{\hbar^2}{2m_e}\nabla_i^2 + V(\mathbf{R}_I, \mathbf{r}_i) \tag{2.2}$$

where the potential $\mathrm{V}(\mathbf{R}_I, \mathbf{r}_i)$ is the sum of all Coulombic terms:

$$V(\mathbf{R}_I, \mathbf{r}_i) = \sum_{I=1}^{N}\sum_{i=1}^{n} -\frac{Z_I\, e}{|\mathbf{r}_i - \mathbf{R}_I|} + \sum_{i>j}^{n} \frac{e^2}{|\mathbf{r}_i - \mathbf{r}_j|} + \sum_{I>J}^{N} \frac{Z_I Z_J}{|\mathbf{R}_I - \mathbf{R}_J|} \tag{2.3}$$

which are electron-nuclear attraction, electron-electron repulsion and nuclear-nuclear repulsion terms respectively.

The time-independent Schrödinger equation for the system can be written as:

$$\hat{H}\Psi(\mathbf{R}_I, \mathbf{r}_i) = E\Psi(\mathbf{R}_I, \mathbf{r}_i). \tag{2.4}$$

This cannot be solved analytically due to the electron – electron interaction terms. The standard way to simplify the problem is to use the Born-Oppenheimer (BO) approximation. The approximation is based on the fact that mass of electrons (m_e) is much smaller than that of nuclei (M_I), so it is possible to assume that electrons would instantaneously adjust their positions to the change in nuclear geometry. The approximation allows us to separate the wavefunction into two parts; the nuclear wavefunction and the electronic wavefunction for a fixed nuclear geometry. The wavefunction can be written as:

$$\Psi(\mathbf{R}_I, \mathbf{r}_i) = \psi_n(\mathbf{R}_I) \times \psi_e(\mathbf{r}_i; \mathbf{R}_I). \tag{2.5}$$

The total exact wavefunction of the system can be expressed as an expansion of complete set of electronic wavefunctions ψ_e with nuclear wavefunctions ψ_n acting as expansion coefficients, which only depend on nuclear geometry:

$$\Psi_{tot}(\mathbf{R}_I, \mathbf{r}_i) = \sum_{k=1}^{\infty} \psi_{nk}(\mathbf{R}_I)\psi_{ek}(\mathbf{r}_i; \mathbf{R}_I). \tag{2.6}$$

The Hamiltonian of electronic motion can be written as:

$$\hat{H}_e = -\sum_i \frac{\hbar^2}{2m_e}\nabla_i^2 + V(\mathbf{R}_I, \mathbf{r}_i) \tag{2.7}$$

and the Schrödinger equation for the electrons becomes:

$$(-\sum_i \frac{\hbar^2}{2m_e}\nabla_i^2 + V(\mathbf{R}_I, \mathbf{r}_i)\,)\psi_e(\mathbf{r}_i; \mathbf{R}_I) = E_e(\mathbf{R}_I)\psi_e(\mathbf{r}_i; \mathbf{R}_I). \tag{2.8}$$

Both ψ_e and E_e depend parametrically on nuclear coordinates. $E_e(\mathbf{R}_I)$ is the electronic energy and $\psi_e(\mathbf{r}_i; \mathbf{R}_I)$ is the electronic eigenfunction of the system when the nuclei are clamped at coordinate $\mathbf{R}_I$. Within the BO approximation, the sum of all possible $E_e(\mathbf{R}_I)$ forms a potential energy surface (PES) upon which nuclei move. PES will be discussed in detail in section 2.11.

The Schrödinger equation for the total energy is:

$$(-\sum_I \frac{\hbar^2}{2M_I}\nabla_I^2 + E_e(\mathbf{R}_I)\,)\Psi_{tot}(\mathbf{R}_I, \mathbf{r}_i) = E_{tot}\Psi_{tot}(\mathbf{R}_I, \mathbf{r}_i) \tag{2.9}$$

substitute eq.(2.6) into eq.(2.9) gives:

$$(-\sum_I \frac{\hbar^2}{2M_I}\nabla_I^2 + E_e(\mathbf{R}_I)\,)\sum_{k=1}^{\infty}\psi_{nk}(\mathbf{R}_I)\,\psi_{ek}(\mathbf{r}_i;\mathbf{R}_I) = E_{tot}\sum_{k=1}^{\infty}\psi_{nk}(\mathbf{R}_I)\psi_{ek}(\mathbf{r}_i;\mathbf{R}_I) \tag{2.10}$$

Using the relationship:

$$\nabla^2(\psi\phi) = \psi\nabla^2\phi + \phi\nabla^2\psi + 2\,(\,\nabla\psi\nabla\phi\,) \tag{2.11}$$

and multiplying from the left by $\psi^*_{ek'}$ and integrating over all electronic coordinates using the orthonormality of ψ_e, we get :

$$(-\sum_I \frac{\hbar^2}{2M_I}\nabla_I^2 + E_e(\mathbf{R}_I) - E_{tot})\,)\,\psi_{nk'} + \sum_k C_{k'k}\,\psi_{nk} = 0 \tag{2.12}$$

with

$$C_{k'k} = -\sum_I \frac{\hbar^2}{2M_I}(\langle\psi_{ek'}|\nabla_I^2|\psi_{ek}\rangle + 2\langle\psi_{ek'}|\nabla_I|\psi_{ek}\rangle\nabla) \tag{2.13}$$

The first term of eq. (2.12) does not contain the electronic wavefunction. Within the BO approximation the second term is neglected as we assume electronic motions are independent of nuclear geometries, i.e. $\nabla_I\psi_e = 0$. So we can write the Schrödinger equation as follows:

$$(-\sum_I \frac{\hbar^2}{2M_I}\nabla_I^2 + E_e(\mathbf{R}_I)\,)\,\psi_n(\mathbf{R}_I) = E_{tot}\,\psi_n(\mathbf{R}_I) \tag{2.14}$$

where $E_e(\mathbf{R}_I)$ is the electronic energy determined by solving the Schrödinger equation for electronic motions at the nuclear coordinates $\mathbf{R}_I$.

In order to obtain more accurate E_{tot}, corrections arising from the neglected $C_{k'k}$ term need to be considered. In the adiabatic approximation, the diagonal first order coupling element is cancelled, i.e. $\langle\psi_{ek'}|\nabla_I|\psi_{ek}\rangle = 0$. Also all the coupling terms $\langle\psi_{ek'}|\nabla_I^2|\psi_{ek}\rangle$ are ignored unless $k' = k = 1$ (ground state). Now eq. (2.12) becomes:

$$(-\sum_I \frac{\hbar^2}{2M_I}\nabla_I^2 + E_e(\mathbf{R}_I) + \Delta V^{AD} - E_{tot})\,\psi_{nk} = 0 \tag{2.15}$$

with

$$\Delta V^{AD} = -\sum_I \frac{\hbar^2}{2M_I}(\langle\psi_{ek}|\nabla_I^2|\psi_{ek}\rangle), \quad k = 1 \tag{2.16}$$

ΔV^{AD} is called the adiabatic or the Born-Oppenheimer diagonal correction (BODC) and is relatively easy to evaluate. Zobov *et al.* [68] calculated the BODC using the self-consistent

field (SCF) wavefunctions. Their results showed the BODC does not give a significant correction to water vibrations as the magnitude of correction is less than 4 cm^{-1}. The BODC effect is stronger for bending than stretching excitation by almost one order of magnitude. Recently, Schwenke [67] calculated the BODC using complete active space self-consistent (CASSCF) wavefunctions, and this data was subsequently refitted by Tennyson *et al.* [83] to stabilise the results of nuclear motion calculation. The major difference between the BODC by calculation using SCF and CASSCF wavefunctions is the results for stretching excitations whereas the bending excitations are similar. In 2003, Schwenke [84] calculated the BODC with the internally contracted multireference configuration interaction (icMRCI) wavefunctions, which should provide high accuracy results. He then compared the BODC by SCF, CASSCF and icMRCI and showed that all three methods gave similar results for the bending excitations but dissimilar results for stretching excitations. The CASSCF method overestimates the effect for stretching excitations. The corrections obtained from icMRCI method always move towards the SCF results although the SCF is not reliable for obtaining the BODC in spectroscopic accuracy.

The non-adiabatic correction, the difference between the full correction and the adiabatic correction, is more difficult to evaluate because interactions between the ground states and all possible excited electronic states need to be considered. In 1980, Bunker and Moss [69] derived an effective Hamiltonian for the non-adiabatic correction for triatomic molecules, in which they treated the non-adiabatic effects as the corrections to the inertia of the nuclei. This was a significant advance in calculating the non-adiabatic effects. The simplest way to include the non-adiabatic correction is to manipulate the masses used in the nuclear motion Hamiltonian. Zobov *et al.* [68] found the best results are obtained when a middle mass of hydrogen – a mass exactly half way between the atomic and nuclear masses, was used. However, this method tends to underestimate the effects for the stretching excitations and overestimate for the bending excitations. Using the effective Hamiltonian by Bunker and Moss, Schwenke [67] developed a model which includes the non-adiabatic correction in the nuclear motion problem. In his paper he developed two models, a full calculation involving three-dimensional coupling surfaces and a simplified version with the vibrationally averaged, diagonal components of coupling surfaces. Interestingly, both models gave similar results. Detailed comparisons between different models can be found in the references [83, 85].

2.2 Coordinate System and the Hamiltonian operator for Water

2.2.1 Coordinate Systems

Once translational motion has been removed, there is no unique nuclear motion Hamiltonian as it can be written in many different coordinate systems [86]. It is therefore important to find the suitable coordinates for the molecule of interest. For a molecule with N atoms, there are 3N degrees of freedom. The centre-of-mass motion takes three degrees of freedom but this needs to be removed as it gives a continuous spectrum. Removing the centre-of-mass motion gives 3N−3 coordinates for rotational and vibrational degrees of freedom. The space-fixed coordinates are not capable of distinguishing between vibrational and rotational motion. Therefore the introduction of the body-fixed coordinates is desirable. In body-fixed coordinates, rotational axes are either fixed or embedded within the molecular framework. The two coordinate systems are linked by the Eular angles (α, β, δ), which are the angles of orientation of the body-fixed axis in relation to the space-fixed axis. The advantage of the body-fixed coordinates is vibrational and rotational motion are separable and some vibration-rotation couplings can be neglected. But on the other hand, they also introduce singularities in the Hamiltonian. Singularities occur at geometry when the Hamiltonian depends on one less coordinate than full set of coordinates. Some strategies to deal with singularities have been considered in the past [87–89].

There are many possible choices of internal coordinates. Sutcliffe and Tennyson [90] introduced a generalised internal coordinate system for triatomic molecules and used it to derive the Hamiltonian for triatomic molecules. This Hamiltonian is called Sutcliffe-Tennyson Hamiltonian and is described in the next subsection. Figure 2.1 shows the general internal coordinate system defined by Sutcliffe and Tennyson. In this generalised coordinate system, a molecule consisting of atoms A_1, A_2 and A_3 is described with two lengths (r_1, r_2) and an angle θ and the two geometric parameters, g_1 and g_2:

$$g_1 = \frac{A_3 - \mathrm{P}}{A_3 - A_2}; \quad g_2 = \frac{A_3 - \mathrm{R}}{A_3 - A_1} \tag{2.17}$$

where the points P and R are determined by the masses of atoms and choice of internal coordinates.

The widely used bond-length-bond-angle coordinates (r_1, r_2, θ) can be obtained from the

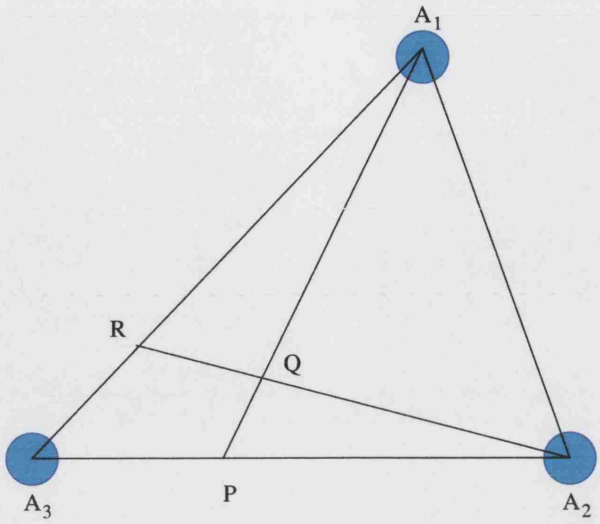

Figure 2.1: Generalised internal coordinate system for triatomic molecules by Sutcliffe and Tennyson. A system is described by two lengths $r_1 = \overline{A_2R}$, $r_2 = \overline{A_1P}$ and the angle $\theta = \widehat{A_1QA_2}$. The positions of points P and R can be defined according to the chosen coordinate system and by the masses of the atoms [90].

general coordinates of Figure 2.1 by setting $r_1 = \overline{A_1A_3}$, $r_2 = \overline{A_2A_3}$ and $\theta = \widehat{A_1A_3A_2}$. In the case of water, A_3 is an oxygen atom and A_1, A_2 are hydrogen atoms, and the geometric parameters g_1 and g_2 are both 0. One disadvantage of bond-length-bond-angle coordinates is that they are not orthogonal and this results in cross-derivative terms in the kinetic energy operator.

For water, Radau coordinates are the preferred choice for many studies [91, 92]. The coordinates were originally proposed by Radau [93] for the planetary three-body problems but are also useful for light-heavy-light triatomic molecules. The geometric parameters for Radau coordinates, which determines the positions of points P and R, are defined as:

$$g_1 = g_2 = \gamma = 1 + \frac{M_O}{M_H} - \sqrt{(1 + \frac{M_O}{M_H})^2 - 1} \approx 0.03 \tag{2.18}$$

where M_O and M_H are the masses of oxygen and hydrogen, respectively. Unlike bond-length-bond-angle coordinates, Radau coordinates are orthogonal and generate a diagonal kinetic energy operator. This is an advantage as it significantly reduces the computational time [94]. For light-heavy-light triatoms like water, Radau coordinates become very similar to bond-length-bond-angle coordinates. Figure 2.2 shows the Radau coordinates for water as defined by Sutcliffe and Tennyson, which is slightly different from the commonly used definition to keep the

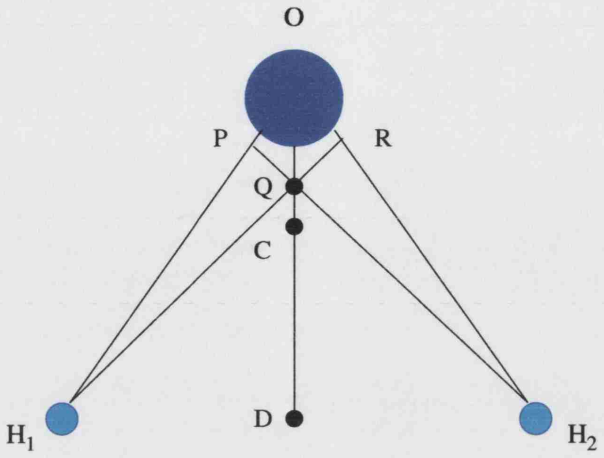

Figure 2.2: Radau coordinates for water as defined by Sutcliffe and Tennyson. C is the centre-of-mass of the molecule, D is the centre-of-mass of two hydrogen atoms and P and R are the points satisfying $g_1 = g_2 = \gamma$. A system is described by the two lengths and the angle; $r_1 = \overline{RH_1}$, $r_2 = \overline{PH_2}$ and $\theta = \widehat{H_1QH_2}$.

consistency between different coordinate systems.

2.2.2 Sutcliffe-Tennyson Hamiltonian for Water

Sutcliffe and Tennyson [90] derived the Hamiltonian which allows an almost entirely arbitrary choice of internal coordinates and body-fixed axes. For water, the combination of Radau coordinates and a bisector embedding is the preferred choice. A bisector embedding is defined as x-axis bisecting the angle θ, with z-axis lying in the plane of the molecule. Figure 2.3 shows a water molecule in Radau coordinates with a bisector embedding.

The Hamiltonian for the body-fixed system has a general form within the BO approximation:

$$\hat{H} = \hat{K}_V + \hat{K}_{VR} + V \tag{2.19}$$

where $\hat{K}_V$ is a purely vibrational kinetic energy operator, $\hat{K}_{VR}$ is a mixed vibration-rotation kinetic energy operator and V is the potential energy surface. The effective radial Hamiltonian operator can be obtained by following the work by Tennyson and Sutcliffe [94]:

$$\hat{H}(r_1, r_2) = \langle j', k' | \hat{H} | j, k \rangle \tag{2.20}$$

with

$$|j, k\rangle = \Theta_{j,k}(\theta) D^J_{M,k}(\alpha, \beta, \gamma) \tag{2.21}$$

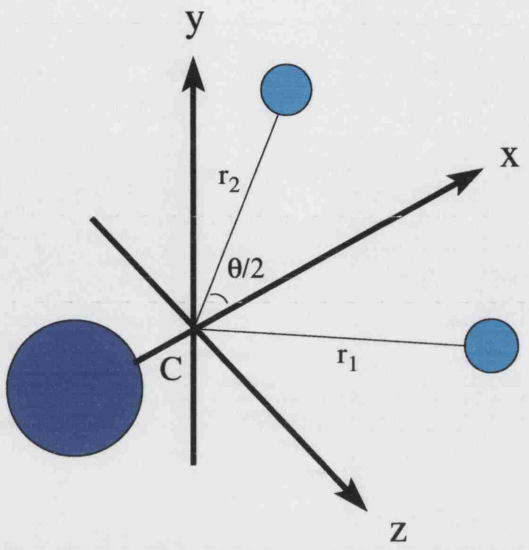

Figure 2.3: Bisector embedding axes in Radau coordinated for water. The origin of the axes is at the centre-of-mass of the molecule (C).

where $|j,k\rangle$ is the angular basis function, $\Theta_{j,k}(\theta)$ is the associated normalised Legendre Polynomial and $D^J_{M,k}(\alpha,\beta,\gamma)$ is the rotational matrices. The rotational matrices convert the space-fixed rotational motions into the body-fixed coordinates with Euler angles (α,β,γ). The subscript k and M are the projection of J onto the body-fixed z-axis and the space-fixed z-axis respectively. M is omitted in the absence of a magnetic field.

The effective radial Hamiltonian operator for water in Radau coordinates with bisector embedding can be written as [85, 90]:

$$\hat{H}(r_1,r_2) = \hat{K}_V^{(1)} + \hat{K}_{VR}^{(1)} + \hat{K}_{VR}^{(2)} + \hat{K}_{VR}^{(3)} + \delta_{k',k}\langle j',k|V(r_1,r_2,\theta)|j,k\rangle_\theta \tag{2.22}$$

where

$$\hat{K}_V^{(1)} = \delta_{j'j}\delta_{k'k}\left[\frac{\hbar^2}{2\mu_1}\frac{\partial}{\partial r_1^2} - \frac{\hbar^2}{2\mu_2}\frac{\partial}{\partial r_2^2} + \frac{\hbar^2}{2}j(j+1)\left(\frac{1}{\mu_1 r_1^2}+\frac{1}{\mu_2 r_2^2}\right)\right] \tag{2.23}$$

$$\begin{aligned}\hat{K}_{VR}^{(1)} &= \delta_{k'k}\frac{\hbar^2}{8}(J(J+1)-3k^2)\left(\frac{1}{\mu_1 r_1^2}+\frac{1}{\mu_2 r_2^2}\right) I^{(1)}_{j',k',j,k} \\ &+\delta_{k',k}\frac{\hbar^2}{16}(J(J+1)-k^2)\delta_{j'j}\left(\frac{1}{\mu_1 r_1^2}+\frac{1}{\mu_2 r_2^2}\right)\end{aligned} \tag{2.24}$$

$$\hat{K}_{VR}^{(2)} = \delta_{k'k\pm1}\frac{\hbar^2}{4}C^{\pm}_{Jk}\left[\left(\frac{1}{\mu_1 r_1^2}-\frac{1}{\mu_2 r_2^2}\right)\left(\delta_{j'j}C^{\pm}_{jk}+(k\pm\frac{1}{2})I^{(2)}_{j',k',j,k}\right)\right] \tag{2.25}$$

$$\hat{K}_{VR}^{(3)} = \delta_{k'k\pm2}\frac{\hbar^2}{32}C^{\pm}_{Jk}C^{\pm}_{Jk}[(\frac{1}{\mu_1 r_1^2}+\frac{1}{\mu_2 r_2^2})(2I^{(1)}_{j',k',j,k}-I^{(3)}_{j',k',j,k})] \tag{2.26}$$

where $C_{jk}^{\pm}$ is the angular factor:

$$C_{jk}^{\pm} = \sqrt{j(j+1) - k(k \pm 1)}, \tag{2.27}$$

and the integrals $\mathrm{I}^{(n)}$ are given by:

$$I_{j',k',j,k}^{(1)} = \langle j'k'| \frac{1}{(1-\cos\theta)} |jk\rangle, \tag{2.28}$$

$$I_{j',k',j,k}^{(2)} = \langle j'k'| \frac{1+\cos\theta}{\sin\theta} |jk\rangle, \tag{2.29}$$

$$I_{j',k',j,k}^{(3)} = \langle j'k'|jk\rangle, \tag{2.30}$$

$$\tag{2.31}$$

A full derivation of this effective radial Hamiltonian can be found in the reference [90, 94].

2.3 Vibrational Motion

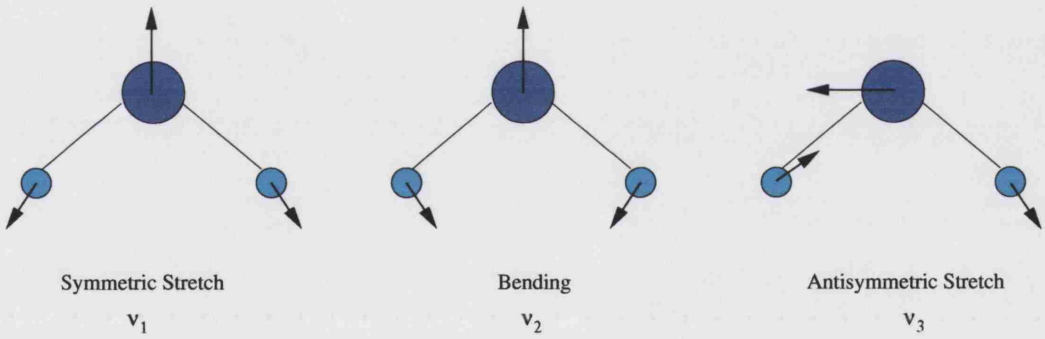

Figure 2.4: Vibrational modes of water in harmonic approximation.

There are 3N−6 vibrational degrees of freedom for a molecule with N atoms. When vibration is assumed to be harmonic, there are three normal modes for water; symmetric stretch (ν_1), bending (ν_2) and antisymmetric stretch (ν_3). Figure 2.4 shows a schematic diagram of vibrational motions of the water molecule. The fundamental wavenumbers for each mode have been experimentally determined. The summary of fundamental wavenumbers for water isotopologues can be found in the Table 2.1. In normal mode notation, each vibrational state is described in (v_1 v_2 v_3) where v_1, v_2, v_3 are quanta corresponding to ν_1, ν_2 and ν_3 respectively. The ground vibrational state is (000) and the lowest excited state is (010), which is the first excited bending motion. Within the harmonic approximation, the energy of each vibrational

Table 2.1: Summary of experimentally observed fundamental wavenumbers for $H_2{}^{16}O$, $H_2{}^{17}O$ and $H_2{}^{18}O$. The data has been taken from references [95–97]. Wavenumbers are given in cm^{-1}.

Isotopologue	ν_1	ν_2	ν_3
$H_2{}^{16}O$ [95]	3656.053323 (4)	1594.74633 (24)	3755.92868 (3)
$H_2{}^{17}O$ [96, 97]	3653.14226 (10)	1591.32565 (5)	3748.31807 (10)
$H_2{}^{18}O$ [96, 97]	3649.68540 (10)	1588.27567 (10)	3741.56678 (10)

state relative to the zero point energy is given as:

$$E(v_1\ v_2\ v_3) = v_1 \cdot \nu_1 + v_2 \cdot \nu_2 + v_3 \cdot \nu_3 \tag{2.32}$$

Although the harmonic oscillator describes low-lying states reasonably well, it fails for the large amplitude motions and the model does not allow for dissociation.

The Morse potential is a more realistic model to describe the stretching vibrational motion of water. The Morse potential is given by:

$$V(r) = D_e\,(1 - e^{-a(r-r_e)})^2 \tag{2.33}$$

where D_e is a dissociation energy, r_e is an equilibrium bondlength and a is the Morse constant which leads to the energy levels getting closer as they get excited.

Normal mode notation is only valid for low lying states. An alternative choice is local mode notation [98], which describes a vibration localised in a single OH bond and gives a better model for high lying stretching states [19, 99]. In local mode notation, vibrational levels are labelled as $mn^{\pm}v_2$, where $m + n = v_1 + v_3$ and superscript $^{\pm}$ shows symmetric (+) or antisymmetric (−) combinations of local quanta. When $m = n$, the combination can only be symmetric hence the superscript is omitted. The levels can be quasi degenerate if the two levels are related such that $(v_1\ v_2\ v_3)$ and $(v_1 - 1\ \ v_2\ \ v_3 + 1)$. For example, normal mode level (400) is 40^+0 (symmetric) in local mode and (301) is 40^-0 (antisymmetric) and they are very close in energy.

Polyads are another way of classifying the vibrational states. The concept originates in the fact that the fundamental frequencies of both stretch modes and two quanta excitations of bending mode are all very close, i.e. $\nu_1 \approx \nu_3 \approx 2\nu_2$. Due to this, the water spectrum shows distinctive clusters called polyads, which contain transitions of similar wavenumber.

The quanta of stretch modes are denoted as ν and of bending mode is as δ where $\nu = 2\delta$. So for even v_2, the polyad number n is $v_1+v_3+(v_2/2)$ and for odd v_2, $n = v_1+v_3+\text{integer}(v_2/2)+\delta$. There are $(n+1)(n+2)/2$ vibrational states for each $n\nu$ and $n\nu+\delta$ polyad.

2.4 Rotational Motion

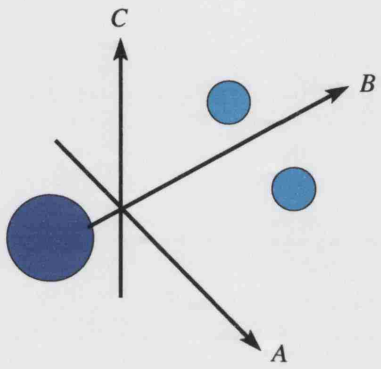

Figure 2.5: The principle axes of inertia. The orientation of axes is a bisector embedding, explained in section 2.2.1.

Water is an asymmetric top molecule, with all three principle moments of inertia, I_A, I_B, I_C, being different. Figure 2.5 shows the three principle axes of water. The spectrum of such molecules is very rich and complicated with billions of transitions [42].

Rotational motion of molecules can be approximated to a rigid rotor model, in which rotational energy for a linear molecule is given by $BJ(J+1)$ where B is a rotational constant determined by the moment of inertia of a rotating molecule. B is defined as:

$$B = \frac{\hbar^2}{2I_B} \tag{2.34}$$

For water, rotational constants are given by:

$$A = \frac{\hbar^2}{2I_A}; \quad B = \frac{\hbar^2}{2I_B}; \quad C = \frac{\hbar^2}{2I_C}$$

where A, B and C are in Hz. The experimentally determined values of rotational constants of three water isotopologues are summarised in Table 2.2. Conventionally, the principle axes are determined to satisfy $A \geq B \geq C$. The rigid rotor model does not allow for the bondlength distortion by the molecular vibration and rotation. Centrifugal and other distortion terms can be added but the model still breaks down for high J.

Table 2.2: Summary of the experimentally determined rotational constants of water isotopologues $H_2^{16}O$, $H_2^{17}O$ and $H_2^{18}O$ in electronic and vibrational ground state (taken from references [100, 101]). Rotational constants A, B, C are given in MHz.

Isotopologue	A	B	C
$H_2{}^{16}O$ [100]	835839.10 (13)	435347.353 (27)	278139.826 (57)
$H_2{}^{17}O$ [101]	830283.720 (43)	435350.739 (26)	277511.307 (22)
$H_2{}^{18}O$ [101]	825367.428 (67)	435353.585 (38)	276950.565 (29)

Rotational levels are usually labelled as $J_{K_aK_c}$ where J is the total angular momentum, K_a is the projection of the total angular momentum J on the A axis and K_c is the projection on the C axis. K_a takes the values $0, 1, ..., J$ and it predominantly influences the energy levels. For a given K_a, K_c takes the value $J - K_a$ or $J - K_a + 1$. There are $2J + 1$ non-degenerate levels for each value of J.

2.5 Quantum Numbers and Symmetry

Table 2.3 shows the summary of quantum numbers used in this thesis.

Water in its equibrium geometry belongs to the C_{2v} point group. The character table of C_{2v} can be found in Table 2.4. Column 1 shows the symmetry types. Column 2 shows the transformation of a wavefunction with the four elements of the group, E (identity transformation), C_2 (rotation about x axis, see figure 2.3), σ_{xz} (reflection through xz plane) and σ_{xy} (reflection through xy plane). Column 3 shows the translation and rotation vectors. Labels x, y, z give the translation vectors which correspond to the change in dipole moments. R_x, R_y, R_z give the rotation vectors about x, y, z axes. A_2 is infrared inactive as it does not involve the change in dipole moments. Column 4 shows the second order combination of Cartesian coordinates. Labels x^2, y^2, z^2, xy, xz, yz give the d orbital symmetrised at the centre of mass. Column 5 shows the symmetry of wavefunction (ϕ). The last columns give the products table for the C_{2v} group.

ROTLEV module of DVR3D program suite writes out energy levels in four symmetry blocks, labelled ee, eo, fe and fo. Table 2.5 shows the relationship of these four symmetry blocks with respect to the values of J, ν_3, K_a, K_c and vibrational and rotational parity p, q respectively.

Table 2.3: Summary of quantum numbers used for calculation of water spectrum.

Rigorous Quantum Numbers		
Quantum Number	Description	Value
J	Total angular momentum	$J \geq 0$
q	Vibrational parity	0 for even v_3, sometimes denoted as "e" 1 for odd v_3, sometimes denoted as "o"
p	Rotational parity	0 for even, sometimes denoted as "e" 1 for odd, sometimes denoted as "f"
ortho (triplet)	The symmetry of H interchange	$K_a + K_c + v_3$ = odd
para (singlet)	The symmetry of H interchange	$K_a + K_c + v_3$ = even
Non-rigorous Quantum Numbers		
v_i	quanta of vibrational mode ν_i	v_1 for symmetric stretch v_2 for symmetric bend v_3 for antisymmetric stretch
K_a	Projection of J onto the A axis	0 to J in integer step
K_c	Projection of J onto the C axis	$J - K_a$ or $J - K_a + 1$

Table 2.4: C_{2v} symmetry point group character table.

C_{2v}	E	C_2	σ_{xz}	σ_{xy}			ϕ	A_1	A_2	B_1	B_2
A_1	+1	+1	+1	+1	x	x^2, y^2, z^2	even-para	A_1	A_2	B_1	B_2
A_2	+1	+1	−1	−1	R_x	yz	odd-para	A_2	A_1	B_2	B_1
B_1	+1	−1	+1	−1	y, R_z	xy	even-ortho	B_1	B_2	A_1	A_2
B_2	+1	−1	−1	+1	z, R_y	xz	odd-ortho	B_2	B_1	A_2	A_1

Table 2.5: The four symmetry blocks used for DVR3D calculations of water spectrum. O is ortho and P is para symmetry of the interchange of hydrogen atoms.

Sym. Block	output	K_a	K_c	p	q	O/P	output	K_a	K_c	p	q	O/P
	ν_3 **even**						ν_3 **odd**					
	J **even**						J **even**					
A_1	ee	even	even	0	0	P	ee	odd	even	0	0	P
A_2	eo	odd	even	0	1	O	eo	even	even	0	1	O
B_1	fe	odd	odd	1	0	P	fe	even	odd	1	0	P
B_2	fo	even	odd	1	1	O	fo	odd	odd	1	1	O
	J **odd**						J **odd**					
A_1	ee	even	odd	0	0	O	ee	odd	odd	0	0	O
A_2	eo	odd	odd	0	1	P	eo	even	odd	0	1	P
B_1	fe	odd	even	1	0	O	fe	even	even	1	0	O
B_2	fo	even	even	1	1	P	fo	odd	even	1	1	P

2.6 Selection Rules

For vibrational transitions, there are no selection rules strictly speaking as $\Delta\nu$ can be any integer. $|\Delta\nu| = 1$ are called the fundamental and within harmonic approximation, this is the only allowed transition. Transitions with $|\Delta\nu| > 1$ are called overtones and they are usually much weaker than fundamentals.

Rotational selection rules mean that ΔJ can be either 0 (Q branch), $+1$ (R branch) or -1 (P branch). For $\Delta J = 0$, only $\Delta p = \pm 1$ transitions are allowed and for $\Delta J = \pm 1$, $\Delta p = 0$ are allowed. ΔK_c is always odd, however ΔK_a depends on the value of $\Delta\nu_3$. When $\Delta\nu_3$ is even ΔK_a is odd and when ν_3 is odd ΔK_a is even. Table 2.6 summarises the selection rules for water.

Table 2.6: Selection rules of water transitions. The stonger transitions are observed with smaller ΔK_a and ΔK_c values.

$\Delta J = 0$	$\Delta J = \pm 1$
$\Delta K_c = \text{odd}$	
$\Delta K_a = \text{odd}$ ($\nu_3 = \text{even}$) $\Delta K_a = \text{even}$ ($\nu_3 = \text{odd}$)	
$\Delta p = \pm 1$	$\Delta p = 0$

2.7 Solving for the Nuclear Motion

Perturbation and variational theory are the two most commonly used methods to solve the Schrödinger equation for multi-atom systems. For a long time, perturbation theory has been used for calculations of high resolution molecular spectroscopy. However, there are situations where the perturbation theory struggles to give high accuracy predictions.

For water, variational methods are the preferred way of solving the Schrödinger equation. The methods are more flexible than perturbation methods and work well for systems for which perturbation theory is unreliable. The main disadvantage is that variational calculations are computationally demanding and thus expensive compared to perturbation methods.

2.7.1 Perturbation Theory

In perturbation theory, the Schrödinger equation is not solved directly but it is assumed that full Hamiltonian is approximately equal to the exact Hamiltonian with a small perturbing term:

$$\hat{H} = \hat{H}_0 + \lambda \hat{H}' \tag{2.35}$$

with

$$\hat{H}_0 \psi_0 = E_0 \psi_0 \tag{2.36}$$

where $\hat{H}$, $\hat{H}_0$, ψ_0 and $\lambda \hat{H}'$ are the full Hamiltonian, the exact Hamiltonian, the exact wavefunction and a perturbing term, respectively. The parameter λ varies between 0 (small perturbation) to 1 (full perturbation), depending on the strength of the perturbation. The wavefunction and eigen-energy is expanded as:

$$\begin{aligned} \Psi &= \psi_0 + \lambda \psi_1 + \lambda^2 \psi_2 + ... \\ E &= E_0 + \lambda E_1 + \lambda^2 E_2 + ... \end{aligned} \tag{2.37}$$

In order for the perturbation theory to be valid, the series needs to converge preferably after a small number of terms. Usually the vibration and rotation motion is considered separately. For the vibrational $\hat{H}_0$, harmonic oscillator is often used and for the rotational $\hat{H}_0$, rigid rotor model is commonly used.

The main problem with the perturbation theory is the assumption of the small amplitude vibrational motion implicit in the harmonic approximation. This is a poor treatment for many molecules and cannot describe the large amplitude motion near dissociation. Another problem is the Hamiltonian for linear and non-linear molecules is different. This means a problem arises when a non-linear molecule reaches linearity [53]. Both problems are significant for water since it undergoes a large amplitude motion and reaches linearity around 11000cm^{-1} [102]. For rotational expansions, the perturbation calculation using the Watson Hamiltonian [53] diverges for $J > 7$ [56], hence it is not suitable for the calculation of room temperature water spectra, which typically have a population of rotational states up to $J = 10$.

2.7.2 The Variational Principle

The variational principle was first proposed by Rayleigh and Ritz [57, 58] and it shows that any approximate wavefunction always gives an energy expectation value greater or equal to the true ground state energy. That is:

$$E_0^{approx} \geq E_0^{exact} \tag{2.38}$$

To prove eq. (2.38), consider a system with a normalised well-behaved approximate function Ψ, such that:

$$\int \Psi^* \hat{H} \Psi d\tau = E^{approx} \tag{2.39}$$

Ψ can be expanded in terms of ψ_n, a complete, orthonormal set of eigenfunctions of $\hat{H}$:

$$\Psi = \sum_n c_n \psi_n \tag{2.40}$$

where c_n is an expansion coefficient and ψ_n is a basis function which satisfies:

$$\hat{H}\psi_n = E_n\psi_n \tag{2.41}$$

Now, consider the case:

$$\int \Psi^*(\hat{H} - E_0)\ \Psi d\tau \tag{2.42}$$

where E_0 is the true ground state energy. Substituting eq. (2.40) into eq. (2.42) gives:

$$\int \Psi^*(\hat{H} - E_0)\ \Psi\ d\tau = \int \sum_m c_m^*\ \psi_m^*(\hat{H} - E_0) \sum_n c_n\ \psi_n\ d\tau \tag{2.43}$$

Using eq. (2.41) we can rewrite eq.(2.43) as:

$$\int \sum_m c_m^*\ \psi_m^* \sum_n c_n(E_n - E_0)\ \psi_n\ d\tau = \sum_n c_n^* c_n(E_n - E_0) = \sum_n |c_n|^2(E_n - E_0) \tag{2.44}$$

E_0 is the lowest possible energy so $(E_n - E_0) \geq 0$ and also $|c_n|^2 \geq 0$. Therefore:

$$\int \Psi^*(\hat{H} - E_0)\ \Psi\ d\tau = \sum_n |c_n|^2(E_n - E_0) \geq 0 \tag{2.45}$$

Rearranging gives:

$$\int \Psi^* \hat{H}\ \Psi\ d\tau \geq E_0 \tag{2.46}$$

If Ψ is not a normalised function, eq. (2.46) becomes:

$$\frac{\int \Psi^* \hat{H} \Psi\ d\tau}{\int \Psi^* \Psi\ d\tau} \geq E_0 \tag{2.47}$$

Equality only occurs when the chosen approximate function Ψ is equivalent to the true ground state wavefunction. Ψ is called a trial function and it needs to be varied to obtain the best estimate of E_0 by minimising the variational integral $\int \Psi^* \hat{H} \Psi \, d\tau$ as the lower the integral the better the approximation to E_0.

The variational principle can also be applied to excited states. MacDonald proved that the i^{th} approximate energy level is an upper bound to the i^{th} exact level [103]. For the exact i^{th} energy level E_i, the relationship with the approximate i^{th} level (ϵ_i) is given as following:

$$E_i \leq \epsilon_i(n+1) \leq \epsilon_i(n) \leq \epsilon_{i+1}(n) \tag{2.48}$$

where n represents the number of terms in the expansion of basis function (See eq. 2.40). This shows that we can minimise the approximate level by increasing the number of expansion terms. To obtain the optimal energy level, it is necessary to test the convergence of n. This property of variational calculations is important for spectroscopy as rotationally and vibrationally excited energy levels are required.

2.8 Finite Basis Representation (FBR)

In the eq. (2.40), the wavefunction is expanded as a linear combination of complete, orthonormal basis function. The finite basis representation (FBR) uses a finite series of basis functions to construct a wavefunction to calculate rotation-vibration spectra. The expectation energy (ϵ) of a Hamiltonian ($\hat{H}$) with a wavefunction Ψ is given as:

$$\begin{aligned} \epsilon &= \frac{\langle \Psi \,|\hat{H}|\, \Psi \rangle}{\langle \Psi \mid \Psi \rangle} = \frac{\sum_{m,n} c_m^* \, c_n \, \langle \psi_m |\, \hat{H} \,| \psi_n \rangle}{\sum_{m,n} c_m^* \, c_n \, \langle \psi_m \mid \psi_n \rangle} \\ &= \frac{\sum_{m,n} c_m \, c_n \, H_{mn}}{\sum_{m,n} c_m \, c_n \, S_{mn}} \end{aligned} \tag{2.49}$$

where $H_{mn} = \langle \psi_m \,|\hat{H}|\, \psi_n \rangle$ is a matrix element of the Hamiltonian matrix $\mathbf{H}$ and $S_{mn} = \langle \psi_m \mid \psi_n \rangle$ is the overlap integral. Because ψ is an orthonormal eigenfunction, $S_{mn} = \delta_{mn}$. Notice that c_m^* is changed to c_m in the last line of the equation (2.49) because the wavefunction is assumed to be real.

To minimise ϵ, the expansion coefficient c_i needs to be optimised using the following equa-

tion:

$$\frac{\partial \epsilon}{\partial c_i} = 0 \quad i = 1, 2, ...n. \tag{2.50}$$

Solving the above equation gives:

$$\sum_n \left[(H_{in} - S_{in}\epsilon)\, c_n \right] = 0. \tag{2.51}$$

Because $S_{in} = \delta_{in}$:

$$\begin{aligned} \sum_n H_{in}\, c_n &= \sum_n \epsilon\, c_n \\ \mathbf{H}\,\mathbf{c} &= \epsilon\,\mathbf{c} \end{aligned} \tag{2.52}$$

where $\mathbf{H}$ is a $n \times n$ square matrix and $\mathbf{c}$ is an n dimensional column vector consisting of elements c_i, $i = 1, 2, ..n$. ϵ is eigenvalues of $\mathbf{H}$ and $\mathbf{c}$ is its eigenvector. For each different eigenvalue there exists a different set of expansion coefficients c_i, therefore in order to obtain different eigenvalues simultaneously it is necessary to construct a $n \times n$ square expansion coefficient matrix, $\mathbf{C}$. Such that:

$$\mathbf{HC} = \mathbf{CE} \tag{2.53}$$

Here $\mathbf{E}$ is a diagonal matrix whose diagonal elements are ϵ, the eigenvalues of $\mathbf{H}$. To find the eigenvalues and eigenvectors of $\mathbf{H}$, we can multiply the equation (2.53) by $\mathbf{C}^{-1}$ from left:

$$\mathbf{C}^{-1}\mathbf{HC} = \mathbf{E}. \tag{2.54}$$

This procedure is called matrix diagonalisation. The matrix elements of the Hamiltonian matrix need to be evaluated numerically.

In FBR, the vibrational wavefunction of a triatomic system in the i^{th} state with coordinates (r_1,r_2,θ) can be written as:

$$\Psi_i = \sum_{m,n,j} c^i_{m,n,j}\, \psi_m(r_1)\psi_n(r_2)\psi_j(\theta). \tag{2.55}$$

The basis functions ψ_m, ψ_n, ψ_j are usually described by polynomials. The angular motion ψ_j can be expanded in terms of Legendre polynomials and the radial motions ψ_m, ψ_n are in Laguerre or Harmite polynomials. When polynomials are employed, Gaussian quadrature schemes based on those polynomials are normally used [104]. The matrix elements of the Hamiltonian matrix becomes:

$$H_{i,i'} = \langle \psi_m \psi_n \psi_j \mid \hat{H} \mid \psi_{m'} \psi_{n'} \psi_{j'} \rangle \tag{2.56}$$

where i is a compound index running over the basis functions used. The eq.(2.55) only accounts for the vibrational motion of a molecule hence when calculating rotation-vibration states, appropriate rotational function needs to be included.

FBR is efficient for predicting the low-lying rotation-vibration states. But for high-lying states with high amplitude motion, the number of basis functions needed for convergence increases. This results in the larger Hamiltonian matrix and hence it becomes computationally very expensive and limited. Use of the Discrete variable representation (DVR) is one of the ways to tackle this problem.

2.9 Discrete Variable Representation (DVR)

Discrete variable representation (DVR) was developed by Light and co-workers [60] in the mid 1980s. It uses the transformation matrices (**T**) introduced by Harris *et al.* [61] to transform the FBR Hamiltonian matrix elements into the grid points determined by Gaussian quadrature scheme for each chosen basis function. Dickison and Certain [105] proved that for a basis set of $(j_{max}+1)$ classical orthogonal polynomials, there exists an orthogonal transformation to $(j_{max}+1)$ weighted Gaussian quadrature points. For 3D DVR grid points in (α,β,γ) coordinates, the matrix elements of the DVR Hamiltonian matrix are written as:

$$H^{DVR}_{\alpha,\beta,\gamma,\alpha',\beta',\gamma'} = \sum_{m,n,j} \sum_{m',n',j'} T^{\alpha,\beta,\gamma}_{m,n,j}\, H^{FBR}_{m,m',n,n',j,j'}\, T^{\alpha',\beta',\gamma'}_{m',n',j'} \tag{2.57}$$

where $\mathrm{H}^{FBR}_{m,m',n,n',j,j'} = \langle \psi_m\psi_n\psi_j \mid \hat{H} \mid \psi_{m'}\psi_{n'}\psi_{j'}\rangle = \langle mnj \mid \hat{H} \mid m'n'j'\rangle$ and $T^{\alpha,\beta,\gamma}_{m,n,j}$ are the transformation matrices in (α,β,γ) which in turn expressed as a product of 1D transformation matrices:

$$T^{\alpha,\beta,\gamma}_{m,n,j} = T^{\alpha}_{m} T^{\beta}_{n} T^{\gamma}_{j} \tag{2.58}$$

The 1D transformation matrices are determined by the points, weights and the Gaussian quadrature scheme used for a particular basis function [106]:

$$T^{\tau}_{i} = \sqrt{w_\tau}\, |i(\tau)\rangle \tag{2.59}$$

where $\tau = \alpha,\beta,\gamma$ (points), $|i\rangle = |m\rangle,|n\rangle,|j\rangle$ (basis function) and w_τ is the weights of associated Gaussian quadrature.

In a DVR, the potential energy operator is diagonal due to the quadrature approximation [105, 106] and requires no integration:

$$\sum_{m,n,j}\sum_{m',n',j'} T^{\alpha,\beta,\gamma}_{m,n,j}\, V^{FBR}_{m,m',n,n',j,j'}\, T^{\alpha',\beta',\gamma'}_{m',n',j'} \simeq V^{DVR}_{\alpha,\alpha',\beta,\beta',\gamma,\gamma'}\, \delta_{\alpha\alpha'}\, \delta_{\beta\beta'}\, \delta_{\gamma\gamma'} \tag{2.60}$$

where $V^{FBR}_{m,m',n,n',j,j'} = \langle mnj \mid V(r_1, r_2, \theta) \mid m'n'j' \rangle$, which is not diagonal, and $V^{DVR}_{\alpha,\alpha',\beta,\beta',\gamma,\gamma'} = V(r_{1\alpha}, r_{2\beta}, \theta_\gamma)$ with $r_{1\alpha}, r_{2\beta}, \theta_\gamma$ representing the value of r_1, r_2, θ at the grid point (α, β, γ).

Because of the transformation DVR is not strictly variational as opposed to FBR, but it often behaves variationally [107]. DVR and FBR are isomorphic therefore it is possible to switch between a DVR and a FBR. This allows us to choose the best representation for the required task.

2.10 The DVR3D program suite

The DVR3D program suite was developed by Tennyson and co-workers [108] at UCL after updating the FBR based program suite called TRIATOM [109–111]. The first version of the DVR3D suite was published in 1995 [108] and the revised version is in press at the time of writing [59]. The program calculates rotation-vibration spectra of triatomic molecules by solving the nuclear motion problems using the DVR methods. It employs so called "two-step procedure" by Tennyson and Sutcliffe [112], which splits the calculations into two steps: Coriolis de-coupled and Coriolis coupled problems, to obtain the full rotation-vibration behaviour. The first step is to calculate the Coriolis de-coupled vibrational wavefunctions using the DVR3DRJZ module. The calculated vibrational wavefunctions are stored and used in the second step by the ROTLEV module which couples the vibrational wavefunctions with Coriolis force and calculates the full rotation-vibration wavefunctions. With the full wavefunctions, transition strengths and spectra can be calculated using DIPOLE3 and SPECTRA respectively.

2.10.1 Basis Functions

It is important to choose the optimal basis functions to obtain a good convergence in variational calculations. For water, the Morse oscillator-like functions defined by Tennyson and

Sutcliffe [88] are selected for the radial basis functions:

$$|t\rangle = H_t(r) = \beta^{\frac{1}{2}}\, N_{t\alpha}\, exp\,(-\frac{y}{2})\, y^{\frac{\alpha+1}{2}}\, L_t^{\alpha}(y) \tag{2.61}$$

$$y = A\, exp\,[-\beta(r - r_e)] \tag{2.62}$$

where

$$A = \frac{4D_e}{\nu_e}, \quad \beta = \nu_e\sqrt{\frac{\mu}{2D_e}}, \quad \alpha = \text{integer (A)}. \tag{2.63}$$

$N_{t\alpha}L_t^{\alpha}(y)$ is the normalised associated Laguerre polynomials, μ is the reduced mass and integer (A) rounds the value of A towards 0, for example 1.3 and 1.7 are both rounded to 1. The parameters r_e, ν_e and D_e can be associated with the equilibrium separation, the fundamental wavenumber and the dissociation energy of the relevant coordinate respectively. These parameters are in practice treated as a variational parameters and needed to be optimised to achieve the best convergence. The following values optimised by Fulton [113] are used in this thesis for the calculation of water linelists: $r_e = 2.55\, a_0$ (Bohr radius = $5.29177249(24) \times 10^{-11}$ m), $\nu_e = 0.25E_h$ (Hartree = $4.3597482(26) \times 10^{-18}$ J) and $D_e = 0.007E_h$. Note that the optimal value of r_e is usually larger than the known equilibrium bondlength.

For the angular basis functions, the normalised associated Legendre Polynomial with the Condon and Shortly [114] phase conventions can be used:

$$|j,k\rangle = \Theta_{j,k}\,(\theta). \tag{2.64}$$

2.10.2 DVR3DRJZ

DVR3DRJZ calculates the first step of the two-step procedure. The module allows users to choose Jacobi (scattering) or Radau coordinates depending on the molecule of interest. Usually Radau coordinate is chosen for the water calculation.

The first part of the calculation is to construct a kinetic energy matrix at DVR points with chosen basis functions. When the problem is purely vibrational, i.e. the total angular momentum $J = 0$, only the Coriolis de-coupled Hamiltonian, $\langle mnj|\ \hat{H}^{J=0}\ |m'n'j'\rangle$, needs to be considered. For $J > 0$, the projection of J along the body-fixed z-axis, k, is introduced. k is an integer that takes $0, 1, ...J$ and is assumed to be a good quantum number. Extra k dependent matrix elements need to be added to the Coriolis de-coupled Hamiltonian in the case of $J > 0$. Detailed explanation can be found in reference [59].

The second part of the calculation is diagonalisation and truncation of the DVR Hamiltonian matrix. First, a series of 2D Hamiltonians are diagonalised, giving the 2D eigenvalues and eigenvectors. The eigenvalues which are lower than a specified cut-off wavenumber are selected to solve the 3D Hamiltonian. This leads to a truncation of 3D Hamiltonian as only a limited number of states needs to be considered. The 3D Hamiltonian matrix is then diagonalised to obtain the full 3D eigenvalues and wavefunctions. Those are stored for the second step calculation by a ROTLEV. The order of solution can be chosen appropriately by users. For water calculations in Radau coordinate, the order of radial → angular is chosen. The successive diagonalisation and truncation nature of DVR3DRJZ allows the final 3D Hamiltonian matrix to contain a very high amount of information with a compact representation.

2.10.3 ROTLEV3B

The second step of the two-step procedure is performed by one of the ROTLEV modules. There are three ROTLEV modules, ROTLEV3 for a standard embedding, ROTLEV3B for a bisector embedding and ROTLEV3Z for a perpendicular embedding. Only ROTLEV3B will be discussed in this section as this was the one used for the water calculations.

ROTLEV3B uses DVR points for all three coordinates. It first selects the lowest N energy solutions of DVR3DRJZ as a basis to solve the full rotation-vibration problem. N is user supplied as IBASS in the input card. The Hamiltonian matrix is very sparse with most of the off-diagonal elements being zero. ROTLEV3B only calculates the diagonal, $k \pm 1$ and $k \pm 2$ elements and stores them. Diagonalisation is performed either in core or iteratively. In water calculation, core diagonalisation was selected. The full rotation-vibration wavefunctions are stored for transition strengths calculations by DIPOLE3.

2.10.4 DIPOLE3

DIPOLE3 calculates transition strengths using the algorithm developed by Tennyson *et al.* [59]. For a transition between an initial state i and a final state f, the transition strength $S(f-i)$ is given by [59]:

$$S(f-i) = \sum_{M'M''\tau} |\langle J'_{M'}\ p'\ l'|\mu^s_\tau|J''_{M''}\ p''\ l''\rangle|^2 \qquad (2.65)$$

where μ_τ^s is the τ component of the space-fixed dipole moment and $|J''_{M''}\ p''\ l''\rangle$ is the l^{th} eigenfunction with angular momentum J and rotational parity p. Transition strengths $S(f-i)$ are given in Debye^2 molecule^{-1} in this module but can be converted to SI unit (C^2·m^2 molecule^{-1}) using the conversion factor, 1 Debye = 3.335×10^{-30} C·m.

The algorithm treats the radial coordinates in DVR. Since the angular coordinate in DVR depends on k, it is first transformed to a k dependent FBR then transformed back into a k independent DVR based on $k = 0$. The number of Gauss-Legendre points required are slightly more than DVR points used to obtain the full wavefunctions [59]. A general form of the transition dipole integral by this algorithm is:

$$\sum_I \psi_i(I)\ \mu(I)\ \psi_f(I) \tag{2.66}$$

where I runs over integration points. The full derivation of transition strength expression can be found in the reference [59].

2.10.5 SPECTRA

SPECTRA creates a spectrum from the transition strengths calculated by DIPOLE3. With user supplied temperature (T), it converts the transition strengths into wavenumber dependent relative intensities and absolute intensities in cm molecule^{-1} (HITRAN unit). The absolute intensities are calculated as a function of wavenumber ν using the formula [59]:

$$I(\nu_{if}) = \frac{A\,\nu_i g_i\,[exp(-\frac{\mathrm{E''}}{k/hc\,T}) - exp(-\frac{\mathrm{E'}}{k/hc\,T})]}{Q(T)}\,S(f-i) \tag{2.67}$$

where A is a conversion factor, $A = 4.162034 \times 10^{-19}$ cm^2 Debye^{-2}), which converts transition strength $S(f-i)$ in Debye^{2}molecule^{-1} into absolute intensity in cmmolecule^{-1}. ν is a transition wavenumber (in cm^{-1}), $Q(T)$ is a partition function, E$'$ is upper state energy, E$''$ is lower state energy (both in cm^{-1}) and g_i is the degeneracy factor depending on the spin statistics. For water, *ortho* state is three times more likely than *para* state so $g_i = 3$ for ortho and $g_i = 1$ for para states. k/hc is the Boltzmann constant, $k/hc = 0.6950356(12)\mathrm{cm}^{-1}\ K^{-1}$. SPECTRA also calculates the partition function if required.

Table 2.7: Summary of spectroscopically determined (purely empirical and semi-empirical) PES for $H_2{}^{16}O$. σ_{vib} shows the standard deviation. No. of vib levels is the number of vibrational levels used for the fit. Max. energy is the maximum energy of the fitted vibrational levels in cm^{-1}.

Reference	Year	σ_{vib} (cm^{-1})	No. vib levels	Max. energy
Hoy, Mills and Strey [115]	1972	214.0	25	13000
Carter and Handy [116]	1987	2.42	25	13000
Halonen and Carrington [117]	1988	5.35	54	18000
Jensen [118]	1989	3.22	55	18000
Polyansky *et al.* [119]	1994	0.60	40	18000
Polyansky *et al.* [65]	1996	0.94	63	25000
Partridge and Schwenke [42]	1997	0.33	42	18000
Shirin *et al.* [66]	2003	0.10	105	25000

2.11 Potential Energy Surface (PES)

When the BO approximation is assumed, the nuclear and electronic motion problems are solved separately, as discussed in the earlier part of this chapter. The solutions to the electronic motion problem at fixed nuclear geometries form a potential energy surface (PES), which is independent of nuclear masses.

An accurate PES is essential for a high accuracy rotation-vibration spectra calculation. There are three types of PES available: empirical, *ab initio* and semi-empirical. An empirical PES can be obtained by the iterative fitting of the parameters in a potential function, solving for the nuclear motion, comparing to the experimental data and then correcting the potential parameters. An *ab initio* PES is derived by solving for the electronic motion on *ab initio* grid points with a particular value of the two bond lengths and the bond angle. A semi-empirical PES is an *ab initio* surface with small empirical adjustments, and for water it is the most accurate of three. Table 2.7 shows the summary of spectroscopically determined (purely empirical and semi-empirical) PES for $H_2{}^{16}O$.

Polyansky *et al.* [119] calculated an empirical PES which gives a standard deviation of 0.36 cm^{-1} for the levels $J \leq 14$. This surface was later improved by including additional potential terms and using more experimental data [65]. This new surface gives a standard deviation of 0.25 cm^{-1}. Although the empirical surfaces give considerably smaller errors than *ab initio*

PESs, they do not give energy level extrapolation beyond the range of observations [42].

In 1997, Partridge and Schwenke [42] (PS) calculated an *ab initio* PES using the cc-pV5Z basis sets – the correlation consistent polarised valence basis sets of Dunning [120], augmented with diffuse s, p, d functions on oxygen and s, p on hydrogen. The multireference configuration interaction (MRCI) approach was employed for the calculation.

PS proposed the *ab initio* PES in the analytical form:

$$V^{ai} = V^{5Z} + \Delta V^{core} \tag{2.68}$$

with

$$V^{5Z}(r_1, r_2, \theta) = V^a(r_1) + V^a(r_2) + V^b(r_{\mathrm{HH}}) + V^c(r_1, r_2, \theta) \tag{2.69}$$

where r_i are the OH bond lengths, θ is the HOH angle, r_{HH} is the distance between the two hydrogen atoms and

$$V^a(r) = D\,[exp(-2a(r - r_0))] - 2D[exp(-a(r - r_0))] \tag{2.70}$$

$$V^b(r) = Aexp(-br) \tag{2.71}$$

$$V^c = c_{000} + exp(-\beta[(r_1 - r_e)^2 + (r_2 - r_e)^2]) \times \sum_{ijk} c_{ijk} \left(\frac{r_1 - r_e}{r_e}\right)^i \left(\frac{r_2 - r_e}{r_e}\right)^j (\cos\theta - \cos\theta_e)^k \tag{2.72}$$

D, a, r_o, A, b and c_{ijk} are determined by an unequally weighed least square fitting to the *ab initio* data, β is fixed at $2a_o^{-2}$ to give fast enough damping and r_e and θ_e are the estimated equilibrium geometry. Fits were made to 355 data points with $i + j \leq 8$ and $k \leq 14 - (i + j)$ to yield 245 different parameters, c_{ijk}. V^{core} is the core-valence correlation term and has the same form as V^c with $i + j + k \leq 6$ for 50 c_{ijk}, fitted to 370 points. The PS *ab initio* surface typically gives a standard deviation of a few cm^{-1} (< 10 cm^{-1}) for water, which is actually significantly worse than the purely empirical surfaces of Polyansky *et al.* [65, 119].

Recently, Polyansky and co-workers [121] published a significantly more accurate *ab initio* PES. They performed a series of calculation using Dunning's [120] aug-cc-pVnZ basis set with n = 3, 4, 5 and 6, where n is the number of basis functions used per physical atomic orbital. For each basis set, 346 points below 30000 cm^{-1} were calculated using the MRCI approach. The extrapolation of the surface to the complete basis set (CBS) was employed to compensate the slow convergence of energies with respect to n. The results showed MRCI calculation to the

CBS limit with the added corrections of core correlation, relativistic, Lamb shift, BODC and non-adiabatic corrections (where applicable), are indeed more accurate than the PS *ab initio* surface.

Partridge and Schwenke [42] also developed a semi-empirical PES which attempts to include the corrections to *ab initio* PES empirically. This semi-empirical PES revolutionised the accuracy of water calculation, giving a typical error less than 0.05 cm^{-1}. Their semi-empirical PES takes the form:

$$\begin{aligned} V^{emp}(r_1,r_2,\theta) &= c^{5Z}V^{5z}(r_1,r_2,\theta) + c^{core}\Delta V^{core}(r_1,r_2,\theta) \\ &+ c^{basis}\Delta V^{basis}(r_1,r_2,\theta) + \Delta V^{rest}(r_1,r_2,\theta) \end{aligned} \tag{2.73}$$

where V^{basis} is the effect of a further basis set enlargement and ΔV^{rest} is the same as V^c in eq. (2.72). The parameters $c^{5Z}, c^{core}, c^{basis}$ and c_{ijk} are determined by fitting to the lines in HITRAN92 with $J \leq 5$.

In 2003, Shirin and co-workers published a new semi-empirical PES [66] which is more accurate than the one by PS. They used the PS *ab initio* potential as a starting point and augmented it with relativistic correction, adiabatic and non-adiabatic corrections and one-electron Lamb shift. The potential was then fitted using the energy levels published by Tennyson *et al.* [95] up to 25000 cm^{-1}. The PES has the general form:

$$V^{emp}(r_1,r_2,\theta) = f^{morp}(r_1,r_2,\theta)V^{ai}(r_1,r_2,\theta) + \Delta V_B(\theta) \tag{2.74}$$

where f^{morp} is a morphing function and the parameters are determined by fitting to the experimental data:

$$\begin{aligned} f^{morp} &= c_{000} + \sum_{ijk} c_{ijk}\, s_1^i s_2^j s_3^k, \\ s_1 &= \frac{r_1 + r_2}{2} - r_e \\ s_2 &= \cos\theta - \cos\theta_e \\ s_3 &= \frac{r_1 - r_2}{2}. \end{aligned} \tag{2.75}$$

$\Delta V_B(\theta)$ is a correction term to the relativistic effects to overcome the problem with the bending

coordinate [102]:

$$\begin{aligned} \Delta V_B(\theta) &= F\,(\frac{\theta^3-\theta_e^3}{\theta_e^3-\pi^3}) + G\,(\frac{\theta^5-\theta_e^5}{\theta_e^5-\pi^5}) \\ &+ (\Delta B + F + G)\,(\frac{\theta^2-\theta_e^2}{\theta_e^2-\pi^2}) \end{aligned} \tag{2.76}$$

where $F = 879.7\ \mathrm{cm}^{-1}$, $G = -381.1\ \mathrm{cm}^{-1}$and $\Delta B = -87.5\ \mathrm{cm}^{-1}$, which gives the change in the height of the barrier to linearity.

Shirin *et al.* made two fits to the experimental data, fits A and B. Fit A uses the midpoint of nuclear and atomic masses [68] for the effective rotational mass whereas fit B uses nuclear masses. The treatment of non-adiabatic corrections included in the nuclear motion Hamiltonian is also different in fit A and B, and the details can be found in reference [66].

For fit A, the semi-empirical PES is:

$$V^A = V^{5Z} + \Delta V^{core} + \Delta V_1^{rel} + \Delta V_2^{rel} + \Delta V^{ad} \tag{2.77}$$

For fit B is:

$$V^B = V^{5Z} + \Delta V^{core} + \Delta V_1^{rel} + \Delta V_2^{rel} + \Delta V^{ad} + \Delta V^{lamb} \tag{2.78}$$

where ΔV^{ad} is the adiabatic correction, ΔV^{lamb} is the one-electron Lamb shift correction and ΔV_1^{rel} and ΔV_2^{rel} are the first-order and the second-order electronic relativistic corrections, respectively.

The PS is very good at predicting low and intermediate wavenumber regions but gives rather poor results in the high wavenumber region due to lack of fit to high lying levels. The PES by Shirin *et al.* was fitted using a very extensive set of energy levels, with the highest energy fitted being 25000 cm^{-1}. This allows the PES to be accurate in the region where PS breaks down. Both surfaces are used for the spectral analysis presented in the later chapters.

2.12 Dipole Moment Surface (DMS)

To calculate the transition strengths with DIPOLE3 module, we need a dipole moment surface (DMS). Water has a permanent dipole along the B axis, see Figure 2.5, and this largely determines the strengths of vibrational and rotational transitions. The strengths of rotational

transitions depend on the size of the permanent dipole moment whereas the strengths of the vibrational transitions depend on the changes in the dipole moment. Interestingly, it was shown by Lynas-Gray *et al.* [80] that an *ab initio* DMS gives smaller errors in calculated intensities than an empirically determined DMS. For this reason, the *ab initio* surfaces are usually used for the calculations of water.

Currently, the best DMS is by Schwenke and Partridge (SP) [122] which is the revised version of their earlier work [42]. The problem with the previous version is that the transition strengths of the bending modes are always overestimated, although stretching modes are more accurate. This is largely due to an insufficient number of angular grid points in the *ab initio* surface. Also, the surface does not return a zero dipole moment for water dissociation.

The analytical presentation of the new DMS by Schwenke and Partridge is given as [122]:

$$\mu(r_1, r_2, \theta) = q(r_1, r_2, \theta)(\mathbf{x}_{H_1} - \mathbf{x}_O) + q(r_2, r_1, \theta)(\mathbf{x}_{H_2} - \mathbf{x}_O) \tag{2.79}$$

with

$$\begin{aligned} q(r_1, r_2, \theta) &= \exp\left(-\beta[r_1 - r_e]^2\right) \left[\sum_{i=0}^{n_r} c_i \left[\frac{r_1 - r_e}{r_e}\right]^i \right. \\ &+ \exp\left(-\beta[r_2 - r_e]^2\right) \sum_{ijk} c_{ijk} \left[\frac{r_1 - r_e}{r_e}\right]^i \\ &\times \left. \left[\frac{r_2 - r_e}{r_e}\right]^j \left[\cos(\theta) - \cos(\theta_e)\right]^k \right] \end{aligned} \tag{2.80}$$

where $\mathbf{x}_H$ and $\mathbf{x}_O$ are the position vectors of the atoms in Radau coordinates and q is an effective charge obtained as a scaler function in eq. (2.80). The parameters c_i and c_{ijk} are determined by a weighted linear least squares fit to the *ab initio* DMS points for $i + j \leq n_r, j + k > 0, k \leq n_\theta - i - j$ and β is set to $2a_0^{-2}$.

For the water calculations presented in this thesis, we used the *ab initio* DMS points computed by Polyansky *et al.* [121] fitted by Lynas-Gray (unpublished, PLG below), which was believed to be the best *ab initio* DMS available at the time of calculation. This DMS was calculated using Dunning's [120] aug-cc-pV6Z basis set but with fewer *ab initio* points than PS [42] and SP [122] to achieve higher accuracy. The relativistic and core valence effects were also tested, but they found to cancel each other out perfectly. However, this surface was later found to be less accurate than SP. The problem is due to the overestimation of the bending

mode strengths due to the artificial "wiggles" in the surface caused by the lack of sufficient angular *ab initio* points for fitting. The same problem was observed in the PS surface but was later corrected in SP by generating a lot of extra artificial points which were used in the fits. The unreliability of PLG surface only became apparent after calculation of the water linelists was complete, therefore the intensities calculated in this thesis are unfortunately not as accurate as we would like, especially for the bending modes. Over the course of writing this thesis, a mistake in the implementation of DMS within the DIPOLE3 codes – the dipole components were not rotated according to the coordinate system used in the calculation, which also led to unreliable intensities – was corrected by researchers at UCL (private communication).

Chapter 3

Spectroscopy

Spectroscopy is the analysis of emitted or absorbed radiation by atoms and molecules. It can be used to determine their identity, structure and physical environment. The radiation recorded is called spectrum and consists of frequency and energy distribution.

Fraunhofer measured the Sun's spectrum in the early 19th century but its full significance was not recognised until the mid 19th century when Kirchhoff and Bunsen confirmed the link between particular wavelengths and atoms. A few elements were since discovered by spectroscopy, including Helium. But it was the introduction of quantum mechanics in the 20th century that dramatically stretched the potential of spectroscopy. Analysis of spectra provides very rich information of atomic and molecular species. Today, it is widely used in many fields of science including chemistry, medicine and astrophysics. In this chapter, two absorption spectroscopic techniques: Fourier transform spectroscopy and cavity ring-down spectroscopy will be discussed.

3.1 Fourier Transform Spectroscopy (FTS)

Fourier transform spectroscopy is one of the most widely used techniques for analysing atoms and molecules. It uses the Michelson interferometer to record an interferogram, which itself does not give direct spectral information but produces a spectrum when Fourier transformed. Fourier transformed spectrometer is a multiplex spectrometer and it measures the intensities of all the wavelengths simultaneously with a single detector. Figure 3.1 shows a schematic setup

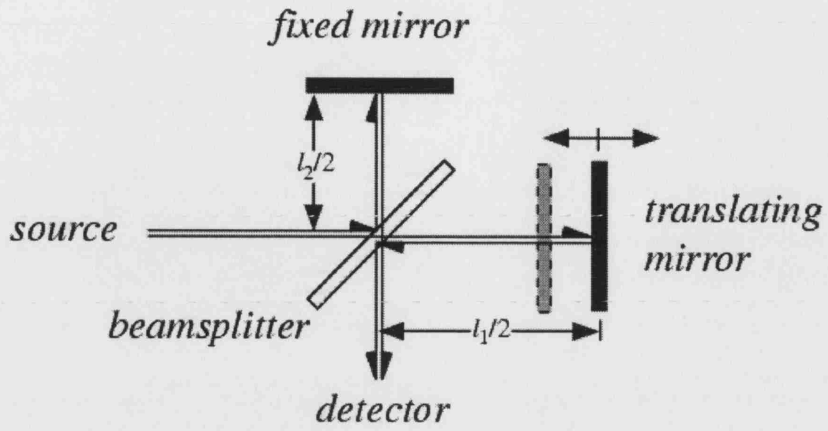

Figure 3.1: The schematic diagram of a Michelson interferometer. The figure was taken from the website "Eric Weisstein's World of Physics" (http://scienceworld.wolfram.com/physics/FourierTransformSpectrometer.html).

of the Michelson interferometer.

The light from the source reaching a beamsplitter is split into two equal beams. One beam is reflected back by a fixed mirror and the other by a movable, translating mirror. Two beams are recombined at the beamsplitter and will form an image on a detector. The path difference of two beams is constantly changed by moving the mirror. When the path difference is equal to an integral number of wavelengths, $n\lambda$, constructive interference occurs and when it is equal to $1/2\ n\lambda$ with odd integer n, destructive interference occurs. The intensity of light reaching the detector (called the interferogram) will vary continuously according to the path difference. The interferogram contains the encoded information of the spectrum, which can be retrieved by digitally decoding the interferogram with a computer. In the following sections, descriptions of FTS will be presented and full details can be found in the references [123–127].

3.1.1 Principles of Fourier Transform Spectroscopy

Consider two coherent monochromatic beams with amplitude A_1 and A_2 recombined at the beamsplitter. The amplitude of light reaching the detector is simply the superposition of two amplitudes:

$$A = A_1 + A_2\, e^{i(2\pi\nu x)} \tag{3.1}$$

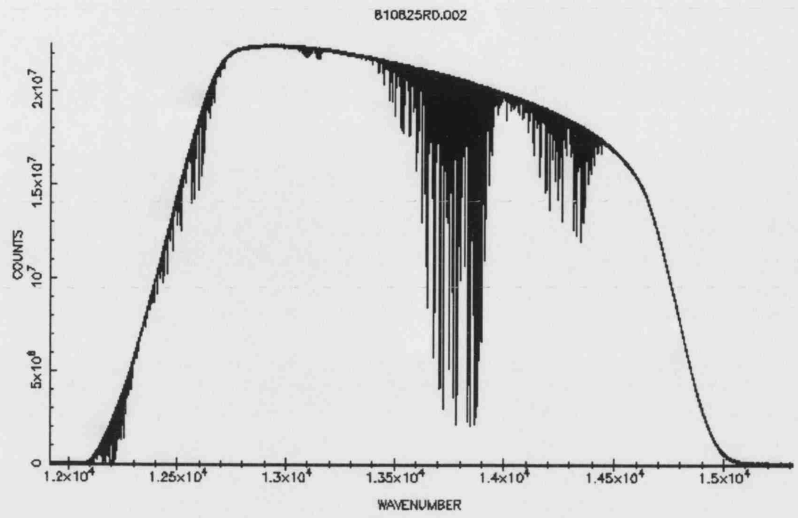

Figure 3.2: The image of a FTS absorption spectrum of $H_2{}^{18}O$ taken from the National Solar Observatory digital library (http://diglib.nso.edu), copyright NOAO/AURA/NSF. The filename 810825R0.002., containing the spectrum of $H_2{}^{18}O$ from 12900 to 14700 cm^{-1} recorded by Camy-Peyret.

where ν is a wavenumber defined by $\nu = 1/\lambda$ measured in cm^{-1} and x is a path difference. The intensity of the interferogram is obtained by multiplying the amplitude by its conjugate, such that:

$$\begin{aligned} I_\nu(\mathrm{x}) = AA^* &= (A_1 + A_2\, e^{i(2\pi\nu \mathrm{x})})(A_1 + A_2\, e^{-i(2\pi\nu \mathrm{x})}) \\ &= A_1^2 + A_2^2 + 2A_1A_2\, \cos(2\pi\nu \mathrm{x}) \\ &= B(\nu)\,(1 + cos(2\pi\nu \mathrm{x})) \end{aligned} \tag{3.2}$$

where $B(\nu)$ is the incident beam intensity, $B(\nu) = A_1^2 = A_2^2$, since $A_1 = A_2$.

The frequency of the light reaching the detector (f in Hz) depends on the rate of change of the path difference (v in $cm{\cdot}s^{-1}$), which is twice the mirror speed and the wavenumber of the light at the source (ν in cm^{-1}):

$$f = \nu v. \tag{3.3}$$

The interferometer acts as a frequency transducer which converts the high speed optical frequencies into the slower audio frequencies, more suitable for detectors.

When the light source contains more than one wavenumber, the superposition of cosines

are observed:

$$\begin{aligned} I_0(\mathrm{x}) &= \int_0^\infty B(\nu)\,(1+\cos(2\pi\nu\mathrm{x}))d\nu \\ &= \bar{I} + \int_0^\infty B(\nu)\cos(2\pi\nu\mathrm{x})d\nu \end{aligned} \tag{3.4}$$

where $\bar{I}$ is the mean value of the interferogram without any modulation. The spectral information is only contained in the second term so we can express the intensity as:

$$I(\mathrm{x}) = I_0(\mathrm{x}) - \bar{I} = \int_0^\infty B(\nu)\cos(2\pi\nu\mathrm{x})d\nu \tag{3.5}$$

The spectral distribution $B(\nu)$ can be recovered by the inverse cosine transform of $I(\mathrm{x})$. The Fourier transform pair is:

$$I(\mathrm{x}) = \int_0^\infty B(\nu)\cos(2\pi\nu\mathrm{x})d\nu \tag{3.6}$$

$$B(\nu) = \int_0^\infty I(\mathrm{x})\cos(2\pi\nu\mathrm{x})d\mathrm{x} \tag{3.7}$$

Mathematically, the eq. (3.7) produces a mirror image of $B(\nu)$ at negative wavenumbers since $\cos(2\pi\nu\mathrm{x}) = cos(-2\pi\nu\mathrm{x})$. The negative wavenumbers are physically unreal but the concept allows the interferogram and the spectrum to be symmetrical. Now to define a symmetric spectral function B^{sym}:

$$B^{sym}(\nu) = \frac{1}{2}[B(\nu) + B(-\nu)] \tag{3.8}$$

The integration limits of the Fourier pair are changed to $-\infty$ to $+\infty$.

$$I(\mathrm{x}) = \int_{-\infty}^\infty B(\nu)\cos(2\pi\nu\mathrm{x})d\nu \tag{3.9}$$

$$B^{sym}(\nu) = \int_{-\infty}^\infty I(\mathrm{x})\cos(2\pi\nu\mathrm{x})d\mathrm{x} \tag{3.10}$$

The experimental interferogram is never symmetric about 0, therefore the sine components also need to be considered by using the complex FT pair rather than the cosine FT pair. Such that:

$$I(\mathrm{x}) = \int_{-\infty}^\infty B(\nu)\, e^{i2\pi\nu\mathrm{x}}\, d\nu \tag{3.11}$$

$$B^{sym}(\nu) = \int_{-\infty}^\infty I(\mathrm{x})\, e^{-i2\pi\nu\mathrm{x}}\, d\mathrm{x} \tag{3.12}$$

When a dichromatic source is used, the two wavenumbers are independently modulated and Fourier transform spectrometer detects the sum of interference patterns. Its interferogram shows the distinctive "beating" patterns. In the case of a polychromatic source, Fourier transform spectrometer records the superposition of the weighted signals according to the intensity at its given wavenumber. The far extremes of the interferogram contain the high-resolution information whereas the central portion contains the low-resolution information [123].

3.1.2 Practical FTS

In the previous subsection, the theory of ideal FTS is described. In reality, there are many practical limitations affecting the quality of spectrum. In this subsection, some of the important effects will be discussed.

In the non-ideal world, the path difference is always finite. The effect of the finite path difference convolutes the spectrum with the sinc function, which is called the instrument function. The siderobes or *feet* of the sinc function is called "ringing", which shows the unphysical negative intensities generated mathematically. When the path difference is varied between $-$L and L, the sinc function has the first zero crossing at $(\nu - \nu_0) = \pm\ 1\ /\ 2\,\mathrm{L}$, where ν_0 is the wavenumber of a monochromatic light source. This value defines the resolution of the instrument (in cm^{-1}):

$$\delta\nu = \frac{1}{2L}. \tag{3.13}$$

The full width at half maximum (FWHM) of the sinc function is 1.207 $\delta\nu$ [123]. It is obvious that higher resolution is obtained with longer path difference L.

The ringing caused by the instrument function needs to be removed or at least reduced as it can cause problems with identifying the weak lines. One method to use is apodisation, literally meaning "cutting the feet off". *Apodisation* is a strategy to suppress the ringing by multiplying the interferogram with a certain function. The use of apodisation needs to be careful because it not only eliminates the ringing but also reduces the resolution and degrades the spectrum. The detailed description of apodisation can be found in the reference [127]. J. Brault [128] suggests the use of "self-apodisation" , where the resolution of instrument ($\delta\nu$) is lower by about a factor of 3 than the FWHM of the physical line shape. When this condition is satisfied, the effect of the instrument function is considered negligible.

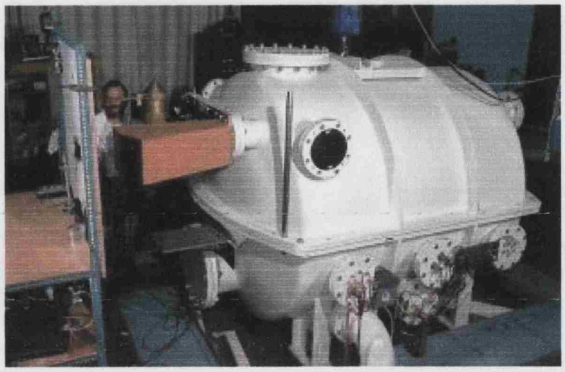

Figure 3.3: The Fourier transform spectrometer vacuum tank at Kitt Peak. The image has been taken from the National Optical Astronomy Observatories website (http://www.noao.edu). Copyright Tom Eglin, Mark Hanna, NOAO/AURA/NSF.

Another effect to be considered is the replication of the spectrum caused by discrete sampling. Although the output from the detector is continuous, the interferogram is sampled with discrete intervals. This results in the replication of the positive and negative images of the true spectrum at certain intervals. The replication is also known as aliasing. The replicas are indistinguishable from the true spectrum therefore a careful treatment is required.

For this thesis, we analysed the spectra of water isotopologues recorded using the McMath-Pierce Fourier transform spectrometer at Kitt PeaK, National Solar Observatory (Arizona, USA). This Fourier transform spectrometer consists of a folded Michelson interferometer contained in the vacuum tank. Figure 3.3 shows the Fourier transform spectrometer vacuum tank at Kitt Peak. It has a maximum path difference of 1 metre and a maximum resolution element of 0.010 cm^{-1}. The spectrum range of 550 to 45 000 cm^{-1} can be measured with a typical wavenumber accuracy of 10^{-3} to 10^{-4} cm^{-1}. The optical arrangement of the Fourier transform spectrometer is shown in Figure 3.4. The absorption spectrum can be recorded using a 6-metre multipass White-type absorption cell, which is capable of creating a pathlength up to 432 metres. Experimental conditions of the water vapour spectra analysed in this thesis can be found in Chapter 6.

The spectrum of natural abundance pure water, recorded using the Fourier transform spectrometer at the Rutherford Appelton Laboratory (RAL) Molecular Spectroscopy Facility (U.K.) [21], was used for identifying the $H_2{}^{16}O$ lines in the isotopically enhanced water spectra recorded at Kitt Peak. The Bruker IFS 120HR Fourier transform spectrometer used at RAL can achieve

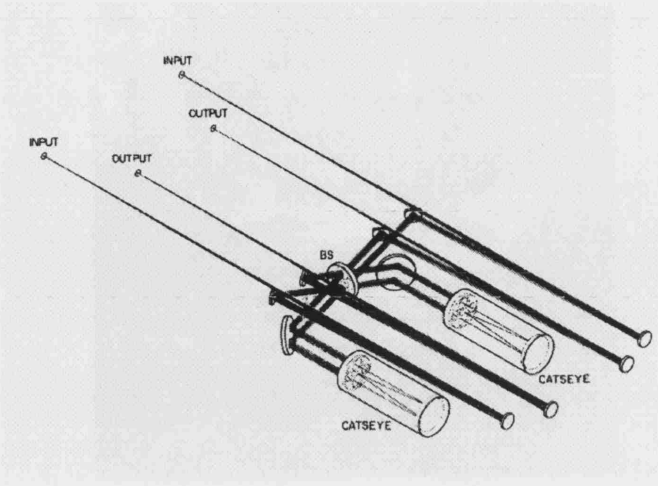

Figure 3.4: The optical arrangement of McMath-Pierce Fourier transform spectrometer at Kitt Peak, National Solar Observatory. The image has been take from the Kitt Peak website (http://nsokp.nso.edu/mp/fts/aboutFTS.html).

a maximum resolution of up to 0.0015 cm^{-1} [129]. The instrument covers the wide spectral range, from far infrared to UV. Figure 3.5 shows a picture of the instrument.

3.2 Cavity Ring-Down Spectroscopy

Cavity ring-down spectroscopy (CRDS) is a relatively new experimental technique which uses a tunable laser and highly reflective mirrors to measure absorption features of samples. It was first introduced in 1988 by O'Keefe and Deacon [130] using a pulsed, tunable laser, which is now known as a "generic" CRDS setup. The technique can be applied to a variety of projects including atmospheric chemistry, molecular spectroscopy and reaction kinetics [131]. CRDS exhibits very high sensitivity partly due to the extremely long path created by the highly reflective mirrors. Absorptions as weak as 10^{-9} cm^{-1} can be detected with a generic CRDS [132].

In a generic CRDS setup, two highly reflective mirrors (reflectivity $\mathcal{R}$ >99.9%) are placed at each end of an empty cavity. The laser pulse entering into the cavity is stored for microseconds and during this time makes thousands of round trips between the mirrors. After each round trip, a small part of the incident pulse is transmitted through a mirror with the rate determined by the reflectivity of the mirrors. The intensity of transmitted light decays exponentially

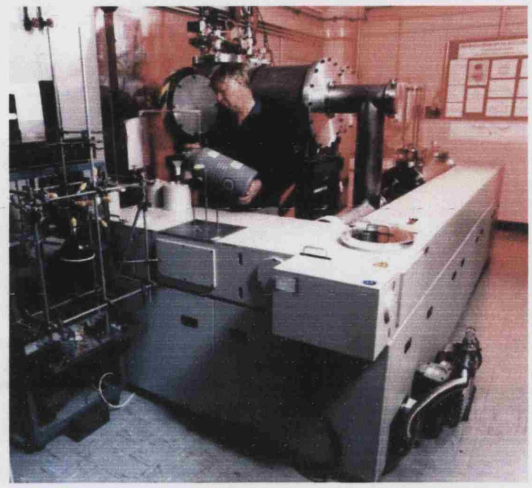

Figure 3.5: The picture of the Bruker IFS 120HR Fourier transform spectrometer at RAL. The image was taken from the RAL Molecular Spectroscopy Facility website (http://www.msf.rl.ac.uk).

and the decay time is called the ring-down time, τ. When a sample is placed in the cavity, the decay time will be reduced due to absorption. By recording the variations in inverse of τ as a function of the incident light wavenumber, it is possible to obtain absorption spectra of a sample. In the following sections, the basic principles of CRDS will be discussed in details.

3.2.1 Principles of Cavity Ring-Down Spectroscopy

Consider a sample with pathlength l and concentration of absorber C, irradiated by light with intensity I_0. The transmitted light intensity, I, can be described by the Beer-Lambert law:

$$I = I_0 \exp\left[-\sigma C l\right] \tag{3.14}$$

where σ is the absorption cross-section of the sample at the particular wavelength of the light. Absorption coefficient α is the product of σ and C and absorbance is the product of σ, C and l. Traditionally, absorption spectroscopy measured the ratios of incident light intensity (I_0) and transmitted light intensity (I) to obtained absorption coefficients because:

$$\alpha = -\frac{1}{l}\left[\ln \frac{I}{I_0}\right] \tag{3.15}$$

This method requires measurements of a very small change in a large intensity fluctuation over time which leads to inaccurate results.

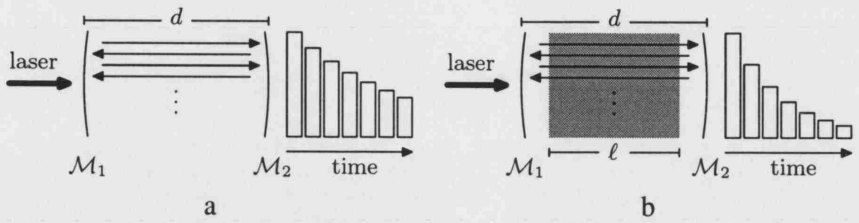

Figure 3.6: The principles of cavity ring-down spectroscopy. It shows the intensity of light decaying in an empty cavity (a) and a cavity filled with an absorber (b). The decay rate for the empty cavity depends solely on the reflectivities of mirrors whereas for the filled cavity it depends on both the mirrors and the absorption in the gas. The figure was provided by M. Sneep (private communication).

The CRDS uses the same principle but with a different approach. In the CRDS experiments, the absorption is determined from the rate of decay of the light leaking out from a cavity. The advantage of this approach is that the result is less sensitive to variations in the laser pulse intensity. For a cavity consisting of two mirrors of reflectivity $\mathcal{R}$, separated by distance l, the ring-down time τ is 2Nl/c, where c is the speed of light and N is the number of round trips made before the light decays to 1 / e of its original intensity. N can be obtained by solving the equation $\mathcal{R}^{2N}$ = 1 / e . From these two relationships, we get:

$$\tau = \frac{l}{\mathrm{c}} \mid \ln \mathcal{R} \mid. \tag{3.16}$$

The light intensity escaping from the cavity decreases exponentially with time:

$$I(t) = I_0 \ \exp\ [-\frac{t}{\tau}] = I_0 \ \exp\ [-\beta t] \tag{3.17}$$

where $\beta = 1/\tau$ is the rate of decay of an empty cavity.

When a sample is placed inside the empty cavity, some light will be absorbed depending on the wavelength. When absorption takes place, the loss of light intensity speeds up, resulting in shorter ring-down time. The light intensity decay is still exponential if the absorption obeys the Beer-Lambert Law:

$$I(t) = I_0 \ \exp\ [-\beta t - \alpha c t] \tag{3.18}$$

α is usually expressed in cm^{-1} and the product of c and t is the effective pathlength for which absorption is measured. The decay rate is now changed to $\beta' = \beta + c\alpha$. If we know the rate of decay of an empty cavity, β, measuring the decay rate of transmitted light intensity as a function of wavenumber allows us to obtain absorption coefficients and hence the absorption

spectrum.

$$\alpha = \frac{\beta' - \beta}{c} \tag{3.19}$$

where β / c represents the background of the ring-down spectrum, which depends on wavenumber as the mirror reflectivity varies according to it. The advantage of CRDS is that absorption features of the sample are not directly measured but contained in the time-evolution of the ring-down signal. This makes CRDS highly sensitive and independent of the fluctuations of the light source, which was the major problem with conventional absorption spectroscopy.

There are several methods to extract spectral information from the recorded exponential decays at each wavenumber. Naus *et al.* [133] showed that the best decay rate was determined by a weighted non-linear least-squares fitting and it produces a reliable estimate of the uncertainty. It is important to note that the decay needs to be mono-exponential, otherwise fitting cannot extract absorption features. Beer-Lambert law (i.e. exponential decay) behaviour requires that the bandwidth of the pulsed laser within the cavity is smaller than the width of the absorption spectral lines. If this condition is not satisfied, the various wavenumber components decay with different rates which results in a non-exponential decay of the signal [134]. This effect is similar to the Fourier transform spectrometer instrument resolution being lower than the width of the absorption features. Hodges *et al.* [135] quantitively investigated the effect and showed the importance of using a narrow bandwidth laser with a well characterised spectrum to achieve high accuracy in intensities. When multiple laser shots are used for each wavelength, averaging is only possible after fitting each decay separately as it is mathematically incorrect to fit the averaged decay [131].

3.2.2 Experimental Setup of Cavity Ring-Down Spectroscopy

Figure 3.7 shows a schematic diagram of the apparatus used in a generic pulsed CRDS experiment. The highly reflective concave mirrors are carefully positioned to create a stable cavity so that pulsed laser light make round trips between the mirrors. A tunable laser pulse of typically 5 ns is coupled into the cavity where most of the laser light reflected back but a small fraction leaks out by transmission through the mirror. The photomultiplier tube (PMT) positioned behind the output mirror detects the intensity of light transmitted. The signal from the PMT is sent to a digital oscilloscope and then to a computer to obtain the decay rate by fitting the

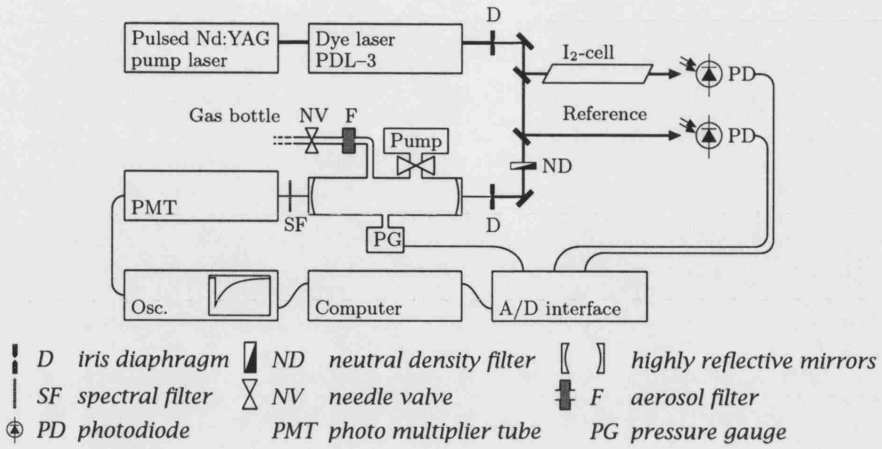

Figure 3.7: Schematic diagram of a generic pulsed CRDS experimental set-up. The figure was provided by M. Sneep (private communication).

digital trace to the first-order exponential function.

3.3 FTS versus CRDS — Advantages and Disadvantages

The basic concepts of FTS and CRDS have been presented in the previous sections. In this section, the advantages and disadvantages of those techniques will be discussed.

The main advantage of FTS is that it gives highly accurate measurements of line positions and intensities. Also, FTS records the spectrum simultaneously and this is an advantage as the experiments can be carried out fairly rapidly. A wide range of wavenumber can be recorded using Fourier transform spectrometer, indeed the Fourier transform spectrometer at Kitt Peak can record spectra over the range $550 - 45000\ \mathrm{cm}^{-1}$ [136]. On the other hand, Fourier trasform spectrometer requires a long absorption cell to create a long pathlength which would certainly be a disadvantage when measuring the water isotopologues that are extremely expensive.

The CRDS is highly sensitive due to the extremely long pathlength created by the highly reflective two mirrors. In a typical CRDS setup, the pathlength can reach 60 km. It can measure very weak absorptions which cannot be detected by other spectrometers. Using an appropriate laser, it is possible to measure the high wavenumber region, such as UV, with a great precision. Also, unlike FTS, only a small sample cell is required for CRDS which is a good news for

measuring expensive species. A disadvantage of CRDS is that it is time consuming as data have to be collected at each wavelength position and the spectral coverage is relatively limited compared to FTS. Another disadvantage is that absorption is underestimated in the case of narrow band absorbers since the finite laser bandwidth interferes with absorption. It is similar to the instrument function in FTS, but it appears inside the exponent, making it impossible to resolve. However, this problem would disappear if a truly narrow-band laser is used.

In this thesis, two spectra recorded using FTS at Kitt Peak and two spectra recorded using CRDS at the Vrije Unitersiteit (Amsterdam, the Netherlands) are analysed. The former spectra were measured by Camy-Payret and co-workers in 1981 and the latter were by Sneep and Ubachs in 2003. The analysis of these spectra will be presented in Chapter 6 and 7.

3.4 Line Profiles

Any observed spectral lines have a finite width, which is the result of a convolution of true line profile with the instrument function (FTS) or the laser bandwidth (CRDS). Three elements contribute to the true line profile; natural broadening, Doppler broadening and pressure broadening.

Natural broadening originates in the fact that excited levels have finite lifetimes and these finite lifetimes cause a spread in energy values due to the uncertainty principle ($\Delta E \Delta t \sim \hbar$). Natural broadening produces a Lorentzian line profile. Doppler broadening occurs as a result of the famous "Doppler effect", which makes the wavelength of a source shorter if it is moving towards the observer and longer if moving away. The thermal motion of atoms or molecules inside a sample cell gives rise to a spread of shifts which results in the broadening of spectral lines. Doppler broadening produces a Gaussian profile. Pressure broadening, often referred to as collision broadening, arises due to the interactions between the sample molecules and particles, including themselves. This broadening results in a Lorentzian profile.

Pressure broadening has a significant importance in atmospheric science, especially for the data retrieval of remote sensing where many strong transitions are highly saturated due to the long pathlength. In this case, the pressure broadening parameter plays an important role for the total absorption of the transitions. There are two types of pressure broadenings,

self-broadening and foreign-broadening. Self-broadening is induced by collisions between the sample molecules themselves, whereas foreign-broadening is by collisions between the sample molecules and other species, such as air. A large number of studies on air, N_2 and other broadenings have been carried out, both theoretically and experimentally, because of its importance for atmospheric studies (see references [137–148] for example). Self-broadening is less significant but, in the case of water, the self broadened width is generally five times larger than the air-broadened width [149]. Self-broadening parameters are included in many water linelists [20, 22, 46, 149].

The true line profile is usually described by a Voigt profile, which is the convolution of a Lorentzian and a Gaussian profile since natural and pressure broadening are in Lorentzian whereas Doppler broadening is in Gaussian. The Voigt profile can be characterised by the damping parameter, b, which is proportional to the FWHM of Lorentzian divided by that of Voigt. When the damping parameter is 0, the profile is a pure Gaussian and when it is 1, a pure Lorentzian. The Voigt function can be written as [124]:

$$V(x,b) = \frac{b}{\pi}\int_{-\infty}^{\infty} \frac{e^{-y^2}}{b^2+(x-y)^2}\,dy \tag{3.20}$$

with

$$b = \frac{\alpha_L}{\alpha_D}\sqrt{\ln 2}, \qquad x = \frac{\nu-\nu_0}{\alpha_D}\sqrt{\ln 2} \tag{3.21}$$

where α_D and α_L are the FWHM of Doppler and Lorentzian profile respectively and ν_0 is the line centre wavenumber.

3.5 Previous Experimental Work

3.5.1 Rotation-Vibration Spectra of $H_2{}^{18}O$

The absorption spectrum of isotopically enriched $H_2{}^{18}O$ in the wide range of wavenumber was recorded at Kitt Peak in the early 1980s. This spectrum has been studied extensively by many workers and a series of papers have been published [23–31]. I analysed the spectrum in the 12400 – 14520 cm^{-1} range. The details of this analysis will be given in Chapter 6. Toth [150] recently analysed the newly recorded pure and isotopically enhanced water vapour spectra in a wide range of wavenumber (500 –8000 cm^{-1}) and the new data will be included in the next

Table 3.1: Previous studies of rotation-vibration spectra of $H_2{}^{18}O$. FTS is the FTS spectrum recorded at Kitt Peak (see Chapter 6). CRDS is the CRDS spectrum recorded at the Vrije Universiteit (see Chapter 7).

Source	Year	Spectral range (cm^{-1})	Method
Toth [150]	2004	500 – 8000	FTS
Toth [26]	1998	590 – 2582	FTS
Toth [27]	1992	1000 – 2225	FTS
Toth [28]	1993	2927 – 3944	FTS
Toth [29]	1994	3223 – 4126	FTS
Toth [30]	1994	6600 – 7640	FTS
Chevillard *et al.* [23]	1985	4400 – 6100	FTS
Chevillard *et al.* [24]	1986	5900 – 8000	FTS
HITRAN 86 [151]	1986	8000 – 9500	unknown
Chevillard *et al.* [25]	1987	9500 – 11500	FTS
Bykov *et al.* [31]	1995	11300 – 12695	FTS
This work		12400 – 14520	FTS
This work		16570 – 17120	CRDS

edition of the HITRAN (HITRAN2004). Table 3.1 shows the summary of previous studies of $H_2{}^{18}O$. For the range of 8000 – 9500 cm^{-1}, no relevant publication was found although it is included in the HITRAN2000. The data is referenced to the old version of HITRAN (HITRAN86) [151], however the source is unclear to us.

The data on $H_2{}^{18}O$ in the current version of the HITRAN database [33] is limited, with the highest wavenumber listed for $H_2{}^{18}O$ being 13900 cm^{-1} whereas for $H_2{}^{16}O$, it extends to over 22600 cm^{-1}. We found that this database appears to lack the entire 2ν polyad region of $H_2{}^{18}O$ which Toth has extensively analysed [30]. In this study, we extended the highest wavenumber of $H_2{}^{18}O$ analysed to 17120 cm^{-1} by analysing the spectrum recorded using the CRDS at the Vrije Universiteit (see Chpter 7 for detils).

3.5.2 Rotation-Vibration Spectra of $H_2{}^{17}O$

Toth analysed the Kitt Peak Fourier transform $H_2{}^{17}O$ enriched spectrum in a wide range of wavenumber [26–30]. The highest wavenumber region published so far is by Camy-Payret *et al.* [32], in which the spectrum was analysed up to 11335 cm^{-1}. In this thesis, we extended the analysis of $H_2{}^{17}O$ up to 17125cm^{-1}, covering the $3\nu + \delta$, 4ν and 5ν polyads. Table 3.2

summarises the previous studies of $H_2{}^{17}O$. The highest wavenumber of $H_2{}^{17}O$ listed in the current version of HITRAN (HITRAN2000) is 11143.99 cm^{-1} [33].

Like for the $H_2{}^{18}O$ lines, the range 7640 – 9711 cm^{-1} can be found in HITRAN2000 with the reference to HITRAN86. There are no relevant publications for this region and the source of this data is unknown to us. New data in the range 500 – 8000 cm^{-1} by Toth [150] will be included in the HITRAN2004 and replace the old HITRAN86 lines.

Table 3.2: Previous studies of $H_2{}^{17}O$. FTS is the FTS spectrum recorded at Kitt Peak (see Chapter 6). CRDS is the CRDS spectrum recorded at the Vrije Universiteit (see Chapter 7).

Source	Year	Spectral range (cm^{-1})	Method
Toth [150]	2004	500 – 8000	FTS
Toth [26]	1998	590 – 2582	FTS
Toth [27]	1992	1000 – 2225	FTS
Toth [28]	1993	2927 – 3944	FTS
Toth [29]	1994	3223 – 4126	FTS
Toth [30]	1994	6600 – 7640	FTS
HITRAN 86 [151]	1986	7640 – 9711	unknown
Camy-Payret *et al.* [32]	1999	9711 – 11335	FTS
This work		11335 – 14517	FTS
This work		16665 – 17125	CRDS

Chapter 4

Calculation of D_2O Energy Levels

D_2O, so called heavy water, is much less abundant than other water isotopologues. Although several studies on the absorption spectra of D_2O vapour can be found [152–161], it is not currently included in the HITRAN database.

Recently, Michael *et al.* [81] observed lasing action by water molecules in the mid-infrared. A supersonic discharge through a He / H_2O mixture was contained in the cavity of an IR cavity-ring down spectrometer. This plasma was initially intended for the measurement of H_3O^+ spectrum. Surprisingly, they actually observed lasing transitions while the ring-down laser itself was turned off. A possible explanation for this is that population inversion occurred as a result of dissociative recombination in the supersonically expanding plasma. Dissociative recombination is the process whereby a molecular ion recombines with an electron and dissociates into neutral fragments. The dominant process in the plasma is:

$$H_3O^+(H_2O)_n + e^- \rightarrow H_2O^* + H + (H_2O)_n \tag{4.1}$$

where H_2O^* is the highly vibrationally excited water which results in the lasing action.

A similar experiment was carried out using a mixture of neon-helium and D_2O to measure pure rotational transitions of D_2O [82]. In this case, the dominant dissociative recombination process in the plasma is:

$$D_3O^+(D_2O)_n + e^- \rightarrow D_2O^* + D + (D_2O)_n. \tag{4.2}$$

It is thought that bending and symmetric stretch vibrational modes are mainly excited through

this process due to the difference in bond angle between D_3O^+ and D_2O [82]. Over 400 laser transitions were observed, of which only around 80 were assigned from the energy levels calculated using the data in references [152, 153, 162, 163]. Even these assignments must be regarded as uncertain. Because of the lack of a model for this laser action in water, making assignments for these transitions is difficult. In order to analyse these lasing transitions further, a set of predicted D_2O energy levels was requested by O. L. Polyansky (private communication). Our ultimate aim is to construct a reliable model for water lasers. In this chapter, the calculation of D_2O energy levels will be presented.

4.1 Calculation of Energy levels

The energy levels of D_2O were calculated using the DVR3D program suite [59]. In this calculation, I used the *ab initio* PES by Partridge and Schwenke [42] with added adiabatic, relativistic and barrier height correction.

The input parameters for DVR3D were first checked by carrying out the convergence tests. Different combinations of radial (which is called NPNT in the input file for DVR3DRJZ) and angular points (NALF) and the size of final Hamiltonians (MAX3D) were tested to obtain the optimal combination. The combinations of (NPNT, NALF) = (21,30), (24,30), (26,30), (21,40), (24,40), (26,40), (21,48) were tested and (21,40) was found to give the best convergence. The MAX3D needs to be considered carefully as the larger the MAX3D, the less approximation we need to make but the CPU time is directly proportional to the cube of MAX3D value. We have tested MAX3D = 500, 600, 800, 1000, 1500 with 21 radial and 40 angular points. The results showed the 1000 and 1500 gave very similar results, therefore we chose 1000 for this calculation. For Morse-like parameters for equilibrium radius (RE1), dissociation energy (DISS1) and fundamental frequency (WE2), we used 2.55 a_h, 0.25 E_h and 0.007 E_h, respectively. These values were extensively tested by Fulton in his PhD thesis [113]. The mass of the deuterium (D) used was 2.0138270 u and the mass of the oxygen (^{16}O) was 15.990726 u, both in atomic mass unit.

Here is the summary of parameters used for the calculation of D_2O energy levels. For vibrational states, Radau coordinates were selected. Twenty one radial points based on a

Morse oscillator-like functions (NPNT1 & NPNT2) and 40 Gauss (associated) Legendre angular grid points (NALF) were used to generate 1000 dimension final vibrational Hamiltonians (MAX3D). For rotationally excited states, the lowest 300 vibrational functions (NVIB) were read for each value of k and final Hamiltonians of dimension $200 \times (J + 1)$ (IBASS) were diagonalised up to J = 12. The descriptions of input parameters for DVR3D can be found in the next chapter (see Table 5.1).

4.2 Results and Discussions

I have calculated the energy levels of D_2O up to $J = 12$. Table 4.1 gives the comparison of known observed band origins to the calculated values. It shows excellent agreement between observed and calculated band origins with differences of the order of 10^{-2} cm^{-1} except for the (401) state. The difference between the observed and calculated for the (401) state is considerably large compared to other levels. The possible reason may be that the calculated levels become less reliable for those higher polyad regions and / or the observed value is incorrect. Since the (401) state is the highest observed vibrational state currently available, the reliability of calculated band origins for other high-lying states cannot be investigated. The list of the first 200 band origins for D_2O, both even and odd parity, can be found in Table 4.2.

The newly discovered water lasers in mid-infrared have a particular significance in atmospheric science as they can be used to study the ion-electron recombination process in the Earth's atmosphere, which is still poorly understood. Currently there is no linelist available to analyse the lasing transitions of water because of unknown population distributions. The intensities cannot be modelled unless we know how the molecules are populated in these lasers. The calculation of the energy levels is the first step to constructing a reliable model of water lasers. Having predicted the band origins of the D_2O so accurately, the analysis of D_2O laser spectrum with these energy levels should increase the number of assigned lines considerably.

Table 4.1: Comparisons of the observed D_2O band origins taken from references [152, 153, 155–158] to the calculated values. Obs − Calc are given in cm^{-1}. Uncertainties of the observed band origins were not provided in the references.

Band	Observed origin	Obs − Calc
(010) or 00 1	1178.38	−0.06
(020) or 00 2	2336.84	−0.02
(100) or 10^+0	2671.65	−0.05
(001) or 10^-0	2787.72	0.02
(030) or 00 3	3474.32	0.04
(011) or 10^-1	3956.01	0.03
(120) or 10^+2	4990.83	−0.01
(200) or 20^+0	5291.72	0.03
(040) or 00 4	4589.30	0.07
(101) or 20^-0	5373.90	0.00
(021) or 10^-2	5105.39	−0.01
(050) or 00 5	5679.60	0.01
(031) or 10^-3	6235.08	−0.11
(210) or 20^+0	6452.98	0.01
(121) or 20^-2	7672.93	0.03
(300) or 30^+0	7852.93	0.12
(201) or 30^-0	7899.82	0.02
(102) or 21^+0	8054.06	−0.09
(003) or 21^-0	8220.18	−0.03
(301) or 40^-0	10358.56	−0.10
(401) or 50^-0	12473.02	−2.89

Table 4.2: Calculated band origins of D_2O. The first 200 band origins for even and odd parity are listed in cm^{-1}.

state	even parity	odd parity	state	even parity	odd parity
1	0.0000	2787.6977	29	9693.1109	12378.0490
2	1178.4383	3955.9827	30	9808.3885	12475.9094
3	2336.8533	5105.3970	31	10048.5361	12618.6433
4	2671.6917	5373.9013	32	10136.0217	12698.7022
5	3474.2843	6235.1908	33	10330.5201	12743.8640
6	3841.5161	6533.2282	34	10340.9945	12934.0838
7	4589.2269	7344.1606	35	10368.1653	13039.6871
8	4990.8376	7672.8894	36	10538.6970	13088.8801
9	5291.6927	7899.8024	37	10556.5926	13362.7398
10	5529.4670	8220.2095	38	10861.1580	13445.6700
11	5679.5411	8430.6040	39	10879.8520	13452.1030
12	6118.9395	8792.6085	40	11128.9950	13717.0070
13	6452.9720	9050.3068	41	11245.1687	13772.3385
14	6686.9483	9366.2234	42	11296.1565	13876.2924
15	6742.1243	9492.0942	43	11434.7206	14015.2155
16	7224.4179	9891.4087	44	11441.1251	14033.2453
17	7593.1258	10179.9607	45	11483.5299	14197.6379
18	7772.1672	10358.6591	46	11679.3538	14217.0789
19	7826.3210	10494.8508	47	11922.4511	14487.4194
20	7852.8133	10524.9922	48	11995.1207	14573.3848
21	8054.1522	10679.8813	49	12184.5202	14794.2964
22	8305.0362	10967.6826	50	12196.7599	14825.5478
23	8711.7444	11289.4738	51	12331.6323	14926.1717
24	8761.3957	11500.2127	52	12365.0623	14978.8322
25	8947.1812	11523.3032	53	12530.3780	15051.9466
26	9005.3783	11605.8883	54	12603.1416	15077.1477
27	9202.6855	11816.6418	55	12738.1539	15113.4620
28	9356.7774	12018.8151	56	12798.9614	15322.8935

Table 4.2: Continued.

state	even parity	odd parity	state	even parity	odd parity
57	12924.3128	15443.3410	86	15295.3366	17831.2195
58	12988.7794	15499.7734	87	15340.6733	17837.9344
59	13112.0920	15677.7571	88	15389.6754	17896.3995
60	13126.0213	15799.6094	89	15430.7964	17966.8657
61	13219.3197	15821.1022	90	15494.4505	18002.7548
62	13264.3577	15853.8652	91	15626.3775	18100.5572
63	13283.8159	15861.0209	92	15647.1585	18173.1034
64	13396.8559	15994.1983	93	15690.4528	18227.2855
65	13598.4633	16064.7688	94	15835.8867	18287.1602
66	13702.1271	16172.3321	95	15896.0187	18315.5921
67	13854.3107	16177.8495	96	15993.8955	18406.5331
68	13869.4607	16409.4935	97	16025.3441	18486.9090
69	13899.9598	16469.2337	98	16066.4473	18507.2410
70	14038.5625	16563.1477	99	16101.2243	18526.5308
71	14121.8906	16708.1074	100	16174.6851	18727.2256
72	14212.2323	16765.9010	101	16318.0435	18762.0344
73	14222.6667	16858.3688	102	16360.7444	18846.7399
74	14274.2684	16890.1371	103	16364.4983	18865.2169
75	14389.1498	16911.6445	104	16451.7366	18893.2002
76	14432.3655	16946.0717	105	16513.3553	19031.8472
77	14642.3354	17129.9644	106	16581.1289	19076.7057
78	14751.0378	17212.8136	107	16582.4528	19149.0716
79	14781.2729	17231.0569	108	16662.5422	19204.6602
80	14961.0381	17296.8586	109	16743.7475	19215.7197
81	14970.2171	17381.3830	110	16858.1042	19234.9946
82	14986.2230	17477.5353	111	16873.7054	19302.9934
83	15050.5594	17590.2766	112	16946.4206	19384.7266
84	15187.9345	17653.9058	113	17058.1818	19451.5022
85	15231.0291	17735.0992	114	17101.8830	19502.1663

Table 4.2: Continued.

state	even parity	odd parity	state	even parity	odd parity
115	17131.7658	19551.2764	145	18709.7972	21172.9796
116	17229.7773	19580.9104	146	18745.8483	21186.2281
117	17261.5482	19634.7524	147	18816.8902	21216.5016
118	17295.5319	19773.9862	148	18827.1572	21256.7057
119	17384.6908	19790.8116	149	18914.5728	21288.5065
120	17408.3284	19899.3741	150	18985.5393	21339.6769
121	17499.4324	19930.8270	151	19037.0557	21412.7584
122	17590.0165	19962.7503	152	19071.3048	21451.0831
123	17604.2878	20024.2067	153	19131.4593	21482.0139
124	17608.1141	20133.2258	154	19204.8850	21516.6949
125	17653.4168	20143.8060	155	19267.8857	21539.2428
126	17713.9455	20182.6778	156	19302.6962	21615.1255
127	17772.8386	20216.9302	157	19356.1787	21657.6449
128	17838.1641	20279.7057	158	19380.2430	21717.8493
129	17867.1250	20353.3539	159	19389.2838	21818.8076
130	17915.8131	20382.5868	160	19402.2445	21829.5015
131	17959.3824	20438.4111	161	19435.5296	21889.4793
132	18055.7243	20448.7973	162	19457.7955	21941.3830
133	18175.7354	20463.7665	163	19504.4502	21966.5220
134	18190.3206	20553.9409	164	19585.6643	21971.1717
135	18192.8156	20588.0511	165	19707.6326	22024.9706
136	18290.1943	20656.9465	166	19726.4540	22112.4436
137	18313.5871	20686.2633	167	19755.9636	22151.2372
138	18402.7758	20733.5193	168	19885.9798	22184.4607
139	18421.2639	20817.0194	169	19897.9618	22196.6829
140	18433.5552	20945.6492	170	19930.9050	22312.8219
141	18445.8801	20949.3478	171	19947.1754	22351.3269
142	18493.7885	20965.8979	172	19976.0269	22380.5283
143	18659.9454	21063.3744	173	20033.0584	22393.8505

Table 4.2: Continued.

state	even parity	odd parity	state	even parity	odd parity
144	18677.3770	21085.7265	174	20154.5086	22451.4633
175	20179.7186	22493.0574	188	20586.1071	23004.9699
176	20202.9772	22513.0329	189	20637.6707	23029.1138
177	20227.6391	22554.7513	190	20729.3266	23060.3037
178	20261.8463	22568.0603	191	20785.7628	23091.5331
179	20327.5314	22652.6716	192	20846.3103	23123.3225
180	20378.4384	22713.6230	193	20931.9177	23196.9652
181	20408.0700	22763.7189	194	20932.9867	23226.0922
182	20419.5353	22783.9628	195	20948.3188	23286.3179
183	20442.2806	22837.0122	196	21010.6223	23329.3182
184	20465.0660	22875.6269	197	21057.3207	23384.3409
185	20466.1649	22883.7294	198	21066.5833	23397.3551
186	20544.4482	22927.0162	199	21105.3107	23414.9867
187	20564.3337	22935.2695	200	21177.9281	23428.2325

Chapter 5

Calculations of Linelists for $H_2{}^{18}O$ and $H_2{}^{17}O$

In this chapter, the calculation of linelists and room temperature spectra for $H_2{}^{18}O$ and $H_2{}^{17}O$ will be presented. Here we use a word "linelist" as the list of possible transitions with transition wavenumbers, dipole moments, transition strengths and Einstein's A-coefficients and a "spectrum" as the synthesised spectrum generated from a linelist for a certain temperature.

The best available linelists for $H_2{}^{18}O$ and $H_2{}^{17}O$ prior to this work were by Partridge and Schwenke (PS) [42]. The linelists were obtained from variational calculations using the FBR method [42, 164] with an exact kinetic energy operator and analytic basis functions. Their semi-empirical PES and *ab initio* DMS (see section 2.11 and 2.12) were used for the calculation. Although those linelists are highly accurate for the low and intermediate wavenumber range, they become increasingly unreliable for predicting both line position and intensity in the high wavenumber range such as 5ν polyad region. In order to assign the experimental spectra in the 5ν polyad region, the new $H_2{}^{18}O$ and $H_2{}^{17}O$ linelists were calculated using the semi-empirical PES by Shirin *et al.* [66] and the *ab initio* DMS computed by Polyansky *et al.* [121], fitted by Lynas-Gray (unpublished, see section 2.12).

5.1 Calculation of $H_2{}^{18}O$ Linelist

Firstly, the linelist for $H_2{}^{18}O$ was calculated to analyse the $H_2{}^{18}O$ spectrum recorded by cavity ring-down spectroscopy (CRDS). The full description of the analysis can be found in Chapter 7. For this calculation, two separate computers, one for ortho and the other for para calculations, were used to speed up the process.

5.1.1 Input parameters

There are two fits for the PES by Shirin *et al.* [66], fit A and B (see section 2.11). After a comparison of $J = 0$ energy levels by two fits against the observed values, fit B was selected as it gave the smaller deviations. The mass of a hydrogen atom used was 1.0072765 and mass of an oxygen atom (^{18}O) was 17.994772, both in atomic mass unit (u). The temperature used in the SPECTRA module to synthesise the spectrum was 296 K (room temperature).

Table 5.1 shows some of the input parameters used in DVR3DRJZ and ROTLEV3B module. Those parameters were supplied by R. Tolchenov (private communication) who has investigated the optimum parameters for his calculation of the $H_2{}^{16}O$ linelist by carrying out the test on convergence. We decided the calculation of energy levels up to $J = 10$ was sufficient enough since our purpose was to construct a linelist to assign the spectrum at room temperature, where rotational states are typically populated in between $J = 0$ to $J = 10$.

5.1.2 The Linelist

The linelist of $H_2{}^{18}O$ is generated for lines involving levels up to $J = 10$. The output of DIPOLE3 module gives transition wavenumbers, transition moments, transition strengths and Einstein A-coefficient. Table 5.2 gives a sample of DIPOLE3 output. The Einstein A-coefficient (in s^{-1}) is defined in terms of linestrength [59]:

$$A_{if} = \frac{64\pi^2}{3c^3h}\nu^3\frac{S(f-i)g_i}{2J'+1}. \tag{5.1}$$

where $S(f-i)$ is the transition strength in Debye^2, ν is the transition wavenumber (cm^{-1}) and J' is the total angular momentum of the upper state. The ratio of constant in the first fraction

Table 5.1: Some input parameters for the DVR3D program suite [59].

DVR3DRJZ		
Parameters	Description	This work
NPNT2	number of DVR points in r_2 from Gauss-associated Leguerre quadrature	34
NALF	number of DVR points in θ from Gauss-associated Legendre quadrature	40
JROT	total angular momentum number of the system J	0 – 10
NEVAL	number of eigenvalues and eigenvectors required	1000
MAX3D	maximum dimension of the final Hamiltonian	2000
RE1 (r_e)	Morse like parameters for equilibrium radius	2.55 a_h
DISS1 (D_e)	Morse like parameters for dissociation energy	0.25 E_h
WE2 (ν_e)	Morse like parameters for fundamental wavenumber	0.007 E_h
ROTLEV3B		
Parameters	Description	This work
NVIB	number of vibrational levels from DVR3DRJZ to be read for each k block	1000
NEVAL	number of eigenvalues required for the first parity	1000
KMIN	parity selection – 0 for f parity, 1 for e parity and 2 for both	2
IBASS	size of final Hamiltonian	$450 \times (J+1)$
NEVAL2	number of eigenvalues required for the second parity	1000

can be set to 3.136186×10^{-7} which converts Debye^2 (transition strength) to s^{-1} (Einstein A-coefficient).

The linelist allows the module SPECTRA to synthesise a spectrum for the user-defined experimental condition. The calculated spectrum contains upper and lower energies for each transition, transition wavenumbers, transition strengths, absolute and relative intensities and Einstein A-coefficient. The absolute intensities are calculated using the eq. (2.67) and relative intensities are the intensities divided by the maximum intensity. Figure 5.1 shows a sample spectrum calculated with the linelist in the region 10000 – 20000 cm^{-1} with temperature 296 K. The comparison of this spectrum with the experimental $H_2{}^{18}O$ spectrum recorded by FTS [23–25] can be found in Chapter 6 (Figure 6.3).

Table 5.3 gives a comparison of the known band origins with PS linelist [42] and this work. Both linelists give accurate results in the low and intermediate wavenumber range but the PS energy levels produce larger errors at wavenumbers over 16000 cm^{-1}. It is impossible to draw

Table 5.2: Sample of DIPOLE3 output for $H_2{}^{18}O$. Transition wavenumbers are in cm^{-1}, transition moments, written as dipole in the table, are in Debye, transition strengths, $S(f-i)$, are in $Debye^2$ and Einstein A-coefficient are in s^{-1}. Dipole in this case is not a vector and is obtained as | x transition + z transition |.

ket energy	bra energy	wavenumber	z transition	x transition	dipole	$S(f-i)$	A-coefficient
-0.000	36.747	36.747	0.977104E-04	-0.186832E+01	0.186822E+01	0.349026E+01	0.181058E-01
-0.000	1628.184	1628.184	-0.400076E-03	0.129074E+00	0.128674E+00	0.165569E-01	0.747085E+01
-0.000	3183.047	3183.047	-0.272511E-05	0.817120E-02	0.816847E-02	0.667240E-04	0.224953E+00
-0.000	3685.647	3685.647	-0.609511E-05	0.142182E-01	0.142121E-01	0.201984E-03	0.105716E+01
-0.000	3765.079	3765.079	0.730773E-01	0.138383E-02	0.744611E-01	0.554445E-02	0.309358E+02
-0.000	4698.459	4698.459	0.151330E-03	0.446920E-03	0.598250E-03	0.357902E-06	0.388071E-02
-0.000	5260.241	5260.241	-0.117649E-03	0.212228E-02	0.200463E-02	0.401853E-05	0.611455E-01
-0.000	5334.021	5334.021	-0.308097E-01	-0.419956E-02	0.350093E-01	0.122565E-02	0.194451E+02
-0.000	6170.133	6170.133	0.919341E-05	-0.119328E-03	0.110134E-03	0.121296E-07	0.297859E-03
-0.000	6798.355	6798.355	0.339412E-04	-0.872716E-03	0.838775E-03	0.703544E-06	0.231091E-01
1588.398	1628.184	39.786	0.246772E-04	-0.183587E+01	0.183584E+01	0.337032E+01	0.221892E-01
1588.398	3183.047	1594.650	-0.502737E-03	0.186139E+00	0.185637E+00	0.344610E-01	0.146085E+02
1588.398	3685.647	2097.249	-0.311561E-04	-0.198069E-01	0.198380E-01	0.393547E-03	0.379513E+00
1588.398	3765.079	2176.681	0.219368E-01	-0.105920E-01	0.113448E-01	0.128704E-03	0.138758E+00
1588.398	4698.459	3110.061	-0.110378E-04	0.132552E-01	0.132442E-01	0.175408E-03	0.551617E+00
1588.398	5260.241	3671.843	0.631566E-04	0.115455E-01	0.116086E-01	0.134760E-03	0.697421E+00
1588.398	5334.021	3745.624	-0.745491E-01	-0.101994E-02	0.755690E-01	0.571068E-02	0.313719E+02
1588.398	6170.133	4581.735	0.296749E-03	0.605082E-03	0.901831E-03	0.813300E-06	0.817751E-02
1588.398	6798.355	5209.957	0.540504E-04	-0.325142E-02	0.319737E-02	0.102232E-04	0.151136E+00
1588.398	6868.166	5279.768	-0.446881E-01	-0.583066E-02	0.505188E-01	0.255215E-02	0.392673E+02

a conclusion on which linelist is more accurate as the observed energy levels for $H_2{}^{18}O$ only goes up to around 17000 cm^{-1}. However, Shirin *et al.* [66] showed in their paper that the error of the PS energy levels gets significantly larger for $H_2{}^{16}O$ when wavenumber is over 20000 cm^{-1}, in fact anything up to 100 cm^{-1}, though the levels calculated with PES by Shirin *et al.* give smaller values of error for wavenumber up to 25000 cm^{-1}.

Table 5.3: Comparisons of the $H_2{}^{18}O$ band origins between the experimental (from references [23–32]), PS linelist [42] and this work. The experimentally observed band origins are shown as "Origins" below (in cm^{-1}). The observed - calculated (cm^{-1}) values for PS linelist and this work are shown under "PS" and "this work" respectively. Uncertainties of the observed band origins were not provided in the references.

Band	Origin	PS	this work
(010) or 00 1	1588.276	−0.036	−0.122
(020) or 00 2	3139.050	−0.005	−0.036
(100) or $10^{+}0$	3649.685	0.012	−0.115
(001) or $10^{-}0$	3741.567	−0.033	0.012
(110) or $10^{+}1$	5221.243	−0.076	−0.262
(011) or $10^{-}1$	5310.467	0.044	0.006
(120) or $10^{+}2$	6755.510	−0.022	−0.150
(021) or $10^{-}2$	6844.599	0.014	0.017
(200) or $20^{+}0$	7185.878	−0.030	−0.011
(101) or $20^{-}0$	7228.878	−0.051	−0.054
(002) or 11 0	7418.724	−0.082	−0.056
(041) or $10^{-}4$	9795.332	−0.062	0.133
(220) or $20^{+}2$	10256.575	−0.014	0.009
(121) or $20^{-}2$	10295.634	0.040	0.045
(022) or 11 2	10483.232	−0.050	−0.039
(300) or $30^{+}0$	10573.917	−0.033	0.059
(201) or $30^{-}0$	10585.285	−0.073	−0.056
(102) or $21^{+}0$	10839.956	−0.049	0.012
(003) or $21^{-}0$	10993.681	−0.064	−0.061
(131) or $10^{-}3$	11774.708	−0.045	0.032
(211) or $30^{-}1$	12116.797	−0.109	−0.108
(112) or $21^{+}1$	12372.707	−0.025	−0.006
(013) or $21^{-}1$	12520.123	−0.013	−0.005
(221) or $30^{-}2$	13612.710	0.157	0.225
(400) or $40^{+}0$	13793.093	−0.097	−0.214
(301) or $40^{-}0$	13795.398	0.041	−0.108
(103) or $31^{-}0$	14276.336	0.004	−0.034
(321) or $40^{-}2$	16775.381	0.504	0.431
(401) or $50^{-}0$	16854.991	0.368	−0.259

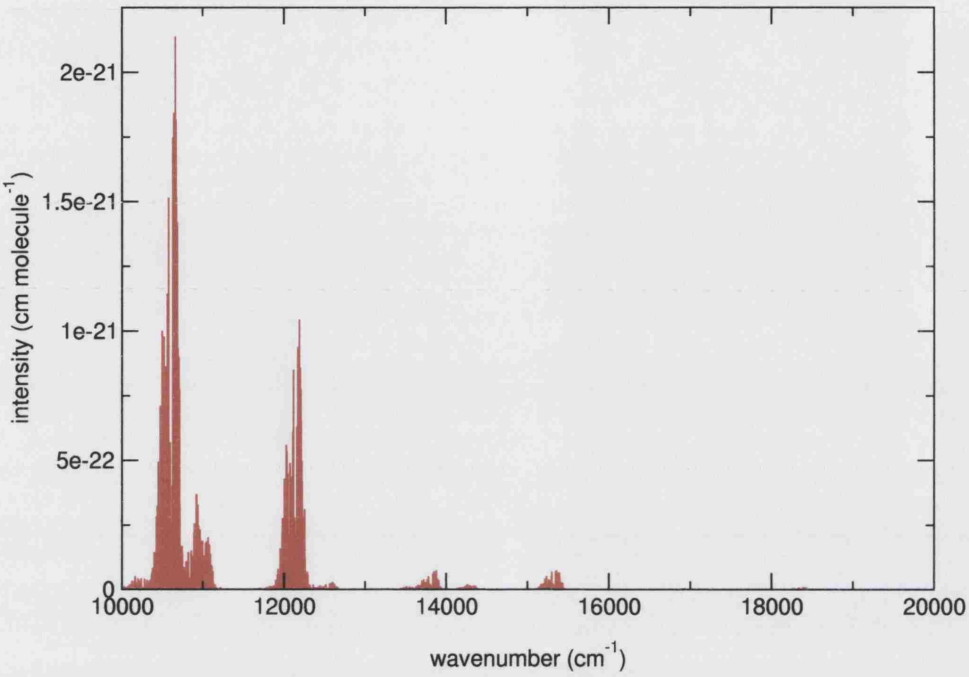

Figure 5.1: A portion of the calculated $H_2{}^{18}O$ spectrum in the range 10000–20000 cm^{-1}. Intensity shown is the absolute intensity. The spectrum was calculated at room temperature (296 K).

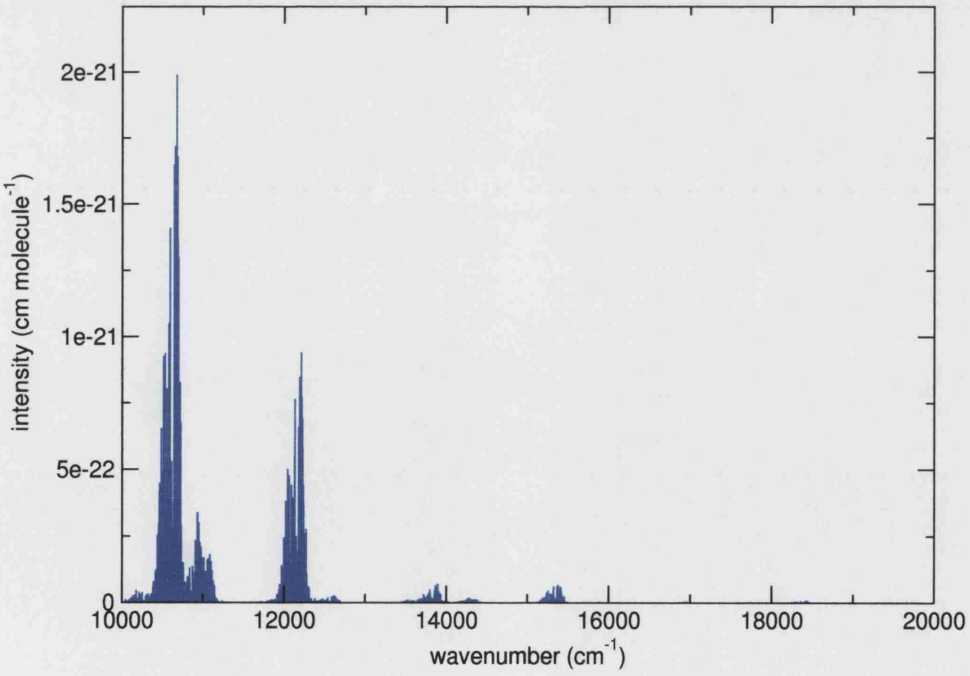

Figure 5.2: A portion of the calculated $H_2{}^{17}O$ spectrum in the range 10000–20000 cm^{-1}. Intensity shown is the absolute intensity.The spectrum was calculated at room temperature (296 K).

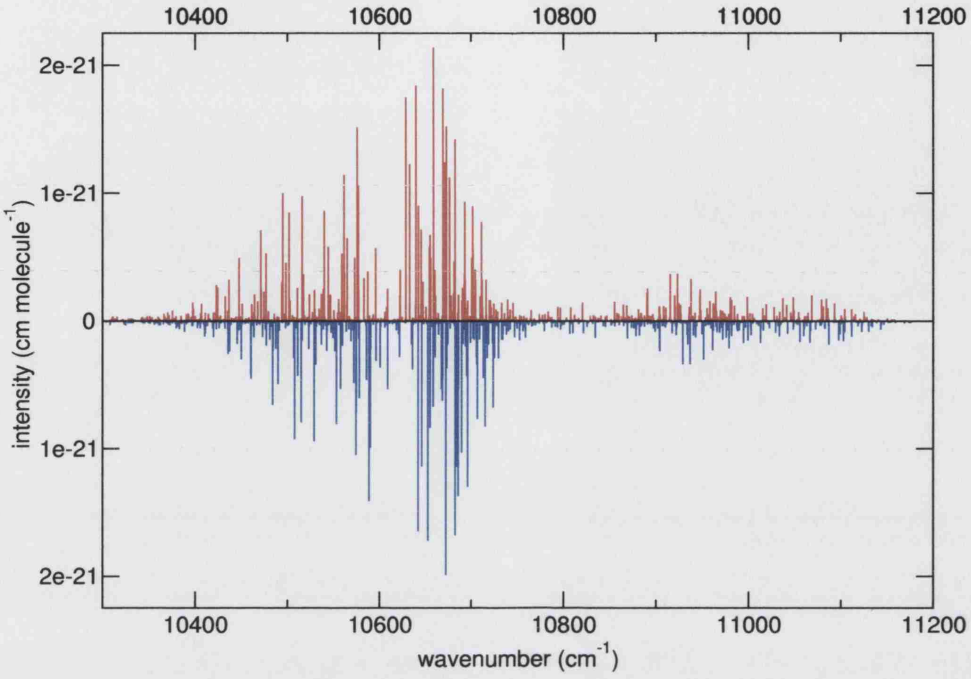

Figure 5.3: Comparison of the calculated $H_2{}^{18}O$ and $H_2{}^{17}O$ spectrum in the range 10300 – 11200 cm^{-1}. The upper red lines are $H_2{}^{18}O$ and the lower blue lines are $H_2{}^{17}O$.

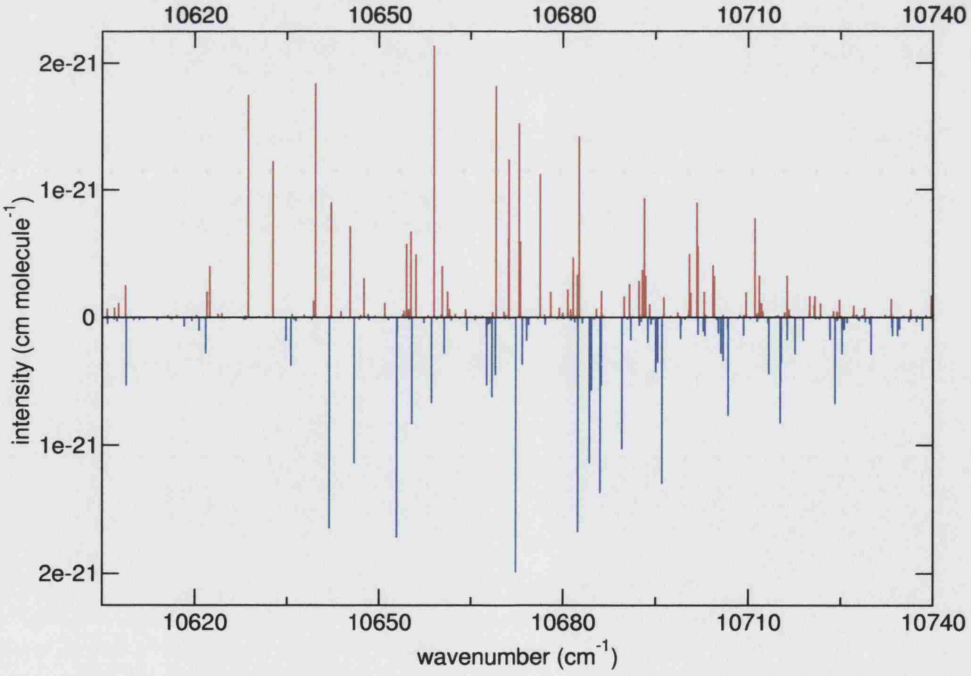

Figure 5.4: Comparison of the calculated $H_2{}^{18}O$ and $H_2{}^{17}O$ spectrum in the range 10605 – 10740 cm^{-1}. The upper red lines are $H_2{}^{18}O$ and the lower blue lines are $H_2{}^{17}O$.

Table 5.4: Labelling of the calculated energy levels. Each level was numbered in the following fashion. The first number (see the last line of each box below, denoted as "0 *j* 0" *etc.*) shows the ortho/para states, para = 0 and ortho = 1. The second number is the value of total angular momentum J. The last number shows the rotational parity p, even = 0 and odd =1. In the case of $J = 0$, when ν_3 is even then the levels are labelled 0 0 0, and when it is odd then they are 1 0 0. The energy levels in each symmetry blocks are numbered from lowest to highest. So for example, the lowest energy level in the $J = 0$, ν_3 even block is expressed as 0 0 0 1, where the fourth number gives the energy ordering of the energy level within the symmetry block.

J even		**J odd**	
ν_3		ν_3	
even	**odd**	**even**	**odd**
ee *para* 0 J 0	**fe** *para* 0 J 1	**ee** *ortho* 1 J 0	**fe** *ortho* 1 J 1
fo *ortho* 1 J 1	**eo** *ortho* 1 J 0	**fo** *para* 0 J 1	**eo** *para* 0 J 0

5.1.3 Labelling the Energy Levels

The energy levels calculated by the DVR3D program suite need to be labelled with the vibrational and rotational quantum numbers. For labelling, each energy level was first numbered according to its symmetry. Table 5.4 shows how each energy level was numbered. Also see Table 2.5 for the DVR3D symmetry blocks. The labelling of quantum numbers was then carried out by comparing the energy level numbers of $H_2{}^{18}O$ with those of $H_2{}^{16}O$, which were already labelled by R. Tolchenov (private communication) starting from the known experimental levels [95]. Assuming that energy level numbers of $H_2{}^{16}O$ and $H_2{}^{18}O$ correspond, $H_2{}^{18}O$ levels were labelled in the same way as $H_2{}^{16}O$ levels. Although many levels are labelled successfully in this manner, there are a few levels that were not. The most common problem was, when two or three energetically close levels were labelled in the wrong order. Because it is crucial to have the correct labelling for each energy level to construct a good linelist, a great deal of time was spent to check the validity of the labels. One way of checking is by taking the ratios of these energy levels to the corresponding known experimental $H_2{}^{16}O$ levels as we know that they are almost constant within a vibrational band. Any energy level whose ratio to $H_2{}^{16}O$ is outside of the usual ratio range will be investigated and re-labelled appropriately. Most levels are properly labelled before starting assignments but still there were occasions when some levels were

found to be mis-labelled as the assignments progressed. Those levels are re-labelled and also the transitions linking to the levels in the linelist are modified. The PS linelist is known to have many energy levels, especially the vibrational states, labelled incorrectly. This became very apparent when we analysed the $H_2{}^{18}O$ spectrum using their linelist.

5.2 Calculation of $H_2{}^{17}O$ Linelist

5.2.1 Input parameters

The same input parameters for DVR3DRJZ and ROTLEV3B were used for the calculation of the $H_2{}^{17}O$ linelist (see Table 5.1). The mass of hydrogen atom used was 1.0072765 u and mass of an oxygen atom (^{17}O) was 16.994743 u. The temperature used in the SPECTRA module to synthesise the spectrum was again 296 K.

5.2.2 The Linelist

Figure 5.2 shows a portion of the synthesised room temperature spectrum in 10000 – 20000 cm^{-1} calculated from the linelist. Labelling of the energy levels was done by following the method discussed in subsection 5.4. Many levels appeared to be mis-labelled when the $H_2{}^{17}O$ spectrum was analysed using this linelist. The ratios of $H_2{}^{17}O$ to $H_2{}^{16}O$ energy levels were checked and re-labelling was done appropriately. All the assignments of transition linking the energy levels are modified accordingly. This procedure was painstaking and time consuming but absolutely crucial for making correct assignments to the spectra.

The observed band origins were compared with those given in the PS linelist [42] and the new linelist of this work. Table 5.5 shows the results of this comparison. Both PS and this work give accurate predictions of band origins throughout, although the (001) vibrational state by PS gives an order of a magnitude larger error than the other states.

Table 5.5: Comparisons of the $H_2{}^{17}O$ band origins between the experimental [26–30, 32], PS linelist [42] and this work. The experimentally observed band origins are shown as "Origins" below (in cm^{-1}). The observed - calculated (cm^{-1}) values for PS linelist and this work are shown under "PS" and "this work" respectively. Uncertainties of the observed band origins were not provided in the references.

Band	Origin	PS	this work
(010) or 10^-1	1591.326	−0.003	−0.124
(020) or 00 2	3144.981	−0.001	−0.040
(100) or 10^+0	3653.142	0.010	0.013
(001) or 10^-0	3748.902	0.557	−0.109
(011) or 10^-1	5320.262	0.055	0.008
(120) or 10^+2	6764.724	−0.020	−0.151
(021) or 10^-2	6857.273	0.018	0.005
(200) or 20^+0	7193.246	−0.019	−0.060
(002) or 11 0	7431.076	−0.085	0.001
(101) or 20^-0	7238.714	−0.047	−0.047
(121) or 20^-2	10311.203	0.053	0.039
(201) or 30^-0	10598.476	−0.057	−0.044
(102) or 21^+0	10853.505	−0.003	0.018
(003) or 21^-0	11011.883	−0.067	−0.055
(211) or 30^-1	12132.993	−0.090	−0.107
(013) or 21^-1	12541.226	−0.019	−0.015
(221) or 30^-2	13631.410	0.087	0.128
(400) or 40^+0	13809.803	0.169	0.043
(301) or 40^-0	13812.158	0.058	−0.107
(103) or 31^-0	14296.282	0.046	−0.025

Table 5.6: Comparisons of the calculated $H_2{}^{17}O$ and $H_2{}^{18}O$ transition wavenumbers. "upper" and "lower" of the first two columns show the upper and lower rotational states in $J_{K_aK_c}$ format. "vib" is the vibrational states, written in $v_1v_2v_3$ normal mode notation. Transition wavenumbers of $H_2{}^{17}O$ and $H_2{}^{18}O$ are given in cm^{-1} and differences ("diff") are calculated as $H_2{}^{17}O - H_2{}^{18}O$, also in cm^{-1}

upper	lower	vib	$H_2{}^{17}O$	$H_2{}^{18}O$	diff
4_{04}	3_{03}	211	12207.738	12191.354	16.384
3_{13}	2_{12}	211	12189.513	12173.237	16.276
5_{15}	4_{14}	211	12218.235	12201.876	16.358
2_{20}	2_{21}	211	12133.656	12117.428	16.228
4_{13}	3_{12}	211	12226.533	12210.293	16.240
2_{02}	1_{01}	211	12177.081	12161.002	16.079
3_{31}	3_{30}	211	12131.662	12115.329	16.333
6_{06}	5_{05}	211	12230.978	12214.549	16.429
2_{11}	1_{10}	211	12183.854	12167.635	16.219
1_{11}	1_{10}	211	12127.262	12111.038	16.224
4_{22}	3_{21}	211	12229.877	12213.671	16.206
3_{13}	4_{14}	211	12044.444	12028.404	16.039
2_{11}	3_{12}	211	12052.931	12036.776	16.155
2_{02}	3_{03}	211	12064.321	12048.424	15.897
5_{24}	4_{23}	211	12236.064	12219.648	16.416
1_{11}	2_{12}	211	12090.224	12074.075	16.149
3_{22}	2_{21}	211	12200.591	12184.312	16.279
0_{00}	1_{01}	211	12109.327	12093.151	16.176
4_{04}	5_{05}	211	12019.625	12003.655	15.970
7_{17}	6_{16}	211	12241.072	12224.553	16.519

5.3 Discussion and Conclusions

Figure 5.3 and 5.4 give the comparisons of $H_2{}^{18}O$ and $H_2{}^{17}O$ spectrum in different wavenumber range. In Figure 5.4, we can see a clear shift in wavenumbers between $H_2{}^{18}O$ and $H_2{}^{17}O$. This is because wavenumbers are inversely proportional to the mass, thus the heavier the mass, the lower the wavenumber. In the case of $H_2{}^{18}O$ and $H_2{}^{17}O$, the wavenumbers of $H_2{}^{18}O$ should be lower than $H_2{}^{17}O$. Some strong lines of the (211) vibrational state were selected to check the shifts between $H_2{}^{18}O$ and $H_2{}^{17}O$. The result is shown in Table 5.6. The table shows consistent shifts ($\approx 16\ cm^{-1}$) between $H_2{}^{18}O$ and $H_2{}^{17}O$ transitions.

In this chapter, I presented the calculation of new linelists for $H_2{}^{18}O$ and $H_2{}^{17}O$ using the DVR3D program suite. Room temperature spectra and the energy levels were also calculated.

I showed that my new $H_2{}^{18}O$ and $H_2{}^{17}O$ linelists give good predictions in the low and intermediate wavenumber range, in fact as good as the PS linelists which were considered to be the best, and can be assumed to be accurate for the high wavenumber region where no experimental data is yet available. The analysis of spectra of water isotopologues using these linelists can be found in the following chapters.

Chapter 6

Analysis of Fourier Transform Spectra of $H_2{}^{18}O$ and $H_2{}^{17}O$

In 1981, Chevillard, Mandin, Flaud and Camy-Peyret [23–25] measured the spectrum of two isotopically enriched samples of water using the McMath-Pierce Fourier transform spectrometer at Kitt Peak. The first sample contained $H_2{}^{18}O$ at 73±1% [24], referred to as "^{18}O" below, and the second sample, "^{17}O" below, contained enriched $H_2{}^{17}O$ and $H_2{}^{18}O$ [25]. These spectra, which achieved a typical uncertainty in their line positions of 0.001 cm^{-1} [31], are publicly available via the Kitt Peak electronic archive. There are a series of papers which analysed these spectra in different wavenumber ranges [23–25, 31, 32].

I first analysed the ^{18}O spectrum in the range of 12400 – 14520 cm^{-1} ($3\nu + \delta$ and 4ν polyad region) using the PS linelist, as this was the most accurate theoretical linelist at the time of work, and assigned 746 out of 911 lines. After this work, I have calculated the new linelist for $H_2{}^{18}O$ (see Chapter 5) and re-analysed the ^{18}O spectrum using it. With help from O. Naumenko (private communication), I have now assigned 905 lines, including 4 lines belonging to $H_2{}^{16}O$. The ^{17}O spectrum in the range of 11335 – 14520 cm^{-1} ($3\nu + \delta$ and 4ν polyad region) was analysed using the new $H_2{}^{17}O$ linelist and 823 out of 845 lines were assigned. In this chapter, the analyses of the ^{18}O and ^{17}O spectrum will be presented.

Table 6.1: Experimental conditions of the spectra analysed in this work. l is the absorption pathlength, P is the total pressure with error of $\pm 1\%$, T is the temperature and R is the resolution (see equation 3.13).

Type of spectrum	l (m)	P (hPa)	T (K)	R (cm^{-1})	Range (cm^{-1})
$H_2{}^{18}O$ enriched	434.0	3.62	300.5	0.0168	12400 – 14520
$H_2{}^{17}O$ enriched	434.0	6.32	301.2	0.0143	11500 – 12800
$H_2{}^{17}O$ enriched	434.0	6.32	301.4	0.0168	12900 – 14500

6.1 Experimental Details

The spectra of ^{17}O and ^{18}O were recorded using the McMath-Pierce Fourier transform spectrometer (see subsection 3.1.2) by Camy-Payret and co-workers. In both experiments, the sample was contained in a 6-m White type cell to create the absorption pathlength of 434 m. The experimental conditions of each spectrum can be found in Table 6.1. The wavenumber calibration was carried out using a sample of N_2O, whose line positions were already known [23]. The uncertainty in line positions was better than 10^{-3} cm^{-1} except for very weak lines, blended lines or noisier regions where signal-to-noise ratio is smaller. The derivation of the uncertainties in line positions and absolute intensities will be discussed in the later section (see section 6.3).

Experimental linelists of ^{17}O and ^{18}O have been created by J. Brault by fitting the lines in both spectra using the GREMLIN program (Brault, unpublished). This program has three fitting routines; derivative linefinder, least square fitting and ring fitting. The derivative linefinder searches for the line positions by taking the first and second order derivatives of experimental lines. This gives reasonably good line positions and rough estimate of strengths. The least square fitting is done by comparing the Voigt profile model to experimental lines and readjusting the model parameters until the square of the sum of deviations reaches minimum. This gives better line positions and a good estimate of strengths and widths. Ring fitting is like the least square fitting but it cuts off all the unobserved wavenumber components produced by "ringing" and effectively fits the lines only using the observed wavenumber components. It usually gives the best results, especially if the spectral resolution is low. A detailed explanation of the fitting procedure can be found in reference [127].

The ^{17}O and ^{18}O spectra contain transitions of $H_2{}^{16}O$, $H_2{}^{17}O$ and $H_2{}^{18}O$ and in some cases even of HDO. In order to filter the transitions due to the isotopologue of interest – $H_2{}^{17}O$ for ^{17}O spectrum and $H_2{}^{18}O$ for ^{18}O – we need to compare the spectra of natural abundance water, ^{17}O and ^{18}O simultaneously. In this work, the Fourier transform spectrum of natural abundance pure water measured by Schermaul *et al.* [21] at the RAL was used instead of the one by Mandin *et al.* [165] recorded at the same time as the isotopically enriched spectra at Kitt Peak. The spectrum by Schermaul *et al.* was selected as it is known to contain many lines that were not observed previously.

The concentration of water isotopologues in each sample was first calculated for the purpose of associating each line with an isotopologue. The total number of molecules in a sample was easily obtained from the pressure, volume and temperature of the sample using $n = PV/RT$, where n is the number of molecules per cm^3. The concentration of $H_2{}^{16}O$, $H_2{}^{17}O$ and $H_2{}^{18}O$ in the natural abundance sample was calculated as (total number of molecules in the sample) $\times$ (natural abundance of the isotopologue). The isotopologue distributions of ^{17}O and ^{18}O samples were deduced using the total number of molecules in each sample and ratios derived by comparing the experimental intensities of transitions observed in more than one spectrum. The resulting isotopologue distributions of the natural abundance, ^{17}O and ^{18}O samples are tabulated in Table 6.2 under the heading of isotopologue distributions.

Using the isotopologue distributions, one can obtain the expected ratios of intensities that each isotopologue would show in the different spectrum. For example, if a transition due to $H_2{}^{16}O$ appears in all three spectra, the intensities of the transition in the natural abundance, ^{17}O and ^{18}O are expected to have the ratio of (4496.90 /4496.90) : (469.02 /4496.90) : (100.73 /4496.90) = 1 : 0.104 : 0.022. The intensity ratios of Table 6.2 give the expected intensity ratios for $H_2{}^{16}O$, $H_2{}^{17}O$ and $H_2{}^{18}O$.

After obtaining the expected intensity ratios, the natural abundance, ^{17}O and ^{18}O spectra were read into a spreadsheet and lines of the same wavenumber were aligned. The intensities of these were ratioed to look for the characteristic patterns discussed above. Figure 6.1 shows a portion of the spreadsheet created by J. Brault (private communication). Most lines are identified as belonging to $H_2{}^{16}O$, $H_2{}^{17}O$ or $H_2{}^{18}O$ according to the intensity ratios although some inconclusive lines, such as blends and HDO lines, are also present in the spectra. For the ^{18}O

Table 6.2: Isotopologue distributions of the samples and the characteristic ratios of intensities. Isotopologue distributions show the number of molecules in the sample (in 10^{19} molecules cm^{-3}).

Isotopologue distribution ($\times 10^{19}$ molecules cm^{-3})			
Isotopologue	Natural	$H_2{}^{17}O$ enriched	$H_2{}^{18}O$ enriched
$H_2{}^{16}O$	4496.90	469.02	100.73
$H_2{}^{17}O$	1.676	32.81	1.05
$H_2{}^{18}O$	9.017	156.62	276.62

Intensity ratios			
Isotopologue	Natural	$H_2{}^{17}O$ enriched	$H_2{}^{18}O$ enriched
$H_2{}^{16}O$	1	0.104	0.022
$H_2{}^{17}O$	0.051	1	0.032
$H_2{}^{18}O$	0.033	0.567	1

spectrum, 911 lines were attributed to $H_2{}^{18}O$ by Brault using the spreadsheet. For the ^{17}O spectrum, I wrote a small computer program, which looks for the characteristic patterns of intensity ratios. This was used as Brault's spreadsheet did not cover the entire wavenumber range that I was interested in. Using this program, 845 lines were attributed to $H_2{}^{17}O$.

Knowing the exact isotopologue composition of the enriched spectra is important for obtaining accurate intensities. In Table 6.2, I find that the ratio of $H_2{}^{18}O$ linestrengths in the ^{18}O to the natural abundance spectrum is 30.7 (= 276.62 ÷ 9.017). My result is consistent with the previous analysis of Chevillard *et al* [24] whose published results can be used to give an intensity enhancement factor of 30.7 with an error of ± 0.5. It is also possible to see that the abundance of $H_2{}^{17}O$ in the ^{17}O spectrum is fairly small, at only about 5% of the total water content. The intensity scaling factor of $H_2{}^{17}O$ is 19.6 (= 32.81÷1.676). The intensities given in the appendix have been divided by 30.7 for $H_2{}^{18}O$ and by 19.6 for $H_2{}^{17}O$ to scale them to natural abundance. The error in this scaling process adds about 2% the uncertainty in the measured intensities.

Figure 6.1: A portion of the spreadsheet used for the isotopologue identification. Column 1 to 5 show transition wavenumber (cm^{-1}), peak height, FWHM (10^{-3} cm^{-1}), damping parameter and equivalent width (EW, in 10^{-3} cm^{-1}) respectively for the natural abundance, ^{17}O and ^{18}O spectra. The lines with the same wavenumber were aligned and the ratio of EWs was taken (the ratios are not shown here). Each line was attributed to $H_2{}^{16}O$ (blue), $H_2{}^{17}O$ (green), $H_2{}^{18}O$ (red) or HDO (pink) according to the ratio.

Natural abundance					O17 enriched					O18 enriched				
13567.610	1.345	52	0.5	89.9	13567.611	0.189	44	0.1	9.45	13567.610	0.037	46	0.1	1.89
					13567.883	0.003	55	0.5	0.21					
13568.019	0.006	44	0.0	0.29	13568.028	0.108	43	0.0	4.91	13568.027	0.194	41	0.1	8.61
					13568.166	0.027	40	0.3	1.30	13568.167	0.046	39	0.2	2.08
13568.662	0.037	51	0.3	2.27	13568.663	0.006	38	0.0	0.24					
13568.986	0.001	60	0.0	0.08	13568.978	0.013	44	0.0	0.61					
13569.236	0.029	49	0.2	1.62	13569.235	0.004	42	0.0	0.19					
13569.339	0.005	47	0.4	0.27										
13570.035	0.002	50	0.0	0.10	13570.031	0.039	41	0.0	1.71	13570.031	0.073	40	0.0	3.14
					13570.086	0.018	40	0.0	0.76	13570.087	0.032	39	0.1	1.39
13570.673	0.029	52	0.2	1.69	13570.672	0.007	16	0.7	0.14					
13571.055	0.217	50	0.3	12.9	13571.056	0.029	45	0.0	1.39	13571.051	0.007	43	1.0	0.49
13571.824	0.002	43	0.0	0.10										
					13571.904	0.010	31	0.0	0.34					
13572.079	0.236	50	0.4	14.4	13572.078	0.031	45	0.0	1.47					
13572.617	0.653	50	0.3	39.4	13572.617	0.092	42	0.2	4.57	13572.619	0.016	56	1.0	1.41
13572.798	0.430	51	0.3	26.7	13572.798	0.055	43	0.2	2.68	13572.802	0.012	43	0.0	0.53
13572.976	0.146	51	0.3	9.06										
					13572.992	0.088	46	0.1	4.52	13572.994	0.147	41	0.1	6.80
13573.112	0.008	53	0.0	0.48										
13573.446	0.668	50	0.4	41.4	13573.447	0.094	43	0.1	4.47	13573.447	0.019	40	0.4	0.97
13573.762	0.023	49	0.0	1.19										
13574.374	0.015	56	0.5	1.11										
13574.533	0.076	55	0.4	5.09	13574.532	0.009	49	0.0	0.49					
13575.090	0.045	53	0.3	2.88	13575.092	0.006	45	0.0	0.26					
					13575.242	0.013	35	0.6	0.59					
13575.543	0.010	46	0.0	0.46										
13575.613	0.005	49	0.0	0.24										
										13575.929	0.009	37	0.4	0.42
					13576.213	0.103	41	0.2	4.92	13576.213	0.188	41	0.1	8.58
13576.313	1.920	52	0.5	130	13576.314	0.272	43	0.1	13.3	13576.314	0.056	41	0.2	2.70
										13576.562	0.005	27	0.0	0.15
13576.728	0.000	11	0.0	0.00										
					13577.197	0.025	37	0.0	0.95	13577.199	0.043	40	0.0	1.84
					13577.257	0.006	47	0.0	0.31					
13577.517	0.003	46	0.0	0.13	13577.521	0.020	39	0.5	1.04	13577.523	0.038	39	0.3	1.77
13577.782	0.043	54	0.6	3.08	13577.788	0.006	44	0.1	0.27					
					13578.086	0.008	36	0.0	0.31	13578.090	0.006	43	0.0	0.28
13578.181	0.002	47	0.5	0.13										
13578.504	0.236	55	0.4	16.3	13578.505	0.036	43	0.4	1.91	13578.507	0.009	33	0.3	0.35

6.2 Assigning the Experimental Spectra

Before I performed a full linelist calculation presented in Chapter 5, I first tried to predict the energy levels and ultimately the transition wavenumbers of $H_2{}^{18}O$ and $H_2{}^{17}O$ using the available $H_2{}^{16}O$ energy levels by Tennyson *et al.* [95]. This method was tested since calculation of full linelist takes a considerable length of time and should be avoided if it is not necessary. Here, the derivation of $H_2{}^{18}O$ energy levels are shown as an example. Within the harmonic approximation, the vibrational energies of pure stretching can be written as:

$$E_v = \hbar\omega(v + \frac{1}{2}); \quad \omega = (\frac{k}{\mu})^{\frac{1}{2}} \tag{6.1}$$

where v is the vibrational quanta, μ is the reduced mass and k is the force constant, $k = \frac{d^2V}{dr^2}|_{r=r_e}$, which is obtained by expanding the harmonic potential in a Taylor series about r_e. The ratio of $H_2{}^{18}O$ to $H_2{}^{16}O$ reduced mass, r, can be approximated as:

$$\frac{\mu^{18}}{\mu^{16}} \sim \frac{18 \cdot 1}{18+1} \times \frac{16+1}{16 \cdot 1} = \frac{153}{152} = r \tag{6.2}$$

Using this value of r, the band origins of pure stretching levels of $H_2{}^{18}O$ can be estimated from that of $H_2{}^{16}O$ as the force constant is the same for both:

$$E_v^{18} = r^{-\frac{1}{2}} E_v^{16} \tag{6.3}$$

For the band origins with both stretching and bending excitations, the $H_2{}^{18}O$ band origins should be:

$$E_v^{18} = E_{vb}^{18} + r^{-\frac{1}{2}} \times (E_v^{16} - E_{vb}^{16}) \tag{6.4}$$

where E_{vb} is the energy of (0 b 0) band origin of pure bending levels.

Within a rigid rotor model, rotational energies are decided by $E_{rot} = \mathrm{B}J(J+1)$ where $\mathrm{B} = \hbar^2/2\mathrm{hcI}$ is the rotational constant with moment of inertia $\mathrm{I} = \mu r^2$. The rotational energies of $H_2{}^{18}O$ are obtained from $H_2{}^{16}O$:

$$E_{rot}^{18} = r^{-1} E_{rot}^{16} \tag{6.5}$$

since the rotational constant is inversely proportional to the reduced mass. Table 6.3 shows the comparison of observed and calculated band origins and Table 6.4 shows the comparison of rotational wavenumbers. As can be seen clearly in the two tables, this approach fails to

Table 6.3: Comparison of $H_2{}^{18}O$ band origins observed and calculated. Observed [23, 25, 31] and calculated band origins and differences between them are given in cm^{-1}. The band origins are calculated following eq.(6.3) and (6.4) using the $H_2{}^{16}O$ rotational wavenumbers in reference [95].

Band origins	Observed	Calculated	Obs. − Calc.
(021)	6844.599	6846.764	−2.165
(200)	7185.876	7177.967	7.911
(201)	10585.285	10578.614	6.671
(112)	12372.707	12365.798	6.691

Table 6.4: Comparison of $H_2{}^{18}O$ rotational wavenumbers observed and calculated. Observed and calculated rotational wavenumbers and differences between them are in cm^{-1} [25, 31]. The rotational wavenumbers are calculated following the eq.(6.5) using the $H_2{}^{16}O$ rotational wavenumbers in reference [95].

Rotational states	Observed	Calculated	Obs. − Calc.
(201)			
$1_{01} - 0_{00}$	21.719	22.995	−1.276
$5_{50} - 0_{00}$	672.270	675.954	−3.684
$9_{09} - 0_{00}$	867.556	865.563	1.993
(112)			
$1_{01} - 0_{00}$	22.814	22.171	0.103
$5_{50} - 0_{00}$	725.954	731.094	−5.140
$8_{08} - 0_{00}$	701.240	699.897	1.343

give consistent predictions of either band origins or rotational wavenumbers. Therefore the idea of calculating $H_2{}^{18}O$ transition wavenumbers from the known $H_2{}^{16}O$ energy levels was abandoned.

6.2.1 Assignment Method

After the failed attempt to predict transition wavenumbers using the known $H_2{}^{16}O$ energy levels, it was decided to employ a theoretical linelist to make assignments. (see Chapter 5 for the detail of linelist calculation.) The following method was established in this work. First I make "trivial" assignments, which are ones linking upper energy levels already determined experimentally. The remaining unassigned lines are compared to a calculated spectrum which contains:

Table 6.5: Sample of the calculated $H_2{}^{18}O$ spectrum. Line positions are in cm^{-1}, intensities are in cm $molecule^{-1}$. v' and v'' are the upper and lower vibrational states, expressed in $v_1v_2v_3$ normal mode notation.

line position	intensity	J'	K_a'	K_c'	J''	K_a''	K_c''	v'	v''
12000.1486	0.193E-28	6	5	2	7	4	3	042	010
12000.2076	0.603E-23	4	3	2	4	4	1	310	000
12000.2396	0.185E-23	7	3	4	7	4	3	310	000
12000.3007	0.494E-26	7	2	6	7	6	1	013	000
12000.3176	0.283E-24	0	0	0	1	0	1	221	010
12000.4138	0.588E-28	10	5	5	9	7	2	211	000
12000.4737	0.191E-26	10	7	4	9	8	1	070	000
12000.4846	0.637E-27	10	1	9	9	8	2	160	000
12000.5041	0.582E-26	7	4	4	7	4	3	221	010
12000.5077	0.110E-27	3	3	1	3	2	2	042	010
12000.5095	0.175E-22	4	2	3	5	1	4	310	000

1. Line positions in cm^{-1}
2. Line intensity in cm $molecule^{-1}$
3. Upper rotational quantum numbers, $J'\ K_a'\ K_c'$
4. Lower rotational quantum numbers, $J''\ K_a''\ K_c''$
5. Upper vibrational quantum numbers, $(v_1'\ v_2'\ v_3')$
6. Lower vibrational quantum numbers, $(v_1''\ v_2''\ v_3'')$

Table 6.5 shows a portion of the calculated $H_2{}^{18}O$ spectrum. Initial assignments are made for each experimental line by selecting the theoretical lines whose line positions fall within the experimental position $\pm$ 0.03 cm^{-1}. The value of error can be varied to narrow or broaden the selection window. Intensities are also taken into consideration to make initial assignments. Usually the intensities of 100 strongest experimental lines are compared with those of the corresponding theoretical lines to take the ratios. These ratios are used as a rough guide for making the initial assignments.

Upper energy levels are then determined by adding the energies of lower levels, which were taken from the HITRAN2000 database [33], to the experimental wavenumbers. All possible

combinations of transitions with those upper energy levels are generated to search for further assignments by combination differences. Upper energy levels that are not confirmed by combination differences are re-considered and any necessary changes are made. The ratios of new upper energy levels to $H_2{}^{16}O$ energy levels are taken to check the reliability of assignments, as these ratios are approximately constant within a vibrational band. For example, in the $H_2{}^{18}O$ (301) vibrational state those ratios are usually 0.9974±0.0001, so if a ratio lies outside this range the assignment is discarded and re-considered. Another way to check the assignments is to look at the differences between the observed and calculated energy levels. The Obs − Calc values tend to be systematic, like the ratios, and can be used to check the validity of energy levels. Some of the newly determined energy levels with the ratios and Obs − Calc are given in Table 6.6.

For making further assignments, I also used a small computer program that calculates all possible combinations of upper and lower energy levels with the observed transition wavenumbers. The program assigns a different combination of J, K_a, K_c for upper and lower levels following the selection rules and calculates the upper energy level by adding the already known lower energy level to the transition wavenumber. If two or more transition wavenumbers have the same upper energy levels then the program will write them out. The upper energy levels obtained by this method do not specify vibrational levels – the levels only have rotational labels, therefore those levels written out have to be matched to the calculated rotation-vibration energy levels to determine the vibrational states.

Table 6.6: Sample of newly determined experimental energy levels of $H_2{}^{18}O$. The columns 1–3 are the rotational states, column 4 gives the vibrational states, column 5 are the newly observed energy levels in cm^{-1}, column 6 are the number of transitions observed to the levels, column 7 is the $H_2{}^{16}O$ energy levels (cm^{-1}), column 8 is the ratio of $H_2{}^{18}O$ to $H_2{}^{16}O$ energy levels, column 9 is the calculated $H_2{}^{18}O$ energy levels, column10 is the difference between the observed and calculated value and column 11 is the ratio of calculated $H_2{}^{18}O$ to $H_2{}^{16}O$ levels. Uncertainties of the observed energy levels is estimated to be 0.2×10^{-2} cm^{-1}(this figure is achieved by averaging the energy levels determined by more than one transitions).

J	K_a	K_c	vib	Obs. $H_2{}^{18}O$		$H_2{}^{16}O$	ratio	Calc. $H_2{}^{18}O$	Obs - Calc	ratio
0	0	0	301	13795.3983	1	13830.9379	0.9974	13795.5063	-0.1080	0.9974
1	0	1	301	13817.7035	2	13853.2703	0.9974	13817.8125	-0.1090	0.9974
1	1	1	301	13828.3093	2	13864.2813	0.9974	13828.4202	-0.1109	0.9974
1	1	0	301	13833.4482	2	13869.3879	0.9974	13833.5606	-0.1124	0.9974
2	0	2	301	13860.8174	3	13896.4764	0.9974	13860.9263	-0.1089	0.9974
2	1	2	301	13867.8052	3	13903.8685	0.9974	13867.9153	-0.1101	0.9974
2	1	1	301	13883.1905	4	13919.1506	0.9974	13883.3041	-0.1136	0.9974
2	2	1	301	13914.9028	2	13951.9016	0.9973	13915.0337	-0.1309	0.9974
2	2	0	301	13916.3610	2	13953.3100	0.9974	13916.4920	-0.1310	0.9974
3	0	3	301	13922.4692	3	13958.1713	0.9974	13922.6292	-0.1600	0.9975
3	1	3	301	13926.2674	4	13962.2547	0.9974	13926.3750	-0.1076	0.9974
3	1	2	301	13956.6303	3	13992.6717	0.9974	13956.7467	-0.1164	0.9974
3	2	2	301	13981.8512	4	14018.9380	0.9974	13981.9819	-0.1307	0.9974
3	2	1	301	13988.4669	4	14025.3508	0.9974	13988.5975	-0.1306	0.9974
3	3	1	301	14047.9309	4	14086.6976	0.9972	14048.0901	-0.1592	0.9973
3	3	0	301	14048.2010	3	14086.9511	0.9972	14048.3618	-0.1608	0.9973
4	0	4	301	14001.7977	4	14038.2649	0.9974	14001.8963	-0.0986	0.9974
4	1	4	301	14002.8390	3	14039.3845	0.9974	14002.9477	-0.1087	0.9974
4	1	3	301	14052.0704	5	14088.3262	0.9974	14052.1889	-0.1185	0.9974
4	2	3	301	14069.8309	3	14107.0816	0.9974	14069.9620	-0.1311	0.9974
4	2	2	301	14086.0908	4	14123.5432	0.9973	14086.0110	0.0798	0.9973
4	3	2	301	14139.5380	4	14178.4011	0.9973	14139.6989	-0.1609	0.9973
4	3	1	301	14141.3222	3	14180.0537	0.9973	14141.4838	-0.1616	0.9973
4	4	1	301	14228.7282	2	14270.3241	0.9971	14228.9361	-0.2079	0.9971
4	4	0	301	14228.7742	3	14270.3606	0.9971	14228.9795	-0.2053	0.9971
5	0	5	301	14097.0137	3	14133.8954	0.9974	14097.1271	-0.1134	0.9974
5	1	5	301	14097.3428	3	14134.2469	0.9974	14097.4538	-0.1110	0.9974
5	1	4	301	14167.1347	3	14203.8361	0.9974	14167.2548	-0.1201	0.9974
5	2	4	301	14177.8912	4	14215.4135	0.9974	14178.0219	-0.1307	0.9974
5	2	3	301	14210.1336	4	14246.9970	0.9974	14210.2716	-0.1380	0.9974
5	3	3	301	14253.7973	5	14292.6884	0.9973	14253.9587	-0.1614	0.9973
5	3	2	301	14260.0800	4	14298.6794	0.9973	14260.2425	-0.1625	0.9973
5	4	2	301	14343.9092	3	14385.6400	0.9971	14344.1176	-0.2084	0.9971
5	4	1	301	14344.2557	4	14385.9494	0.9971	14344.4635	-0.2078	0.9971
5	5	1	301	14461.4440	1	14508.5326	0.9968	14461.7257	-0.2817	0.9968

6.3 Assignments of the ^{18}O spectrum

The absolute intensities of transitions are calculated using the following equation:

$$I = \frac{T}{T_0 L_0} \frac{A_I}{P_{H_2O}\, l} \tag{6.6}$$

where L_0 is the Loschmidt number, A_I is the integrated absorbance, l is the pathlength (in cm) and P_{H_2O} is the pressure of the sample (in atm). The Loschmidt number gives the number of particles of an ideal gas at standard pressure $P_0 = 1$ atm and $T_0 = 273.15$ K, and is defined as $L_0 = 2.68673 \times 10^{19}$ cm^{-3}atm^{-1}. A_I (in cm^{-1}) is included in the experimental linelist as the equivalent width (EW). The absolute intensities are given in cm molecule^{-1} (HITRAN unit). For ^{18}O spectrum, the intensities of $H_2{}^{18}O$ in natural abundance are obtained by $2.6087 \times 10^{-26} \times$EW / 30.7 (including the scaling factor).

The uncertainties in the line positions and the absolute intensities were estimated using the following equation [39]:

$$\frac{\Delta\nu}{\text{FWHM}} \sim \frac{\Delta A_I}{A_I} = \frac{k}{(S/N)\sqrt{\text{FWHM/Resolution}}} \tag{6.7}$$

were k is a constant which can be set to 0.8 for the uncertainties in the line positions and 2.0 for the intensities [39]. S/N is the signal-to-noise ratio and is given by the ratio of the peak height to the *rms* at the line position. The uncertainties in the line positions and the absolute intensities are included in the list of observed transitions given in Appendix (Table A.1).

6.3.1 Assignments using the PS linelist

The ^{18}O spectrum was first analysed using the PS linelist [42], which was the best available linelist at the time of work – before the calculation of $H_2{}^{18}O$ linelist presented in Chapter 5. Figure 6.2 shows the comparison of experimental spectrum to the PS linelist. It is interesting to notice that the intensities of lines in the experimental spectrum and the PS linelist do not agree very well in the 14000 – 14500 cm^{-1} region although they seem to have excellent agreements in the lower wavenumber region. Assignments were made by following the procedure discussed in a previous section (see subsection 6.2.1). Although many transitions are assigned using the PS linelist, it became apparent that in many cases the vibrational labels of their linelist were incorrect. The most notable mis-labelled levels were (302) $\longleftrightarrow$ (301), (400) $\longleftrightarrow$ (202),

(320) $\longleftrightarrow$ (122) and (310) $\longleftrightarrow$ (112), where $\longleftrightarrow$ means the two labels needed to be swapped around in many cases. The ratios of $H_2{}^{18}O$ to known $H_2{}^{16}O$ energy levels were useful to check the validity of the labels. The expected ratio for each vibrational level was as follows: (112) 0.9972, (103) 0.9964, (221) 0.9971, (400) 0.9975, (301) 0.9974, (202) 0.9977, (103) 0.9970. Indeed, these ratios were found to be fairly constant within the vibrational bands. The wrong labels were relabelled appropriately.

Assignments were made for 746 lines out of 911 lines attributed to $H_2{}^{18}O$. Lines are assigned to 14 different upper vibrational levels. Three of these, (013), (112) and (211), were already extensively studied by Bykov *et al* [31]. The other states have not been previously observed for $H_2{}^{18}O$. My new assignments can be used to characterise further $H_2{}^{18}O$ energy levels. The energy levels that were determined by more than one transitions were averaged and standard deviations are calculated for uncertainties. Table 6.8 gives newly derived energy levels for vibrational states (221), (400), (301), (202) and (103) which covers most of the new data. For these states, vibrational band origins have been determined at 13612.71, 13793.09, 13795.40, 14188.82 and 14276.34 cm^{-1} respectively. Because each band origin was determined from a single transition, uncertainty is not available. The small splitting between the (400) and (301) band origins shows, as has been noted previously [19], that stretching states in the 4ν polyad for water are local-mode like. Table 6.8 therefore labels the vibrational states using both normal and local mode notations. Table 6.7 shows the summary of assignment results obtained by using the PS linelist.

Figure 6.4 compares the experimental line intensities given in HITRAN2000 with those analysed in this work. For ease of analysis I plot the intensities from the ^{18}O spectrum directly without scaling for enhanced $H_2{}^{18}O$ abundance. The ratio of my intensities to HITRAN2000 is 34.6 ± 8.9 with two outliers removed. This result is consistent with my result of 30.7 ± 0.5.

Table 6.7: Summary of experimental $H_2{}^{18}O$ energy levels determined with the PS linelist. Bands are labelled using normal mode (left) and local mode (right) notations. No. of levels shows the number of newly determined energy levels. No. of trans. shows the number of transitions to the vibrational bands. Uncertainties of the band origins are estimated to be 0.2×10^{-2} cm^{-1} by taking the average of the uncertainties of energy levels determined by more than one transitions.

Band	Origin (cm^{-1})	No. of levels	No. of trans.
(112) or $21^{+}1$	—	42	57
(013) or $21^{-}1$	12520.123	62	95
(211) or $30^{-}1$	—	7	12
(141) or $20^{+}4$	—	1	2
(042) or 11 4	—	1	2
(004) or 22 0	—	3	3
(221) or $30^{-}2$	13612.710	63	140
(122) or $21^{+}2$	—	9	10
(023) or $21^{-}2$	—	11	15
(400) or $40^{+}0$	13793.093	45	101
(301) or $40^{-}0$	13795.398	47	122
(202) or $31^{+}0$	14188.823	38	82
(103) or $31^{-}0$	14276.336	43	95
	Total	**384**	**746**

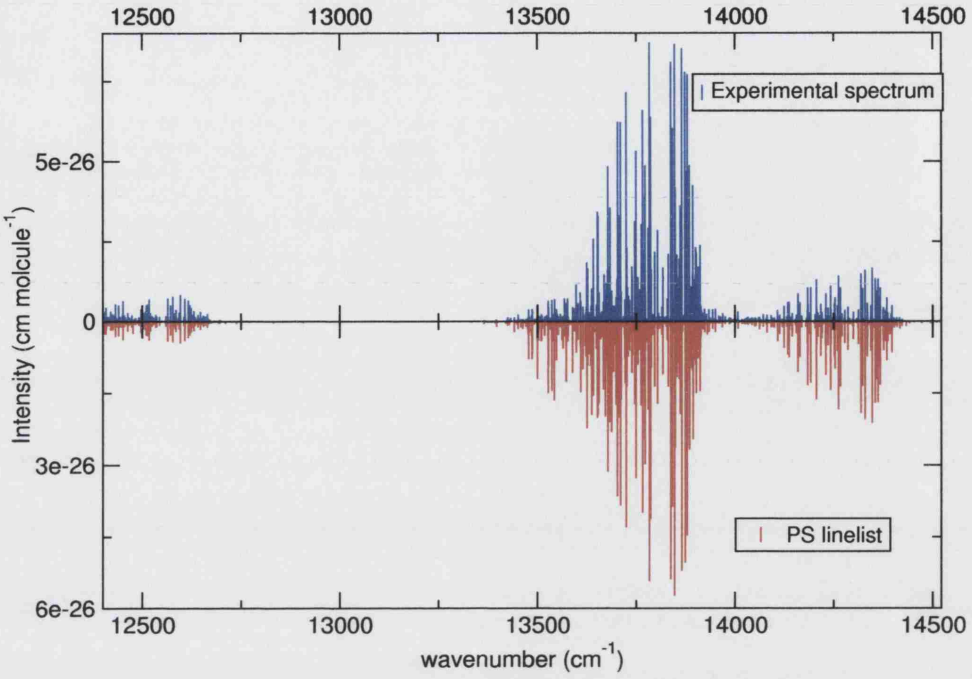

Figure 6.2: Comparison of experimental $H_2{}^{18}O$ spectrum with the PS linelist. The absolute intensities of PS lines are scaled for the natural abundance of $H_2{}^{18}O$.

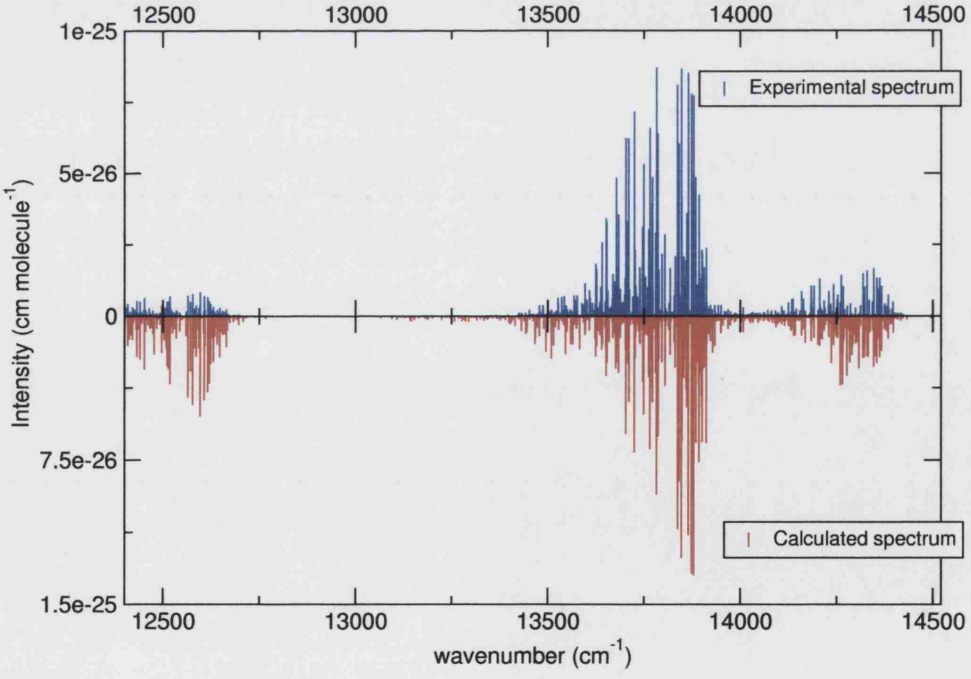

Figure 6.3: Comparison of experimental $H_2{}^{18}O$ spectrum with the newly calculated spectrum. The absolute intensities of calculated spectrum are scaled to match the natural abundance of $H_2{}^{18}O$.

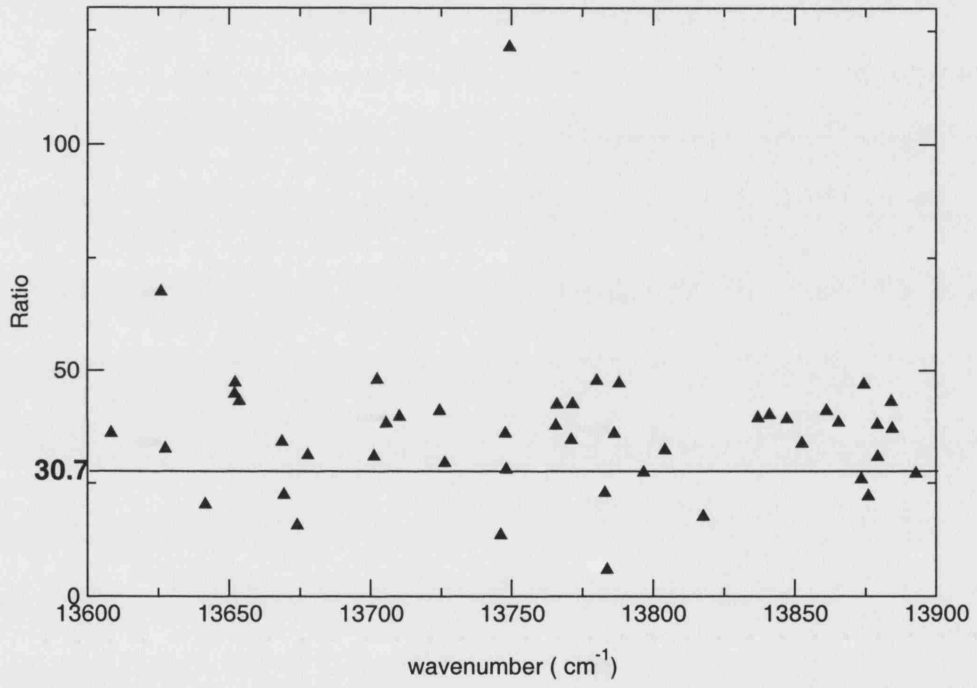

Figure 6.4: Ratio of $H_2{}^{18}O$ experimental line intensities obtained in this work (unscaled for isotopic enrichment) to those given in HITRAN2000.

Table 6.8: $H_2{}^{18}O$ experimental energy levels determined using the PS linelist. Energy levels are given in cm^{-1}, and the uncertainties (Δ) are in 10^{-4} cm^{-1}. The levels determined from more than one transitions were averaged and the standard deviations are given as the uncertainties. Uncertainties for the levels determined from a single transition are not given but they are estimated to be 2.0×10^{-2} cm^{-1} by taking the average of the uncertainties of energy levels determined by more than one transitions. The number of transitions assigned to each level (no.) are also given below.

J	K_a	K_c	(221) or 30^-2	Δ	no.	(400) or 40^+0	Δ	no.	(301) or 40^-0	Δ	no.
0	0	0	13612.7103		1	13793.0926		1	13795.3983		1
1	0	1	13635.2004		1	13815.5999		1	13817.7034	7	2
1	1	1	13651.9827	7	2	13826.2109		1	13828.3093	1	2
1	1	0	13657.8443	2	2	13829.9690		1	13833.4482	1	2
2	0	2	13679.5579	21	2	13858.8235	19	2	13860.8174	10	3
2	1	2	13691.7911	3	3	13865.8901	91	4	13867.8052	2	3
2	1	1	13709.2788	3	3				13883.1905	7	4
2	2	1	13757.7913	1	2	13912.9581	12	3	13914.9028	2	2
2	2	0	13759.0997	11	2				13916.3610	11	2
3	0	3				13920.6416	12	2	13922.4692	43	3
3	1	3	13750.4052	5	3	13924.6092	4	3	13926.2674	19	4
3	1	2	13785.3650	4	2	13954.5992	7	3	13956.6303	5	3
3	2	2	13826.2273	5	4	13980.0017	76	3	13981.8515	4	3
3	2	1	13832.3323	8	3	13986.4867	36	2	13988.4675	44	3
3	3	1	13919.9525	19	4	14045.8081		1	14047.9309	21	4
3	3	0	13920.1799	7	2	14046.3804	11	2	14048.2010	8	3
4	0	4	13824.2031	6	3	13999.4307	13	2	14001.7977	11	4
4	1	4	13827.7712		2	14000.3791	9	3	14002.8390	9	3
4	1	3	13884.6210	17	3	14050.1509	95	3	14052.0704	17	5
4	2	3	13916.5292	41	2	14068.1270	10	5	14069.8309	4	3
4	2	2	13932.6060	35	4	14084.7983	105	3	14086.7496	4	4
4	3	2	14013.5682	12	4	14137.8052	9	5	14139.5380	12	4
4	3	1	14014.7078	29	3	14139.4784	28	2	14141.3222	4	3
4	4	1	14137.0536		1	14226.9808	11	3			
4	4	0	14137.0858	12	3	14227.0266		1	14228.7742	6	3
5	0	5	13921.2439	22	2				14097.0137	17	3
5	1	5	13922.9672	18	3				14097.3428	2	3
5	1	4	14004.8183	14	3	14165.4097	42	3	14167.1347	4	3
5	2	4				14176.3807		1	14177.8912	4	4
5	2	3	14059.5109	6	3	14208.1546	20	3	14210.2536		1
5	3	3	14130.1770	7	3	14252.1247		1	14253.7968	29	4
5	3	2	14134.6573	8	3	14258.1806	14	4	14260.0800	8	4
5	4	2	14254.3017	41	3	14342.2201		1	14343.9092		3
5	4	1				14342.5676	97	3	14344.4290		1
5	5	1	14403.0236	36	2	14464.7906	9	2	14461.4440		1
6	0	6	14034.7591	1	2	14208.9443		1	14208.9358		1
6	1	6	14035.6594	8	2	14208.4965	2	3	14209.4131	3	3
6	1	5	14143.3787	20	2	14298.2445		1	14299.7517	8	3
6	2	5	14155.6999	18	2						
6	2	4	14212.5790	7	3	14355.0147		1			
6	3	4	14269.3167	15	2	14388.3862	51	3			
6	3	3	14281.0237	10	2	14403.0730	46	2			
6	4	3	14395.0922	2	2	14480.7446		2			

Table 6.8: Continued.

J	K_a	K_c	(221) or 30^-2	Δ	no.	(400) or 40^+0	Δ	no.	(301) or 40^-0	Δ	no.
6	4	2	14396.3270	11	4						
6	5	2				14598.9304	52	2			
6	5	1	14543.0611	37	3	14599.7860		1			
6	6	1				14699.0658		1			
6	6	0							14710.5590	16	2
7	0	7	14164.9836		2						
7	1	7	14166.1598	71	2	14338.1602	12	3	14338.1975	6	3
7	1	6	14299.3434	4	2						
7	2	6	14305.5408	9	2	14446.0799		1	14452.0020		1
7	3	5	14430.3129	24	2						
7	4	4	14559.9502	4	3						
8	0	8	14312.7813		2						
8	1	8	14310.2322		1	14484.2874	7	2	14485.3754		1
8	1	7	14470.9302	37	2				14611.0603		1
8	2	7				14613.4122	23	4			
8	3	6							14724.8902	31	2
8	3	5	14656.4642	55	2				14774.0263		1
8	4	5	14746.5233		1				14828.2123		1
8	4	4	14755.6783	1	2				14841.3566		1
8	6	3	14987.0551		1						
9	1	9	14475.0213		1						
9	1	8	14658.7198		1						
9	2	8	14658.6119	20	2						
9	3	7	14812.5563		1						
9	4	5	14974.8154		1						
9	7	3							15401.7031		1
10	1	10	14654.1017		1						
10	3	7	15126.1192		1						
11	2	10	15086.3967		1						

J	K_a	K_c	(202) or 31^+0	Δ	no.	(103) or 31^-0	Δ	no.
0	0	0	14188.8228		1	14276.3359		1
1	0	1	14210.3232	1	2	14298.9114	4	2
1	1	1	14221.0194	28	2	14308.7859	1	2
1	1	0	14226.2077	26	2	14314.0810	5	2
2	0	2	14253.4814	3	2	14342.3991	8	3
2	1	2	14260.4834	8	3	14348.7113	2	3
2	1	1	14276.0095		1	14364.5436	6	3
2	2	1	14307.8861	9	3	14393.9667	2	2
2	2	0	14309.3246		1	14395.5913	6	3
3	0	3	14315.1553	8	3	14404.3083	4	2
3	1	3	14318.8304	20	3	14407.7113	1	3
3	1	2	14349.5438	4	3	14438.8567	10	3
3	2	2	14374.7880		1	14462.3015	8	4
3	2	1	14381.3003	36	4	14469.3583	7	4
3	3	1	14440.7748	74	2	14524.2601	2	2
3	3	0	14440.7990	1	3	14524.5928	2	2
4	0	4	14393.7346	23	3	14483.1308	22	3
4	1	4	14395.3796	21	3	14486.1095	1	2
4	1	3	14445.0560		1	14535.0402	7	3
4	2	3	14462.7497	17	4	14552.0724	12	2

Table 6.8: Continued.

J	K_a	K_c	(202) or 31^+0	Δ	no.	(103) or 31^-0	Δ	no.
4	2	2	14478.3493	12	2	14569.3897	1	3
4	3	2	14532.1947	52	2	14625.1578		2
4	3	1	14532.9298		1	14625.8542	1	3
4	4	1	14614.4146	9	3	14700.0198	56	2
4	4	0	14612.9837	15	2	14700.1157	14	2
5	0	5	14488.9206	70	3	14578.7052	83	4
5	1	5	14489.5947		1	14578.8424	1	3
5	1	4	14560.1005	17	4	14650.3978	46	2
5	2	4	14570.8065		1	14663.4071	8	2
5	2	3	14604.0242	16	2			
5	3	3	14648.9023	8	2			
5	3	2	14649.2840	15	3			
5	4	2	14729.9790		1	14814.5346	6	3
5	4	1				14815.0096		1
5	5	1				14920.6197		1
6	1	6	14601.1513	12	2			
6	1	5				14782.6682	20	2
6	2	5	14697.9910	2	2			
6	2	4				14842.6295		1
6	3	3	14802.0963		1	14892.3876	27	3
6	4	3	14869.8231	15	2	14952.4420	5	2
6	4	2				14954.7374		1
7	0	7				14821.2357		1
7	1	7				14821.6003		1
7	1	6				14931.2044		1
7	2	6				14932.0270		1
7	3	4				15065.0979		1
7	5	3	15153.4500	47	2			
8	1	8				14967.9093	6	2

6.3.2 Assignments using the newly calculated linelist

The PS linelist was used to analyse the ^{18}O spectrum as it was the most accurate linelist available at the time of work. After this analysis, the new linelist for $H_2{}^{18}O$ has been generated (see Chapter 5) for the purpose of assigning the cavity ring-down spectrum which lies in the 5ν polyad region where the PS linelist is less reliable. The analysis of the cavity ring-down spectrum can be found in the next chapter.

Using the new $H_2{}^{18}O$ linelist, I have re-analyses the ^{18}O spectrum in the hope of making more assignments. Figure 6.3 shows the comparison of the experimental spectrum to the calculated. The figure shows a clear overestimation of intensities around 12500 cm^{-1} and also for a small region near 14250 cm^{-1}. This is due to the overestimated line strengths of the bending modes caused by the *ab initio* DMS used for the calculation, which was discussed in the previous chapter (see section 2.12).

The same assignment procedure used for the analysis with the PS linelist (see section 6.3.1) was used with the new linelist. The ratios for each vibrational level were the same as the previous analysis. I extended the number of assigned lines significantly, from 746 to 910 including 4 lines belonging to $H_2{}^{16}O$. This leaves only 15 lines unassigned. Comparisons between the previous analysis using the PS linelist (PS work, below) and the new work are following. The same assignments in both works were found for 616 lines and different assignments for 125 lines. One hundred sixty nine unassigned lines in PS work are newly assigned in this work, including 4 lines (at 13563.32, 13907.03, 14163.20 and 14386.61 cm^{-1}) attributed to $H_2{}^{16}O$. Five lines assigned in PS work were not assigned in this work and 10 lines were unassigned in both works.

Table 6.9 gives the summary of $H_2{}^{18}O$ energy levels determined using the new linelist. The table shows the lines are assigned to 17 different upper vibrational bands, giving 459 new energy levels. This is a great improvement compared to the previous analysis with the PS linelist, in which 384 new energy levels were determined (see Table 6.7). In particular, (301) vibrational level is significantly improved as almost twice as many levels are obtained in this work. The band origin of the (112) band is newly derived at 12408.797 cm^{-1}, though that of (202), which was determined in the previous analysis, was not included because I decided the

previous assignment of this transition was incorrect. Table 6.10 gives the derived energy levels for the same vibrational states as Table 6.8.

The significant improvement in assignments is not due to the better accuracy of the newly calculated linelist, in fact the PS linelist can be more accurate in the wavenumber region analysed in this work. It is down to useful discussions and correspondences with O. Naumenko (private communication), who kindly provided her assignments of the spectrum which she made using the linelist generated by Tashkun following the method in reference [42] with the PES by Partridge and Schwenke [42] and the *ab initio* DMS by Schwenke and Partridge [122]. Two assignments, one by myself and the other by Naumenko, were thoroughly compared to achieve the best possible results. O. Naumenko pointed out the main problem in PS work was that many transitions were wrongly assigned because the intensities were not properly taken into account when making assignments. Some strong lines are assigned as weak lines and vice versa. Reconsidering the intensities gave immediate improvement in assignments.

Table 6.9: Summary of $H_2{}^{18}O$ energy levels determined with the newly calculated linelist. Bands are labelled using normal mode (left) and local mode (right) notations. No. of levels shows the number of newly determined energy levels. No. of trans. shows the number of transitions to the vibrational bands.

Band	Origin (cm^{-1})	No. of levels	No. of trans.
(070) or 00 7	—	1	1
(230) or $20^{+}3$	—	1	1
(310) or $30^{+}1$	—	8	8
(211) or $30^{-}1$	—	3	3
(112) or $21^{+}1$	12408.797	37	52
(013) or $21^{-}1$	12520.123	63	96
(141) or $20^{+}4$	—	1	1
(320) or $30^{+}2$	—	16	18
(221) or $30^{-}2$	13612.710	66	141
(042) or 11 4	—	3	4
(122) or $21^{+}2$	—	10	14
(023) or $21^{-}2$	—	12	15
(400) or $40^{+}0$	13793.093	51	112
(301) or $40^{-}0$	13795.398	80	219
(202) or $31^{+}0$	—	43	89
(103) or $31^{-}0$	14276.336	58	125
(071) or $10^{-}7$	—	1	2
	Total	**454**	**901**

Table 6.10: $H_2{}^{18}O$ experimental energy levels using the newly calculated linelist. Energy levels are given in cm^{-1}, and the uncertainties (Δ) are in 10^{-4} cm^{-1}. The levels determined from more than one transitions were averaged and the standard deviations are given as the uncertainties. Uncertainties for the levels determined from a single transition are not given but they are estimated to be 2.0×10^{-2} cm^{-1} by taking the average of the uncertainties of energy levels determined by more than one transitions. The number of transitions assigned to each level (no.) are also given below.

J	K_a	K_c	(221) or 30^-2	Δ	no.	(400) or 40^+0	Δ	no.	(301) or 40^-0	Δ	no.
0	0	0	13612.7103		1	13793.0926		1	13795.3983		1
1	0	1	13635.4751		1	13815.5999		1	13817.7035	7	2
1	1	1	13651.9826	7	2				13828.3093	1	2
1	1	0	13657.8443	2	2				13833.4482	1	2
2	0	2	13679.5579	21	2	13858.8235	19	2	13860.8174	10	3
2	1	2	13691.7911	3	3	13865.8918	102	3	13867.8052	2	3
2	1	1	13709.2788	3	3				13883.1905	7	4
2	2	1	13757.7913	1	2	13912.9581	12	3	13914.9028	2	2
2	2	0	13759.0998	11	2				13916.3610	11	2
3	0	3	13743.8280	6	2	13919.9539	5	2	13922.4692	43	3
3	1	3	13750.4052	5	3	13924.6092	4	3	13926.2674	19	4
3	1	2	13785.3650	4	2	13954.5992	7	3	13956.6303	5	3
3	2	2	13826.2274	5	4	13980.0017	76	3	13981.8512	6	4
3	2	1	13832.3323	8	3	13986.4867	36	2	13988.4669	38	4
3	3	1	13920.6416	12	2	14046.1129		1	14047.9309	21	4
3	3	0	13920.1799	7	2	14046.3804	11	2	14048.2010	9	3
4	0	4	13824.2031	6	3	13999.4308	13	2	14001.7977	11	4
4	1	4	13827.7712	0	2	14000.3791	9	3	14002.8388	12	2
4	1	3	13884.6210	17	3	14050.1466	22	3	14052.0704	17	5
4	2	3	13916.5292	41	2	14068.1269	11	4	14069.8309	4	3
4	2	2	13932.6078	4	3	14084.7925		1	14086.0908	6	4
4	3	2	14013.5679	14	3	14137.0857	17	2	14139.5380	12	4
4	3	1	14014.7079	29	3	14139.4784	28	2	14141.3222	4	3
4	4	1	14136.8379		1	14226.9808	11	3	14228.7282	10	2
4	4	0	14137.8052	9	5	14227.0249	24	2	14228.7741	6	3
5	0	5	13921.2440	22	2	14094.8552	23	2	14097.0137	17	3
5	1	5	13922.9672	18	3				14097.3428	2	3
5	1	4	14004.8182	14	3	14165.4121	10	2	14167.1347	4	3
5	2	4				14176.3801	9	2	14177.8912	4	4
5	2	3	14059.5109	6	3	14208.1546	20	3	14210.1337	13	4
5	3	3	14130.1770	7	3	14252.1194	105	3	14253.7973	27	5
5	3	2	14134.6573	8	3	14258.1817	27	5	14260.0800	8	4
5	4	2	14254.2984		1	14342.2264	88	2	14343.9092	0	3
5	4	1	14254.5804		1	14342.5618	13	3	14344.2557	15	4
5	5	1	14403.0236	36	2				14461.4440		1
5	5	0				14459.5242		1			
6	0	6	14034.7591	1	2				14208.4962	5	4
6	1	6	14035.6594	8	2				14209.4130	4	3
6	1	5	14143.3787	20	2	14298.2445		1	14299.7542	58	5
6	2	5	14155.6999	18	2	14303.8588	47	5	14305.0913	2	4
6	2	4	14212.5790	7	3	14354.7361	17	2	14356.6656	3	4
6	3	4	14269.3167	15	2	14388.3834	5	3	14389.9618	25	5
6	3	3	14281.0238	10	2				14405.5151	2	3
6	4	3	14395.0922	2	2	14480.7465	28	4	14482.3868	12	3

Table 6.10: Continued.

J	K_a	K_c	(221) or 30^-2	Δ	no.	(400) or 40^+0	Δ	no.	(301) or 40^-0	Δ	no.
6	4	2	14396.3270	11	4				14483.9588	3	3
6	5	2				14598.9304	52	2	14543.0382		1
6	5	1	14600.9079	25	2				14543.0611	37	3
6	6	0				14699.0618		1			
7	0	7	14164.9836	0	2	14336.0044		1	14338.1602	12	3
7	1	7	14166.1597	71	2				14338.1974	6	3
7	1	6	14299.3434	4	2	14450.0812	16	3	14449.5807	4	2
7	2	6	14305.5409	9	2	14445.6352	100	2	14451.9449	16	3
7	2	5							14523.7575	7	2
7	3	5	14430.3129	24	2				14546.8882	16	3
7	3	4							14577.2812	12	3
7	4	4	14559.9502	4	3	14642.2322	52	2	14643.8942	8	3
7	4	3	14563.0373		1				14648.9023	8	2
7	5	3	14763.8089	24	3				14706.2891	22	4
7	5	2				14762.1947	40	2			
7	6	1				14861.2120	7	2			
7	7	1							15006.2720		1
8	0	8	14312.7813	0	2						
8	1	8	14310.2322		1	14484.2873	7	2	14484.3124		1
8	1	7	14470.9302	37	2	14610.5644		1	14613.4122	23	4
8	2	7				14611.1853		1	14613.8362	5	2
8	2	6				14706.3899		1	14708.9413	43	3
8	3	6							14723.8631		1
8	3	5	14656.4643	55	2				14773.4976	14	4
8	4	5	14746.5233		1	14826.1678		1	14827.7929		1
8	4	4	14755.6783	1	2				14840.1757	14	3
8	6	3				15046.4460		1			
8	7	1							15191.2531		1
9	0	9	14470.2439		1				14647.3842		1
9	1	9	14474.7645	18	2				14647.4397	45	2
9	1	8	14658.7198		1				14794.3963		1
9	2	8	14658.6105		1				14794.5248	5	2
9	2	7				14909.1249		1	14910.6427		1
9	3	7	14812.2349		1	14918.5447		1	14919.6389	10	2
9	4	6	14955.6287		1				15033.5558		1
10	0	10	14654.0697		1						
10	1	10							14827.4381		1
10	1	9							14992.2903	8	2
10	2	9							14992.3138		1
10	2	8	15028.6428		1				15132.6753		1
10	3	7							15229.0747		1
10	4	6							15301.9545		1
11	0	11							15024.3113	96	2

J	K_a	K_c	(202) or 31^+0	Δ	no.	(103) or 31^-0	Δ	no.
0	0	0				14276.3359		1
1	0	1	14210.3232	1	2	14298.9114	4	2
1	1	1	14221.0193	28	2	14308.7859	2	2
1	1	0	14226.2077	26	2	14314.0810	5	2
2	0	2	14253.4815	3	2	14342.3991	8	3
2	1	2	14260.4834	8	3	14348.7112	2	3

Table 6.10: Continued.

J	K_a	K_c	(202) or 31^+0	Δ	no.	(103) or 31^-0	Δ	no.
2	1	1	14276.0095		1	14364.5436	6	3
2	2	1	14307.8861	9	3	14393.9666	2	2
2	2	0	14309.3246		1	14395.5913	6	3
3	0	3	14315.1553	8	3	14404.3083	4	2
3	1	3	14318.8304	20	3	14407.7113	1	3
3	1	2	14349.5438	4	3	14438.8567	10	3
3	2	2				14462.3015	8	4
3	2	1	14381.3003	36	4	14469.3583	7	4
3	3	1	14440.7695		1	14524.2601	2	2
3	3	0	14440.7990	1	3	14524.5928	2	2
4	0	4	14393.7347	23	3	14483.1308	22	3
4	1	4	14395.3795	21	3	14486.1095	1	2
4	1	3	14445.0560		1	14535.0402	7	3
4	2	3	14462.7497	17	4	14552.0724	12	2
4	2	2	14478.3493	12	2	14569.3897	1	3
4	3	2	14532.1947	52	2	14625.1578	0	2
4	3	1	14532.9298		1	14625.8542	1	3
4	4	1	14614.4146	9	3	14700.0198	56	2
4	4	0	14612.9837	15	2	14700.1157	14	2
5	0	5	14488.9206	70	3	14578.7011	21	3
5	1	5	14489.5928	26	2	14578.8425	1	3
5	1	4	14560.1010	7	2	14650.3978	46	2
5	2	4	14570.8065		1	14663.4071	8	2
5	2	3	14604.0242	16	2	14694.4529		1
5	3	3				14742.8495	18	3
5	3	2	14649.2840	15	3	14746.0662		1
5	4	2	14729.9790		1	14814.5346	6	3
5	4	1	14725.9840	10	3	14815.0096		1
5	5	1				14920.6197		1
6	0	6	14600.7755	0	2	14691.2101	16	3
6	1	6	14601.1513	12	2	14691.3096		1
6	1	5				14782.6683	20	2
6	2	5	14697.9909	2	2			
6	2	4	14750.6261		1	14842.3680	63	3
6	3	4	14782.0104		1	14883.0957		1
6	3	3	14802.0963		1	14892.3877	27	3
6	4	3	14869.8231	15	2	14952.4420	5	2
6	4	2	14862.3144		1	14954.5256	16	3
6	5	1				15058.8015		1
6	6	0				15185.2688		1
7	0	7	14729.6894		1	14820.7780	4	2
7	1	7				14821.3230	9	2
7	1	6				14931.1109		1
7	2	6				14931.6760	2	2
7	2	5	14918.2196		1			
7	3	5	14933.6375		1	15047.5328		1
7	3	4				15065.0979		1
7	4	4				15113.4463	38	2
7	4	3	15021.0019		1			

Table 6.10: Continued.

J	K_a	K_c	(202) or 31^+0	Δ	no.	(103) or 31^-0	Δ	no.
8	0	8	14875.2877		1	14967.2701	20	2
8	1	8	14875.9565		1	14967.3069		1
8	1	7				15095.9865	3	2
8	2	6				15196.7908		1
8	3	5				15261.9776		1
9	0	9				15130.9364		1
9	1	9				15130.9443		1
10	0	10				15311.6181	52	2

6.3.3 Discussion and Conclusions

In my first analysis of the ^{18}O spectrum using the PS linelist, many transitions were incorrectly assigned because the intensities were not considered carefully when making assignments. Strong emphasis was put on the transition wavenumbers, using the very small error in wavenumbers to search for the theoretical lines matching the experimental line, and less emphasis on the intensities. This caused some strong lines assigned to weak theoretical lines and vice versa. In the re-analysis with the newly calculated linelist, both wavenumbers and intensities were fully taken into account to make assignments.

Table 6.11 gives the comparison of strong transitions observed in the PS linelist and the new linelist used in this work. The table shows both PS and this work gives good predictions of transition wavenumbers in all vibrational levels compared. Although the line positions are accurately predicted, the newly calculated linelist exhibits somewhat higher intensities for bending states due to the problem with the *ab initio* DMS. This overestimation of intensities is apparent in Figure 6.3 especially in 12500 cm^{-1} region, however, for 14000 – 15000 cm^{-1} region the PS linelist seems to be less reliable than mine (see Figure 6.2).

The natural abundance spectrum of pure water vapour by Schermaul *et al.* [21] contained some transitions due to $H_2{}^{18}O$. These transitions are compared to the ones analysed in this work. More than half of the transitions, indeed 19 out of 32, are found to have the same assignments. Six transitions seem to disagree, of which two are due to wrongly labelled vibrational levels. Seven transitions are not found in the ^{18}O spectrum studied here. The reason may be that those transitions are wrongly attributed to $H_2{}^{18}O$. The transition wavenumbers in both spectra show excellent agreement, with a small systematic difference of 0.005 cm^{-1}. This confirms the unreliability of those seven transitions that were not observed in this work.

A major reason for analysing the ^{18}O spectrum presented here is so that the data can be included in databases for use in atmospheric and other models. HITRAN2000 [33] contained 51 transitions assigned to $H_2{}^{18}O$ by Mandin *et al.* [165] in the region studied here, which are confined to the wavenumber range 13608 – 13893 cm^{-1}. My analysis confirms the assignments given in HITRAN, with some exceptions which are listed below. The upper energy levels of three transitions, at 13641.585, 13788.125 and 13875.953 cm^{-1}, are assigned to 4_{22} (301) but

the vibrational level seems to be mis-labelled and should be replaced by 4_{14} (122). The line at 13847.279 cm^{-1}, which I assign to $3_{13} - 2_{12}$ 301–000 but the assignment in HITRAN is mis-typed. And the transition at 13677.131 cm^{-1} in HITRAN, which are assigned to $4_{14} - 5_{15}$ 301–000, was not observed in this study.

A new version of HITRAN (HITRAN2004) is in preparation and all the experimental transitions analysed in this work have been accepted for inclusion in this edition. Those 51 common lines mentioned previously have all been replaced by the new lines obtained in this work. The spectrum was recorded at temperature of 300.5 K, which is slightly higher than the standard room temperature used in HITRAN (296 K). Since intensities are temperature dependent, which can be seen in the eq. (2.67), they have to be converted to match the HITRAN temperature. The following equation has been derived from the eq. (2.67) for this purpose:

$$I_h = [\frac{Q(T_e)}{Q(T_h)} \cdot \frac{\exp(-\frac{E''}{k/hc\,T_h}) - \exp(-\frac{E'}{k/hc\,T_h})}{\exp(-\frac{E''}{k/hc\,T_e}) - \exp(-\frac{E'}{k/hc\,T_e})}] \cdot I_e \tag{6.8}$$

where $Q(T)$ is the partition function, E'' and E' are the lower and upper energies, and the subscripts e and h indicate experiment and HITRAN respectively. In practice, the terms $exp(-\frac{E'}{kT_{e,h}})$ in numerator and denominator are ignored as they are close to zero at T $\simeq$ 300K in the wavenumber region studied here. The partition function for each temperature is obtained from the HITRAN ftp site (*cfa-ftp.harvard.edu*) where they are given in 1 K intervals from 70 K to 3000 K. To obtain the partition function of 300.5 K, the average of functions of 300 K and 301 K was taken. The following values were used for the intensity conversion: Q(296) = 175.113, Q(300.5) = 179.135 (uncertainties not provided), and k/hc = 0.6950356(12) cm^{-1} K^{-1} (Boltzmann constant). The intensities given in the Appendix (Table A.1) are normalised to the corresponding values at 296 K.

In this work, the spectrum of $H_2{}^{18}O$ enriched water vapour was analysed using two different linelists, PS linelist and the new linelist calculated in this thesis. The first analysis was done with the PS linelist, which lead to the assignments of 746 out of 911 lines. The second analysis using the new linelist improved the assignments to 905 lines, of which 4 lines are identified as belonging to $H_2{}^{16}O$, leaving only 15 lines unassigned. The assignment techniques are well established in this work and can be applied to the analysis of other spectra.

Table 6.11: Comparison of observed strong $H_2{}^{18}O$ lines in the PS linelist and the linelist used in this work. Five strongest transition lines are selected for vibrational bands (221), (400), (301), (202) and (103). "Obs. wn." shows the observed wavenumbers in cm^{-1}, "Obs. int." is the observed intensities in cm $molecule^{-1}$. The observed − calculated values for PS linelist and this work are shown "PS" and "this work" respectively (in cm^{-1}).

upper			lower			vib	Obs. wn.	Obs. int.	PS	this work
6	2	4	5	0	5	221	13888.5317	0.109E-25	0.025	0.100
2	2	0	2	2	1	221	13625.6249	0.102E-25	0.154	0.167
4	0	4	3	0	3	221	13687.8664	0.967E-26	0.165	0.218
5	5	1	5	5	0	221	13669.3433	0.961E-26	−0.071	−0.149
4	1	3	3	1	2	221	13711.7410	0.938E-26	0.184	0.206
8	1	8	7	0	7	400	13900.5087	0.231E-25	—	−0.145
6	2	5	5	1	4	400	13905.4961	0.145E-25	−0.094	−0.117
4	1	4	3	0	3	400	13864.0427	0.112E-25	0.010	−0.063
3	1	3	2	0	2	400	13854.6822	0.109E-25	0.039	−0.076
3	0	3	3	3	0	400	13637.6465	0.102E-25	−0.128	0.094
2	2	0	2	2	1	301	13782.8862	0.871E-25	0.044	−0.133
3	1	3	2	1	2	301	13847.2785	0.866E-25	0.031	−0.111
4	0	4	3	0	3	301	13865.4615	0.852E-25	−0.043	−0.103
2	0	2	1	0	1	301	13837.0634	0.810E-25	0.042	−0.109
5	1	5	4	1	4	301	13873.5146	0.778E-25	−0.144	−0.121
4	4	1	4	3	2	202	14235.1234	0.424E-26	0.003	−0.064
3	2	1	3	1	2	202	14208.4158	0.238E-26	−0.027	0.050
5	4	1	5	3	2	202	14220.2559	0.232E-26	−0.104	−0.076
4	1	4	5	0	5	202	14071.3350	0.221E-26	−0.037	0.055
1	1	0	1	0	1	202	14202.4546	0.218E-26	−0.021	0.075
4	0	4	3	0	3	103	14346.7957	0.167E-25	−0.052	−0.039
3	1	3	2	1	2	103	14328.7232	0.160E-25	0.002	−0.037
2	0	2	1	0	1	103	14318.6448	0.150E-25	0.010	−0.035
2	2	0	2	2	1	103	14262.1167	0.143E-25	0.018	−0.051
5	1	5	4	1	4	103	14355.0145	0.134E-25	-0.120	−0.046

6.4 Assignments of the ^{17}O spectrum

The absolute intensities of ^{17}O spectrum was calculated using the eq. (6.6), which gives:

$$I = 1.4984 \times 10^{-26} \times EW/19.6 \tag{6.9}$$

in cm molecule^{-1}, including the scaling factor for natural abundance. The intensities given in the Appendix (Table A.3) are scaled for natural abundance and normalised at 296 K using the partition functions Q(301) = 1074.801 and Q(296) = 1047.931 (from *cfa-ftp.harvard.edu*, uncertainties not provided).

The ^{17}O spectrum covers the $3\nu + \delta$ and 4ν polyad region, which is next to the spectral region previously studied by Camy-Payret *et al.* [32]. Analysis of the ^{17}O spectrum was made using the calculated $H_2{}^{17}O$ spectrum (see section 5.2). Figure 6.5 shows the comparison of experimental and calculated spectrum in the range 11330 – 14520 cm^{-1}. The intensities of both spectra are scaled to match the natural abundance, however the different scales for intensity axes are used to get a clearer comparison. In the calculated spectrum the first region, $3\nu + \delta$ polyad, is much stronger than the second region, 4ν polyad, but in the experimental spectra these two regions show similar strengths. As the figure shows, the intensities of two spectra agree in $3\nu + \delta$ polyad region but strongly disagree in 4ν region. Figure 6.6 gives the same comparison covering only the 4ν region using similar scales for the intensity axes. The two spectra seem to agree well, although some weak lines in 14000 – 14500 cm^{-1} were not observed experimentally. Comparing Figure 6.5 and 6.6, I found that the intensities of two spectra in the $3\nu + \delta$ region strongly disagree. The possible reasons may be the overestimation of bending mode strengths in the calculated spectrum caused by the *ab initio* DMS used and incorrect derivations of the experimental intensities. Two separate experimental runs, one for $3\nu + \delta$ and the other for 4ν polyad, are combined in this work for analysis. Two spectrum were measured in very similar conditions (see section 6.1) and the intensities of each spectrum were calculated according to its condition. The derivation of the intensities was thoroughly checked and no mistake could be found.

In order to see the effect of the *ab initio* DMS on the calculated intensities, Figure 6.7 was plotted using the $H_2{}^{16}O$ lines taken from the HITRAN2000 database [33]. The intensities for $3\nu + \delta$ and 4ν polyad are in fact similar in this figure, suggesting that there is a severe

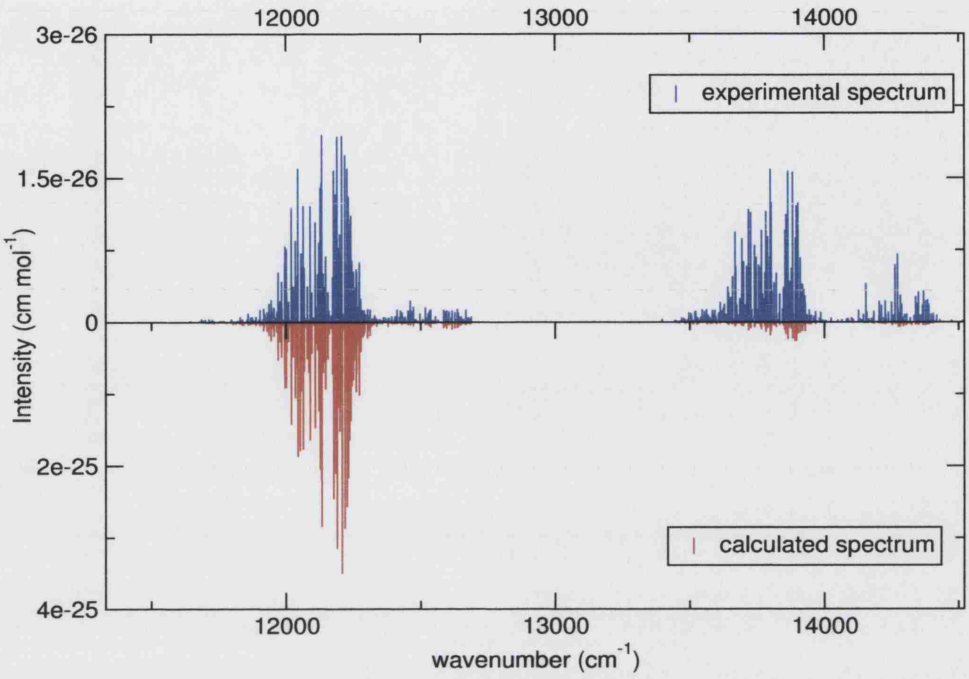

Figure 6.5: Comparison of experimental $H_2{}^{17}O$ spectrum with the calculated spectrum in the range 11330 – 14520 cm^{-1}. The intensities of experimental and calculated spectrum are scaled for the natural abundance of $H_2{}^{17}O$.

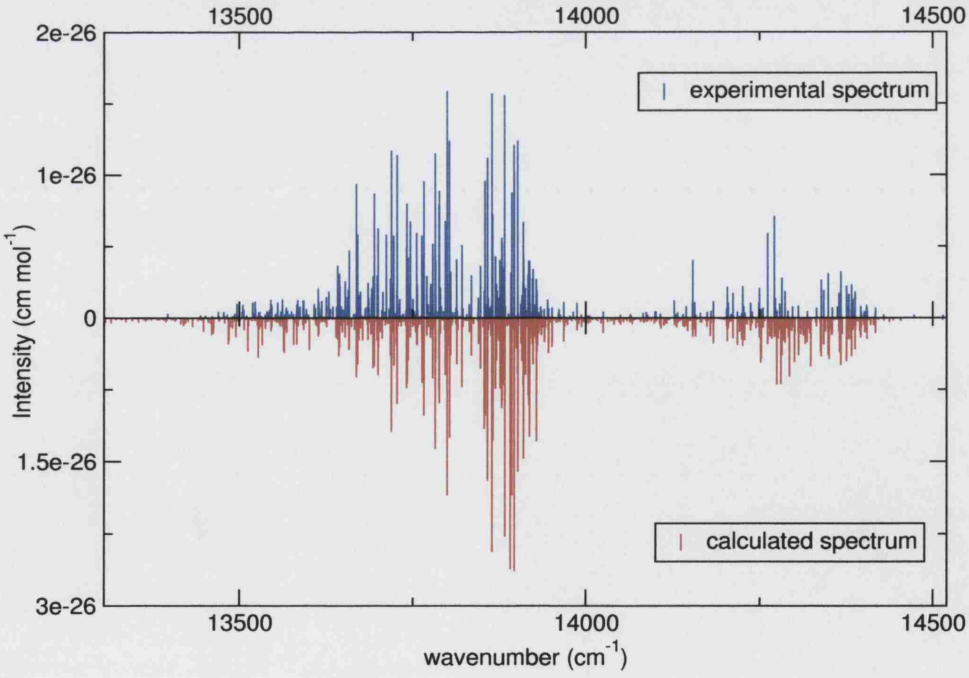

Figure 6.6: Comparison of experimental $H_2{}^{17}O$ spectrum with the calculated spectrum in the range 13330 – 14520 cm^{-1}. The 4ν polyad of the above graph is shown using different scales in the intensity axes.

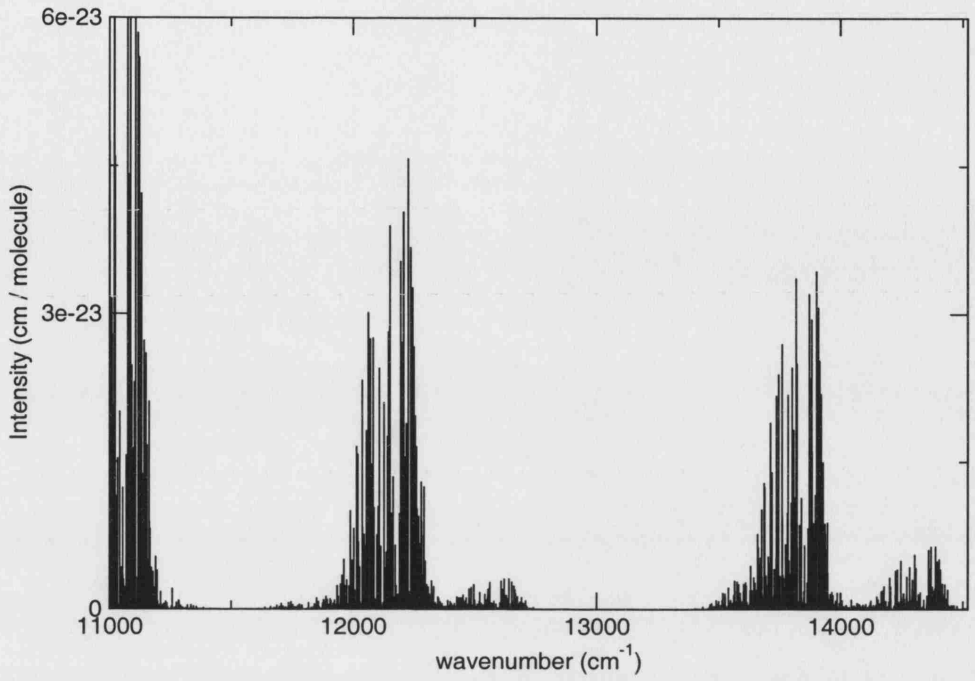

Figure 6.7: Spectrum of $H_2{}^{16}O$ in the range 11000 – 14520 cm^{-1}. The data was taken from the HITRAN2000 [33].

overestimation of the intensity for the bending mode in the calculated spectrum. For making assignments, the calculated intensities of two polyad regions should be scaled differently to match the experimental spectrum. This could be done by selecting a few strongest experimental lines in each region and comparing them with the calculated lines to get the ratios of intensities.

In this work, I assigned 823 lines out of 845 lines attributed to $H_2{}^{17}O$, leaving only 22 lines unassigned. Assignments were first made by following the procedure established in the earlier work (see subsection 6.2.1) using the calculated $H_2{}^{17}O$ spectrum. Those assignments were later re-analysed by O. Naumenko (private communication) using the linelist generated by Tashkun (see subsection 6.3.2) to obtain the best assignments. Table 6.12 gives the summary of the observed energy levels determined in this work. All the lines originate in the (000) ground vibrational level and are assigned to 15 different upper vibrational levels. Band origins of (131), (211), (013), (221), (301) and (103) are newly observed at 11792.827, 12132.993, 12541.226, 13631.500, 13812.158 and 14296.280 cm^{-1}, respectively. As was recognised in the analysis of the ^{18}O spectrum, the ratios of $H_2{}^{17}O$ to $H_2{}^{16}O$ energy levels were constant within the vibrational levels. Also the systematic differences in observed and calculated en-

Table 6.12: Summary of $H_2{}^{17}O$ energy levels determined with the newly calculated linelist. Bands are labelled using normal mode (left) and local mode (right) notations. No. of levels shows the number of newly determined energy levels. No. of trans. shows the number of transitions to the vibrational bands. Uncertainties of the band origins are estimated to be 0.3×10^{-2} cm^{-1} by taking the average of the uncertainties of energy levels determined by more than one transitions.

Band	Origin (cm^{-1})	No. of levels	No. of trans.
(003) or 21^-0	—	1	1
(131) or 10^-3	11792.827	31	47
(310) or 30^+1	—	25	35
(211) or 30^-1	12132.993	77	189
(112) or 21^+1		45	45
(013) or 21^-1	12541.226	38	65
(141) or 20^+4	—	1	1
(320) or 30^+2	—	3	5
(221) or 30^-2	13631.500	46	100
(042) or 11 4	—	1	1
(400) or 40^+0		31	55
(301) or 40^-0	13812.158	74	192
(202) or 31^+0	—	13	19
(103) or 31^-0	14296.280	35	65
(071) or 10^-7	—	2	3
	Total	**402**	**823**

ergy levels were seen, which helped to check the validity of the energy levels derived. Many levels were confirmed by combination differences, especially those in (211) and (301) vibrational states, which makes the derived energy levels much more reliable. Table 6.13 gives the newly determined energy levels of the $3\nu + \delta$ polyad, (131), (310), (112), (211) and (013) and Table 6.14 gives the energy levels of the 4ν polyad, (221), (400), (301), (202) and (103). The number of lines assigned to each level is also given in those tables. I noticed that not many transitions belonging to the (400) and (202) vibrational states were observed compared to $H_2{}^{18}O$. Large number of lines are assigned to the (211) and (301) states, which are the strongest bands in $3\nu + \delta$ and $4\ \nu$ polyad respectively.

Table 6.13: $H_2{}^{17}O$ experimental energy levels for $3\nu + \delta$ polyad determined determined using the newly calculated linelist. Energy levels are given in cm^{-1}, and the uncertainties (Δ) are in 10^{-4} cm^{-1}. The levels determined from more than one transitions were averaged and the standard deviations are given as the uncertainties. Uncertainties for the levels determined from a single transition are not given but they are estimated to be 0.3×10^{-2} $cm^{-1}$by taking the average of the uncertainties of energy levels determined by more than one transitions. The number of transitions assigned to each level (no.) are also given below.

J	K_a	K_c	(131) or 30^-2	Δ	no.	(310) or 40^+0	Δ	no.	(112) or 40^-0	Δ	no.
0	0	0	11792.8270		1						
1	0	1	11816.0537		1	12144.9824		1	12411.9340	18	2
1	1	1	11838.4418	5	2	12158.9712	3	2			
1	1	0							12430.9219	19	2
2	0	2	11861.3331	16	2				12456.1601		1
2	1	2				12198.0412	1	2	12465.4507	147	2
2	1	1	11897.1730	5	2						
2	2	1	11962.4996		1	12256.3772	74	2	12522.3828	58	3
2	2	0	11963.6154	23	2						
3	0	3				12252.4503		1	12519.5698	46	3
3	1	3	11938.3818	49	2	12257.6918		1	12524.7876	93	3
3	1	2	11975.0421	62	3	12290.7250		1	12557.8350	7	2
3	2	2	12032.2341	17	3	12324.8421		1	12590.8993	103	2
3	2	1				12330.8805		1	12597.3024		1
3	3	1	12151.8310		1				12671.0575	65	2
3	3	0	12151.9570		1				12671.5166	22	2
4	0	4	12009.8451	2	2				12600.4251	2	2
4	1	4	12016.9164		1	12335.5713		1	12602.6656	8	2
4	1	3	12076.7843	2	2						
4	2	3				12415.0421	76	3	12681.0430	11	2
4	2	2	12138.6551	43	2				12697.7851		1
4	3	2	12246.9012		1	12499.8092		1	12765.0880		1
4	4	0	12402.7287		1	12609.0992		1			
5	0	5				12430.2763		1	12696.9954	55	2
5	1	5				12431.3983		1			
5	1	4							12775.5867	62	2
5	2	4	12237.6980		1	12526.3787	65	3			
5	2	3							12824.4443	171	2
5	3	3	12365.5396		1				12881.8836		1
5	3	2				12621.4338		1			
5	4	2	12521.6251	30	2						
5	5	1	12711.0736		1	12860.9134		1			
5	5	0				12860.9565		1			
6	0	6	12226.1379	91	2				12811.3285		1
6	1	6				12544.7486		1			
6	1	5	12346.8674		1						
6	2	5	12372.0140		1	12653.0895	37	3			
6	3	4				12755.6059		1			
6	3	3	12516.2817		1						
6	4	3	12668.3660	48	2				13130.3224		1
6	5	2				13001.7367		1			
6	5	1	12855.1317		1						
7	0	7							12942.5099		1
7	1	6							13066.5339		1

Table 6.13: Continued.

J	K_a	K_c	(131) or 30^-2	Δ	no.	(310) or 40^+0	Δ	no.	(112) or 40^-0	Δ	no.
7	2	6				12805.9320		1			
7	3	5	12670.6542	32	2	12916.3128		1			
7	4	4	12833.0718		1						
7	5	2	13022.6950		1						
8	3	6				13099.6200		1			
9	3	7							13293.1931		1

J	K_a	K_c	(211) or 31^+0	Δ	no.	(013) or 31^-0	Δ	no.
0	0	0	12132.9926		1	12541.2255		1
1	0	1	12155.5984		1	12564.3523		1
1	1	1	12169.3362	1	2	12576.6252	19	2
1	1	0	12174.8813	4	2	12582.3249		1
2	0	2	12200.7670	8	4	12608.9977	21	2
2	1	2	12209.3528	11	3	12617.1894		1
2	1	1	12225.9269	1	2	12634.2644	19	3
2	2	1	12266.2846	1	2	12670.6950		1
2	2	0	12267.6658	14	3	12672.2563	64	2
3	0	3	12263.6774	16	3	12672.9042	78	2
3	1	3	12268.6267	10	4	12677.1228	25	2
3	1	2	12301.3584	8	3	12710.8800		1
3	2	2	12334.6017	3	4	12740.1756	21	3
3	2	1	12340.9859	7	4	12747.3071	1	2
3	3	1	12415.2616	5	2	12814.6859	29	2
3	3	0	12415.4868	2	2	12814.9707		1
4	0	4	12344.1671	14	3	12753.4093	13	2
4	1	4	12346.5119	2	3	12755.6796	2	2
4	1	3	12399.5286	2	3	12810.2971	116	2
4	2	3	12424.5479	1	4			
4	2	2	12441.1762	88	5	12849.6845	8	2
4	3	2	12508.6554	3	3			
4	3	1	12510.1495	6	4	12912.0019	21	2
4	4	1	12616.3927	107	2			
4	4	0	12616.4180	5	2	13008.4913	16	2
5	0	5	12441.4249	5	3	12851.1988		1
5	1	5	12442.4230	9	3	12852.3327	65	3
5	1	4	12517.8863	9	3	12929.9133	50	2
5	2	4	12535.3605	7	4	12943.3543	66	3
5	2	3	12567.5903	29	3			
5	3	3	12625.1817	63	3	13029.0456	33	3
5	3	2	12630.5907	9	2			
5	4	2	12733.6258		2	13131.3836		1
5	4	1	12733.8941	22	3			
5	5	1	12868.9415		1	13250.3335		1
6	0	6	12555.5284	84	3	12965.8737	39	2
6	1	6	12555.9686	3	2			
6	1	5	12658.9386	41	4	13067.1649	3	2
6	2	5	12662.1023		1			
6	2	4	12718.4670	32	4	13131.2210		1
6	3	4	12764.1664	51	3			
6	3	3	12778.0408	4	4	13186.7117		1

Table 6.13: Continued.

J	K_a	K_c	(211) or 31^+0	Δ	no.	(013) or 31^-0	Δ	no.
6	4	3	12874.5182	82	2			
6	4	2	12875.7361	138	5			
6	5	2	13009.9996		1			
6	5	1	13010.0119	53	2	13392.3455		1
6	6	0	13175.3684		1			
7	0	7	12686.6444		1			
7	1	7	12687.1818	73	3	13097.7781	10	2
7	1	6	12811.8811	7	2			
7	2	6	12813.5677	19	4	13226.4309		1
7	2	5	12891.4722		1			
7	3	5	12924.6604	6	3			
7	3	4	12952.6081	59	2			
7	4	4	13038.7866	48	3			
7	5	3	13174.6700	31	2			
7	6	2	13339.9786		1			
7	7	1	13463.0968		1			
8	0	8	12835.2843	17	2	13246.7796		1
8	1	8	12834.2447	98	3			
8	1	7	12979.8316	96	2	13390.7644		1
8	2	7	12981.2561	6	2			
8	2	6	13083.8433	3	2			
8	3	5	13152.8584	104	3			
8	4	4	13236.1303		1			
8	5	3	13363.6235	104	2			
9	0	9	12999.1309		1			
9	1	9	12999.8610	1	2			
9	1	8	13166.3908		1			
9	2	8	13166.4592	29	2			
9	3	6	13376.2800		1			
9	4	6	13435.8965		1			
10	0	10	13181.6211	10	2			
10	1	10	13181.5762		1			
10	1	9	13365.2113		1			
10	2	9	13368.7393		1			
10	2	8	13524.2799		1			
10	3	7	13618.9376		1			
10	4	6	13703.5978		1			
11	1	11	13380.8360		1			
11	2	10	13586.3256		1			

Table 6.14: $H_2{}^{17}O$ experimental energy levels for 4ν polyad determined determined using the newly calculated linelist. Energy levels are given in cm^{-1}, and the uncertainties (Δ) are in 10^{-4} cm^{-1}. The levels determined from more than one transitions were averaged and the standard deviations are given as the uncertainties. Uncertainties for the levels determined from a single transition are not given but they are estimated to be 0.3×10^{-2} $cm^{-1}$by taking the average of the uncertainties of energy levels determined by more than one transitions. The number of transitions assigned to each level (no.) are also given below.

J	K_a	K_c	(221) or 30^-2	Δ	no.	(400) or 40^+0	Δ	no.	(301) or 40^-0	Δ	no.
0	0	0	13631.4998		1				13812.1581		1
1	0	1	13654.2642	16	2	13832.0822		1	13834.4868	2	2
1	1	1	13670.9894	22	2				13845.2106	2	2
1	1	0	13676.8512	102	2				13850.3361	31	2
2	0	2	13698.3033	1	2	13875.3762		1	13877.9188	126	3
2	1	2	13710.8775	25	2	13882.6000	63	2	13884.7502	2	3
2	1	1	13728.2833	10	3				13900.0868	11	4
2	2	1	13777.3865	12	2	13930.0874	27	2	13932.2834	13	2
2	2	0	13778.6777	29	2				13933.7251	107	3
3	0	3	13762.7558	12	2	13937.3000		1	13939.1615	5	3
3	1	3	13769.5453	37	3	13941.4661	30	3	13943.3478	9	4
3	1	2	13804.3964	70	2	13971.2770		1	13973.5643	8	3
3	2	2	13845.8696	116	3	13997.1913	24	2	13999.2750	12	4
3	2	1	13851.8891	22	3				14005.7926	6	3
3	3	1	13940.4279	66	4				14066.1348	1	2
3	3	0	13940.6957	22	3				14066.3992	24	2
4	0	4	13843.3683	16	2	14016.2968	144	2	14018.9488	24	4
4	1	4	13847.0242	82	2	14017.3155		1	14020.0155	8	3
4	1	3	13903.7095	69	4	14066.9301		1	14069.1084	36	4
4	2	3	13936.4372		1	14085.4137	13	2	14087.3319	6	4
4	2	2	13952.1476	28	3				14104.0135	6	4
4	3	2	14034.0933	39	3	14155.8038	94	3	14157.7875	19	3
4	3	1	14035.2100	2	2				14159.5107	41	4
4	4	1	14158.7317		1	14246.2406		1	14248.2433	16	2
4	4	0	14158.7618	9	2				14248.2803	12	2
5	0	5	13940.6331		1	14111.9169	57	2	14114.3492	47	3
5	1	5	13942.4014	97	3				14114.6857	11	2
5	1	4	14024.0463	28	2	14182.4381	5	2	14184.3826	10	3
5	2	4	14044.4375		1	14193.8149	89	2	14195.5210	19	4
5	2	3	14079.0616	1	2	14225.1621	70	2	14227.4520	16	4
5	3	3	14150.7493	34	3				14272.0880	6	4
5	3	2				14276.1663	61	4	14278.2068	32	3
5	4	2							14363.4819	53	4
5	4	1	14276.2372		1	14361.8791		1	14363.8161	33	2
5	5	1							14483.4614	39	2
6	0	6	14054.3897	19	2	14225.0239		1	14226.2142	51	4
6	1	6	14055.3348	5	2				14227.0428	5	2
6	1	5	14163.5847		1	14315.6531		1	14317.3842	49	4
6	2	5	14176.1235		1	14321.5460	46	4	14322.9211	70	3
6	2	4	14231.9413	27	4				14374.0987	27	4
6	3	4				14406.5968	49	6	14408.2357	21	2
6	3	3	14301.2455	48	3	14421.3248		1	14423.5510	49	5
6	4	3				14500.1621		1	14502.0563	48	3
6	4	2	14417.9574	91	3				14503.5418	41	3

Table 6.14: Continued.

J	K_a	K_c	(221) or 30^-2	Δ	no.	(400) or 40^+0	Δ	no.	(301) or 40^-0	Δ	no.
6	5	1	14623.1371		1				14565.4267	74	3
6	6	0	14657.6201		1				14724.6010		1
7	0	7							14356.0059	2	2
7	1	7	14186.2854	45	2				14356.0166	3	3
7	1	6				14460.9097		1	14467.5783	81	3
7	2	6	14325.9349		1	14463.7052		1	14468.2797	38	2
7	2	5				14538.8675		1	14541.4606	34	3
7	3	5	14451.0921		1	14563.6204		1	14565.4924	53	3
7	3	4							14595.2907	53	2
7	4	4	14581.5782		1				14663.6429		1
7	4	3							14668.4256		1
7	5	3	14786.2136		1				14728.5412	2	2
7	6	2							14885.7617		1
8	0	8	14333.1480		1				14502.3917	113	3
8	1	8							14502.4304		1
8	1	7	14491.3829		1				14631.7914	14	3
8	2	7							14632.2455	39	2
8	2	6							14727.0458	84	2
8	3	6	14632.4765		1	14741.2305		1	14742.5394	79	2
8	3	5							14791.5588	60	3
8	4	4							14859.7879		1
9	0	9							14665.8194		1
9	1	9							14665.9263	5	2
9	1	8							14813.1795	103	2
9	2	8	14679.5280		1				14813.3265		1
9	3	7							14938.8225		1
9	4	6							15053.7963		1
10	0	10							14846.2066	21	2
10	1	10							14846.1965		1
10	1	9	14887.3177		1				15011.5292	58	2
10	2	9							15011.5906		1

J	K_a	K_c	(202) or 31^+0	Δ	no.	(103) or 31^-0	Δ	no.
0	0	0				14296.2795		1
1	0	1	14225.9041		1	14318.8785	76	2
1	1	1				14328.8804	24	2
1	1	0	14241.9308		1	14334.1611	18	2
2	0	2				14362.4255	17	2
2	1	2	14276.2847	40	2	14368.8583	38	3
2	1	1	14291.7384	57	2	14384.6451	20	3
2	2	1				14414.4601	12	2
2	2	0				14416.0613	7	2
3	0	3	14330.9227	51	3	14424.4517		1
3	1	3				14427.9272	24	3
3	1	2	14365.3140	30	2			0
3	2	2				14482.7874	103	3
3	2	1	14397.4700		1	14489.7984	1	2
3	3	1				14545.4210	109	2
3	3	0						
4	0	4				14503.4441		1
4	1	4	14411.4056	9	2	14505.9555	43	2

Table 6.14: Continued.

J	K_a	K_c	(202) or 31^+0	Δ	no.	(103) or 31^-0	Δ	no.
4	1	3				14555.3207	1	2
4	2	3				14572.5421		1
4	2	2				14589.8338	5	3
4	3	1				14645.5994	90	2
4	4	1	14633.9099		1			
4	4	0				14722.2256		1
5	0	5				14599.2170	37	2
5	1	5				14599.2452	10	2
5	1	4				14670.8963	81	2
5	2	4				14683.4617	9	2
5	2	3	14620.3715		1	14714.9744		1
5	3	3				14762.5942		1
5	4	1	14745.6150		1			
6	0	6				14711.9508	16	2
6	1	6				14712.0534		1
6	1	5				14803.4604	9	2
6	2	4				14863.0522	79	2
6	3	3	14820.1068		1			
6	5	2	15009.2314		1			
7	0	7				14841.6965		1
7	1	7				14841.5538	8	2
7	2	6				14952.6422		1
7	2	5				15031.1727		1
8	0	8				14988.5684		1

6.4.1 Discussion and Conclusions

The spectrum of isotopically enriched $H_2{}^{17}O$ water vapour covering the $3\nu + \delta$ and 4ν polyad was analysed in this work. The original experimental spectrum contained a significant number of lines belonging to $H_2{}^{16}O$ and $H_2{}^{18}O$ because of high concentrations of those isotopologues in the sample. A great deal of time was spent to attribute each line to an appropriate water isotopologue. There were nearly 4000 lines observed between 11335 – 14520 cm^{-1}, of which 845 lines were attributed to $H_2{}^{17}O$.

The problem with the *ab initio* DMS used in the calculation of the linelist (see section 2.12) caused the severe overestimation of intensities in the $3\nu + \delta$ polyad. The severity of overestimation was less apparent in the previous ^{18}O analysis because the spectrum covered only the higher end of the polyad. The ^{17}O spectrum, on the other hand, covers the entire $3\nu + \delta$ polyad and gave a clear picture to this problem. It is estimated that the calculated intensities in this polyad region are about 15 times stronger than the experimentally observed values.

In this work, the spectrum of $H_2{}^{17}O$ water vapour was analysed and 823 out of 845 lines were assigned in the range of 11335 – 14520 cm^{-1}. The highest wavenumber listed for $H_2{}^{17}O$ in the HITRAN2000 is 11143 cm^{-1}, which is considerably low compared to that for $H_2{}^{16}O$ and $H_2{}^{18}O$. Unlike the $H_2{}^{18}O$ lines analysed in the previous section, the $H_2{}^{17}O$ lines analysed here will not be included in the next edition of the HITRAN because this work was completed when the preparation for the next HITRAN was well under way. The results presented in this thesis, however, should be included in the HITRAN in the near future as the line assignments given here show high reliabilities.

Chapter 7

Analysis of Cavity Ring-Down Spectra of $H_2{}^{18}O$ and $H_2{}^{17}O$

M. Sneep and W. Ubachs at the Vrije Universiteit (Amsterdam, the Netherlands) recorded absorption spectra of $H_2{}^{18}O$ and $H_2{}^{17}O$ water vapour in 16570 – 17125 cm^{-1} range using the cavity ring-down spectroscopy (CRDS). The spectra cover the entire 5ν polyad, which lies in a window used for the remote sensing [49] and the highest wavenumber region analysed to date for $H_2{}^{18}O$. Earlier, Naus *et al.* [16] studied the same wavenumber region for natural abundance water using the same CRDS technique. This work concentrated on $H_2{}^{16}O$ lines but also tentatively identifies some transitions due to $H_2{}^{18}O$.

In this work, I have first analysed the $H_2{}^{18}O$ spectrum using the newly calculated linelist presented in Chapter 5 and assigned 375 out of 596 lines identified as belonging to $H_2{}^{18}O$. I then analysed the $H_2{}^{17}O$ spectrum using the calculated $H_2{}^{17}O$ linelist and assigned 261 out of 375 lines attributed to $H_2{}^{17}O$. In this chapter, the analyses of two spectra will be presented.

7.1 Analysis of the $H_2{}^{18}O$ spectrum

7.1.1 Experimental Details

The following details were supplied by M. Sneep (private communication) who carried out the measurement of the $H_2{}^{18}O$ spectrum using the CRDS.

Wavelength tunable laser pulses with a bandwidth of $\sim$ 0.06 cm^{-1}, produced by a Nd:YAG pumped dye laser system (Quanta Ray PDL-3) were used in a generic pulsed CRD experiment. The ring-down cell was 86.5 cm long and a single mirror set, with reflectivities varying between 99.97 % near 16500 cm^{-1} and 99.995 % near 17000 cm^{-1}, was used over the entire wavelength range. The radius of curvature of the mirrors is 1 m, and the stable cavity was aligned such that the statistics on the weighted residuals of a least squares fit were fully explained by contributions from Gaussian noise caused by the electronics and Poisson noise caused by the photon shot noise [133].

Before starting the measurements, the cell was heated to about 60 °C and flushed with dry nitrogen to remove as much of the natural water vapour from the cell as possible, without risk of damage to the mirrors. The liquid isotope enriched water — Euriso-top 96.5 % atom ^{18}O, 0.6 % atom ^{17}O, 2.9 % atom ^{16}O — was injected into the cavity while flushing the opening with a continuous dry nitrogen flow. The cell was then closed and partly evacuated, and several hours was allowed for the pressure to stabilise. In order not to loose isotopically enriched water, part of the dry nitrogen was left in the cell. The temperature in the cell was measured and the partial water vapour density in the cell was calculated assuming saturation density. The partial water vapour pressure at the set temperature corresponds to 24 mbar. To avoid condensation on the mirrors, the mirror-mounts were gently heated.

Data points were taken at a step size of 0.008 cm^{-1} with averaging of five laser pulses at each laser frequency. The decay transients were detected using a photomultiplier tube, fed into a digital storage oscilloscope and then transferred to a computer where a least squares fitting routine was used to estimate the decay rates. This fitting routine is the same as the one used in aligning the cavity. These decay rates contain both the water vapour absorption spectrum and a background signal caused by the losses of the empty cavity; this smooth background was subtracted from the spectrum before analysing the resonance features. By recording an iodine spectrum simultaneously with the cavity ring-down spectrum a wavenumber calibration was obtained by comparing and interpolating the iodine spectrum against a reference atlas [166].

The spectra were searched by a computer program for possible locations of resonance features. A Voigt profile was then fitted to each of these candidate locations, yielding the central wavenumber, line width and intensity. The entire spectrum was visually inspected to ensure

that all the fitted features were actual lines. Given the step size, the laser bandwidth and the width of the fitted lines, the one standard deviation uncertainty on the central wavenumber is estimated to be $0.01\,cm^{-1}$. The integrated line intensities, before corrections associated with $H_2{}^{16}O$ contamination in the sample, were calculated using the fitted line parameters. Several uncertainty contributions can be distinguished in cavity ring down spectroscopy: statistical effects, on the order of a few per cent in this experiment, a systematic underestimated absorption cross section on narrow band absorbers [135] and saturation effects related to non-exponential decay in the ring down transients of the strongest lines. An additional uncertainty that is specific for this experiment is the uncertainty in the isotopic content of the ring-down cell. An estimate of the isotope ratio of $H_2{}^{16}O$ and $H_2{}^{18}O$ is given below, but a few per cent uncertainty must be added to the uncertainty budget. The total uncertainty on the line intensities is estimated to be 15 %.

Despite best efforts to avoid contamination of the isotope enriched sample, several lines of $H_2{}^{16}O$ were visible in the measured spectrum. To weed out these $H_2{}^{16}O$ lines and identify which lines are $H_2{}^{18}O$ lines, we compared our new spectrum with the previously measured spectrum by Naus, by plotting both in a single graph and manually assigning each line to either $H_2{}^{16}O$ or $H_2{}^{18}O$; see figure 7.1 for a short section of both spectra. In figure 7.1 the vertical axes are given in terms of a cross section per molecule. From the integrated intensity ratio of the $H_2{}^{16}O$ lines in both spectra, the isotope ratio in the spectra can be estimated. Using this approach yields a $H_2{}^{16}O$ contamination of about 10 %. The integrated line intensities in the full spectrum are corrected for the isotope ratio in the cell.

The comparison between the measurements on the two isotopes clearly shows that the $H_2{}^{18}O$ lines are broader than the $H_2{}^{16}O$ lines, the difference being caused by the pressure conditions during the measurements. The FWHM of the lines is $\sim 0.13\,cm^{-1}$ after fitting the lines to a Voigt profile. This broadening beyond the laser linewidth of $0.06\,cm^{-1}$ is a result of collision broadening. Doppler broadening and self broadening at 24 mbar of water vapour yields a width of $0.09\,cm^{-1}$, the remainder of the broadening is attributed to nitrogen left behind in the cell during partial evacuation. The integrated intensities should be unaffected by the collisional broadening, and since the cell was saturated with water vapour, the density of the water vapour is known.

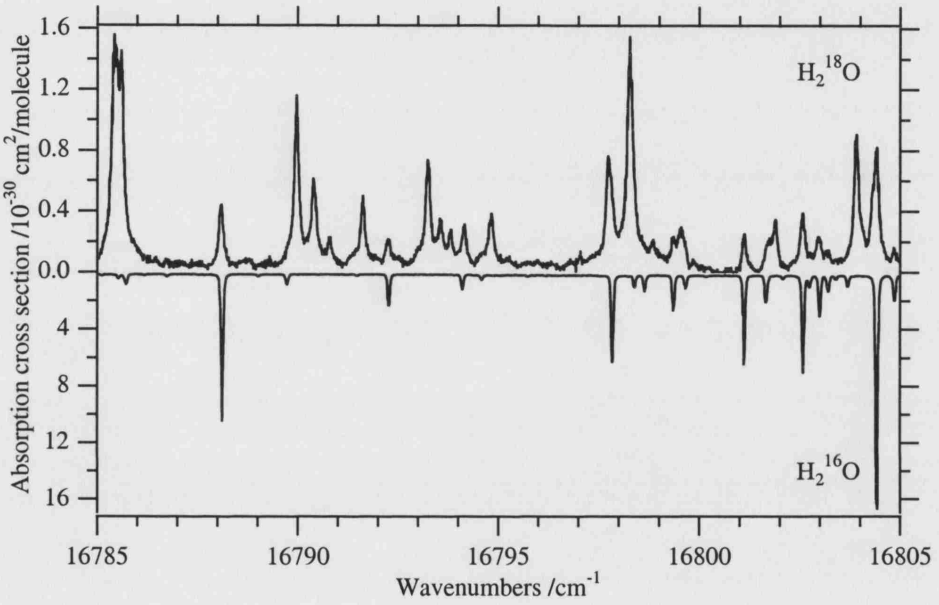

Figure 7.1: A portion of the measured spectrum in $H_2{}^{18}O$ enriched water (top), compared with the natural water vapour spectrum previously measured by Naus *et al.* [16] (bottom). Lines only present in the top graph are $H_2{}^{18}O$ lines. The pressure at which the top graph was measured was 24 mbar, while the bottom graph was measured at about 16 mbar. The vertical axis in the top graph is a cross section per molecule $H_2{}^{18}O$, the lines of $H_2{}^{16}O$ in this graph are scaled with the isotope ratio. The figure is provided by M. Sneep (private communication).

7.1.2 Assignment Results

Absolute intensities in HITRAN unit (cm molecule^{-1}) were calculated using an approximated Voigt profile, which is created by a linear combination of a Gaussian and a Lorentzian profile. The intensity is obtained as a linear combination of Gaussian and Lorentzian intensities with ratio decided by the damping parameter b, such that:

$$I = h \times \Gamma \times \frac{1}{c\rho} \times [(1-b)\frac{\pi}{2} + b\frac{\sqrt{\pi}}{2\sqrt{\ln 2}}] \tag{7.1}$$

where h is the line profile height (in s^{-1}), Γ is the FWHM of the profile (in cm^{-1}), c is the speed of light (3×10^{10} cm s^{-1}), ρ is the density (5.91×10^{17} cm^{-3}) and b is the fraction of Gauss in the Voigt profile used in the fit. Eq. (7.1) can be rewritten as;

$$I = A \times 5.640 \times 10^{-29} \tag{7.2}$$

where A, the fit area (in cm^{-1} s^{-1}), is $h \times \Gamma \times [(1-b)\frac{\pi}{2} + b\frac{\sqrt{\pi}}{2\sqrt{\ln 2}}]$, which is determined by the experimental spectrum. For HITRAN, intensities should be scaled to natural abundance of $H_2{}^{18}O$. The natural abundance of $H_2{}^{18}O$ according to HITRAN [33] is 0.199983 %. In this experiment, the sample contained 96.5 % of $H_2{}^{18}O$ but the contamination of $H_2{}^{16}O$ is estimated to about 10 %, this leaves about 90 % of $H_2{}^{18}O$ present in the sample. The scaling factor of intensities would be 0.199983 / 90. Eq. (7.2) changes to:

$$I = A \times 1.25 \times 10^{-31} \tag{7.3}$$

The intensities given in the Appendix (Table A.2) are scaled to the natural abundance.

The assignments were carried out using the newly calculated linelist presented in Chapter 5. One of the motivations for calculating the new linelist was to analyse this experimental spectrum. The PS linelist [42] does not contain many transitions in this region and the uncertainties in wavenumbers are often large. Figure 7.2 shows the comparison of the measured $H_2{}^{18}O$ spectrum with the calculated spectrum. In the figure, disagreements in intensity can be seen in some regions, particularly in the 16900 – 17000 cm^{-1} range. There are two possible causes for this, i) the underestimation of intensity in the cavity ring-down spectrum, ii) the overestimation of intensity for bending modes due to the problem in the *ab initio* DMS, which was discussed previously. Unlike FTS spectrum, less reliance could be placed on intensities when making the assignments.

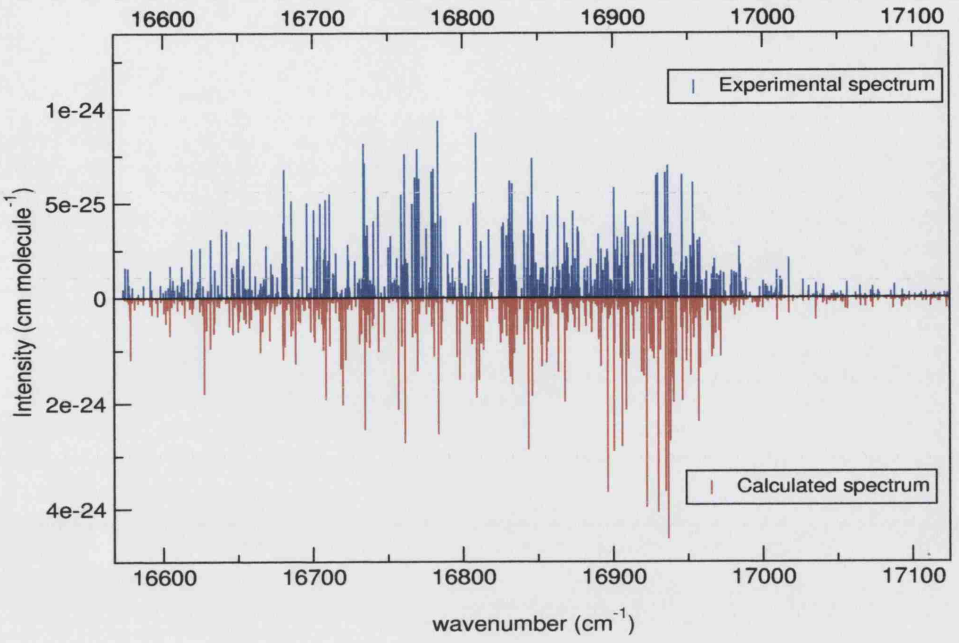

Figure 7.2: Overview of the $H_2{}^{18}O$ experimental spectrum and the calculated spectrum in the 5ν polyad region.

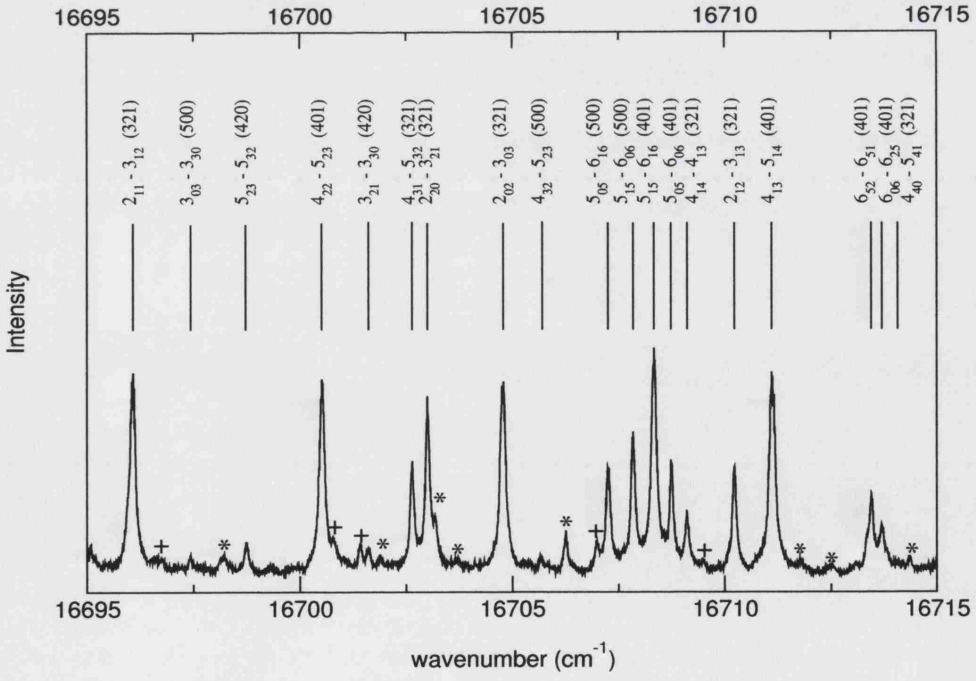

Figure 7.3: Experimental spectrum in the 16695 – 16715 cm^{-1} range with the assignments. * indicates $H_2{}^{16}O$ lines and + indicates unassigned $H_2{}^{18}O$ lines.

Table 7.1: Summary of $H_2{}^{18}O$ energy levels determined in this study. Bands are labelled using normal mode (left) and local mode (right) notations. No. of levels shows the number of newly determined energy levels. No. of trans. shows the number of transitions to the vibrational bands.

Band	Origin (cm^{-1})	No. of levels	No. of trans.
(340) or $30^{+}4$	—	11	20
(241) or $30^{-}4$	—	7	12
(043) or $21^{-}4$	—	3	3
(142) or $21^{+}4$	—	12	19
(222) or $31^{+}2$	—	9	7
(420) or $40^{+}2$	—	29	39
(321) or $40^{-}2$	16775.381	42	83
(302) or $41^{+}0$	—	1	2
(500) or $50^{+}0$	16854.84	43	80
(401) or $50^{-}0$	16854.991	50	110
	Total	**207**	**375**

We assigned 375 of the 596 lines to 10 different upper vibrational levels. Table 7.1 gives the summary of the result. All transitions originate in the (000) ground vibrational level. Two new vibrational band origins were determined directly by transitions to their 0_{00} states: (321) at 16775.381 cm^{-1} and (401) at 16854.991 cm^{-1}. The band origin for (500) can be estimated to be 16854.84 $\pm$ 0.02 cm^{-1} using the empirically determined levels for this state with $J > 0$ and the systematic uncertainty in our calculations. Estimation of energy levels in this manner has been shown to work well in the past [45]. Table 7.2 shows the newly determined energy levels for (321), (500) and (401) vibrational bands labelled with both normal and local mode notations. Obs − Calc shows the differences between an experimentally determined and the theoretically predicted energy level. The systematic differences in Obs − Calc values were observed in all the vibrational bands. These values were useful to check the reliability of empirically determined energy levels.

Naus *et al.* [16] assigned 6 of their transitions recorded using natural abundance water to $H_2{}^{18}O$. We find one of their lines was previously mis-assigned. The 16761.672 cm^{-1} line was assigned to $3_{13} - 4_{14}$ 401–000 ($H_2{}^{18}O$) but the correct assignment is $5_{24} - 5_{33}$ 142–000 ($H_2{}^{16}O$). The $3_{13} - 4_{14}$ 401–000 ($H_2{}^{18}O$) line lies at 16761.004 cm^{-1}.

Table 7.2: $H_2{}^{18}O$ experimental energy levels for the (321), (500) and (401) vibrational states.Energy levels are given in cm^{-1}, and the uncertainties (Δ) are given in 10^{-4} cm^{-1}. The levels determined from more than one transitions were averaged and the standard deviations are given as the uncertainties. Uncertainties for the levels determined from a single transition are not given but they are estimated to be 0.7×10^{-2} $cm^{-1}$by taking the average of the uncertainties of energy levels determined by more than one transitions. Also given are the number of transitions assigned to each level and observed − calculated values (Obs−Calc).

J	K_a	K_c	(321) or 40^-2	Δ	no.	Obs−Calc	(500) or 50^+0	Δ	no.	Obs−Calc
0	0	0	16775.381		1	0.431				
1	0	1	16797.751	113	2	0.436	16876.838		1	−0.152
1	1	1	16812.558		1	0.176	16887.674	84	2	−0.164
1	1	0	16818.257		1	0.132	16892.781		1	−0.145
2	0	2	16841.104	127	2	0.451	16919.565		1	−0.177
2	1	2	16851.770	127	2	0.410	16926.727	95	3	−0.166
2	1	1	16868.947	120	2	0.405	16941.961		1	−0.187
2	2	1	16912.252		1	−0.042	16975.261		1	−0.297
2	2	0	16913.804	7	2	0.281	16977.073		1	0.126
3	0	3	16903.088	141	2	0.423	16979.733	48	4	−0.070
3	1	3	16905.182	28	2	0.061	16984.457	113	2	−0.148
3	1	2	16943.465	77	2	0.392	17014.705	96	3	−0.145
3	2	2	16979.495	50	3	0.285	17041.940	21	2	−0.114
3	2	1	16986.445	91	2	0.249	17048.278	14	2	−0.104
3	3	1	17115.166	84	2	−0.054	17059.953	28	2	−0.328
3	3	0	17115.365	70	2	−0.085	17060.270	52	3	−0.258
4	0	4	16979.033	70	2	0.384	17058.157		1	−0.181
4	1	4	16983.912		1	−0.020	17060.221		1	−0.196
4	1	3	17040.529	107	3	0.359	17109.231	113	2	−0.165
4	2	3	17067.391		1	0.284	17129.480		2	−0.060
4	2	2	17084.209	102	3	0.275	17145.664	56	2	−0.104
4	3	2	17206.628		1	−0.292	17150.823	98	2	−0.125
4	3	1	17208.361	77	3	−0.065	17152.405	56	2	0.014
4	4	1					17250.003		1	−0.291
4	4	0	17318.857	127	2	0.217	17250.447	84	2	0.112
5	0	5	17076.303		1	0.033	17152.600	68	3	−0.154
5	1	5	17077.137		1	0.403	17152.692	127	2	−0.153
5	1	4	17157.904	130	3	0.310	17223.347		1	−0.232
5	2	4	17175.241	107	3	0.252	17237.120		1	−0.074
5	2	3	17207.731	49	4	0.259	17268.684	63	2	−0.044
5	3	3	17321.491	108	4	0.146	17263.668	116	3	−0.052
5	3	2	17326.788	70	2	−0.012	17269.334	55	3	−0.062
5	4	2	17435.397		1	0.287	17363.369		1	−0.082
5	4	1	17435.068	7	2	−0.256	17363.475	55	3	−0.322
5	5	1	17496.634		1	−0.217	17456.692		2	0.020

Table 7.2: Continued.

J	K_a	K_c	(321) or 40^-2	Δ	no.	Obs−Calc	(500) or 50^+0	Δ	no.	Obs−Calc
5	5	0					17456.703	56	2	0.025
6	1	6					17263.546	14	2	−0.142
6	1	5	17293.138	51	3	0.238	17355.452		1	−0.087
6	2	5					17364.686		1	0.047
6	3	4	17458.118	86	3	−0.012	17399.119	63	2	0.475
6	3	3	17471.645	28	3	−0.019	17411.699		1	0.388
6	4	3					17499.669		1	0.255
6	4	2	17575.652		1	−0.385				
7	1	6					17503.917	84	2	0.237
7	2	6	17447.102		1	0.159				
7	3	5	17616.343	56	2	0.097				
7	3	4	17642.801	91	2		17575.265	80	3	−0.377

J	K_a	K_c	(401) or 50^-0	Δ	no.	Obs−Calc
0	0	0	16854.991		1	−0.259
1	0	1	16877.127	84	2	−0.165
1	1	1	16887.956		1	−0.180
1	1	0	16893.063	35	2	−0.173
2	0	2	16919.869		1	−0.202
2	1	2	16926.995	98	3	−0.166
2	1	1	16942.284	58	3	−0.164
2	2	1	16975.532		1	−0.165
2	2	0	16976.948	62	3	−0.155
3	0	3	16980.198	49	2	−0.117
3	1	3	16984.835	42	2	−0.120
3	1	2	17015.001	7	2	−0.140
3	2	2	17041.964	42	2	−0.162
3	2	1	17048.333		1	−0.171
3	3	1	17061.423	107	4	0.071
3	3	0	17061.659		1	0.060
4	0	4	17058.363		1	−0.147
4	1	4	17060.411	42	2	−0.163
4	1	3	17109.490	123	3	−0.159
4	2	3	17129.345	14	2	−0.145
4	2	2	17145.670	87	4	−0.131
4	3	2	17151.466	115	3	−0.026
4	3	1	17152.249	108	3	−0.057
4	4	1	17250.636		1	−0.259
4	4	0	17250.811		1	−0.060

Table 7.2: Continued.

J	K_a	K_c	(401) or 50^-0	Δ	no.	Obs−Calc
5	0	5	17153.584	30	3	−0.148
5	1	5	17153.671	87	3	−0.150
5	1	4	17223.609	50	3	−0.146
5	2	4	17236.784	55	4	−0.122
5	2	3	17268.425	7	2	−0.110
5	3	3	17264.399	103	4	−0.077
5	3	2	17268.533	106	2	−0.401
5	4	2	17363.554	14	2	−0.343
5	4	1	17363.609	98	2	0.065
5	5	1	17456.947	91	2	−0.004
5	5	0	17456.722		1	−0.236
6	0	6	17264.145	91	2	−0.133
6	1	6	17264.166	141	2	−0.131
6	1	5	17355.477	26	3	−0.102
6	2	5	17363.699	113	2	0.200
6	2	4	17411.992	112	3	−0.122
6	3	4	17399.527	101	5	−0.077
6	3	3	17409.519		1	−0.152
6	4	3	17499.726	28	2	−0.341
6	4	2	17501.234	77	2	−0.374
6	5	2	17593.567	42	2	0.047
6	5	1	17593.561	14	2	−0.023
6	6	0	17726.192		1	−0.215
7	1	7	17391.441	14	2	−0.141
8	0	8	17535.562	21	2	−0.128

7.1.3 Discussion and Conclusions

The $H_2{}^{18}O$ spectrum analysed here will not be included in the next version of HITRAN (HITRAN2004) but it can be in the near future. The CRDS data are not favoured by HITRAN due to unreliability of the absolute intensities, and currently no data by CRDS is compiled in the database. Although the uncertainties in the intensities in this experiment can be as high as 15 %, this is still an acceptable level considering some of the intensities of water lines in HITRAN have more than 20 % uncertainties and HITRAN lacks all data for $H_2{}^{18}O$ above 15000 cm^{-1}. Since this spectrum lies in the visible region where the solar radiation flux peaks, the significance to the atmospheric science is undoubted.

In order to prepare for HITRAN, the absolute intensities need to be normalised to the corresponding values at 296 K. The temperature of this experiment was 294 K. The effect of heating the mirror mount to the sample temperature is considered to be minimal. The intensities are normalised by following the procedure discussed in subsection 6.3.3. The partition function

for 294 K is 173.336 and for 296 K is 175.113 (from *cfa-ftp.harvard.edu*, uncertainties not provided). The intensities given in the Appendix (Table A.2) are scaled for natural abundance and normalised at 296 K.

In this work, the analysis of $H_2{}^{18}O$ spectrum in the range 16570 – 17120 cm^{-1} measured using CRDS has been presented. We assigned 375 out of 596 lines attributed to $H_2{}^{18}O$ using the newly calculated linelist. The wavenumber range analysed in this work is the highest for $H_2{}^{18}O$ to date and the results should be useful for atmospheric and other studies.

7.2 Analysis of the $H_2{}^{17}O$ spectrum

7.2.1 Experimental Details

The experimental procedure and conditions are very similar to the $H_2{}^{18}O$ measurements (see subsection 7.1.1). Isotopic composition of the sample water was: 83.8 % atom ^{17}O, 8.3 % atom ^{16}O and 7.9 % atom ^{18}O. The contamination of $H_2{}^{16}O$ was estimated to be about 10 % and that of $H_2{}^{18}O$ is roughly the same because of the residuals from the sample cell and mirrors, which were used for the previous $H_2{}^{18}O$ measurements. This leaves about 80 % of sample water belonging to $H_2{}^{17}O$, with an estimated error of about 5 %. To eliminate the $H_2{}^{16}O$ and $H_2{}^{17}O$ lines and to identify the lines belonging to $H_2{}^{17}O$, the spectrum of natural abundance water vapour by Naus *et al.* [16] and the $H_2{}^{18}O$ spectrum analysed in the previous section (section 7.1) were plotted with the $H_2{}^{17}O$ spectrum in a single graph. Figure 7.4 shows a portion of the graph with the natural abundance (top), $H_2{}^{17}O$ (middle) and $H_2{}^{18}O$ spectrum (bottom). The $H_2{}^{16}O$ lines are narrower than the $H_2{}^{17}O$ and $H_2{}^{18}O$ lines because of the different pressure conditions used in the experiments. Each line in the $H_2{}^{17}O$ spectrum was manually attributed to $H_2{}^{16}O$, $H_2{}^{17}O$ or $H_2{}^{18}O$ by M. Sneep (private communication). After this procedure, 357 lines are identified as belonging to $H_2{}^{17}O$.

7.2.2 Assignment Results

Absolute intensities (in cm molecule^{-1}) were calculated as follows:

$$I = A \times 3.161 \times 10^{-32} \tag{7.4}$$

where A is the fit area (cm^{-1} s^{-1}) provided in the experimental spectrum. The density of $H_2{}^{17}O$ in the sample was 4.90×10^{17} cm $^{-3}$. Natural abundance of $H_2{}^{17}O$ is 0.0372 % in HITRAN [33], therefore the intensity scaling factor is 0.0372/80. Eq. (7.4) includes the scaling factor. Intensities listed in the Appendix (Table A.4) are scaled to the natural abundance and normalised at 296 K (HITRAN temperature) using the partition function Q(294) = 1037.253 and Q(296) = 1047.931 (from *cfa-ftp.harvard.edu*).

Figure 7.5 shows a comparison of the experimental spectrum with the calculated spectrum. Similar to that of $H_2{}^{18}O$ spectrum, disagreements in intensities are observed throughout due to

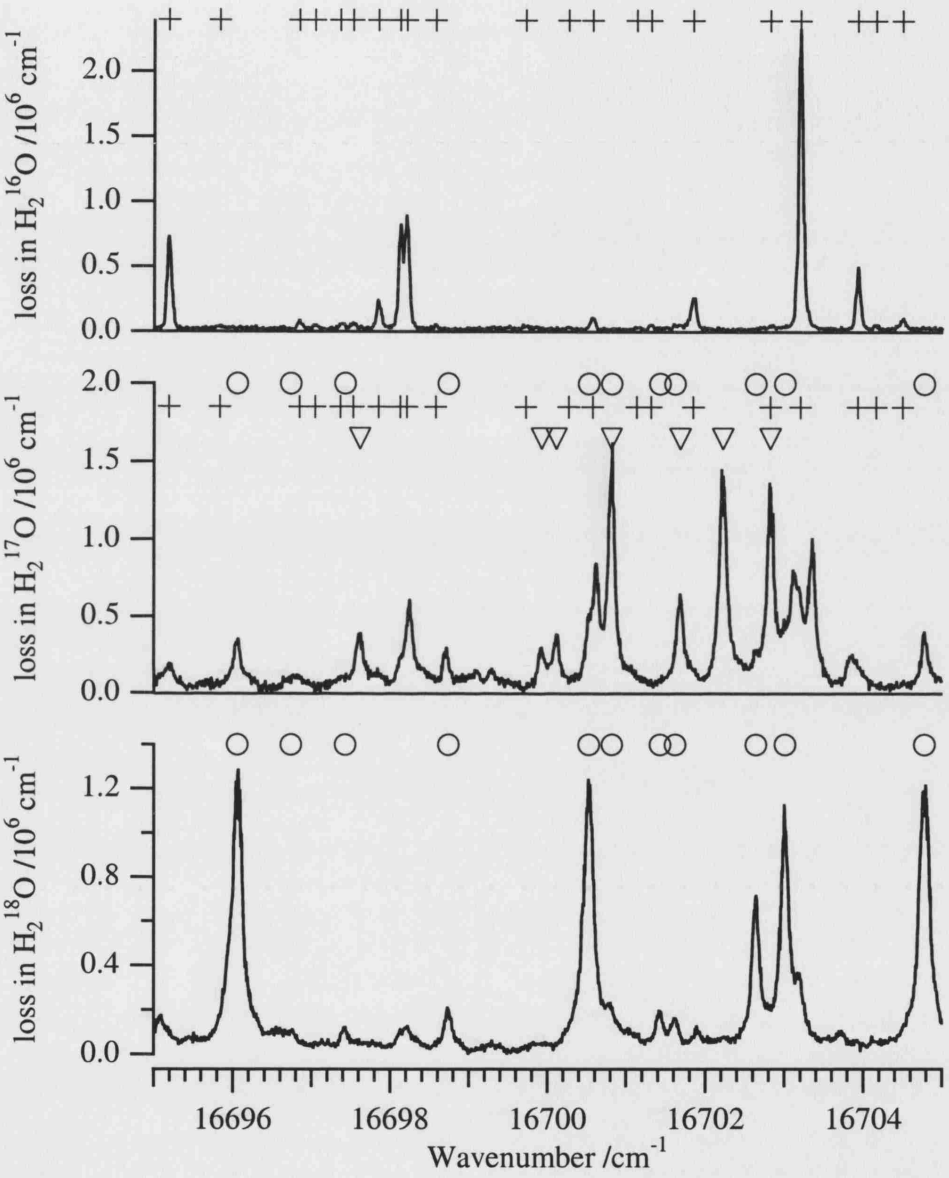

Figure 7.4: A portion of the measured spectrum of $H_2{}^{17}O$ (middle) compared with natural abundance spectrum by Naus *et al.* [16] (top) and $H_2{}^{18}O$ spectrum analysed in the previous section (bottom). The markers indicate line positions of the different isotopologues – $H_2{}^{16}O$ (+), $H_2{}^{17}O$ ($\bigtriangledown$) and $H_2{}^{18}O$ ($\bigcirc$). The figure is provided by M. Sneep (private communication).

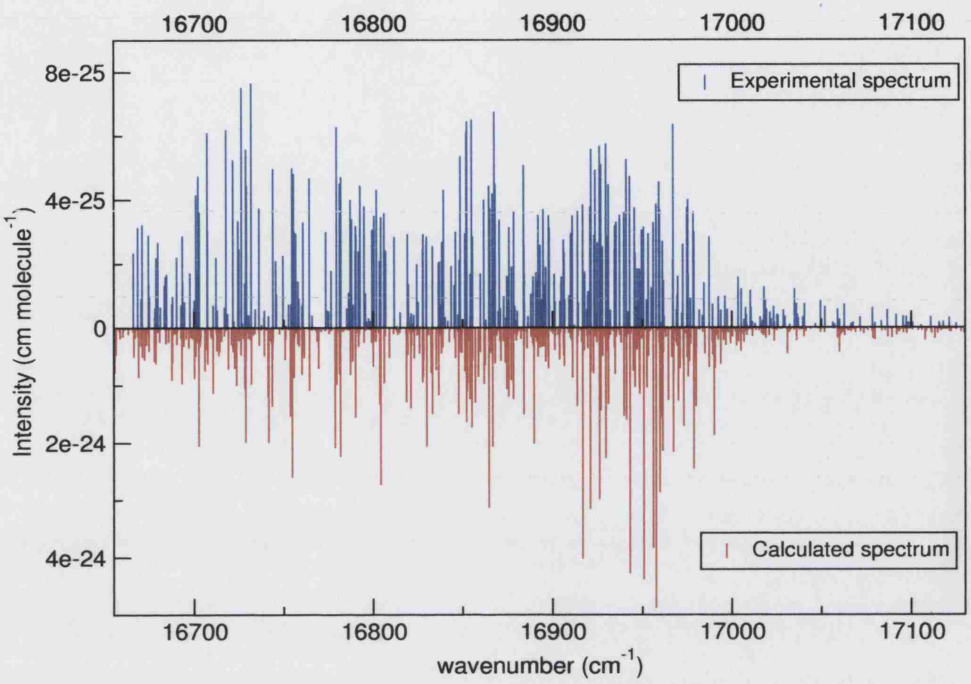

Figure 7.5: Overview of the $H_2{}^{17}O$ experimental spectrum and the calculated spectrum in the 5ν polyad region. The intensities of the experimental spectrum are not scaled to its natural abundance.

less reliable intensity measurements in CRDS experiments and the problem with the *ab initio* DMS used for the calculation. However, it is not possible to determine which factor affects more strongly.

In this work, 261 out of 357 lines attributed to $H_2{}^{17}O$ have been assigned. All the transitions originate in (000) vibrational ground level and are assigned to 9 different upper levels including (321), (500) and (401). The summary of energy levels derived can be found in Table 7.3. The band origins for (321) and (401) are newly determined at 16796.723 and 16875.620 cm^{-1} respectively and for (500), it is estimated at 16875.40 $\pm$ 0.02 cm^{-1} from the calculated energy levels as it was not directly observed experimentally. The band origin for (500) has not been observed for either $H_2{}^{16}O$ or $H_2{}^{18}O$. The ratios of $H_2{}^{17}O$ to $H_2{}^{16}O$ energy levels were again constant within each vibrational level. The differences in observed and calculated $H_2{}^{17}O$ energy levels, Obs−Calc, were pretty systematic although for (321) level, the trend was less obvious. The energy levels and Obs−Calc values for the (321), (500) and (401) vibrational levels are tabulated in Table 7.4.

Table 7.3: Summary of $H_2{}^{17}O$ energy levels determined in this study. Bands are labelled using normal mode (left) and local mode (right) notations. No. of levels shows the number of newly determined energy levels. No. of trans. shows the number of transitions to the vibrational bands.

Band	Origin (cm^{-1})	No. of levels	No. of trans.
(340) or 30^+4	—	4	5
(241) or 30^-4	—	6	6
(043) or 21^-4	—	3	3
(142) or 21^+4	—	10	10
(222) or 31^+2	—	7	7
(420) or 40^+2	—	28	38
(321) or 40^-2	16796.723	41	53
(500) or 50^+0	16875.40	38	50
(401) or 50^-0	16875.620	54	89
	Total	**191**	**261**

7.2.3 Discussion and Conclusions

Fewer lines were attributed to $H_2{}^{17}O$ in this spectrum compared to the $H_2{}^{18}O$ lines in the $H_2{}^{18}O$ spectrum. This is because the sample used in this experiment contained lower concentration of $H_2{}^{17}O$ and also the spectrum was significantly contaminated by $H_2{}^{16}O$ and $H_2{}^{18}O$. For the strongest vibrational level in this polyad region, the (401) vibrational mode, many energy levels are confirmed by combination differences, however, for the less strong mode like (321) and (500), energy levels were determined from a single transition in many cases. The energy levels determined from a single transition is less reliable than those confirmed by combination differences.

The $H_2{}^{17}O$ water vapour spectrum in the 5ν polyad measured by CRDS has been analysed and 261 out of 357 lines are now assigned. This is the highest wavenumber region to be studied for $H_2{}^{17}O$. This spectral region has significant importance in atmospheric modelling as it is close to the absorption peak of solar radiation. This work should contribute to solving the missing absorption problem of the Earth's atmosphere.

Table 7.4: $H_2{}^{17}O$ experimental energy levels for the (321), (500) and (401) vibrational states.Energy levels are given in cm^{-1}, and the uncertainties (Δ) are given in 10^{-4} cm^{-1}. The levels determined from more than one transitions were averaged and the standard deviations are given as the uncertainties. Uncertainties for the levels determined from a single transition are not given but they are estimated to be 0.6×10^{-2} $cm^{-1}$by taking the average of the uncertainties of energy levels determined by more than one transitions. Also given are the number of transitions assigned to each level and observed − calculated values (Obs−Calc).

J	K_a	K_c	(321) or 40^-2	Δ	no.	Obs−Calc	(500) or 50^+0	Δ	no.	Obs−Calc
0	0	0	16796.723		1	−0.022				
1	0	1					16897.358		1	−0.121
1	1	1	16834.239		1	−0.084				
1	1	0	16839.895		1	−0.144	16913.581		1	−0.070
2	0	2	16860.493		1	0.199	16940.221		1	−0.112
2	1	2	16873.201		1	−0.136	16947.565		1	−0.123
2	1	1	16890.599		1	0.163	16962.956	60	2	0.028
2	2	1	16934.567		1	0.075				
2	2	0	16935.851	26	2	0.202				
3	0	3	16924.442		1	−0.137	17000.660	89	3	−0.058
3	1	3					17005.384	55	2	−0.143
3	1	2	16964.758		1	−0.194	17035.598		1	−0.144
3	2	2	17001.663	3	2	0.263				
3	2	1	17008.210		1	0.020	17070.019	46	2	−0.072
3	3	1	17138.737	84	2	−0.043				
3	3	0	17138.963		1	−0.038	17082.702		1	0.042
4	0	4	17003.339		1	0.135	17079.164		1	−0.125
4	1	4	17006.506		1	−0.154				
4	1	3	17061.924		1	−0.148	17130.379		1	−0.120
4	2	3	17089.330		1	0.026				
4	2	2	17106.188	35	3	0.260				
4	3	2	17230.588		1	−0.054	17173.162		1	0.005
4	3	1	17232.052	79	3	−0.045	17174.865		1	0.173
4	4	1					17272.679		1	−0.104
4	4	0	17345.032		1	−0.018	17273.017		1	0.197
5	0	5					17173.814		1	−0.146
5	1	5	17098.992		1	−0.119	17173.949		1	−0.115
5	1	4	17179.875	16	2	0.285	17244.973		1	−0.069
5	2	4	17197.460		1	0.237	17259.522		1	−0.093
5	2	3					17290.816	118	2	−0.044
5	3	3	17345.311	22	2	−0.028	17285.972	40	2	0.058
5	3	2	17349.543		1	−0.071	17291.755		1	−0.082
5	4	2	17461.650		1	−0.037				
5	4	1	17462.065	42	2	0.176	17386.180		1	−0.147
5	5	1	17524.946		1	−0.147	17481.352		1	−0.011
5	5	0					17481.455		1	0.087

Table 7.4: Continued.

J	K_a	K_c	(321) or 40^-2	Δ	no.	Obs−Calc	(500) or 50^+0	Δ	no.	Obs−Calc
6	1	6					17285.105		1	−0.069
6	2	5	17324.302		1	0.188	17386.174	87	3	−0.064
6	3	4	17482.344		1	0.002				
6	3	3					17434.963	55	2	0.141
6	4	3					17522.360		1	0.069
6	5	2					17618.013		1	0.129
6	6	1					17744.243		1	0.121
7	1	7					17412.672	24	2	−0.110
7	1	6					17527.015	24	2	−0.146
7	2	6	17469.223		1	−0.188				
7	2	5					17539.699		1	−0.203
7	3	5	17640.767		1	−0.023	17575.889		1	−0.225
7	3	4	17666.842		1		17601.997		1	0.177
7	4	4	17765.072		1	−0.142				
7	5	3					17776.716		1	−0.139
8	0	8	17480.219		1	0.224				
8	1	8	17469.060		1	−0.079				
8	1	7	17629.490	85	2	0.109				
8	2	6	17729.099		1	0.102				
8	3	5	17860.117	113	2	0.303				

J	K_a	K_c	(401) or 50^-0	Δ	no.	Obs−Calc
0	0	0	16875.620		1	−0.147
1	0	1	16897.680		1	−0.156
1	1	1	16908.723	18	2	−0.195
1	1	0	16913.845		1	−0.169
2	0	2	16940.705		1	−0.037
2	1	2	16947.859	115	2	−0.144
2	1	1	16963.088	140	2	−0.194
2	2	1	16997.232	59	2	−0.123
2	2	0	16998.659	65	2	−0.065
3	0	3	17001.078	41	2	−0.105
3	1	3	17006.098		2	0.039
3	1	2	17035.921	45	3	−0.145
3	2	2	17063.768	59	3	−0.127
3	3	1	17081.925		1	−0.028
3	3	0	17083.856	4	2	0.022
4	0	4	17079.357	25	2	−0.135
4	1	4	17081.529	48	2	−0.144
4	1	3	17130.664	147	3	−0.129
4	2	3	17151.319	86	2	−0.112
4	2	2	17167.449	67	3	−0.115
4	3	2	17174.187	33	2	−0.005
4	3	1	17175.675	3	2	−0.021
4	4	1	17273.063	17	2	−0.278
4	4	0	17272.985	21	2	0.098

Table 7.4: Continued.

J	K_a	K_c	(401) or 50^-0	Δ	no.	Obs−Calc
5	0	5	17174.901		1	−0.127
5	1	5	17174.994	33	2	−0.135
5	1	4	17245.125		1	−0.105
5	2	4	17259.000	67	2	−0.092
5	2	3	17290.268		1	−0.251
5	3	3	17286.834	98	3	−0.068
5	3	2	17292.623		1	−0.059
5	4	2	17386.455		1	−0.039
5	5	1	17481.603		1	−0.012
5	5	0	17481.579	9	2	−0.042
6	0	6	17285.718	66	2	−0.144
6	1	6	17285.975		1	0.090
6	1	5	17377.449		1	−0.096
6	2	5	17385.931		1	−0.078
6	2	4	17435.672		1	−0.151
6	3	4	17421.755	11	2	−0.097
6	3	3	17434.894		1	−0.114
6	4	3	17520.659		1	−0.144
6	4	2	17521.581		1	−0.086
6	5	2	17617.886		1	−0.046
6	5	1	17617.910	136	2	−0.083
7	0	7	17413.040		1	−0.123
7	1	7	17413.345	70	3	−0.107
7	2	6	17531.408		1	−0.051
7	4	4	17675.880		1	0.154
7	4	3	17685.573		1	−0.002
8	1	8	17557.770		1	−0.195
8	1	7	17684.854	94	2	−0.030
8	3	5	17800.119	142	2	−0.068
8	5	3	17959.350		1	0.031

Chapter 8

Conclusions

8.1 Summary of the Thesis

Calculations of isotopically substituted water vapour and analyses of experimental spectra have been presented in this thesis. The energy levels of D_2O were calculated up to $J = 12$ using the DVR3D program suite [59] in an attempt to model the lasing actions by D_2O [82]. Linelists for $H_2{}^{17}O$ and $H_2{}^{18}O$ up to $J = 10$ have been also calculated using the DVR3D suite with the semi-empirical potential energy surface (PES) by Shirin *et al.* [66] and the *ab initio* dipole moment surface (DMS) by Polyansky *et al.* (unpublished), which were the best surfaces at the time of calculation. Good agreements with the observed energy levels were seen for both $H_2{}^{17}O$ and $H_2{}^{18}O$ calculated energy levels. The intensities, however, were not as accurate as we would like, especially for the bending mode transitions, because of the problem with the *ab initio* DMS used for the calculation. These problems are currently being addressed (J. Tennyson; private communication).

The Fourier transform spectrum of isotopically enriched $H_2{}^{18}O$ water vapour recorded at Kitt Peak National Solar Observatory (Arizona, USA) was analysed using the theoretical linelist generated by Partridge and Schwenke [42] and the new theoretical linelist generated in this work. The spectrum was measured in the range of 12400 – 14520 cm^{-1} and covered the $3\nu + \delta$ and 4ν polyads. In this work, the new band origins for (112), (013), (221), (400), (301) and (103) vibrational states were newly determined. We have assigned 911 out of 926 lines belonging to $H_2{}^{18}O$. The results of this analysis will be included in the next edition of

HITRAN, HITRAN2004.

We have also analysed the Fourier transform spectrum of isotopically enriched $H_2{}^{17}O$ water vapour recorded at Kitt Peak. This spectrum was in 11335 –14520 cm^{-1}, covering the entire $3\nu + \delta$ and 4ν polyads. New band origins for (131), (211), (013), (221), (301) and (103) were determined. In this analysis, we have found that the intensities of calculated lines were severely overestimated in the $3\nu + \delta$ polyad region.

The spectra of $H_2{}^{17}O$ and $H_2{}^{18}O$ in the region of the 5ν polyad were analysed using the linelists calculated in this thesis. The spectra were measured at the Vrije Universiteit (Amsterdam, the Netherlands) using the cavity ring-down spectroscopy (CRDS). In both spectra, the band origins for (321) and (401) were experimentally determined and those for (500) were estimated from the calculated energy levels since they were not experimentally observed. The spectra analysed here lie close to the region where absorption of the solar radiation peaks in the atmosphere. This work should provide a valuable information for atmospheric modelling and contribute to improve our understanding of the energy budget.

8.2 Future Work

The results of spectral analyses presented in this thesis will be included in the HITRAN database in due course, where they will supplement our Fourier transform $H_2{}^{18}O$ lines which are already accepted for inclusion in the HITRAN2004. The new data, especially for the 5ν polyad region, has a huge significance to atmospheric modelling. The data can be also useful for monitoring the non-uniform isotopic distribution and the fractionation effects in the Earth's atmosphere.

As well as for atmospheric science, our results can be used to improve the quality of semi-empirical PESs, which are obtained by fitting *ab initio* surfaces to experimental data. Shirin *et al.* [167], for example, are using the energy levels determined in this thesis to improve the *ab initio* PES by Polyansky *et al.* [121] with the aim of producing a high accuracy surface for water isotopologues including $H_2{}^{17}O$ and $H_2{}^{18}O$. Another use of the data is to calculate partition functions. The vibration-rotation partition function can be calculated by explicit summation of the vibration-rotation energy levels, therefore accurate energy levels are essential for obtaining

accurate partition functions. The calculated and observed energy levels presented in this thesis can be used to improve accuracy of the partition functions for $H_2{}^{17}O$ and $H_2{}^{18}O$, especially those for high temperature where current functions are less reliable. Such an approach has already been used for $H_2{}^{16}O$ by Vidler and Tennyson [168] as well as for HDO and D_2O by Hewitt *et al.* [169].

In this work, the *ab initio* DMS of Polyansky, Lynas-Gray and co-workers (unpublished) used for linelist calculations was found to overestimate the line strengths of bending mode excitations. This problem is being addressed (J. Tennyson; private communication) and corrections to the surface should be made in the near future to achieve better accuracy in calculation of line strengths.

In order to provide more complete data for water isotopologues, the spectra of $H_2{}^{17}O$ and $H_2{}^{18}O$ in the $4\nu + \delta$ polyad region (14500 – 16700 cm^{-1}) need to be analysed. This region was not covered in this work and, as far as we are aware, no experimental spectrum is available at the time of writing. The success of analysing the $H_2{}^{17}O$ and $H_2{}^{18}O$ spectra in this work should encourage the measurements of isotopically enhanced spectra in the $4\nu + \delta$ and higher polyad regions.

The natural abundance of $H_2{}^{17}O$ and $HD^{16}O$ is similar, this means that $HD^{16}O$ could also have some significance in absorption of solar radiation in the atmosphere. The highest frequency listed for $HD^{16}O$ in the HITRAN2000 is 7514 cm^{-1}, and there is currently no data for this isotopologue in the visible region in the database. Extensive studies on HDO in the visible region have been carried out [170–174], but those results are not compiled in the HITRAN as the lines were not measured with absolute intensities. Recently, a new HDO spectrum with absolute intensities has been measured (P. F. Coheur; private communication) using a Fourier transform spectrometer with 50 m White cell. Assignment of this spectrum requires a high accuracy linelist, however calculation of a linelist for HDO is considerably harder than for H_2O because of loss of symmetry and the higher density of states due to deutration. But thanks to recent advances in computer, such calculation is now possible. It will be an interesting and challenging future project to generate the new linelist for HDO and analyse the spectrum.

The assignment procedure established for $H_2{}^{17}O$ and $H_2{}^{18}O$ in this work can be applied to the analysis of spectra of other molecules. The method presented in this thesis can contribute

to improving the spectroscopic knowledge of water isotopologues and other molecules.

Appendix A

Experimental Line Positions and Intensities of $H_2{}^{18}O$ and $H_2{}^{17}O$

Table A.1: The observed line positions (cm^{-1}) and absolute intensities (cm $molecule^{-1}$) of $H_2{}^{18}O$ observed in the range 12400 – 14520 cm^{-1}. The absolute intensities are scaled to match the natural abundance of $H_2{}^{18}O$ and normalised at 296 K. Uncertainty in line position is given in 10^{-4} cm^{-1} ($\Delta\nu$ in column 2) and for intensity is given in 10^{-28} cm $molecule^{-1}$ (ΔI in column 4). Vibrational states are presented in $v_1v_2v_3$ normal mode notation in column 11.

wavenumber	$\Delta\nu$	intensity	ΔI	J′	K'_a	K'_c	J″	K''_a	K''_c	vib
12402.9673	18	0.349E-27	4.620							
12404.8751	2	0.298E-26	0.451	3	1	2	3	0	3	112
12405.9477	14	0.945E-27	0.920	4	2	2	4	1	3	112
12407.4054	4	0.324E-26	0.902	3	2	1	3	1	2	112
12407.9412	1	0.441E-26	0.476	4	0	4	5	0	5	013
12408.7966	7	0.638E-27	4.099	1	1	1	0	0	0	112
12408.9458	4	0.171E-26	0.485	4	1	4	5	1	5	013
12408.9810	3	0.151E-26	0.403	5	2	3	5	1	4	310
12410.6766	10	0.350E-27	3.785	7	3	4	7	2	5	310
12411.1915	5	0.114E-26	0.481	3	2	1	4	2	2	013
12411.5318	7	0.740E-27	4.471	6	4	2	5	2	3	211
12411.9559	6	0.118E-26	0.469	2	2	0	2	1	1	112
12412.3108	0	0.387E-27	0.000	6	6	1	5	5	0	310
12413.0633	5	0.135E-26	0.471	3	3	1	4	3	2	013
12414.7409	4	0.158E-26	0.455	3	1	2	4	1	3	013
12415.9447	10	0.550E-27	4.379	5	4	2	4	2	3	211
12418.4464	8	0.933E-27	0.572	4	1	3	4	0	4	112
12419.8255	2	0.321E-26	0.485	3	2	2	4	2	3	013
12423.9617	4	0.169E-26	0.466	3	0	3	2	1	2	112
12424.1787	4	0.134E-26	0.450	5	3	2	5	2	3	112
12425.0884	5	0.238E-26	0.879	2	1	2	1	0	1	112

Table A.1: Continued.

wavenumber	$\Delta\nu$	intensity	ΔI	J′	K'_a	K'_c	J″	K''_a	K''_c	vib
12426.3520	9	0.166E-26	0.960	2	2	1	2	1	2	310
12429.9626	3	0.192E-26	0.487	3	0	3	4	0	4	013
12431.9006	1	0.551E-26	0.463	3	1	3	4	1	4	013
12433.3636	9	0.630E-27	5.102	4	0	4	4	2	3	013
12433.5625	16	0.387E-27	4.494	8	3	5	7	1	6	211
12434.0477	12	0.493E-27	4.346	4	3	1	4	2	2	112
12434.5913	8	0.114E-26	0.824	5	1	4	5	0	5	112
12438.1499	8	0.801E-27	4.534	3	1	3	2	0	2	112
12439.8140	2	0.324E-26	0.506	2	2	0	3	2	1	013
12440.0024	0	0.164E-26	0.000	4	2	3	4	1	4	112
12440.1094	1	0.515E-26	0.450	2	1	1	3	1	2	013
12441.9470	0	0.686E-27	0.000	4	0	4	3	1	3	112
12442.8746	4	0.153E-26	0.507	3	3	0	3	2	1	112
12444.2661	6	0.898E-27	0.470	2	2	1	3	2	2	013
12448.5183	5	0.130E-26	0.468	4	3	2	4	2	3	112
12449.2846	15	0.446E-27	4.602	5	2	4	5	1	5	112
12449.4743	3	0.216E-26	0.460	4	1	4	3	0	3	112
12451.4773	1	0.654E-26	0.466	2	0	2	3	0	3	013
12452.0885	16	0.757E-27	7.086	6	3	4	6	2	5	112
12454.3223	3	0.207E-26	0.473	2	1	2	3	1	3	013
12456.2687	0	0.140E-26	0.000	5	0	5	4	1	4	112
12459.4903	0	0.584E-27	0.000	6	2	5	6	1	6	112
12460.0168	0	0.336E-27	0.000	5	1	4	4	2	3	112
12460.2319	14	0.413E-27	4.345	5	1	5	4	0	4	112
12461.2429	16	0.352E-27	4.587	8	4	5	8	3	6	112
12463.3178	2	0.282E-26	0.483	2	2	1	1	1	0	112
12464.5331	7	0.914E-27	0.498	5	4	1	5	3	2	112
12465.1917	12	0.526E-27	5.959	7	1	6	7	0	7	112
12465.8932	12	0.456E-27	4.324	6	4	3	6	3	4	112
12466.2952	5	0.138E-26	0.467	1	1	0	2	1	1	013
12470.0065	9	0.895E-27	0.506	7	2	6	7	1	7	112
12470.6275	0	0.808E-27	0.000	6	1	6	5	0	5	112
12473.3019	3	0.210E-26	0.483	1	0	1	2	0	2	013
12473.5862	8	0.686E-27	4.273	4	4	1	4	3	2	112
12476.2195	17	0.477E-27	4.933	5	2	4	5	2	3	013
12479.0074	9	0.623E-27	4.300	3	2	2	2	1	1	112
12479.2612	41	0.236E-27	8.361	6	6	0	6	6	1	013
12479.5790	45	0.871E-27	1.313	7	0	7	6	1	6	112
12482.8453	6	0.120E-26	0.503	3	1	3	3	1	2	013
12487.9433	14	0.442E-27	5.883	6	5	2	6	5	1	013
12488.0519	14	0.307E-27	3.946							
12488.2156	8	0.455E-27	3.835	6	5	2	6	4	3	112
12490.9488	4	0.131E-26	0.447	4	2	3	3	1	2	112
12492.2698	5	0.123E-26	0.457	5	5	1	5	5	0	013
12493.8693	5	0.114E-26	0.478	5	5	0	5	4	1	112
12495.1227	12	0.413E-27	4.147	4	2	3	4	2	2	013
12496.3680	0	0.399E-26	0.000	0	0	0	1	0	1	013
12499.6992	23	0.272E-27	4.483	5	2	4	4	1	3	112

Table A.1: Continued.

wavenumber	$\Delta\nu$	intensity	ΔI	J′	K'_a	K'_c	J″	K''_a	K''_c	vib
12500.8372	7	0.721E-27	4.308	5	3	3	5	3	2	013
12501.0999	8	0.776E-27	4.419	2	1	2	2	1	1	013
12501.3015	11	0.122E-26	0.913	3	2	1	2	1	2	112
12502.5237	7	0.891E-27	0.463	4	4	1	4	4	0	013
12502.6002	0	0.275E-26	0.000	4	4	0	4	4	1	013
12506.4793	12	0.514E-27	4.451	6	2	5	5	1	4	112
12507.0490	9	0.678E-27	4.530	4	3	2	4	3	1	013
12507.6476	2	0.323E-26	0.472	3	2	2	3	2	1	013
12510.0487	0	0.518E-26	0.000	3	3	1	3	3	0	013
12510.3552	3	0.212E-26	0.460	4	3	1	4	3	2	013
12510.5552	3	0.171E-26	0.442	3	3	0	3	3	1	013
12513.3479	1	0.547E-26	0.473	1	1	1	1	1	0	013
12514.2426	2	0.249E-26	0.484	2	2	1	2	2	0	013
12517.1395	0	0.707E-26	0.465	2	2	0	2	2	1	013
12518.8335	7	0.863E-27	0.449	3	3	1	2	2	0	112
12518.9772	13	0.270E-27	3.704	6	3	3	6	3	4	013
12520.1975	2	0.267E-26	0.457	3	3	0	2	2	1	112
12520.8956	5	0.116E-26	0.510	3	2	1	3	2	2	013
12524.3343	0	0.179E-26	0.000	1	1	0	1	1	1	013
12529.3886	5	0.133E-26	0.495	4	2	2	4	2	3	013
12534.0042	3	0.221E-26	0.462	2	1	1	2	1	2	013
12536.3409	4	0.166E-26	0.496	4	3	2	3	2	1	112
12543.2303	0	0.147E-26	0.000	1	0	1	0	0	0	013
12543.7515	13	0.473E-27	4.413	4	3	1	3	2	2	112
12547.9720	0	0.331E-27	0.000	3	1	2	3	1	3	013
12549.6564	0	0.177E-27	0.000	5	3	3	4	2	2	310
12557.3732	26	0.198E-27	4.180	6	3	4	5	2	3	112
12559.1408	3	0.178E-26	0.456	2	1	2	1	1	1	013
12564.0600	0	0.742E-26	0.000	2	0	2	1	0	1	013
12565.0251	11	0.540E-27	4.434	4	1	3	4	1	4	013
12570.5734	0	0.164E-26	0.000	4	4	1	3	3	0	112
12570.7191	0	0.584E-27	0.000	5	3	2	4	2	3	112
12570.7853	0	0.456E-27	0.000	4	4	0	3	3	1	310
12570.9693	1	0.524E-26	0.474	2	1	1	1	1	0	013
12576.7414	0	0.798E-26	0.000	3	1	3	2	1	2	013
12581.2699	2	0.271E-26	0.481	3	0	3	2	0	2	013
12582.1069	22	0.332E-27	4.690	3	2	2	3	0	3	013
12583.6921	27	0.259E-27	4.628	3	3	1	2	0	2	112
12584.9711	0	0.381E-26	0.000	3	2	2	2	2	1	013
12589.4803	24	0.325E-27	4.771	5	4	2	4	3	1	112
12590.8707	5	0.115E-26	0.437	3	2	1	2	2	0	013
12590.9658	0	0.810E-27	0.000	5	4	1	4	3	2	112
12592.5902	2	0.299E-26	0.497	4	1	4	3	1	3	013
12594.7553	0	0.251E-26	0.000	3	1	2	2	1	1	013
12595.6520	0	0.856E-26	0.000	4	0	4	3	0	3	013
12604.8205	0	0.156E-26	0.000	4	2	3	3	2	2	013
12605.5551	0	0.209E-27	0.000	6	4	3	5	3	2	112
12605.6598	0	0.724E-27	0.000	4	3	2	3	3	1	013

Table A.1: Continued.

wavenumber	$\Delta\nu$	intensity	ΔI	J′	K'_a	K'_c	J″	K''_a	K''_c	vib
12606.8327	0	0.720E-26	0.475	5	1	5	4	1	4	013
12608.2913	2	0.250E-26	0.492	5	0	5	4	0	4	013
12610.8042	23	0.298E-27	4.567	4	3	2	3	0	3	112
12615.9704	1	0.670E-26	0.488	4	1	3	3	1	2	013
12617.2101	0	0.444E-26	0.000	4	2	2	3	2	1	013
12618.7837	4	0.166E-26	0.477	6	1	6	5	1	5	013
12619.9627	1	0.521E-26	0.470	6	0	6	5	0	5	013
12622.7563	0	0.434E-26	0.000	5	2	4	4	2	3	013
12626.2436	4	0.148E-26	0.456	5	4	2	4	4	1	013
12626.4291	0	0.613E-27	0.000	5	4	1	4	4	0	013
12627.2742	3	0.227E-26	0.462	5	3	3	4	3	2	013
12630.3279	2	0.334E-26	0.458	7	1	7	6	1	6	013
12630.7587	0	0.116E-26	0.000	7	0	7	6	0	6	013
12632.4654	8	0.677E-27	4.359	5	3	2	4	3	1	013
12633.4620	0	0.149E-26	0.000	5	1	4	4	1	3	013
12638.7160	7	0.905E-27	0.448	6	2	5	5	2	4	013
12640.4038	0	0.614E-27	0.000	8	1	8	7	1	7	013
12640.6272	0	0.211E-26	0.000	8	0	8	7	0	7	013
12642.1593	0	0.122E-26	0.000	5	2	3	4	2	2	013
12646.8792	0	0.306E-26	0.000	6	1	5	5	1	4	013
12647.4778	0	0.545E-27	0.000	6	3	4	5	3	3	013
12649.1148	0	0.394E-27	0.000	6	4	3	5	4	2	013
12649.2816	0	0.112E-26	0.000	9	1	9	8	1	8	013
12649.3592	0	0.330E-27	0.000	9	0	9	8	0	8	013
12649.9228	6	0.109E-26	0.474	6	4	2	5	4	1	013
12654.0072	0	0.192E-26	0.000	7	2	6	6	2	5	013
12657.0934	15	0.659E-27	5.281	10	0	10	9	0	9	013
12657.3674	0	0.608E-27	0.000	7	6	2	6	1	5	230
12658.6297	4	0.159E-26	0.479	6	3	3	5	3	2	013
12662.2098	27	0.278E-27	4.786	8	7	1	7	2	6	070
12663.7161	24	0.273E-27	4.536	5	4	2	5	2	3	013
12664.1903	0	0.241E-26	0.000	6	2	4	5	2	3	013
12665.0856	0	0.663E-27	0.000	7	6	1	6	3	4	310
12666.4750	0	0.964E-27	0.000	8	1	7	7	1	6	013
12667.0270	0	0.387E-27	0.000	7	3	5	6	3	4	013
12668.8923	0	0.505E-27	0.000	6	6	1	5	5	0	112
12669.6800	48	0.147E-27	4.758	12	0	12	11	0	11	013
12670.6255	0	0.628E-27	0.000	7	4	4	6	4	3	013
12682.2131	0	0.381E-27	0.000	7	2	5	6	2	4	013
12682.5411	29	0.189E-27	4.365	10	1	9	9	1	8	013
12684.1984	27	0.268E-27	4.750	7	3	4	6	3	3	013
12689.3155	32	0.254E-27	4.916	8	6	2	7	3	5	310
12691.6703	21	0.304E-27	5.622	4	2	2	3	0	3	013
12695.5518	0	0.558E-27	0.000	8	2	6	7	2	5	013
12696.9077	0	0.317E-27	0.000	8	4	4	7	4	3	013
12699.8582	29	0.160E-27	4.122	9	3	7	8	3	6	013
13364.9612	0	0.241E-27	0.000	9	1	9	10	1	10	221
13393.9402	0	0.167E-27	0.000	8	1	8	9	1	9	221

Table A.1: Continued.

wavenumber	$\Delta\nu$	intensity	ΔI	J′	K'_a	K'_c	J″	K''_a	K''_c	vib
13396.1698	21	0.290E-27	4.530	8	1	7	9	1	8	221
13396.5213	0	0.547E-27	0.000	8	0	8	9	0	9	221
13419.8497	0	0.154E-27	0.000	7	1	6	8	1	7	221
13423.6252	0	0.627E-27	0.000	7	2	6	8	2	7	221
13424.0725	0	0.344E-27	0.000	7	0	7	8	0	8	221
13425.1557	0	0.120E-26	0.000	7	1	7	8	1	8	221
13428.6052	14	0.434E-27	4.562	7	3	5	8	3	6	221
13432.1268	7	0.106E-26	0.491	6	2	4	7	2	5	221
13441.4730	0	0.637E-27	0.000	6	3	3	7	3	4	221
13441.6842	0	0.120E-26	0.000	6	1	5	7	1	6	221
13443.3137	0	0.318E-27	0.000	7	4	4	8	4	5	221
13449.1016	19	0.345E-27	4.567	6	2	5	7	2	6	221
13450.9802	0	0.211E-26	0.000	6	0	6	7	0	7	221
13451.6738	0	0.715E-27	0.000	6	1	6	7	1	7	221
13456.5568	0	0.297E-27	0.000	6	3	4	7	3	5	221
13458.2733	0	0.693E-27	0.000	5	2	3	6	2	4	221
13459.9213	0	0.318E-27	0.000	7	5	3	8	5	4	301
13460.2016	0	0.424E-27	0.000	6	1	5	7	3	4	301
13463.6386	0	0.701E-27	0.000	5	1	4	6	1	5	221
13470.6246	10	0.715E-27	4.768	6	4	2	7	4	3	221
13473.1151	0	0.333E-27	0.000	11	0	11	12	0	12	301
13473.7479	0	0.291E-27	0.000	10	1	9	11	1	10	301
13475.2793	0	0.728E-27	0.000	5	3	2	6	2	5	042
13476.0483	0	0.452E-27	0.000	5	3	2	6	3	3	221
13476.3964	6	0.112E-26	0.480	5	0	5	6	0	6	221
13477.6201	0	0.365E-26	0.000	5	1	5	6	1	6	221
13479.3501	0	0.128E-26	0.000	9	3	7	10	3	8	301
13484.7945	4	0.175E-26	0.467	5	3	3	6	3	4	221
13486.2588	1	0.376E-26	0.473	4	1	3	5	1	4	221
13487.4492	0	0.321E-26	0.000	4	2	2	5	2	3	221
13491.8593	0	0.598E-27	0.000	6	5	1	7	5	2	301
13493.6993	9	0.702E-27	4.671	8	3	5	9	3	6	301
13500.1565	0	0.528E-26	0.000	4	0	4	5	0	5	221
13502.3651	7	0.155E-26	0.545	4	2	3	5	2	4	221
13502.5562	4	0.168E-26	0.471	4	1	4	5	1	5	221
13503.2654	6	0.111E-26	0.467	5	4	2	6	4	3	221
13505.9450	7	0.134E-26	0.516							
13506.2564	0	0.755E-27	0.000	9	2	8	10	2	9	301
13506.6623	19	0.302E-27	4.485	9	1	8	10	1	9	301
13508.9805	3	0.214E-26	0.476	4	3	1	5	3	2	221
13510.5623	0	0.193E-26	0.000	3	1	2	4	1	3	221
13510.7395	0	0.777E-27	0.000	8	2	6	9	2	7	301
13512.9735	0	0.769E-27	0.000	4	3	2	5	3	3	221
13517.4411	31	0.187E-27	4.451	7	5	3	8	5	4	221
13517.8735	5	0.144E-26	0.485	3	2	1	4	2	2	221
13519.9807	27	0.265E-27	4.630	3	1	3	4	0	4	320
13520.2758	0	0.567E-27	0.000	7	4	3	8	3	6	042
13522.5946	0	0.194E-26	0.000	3	0	3	4	0	4	221

Table A.1: Continued.

wavenumber	$\Delta\nu$	intensity	ΔI	J′	K'_a	K'_c	J″	K''_a	K''_c	vib
13522.9440	11	0.969E-27	0.540	5	5	1	6	5	2	221
13524.3057	15	0.516E-27	4.906	8	0	8	9	2	7	023
13524.6083	15	0.384E-27	4.351	5	1	5	5	1	4	221
13525.5835	19	0.440E-27	4.920	4	0	4	4	2	3	221
13526.5776	0	0.648E-26	0.000	3	1	3	4	1	4	221
13527.2576	7	0.943E-27	0.460	7	4	4	8	4	5	301
13527.6075	1	0.430E-26	0.470	3	2	2	4	2	3	221
13529.9549	0	0.647E-27	0.000	7	3	4	8	3	5	301
13532.2929	6	0.104E-26	0.462	4	4	1	5	4	2	221
13533.0133	20	0.376E-27	4.810	4	4	0	5	4	1	221
13536.3967	1	0.673E-26	0.490	2	1	1	3	1	2	221
13537.5962	0	0.879E-27	0.000	9	0	9	10	0	10	301
13537.6345	0	0.217E-26	0.000	9	1	9	10	1	10	301
13537.9276	10	0.567E-27	4.445	8	2	7	9	2	8	301
13538.6481	3	0.219E-26	0.474	8	1	7	9	1	8	301
13539.4773	0	0.598E-27	0.000	3	3	0	4	3	1	221
13540.6622	3	0.202E-26	0.466	3	0	3	4	3	2	400
13541.9763	21	0.491E-27	6.671	6	2	4	7	3	5	400
13543.2204	0	0.707E-26	0.000	2	0	2	3	0	3	221
13543.5350	0	0.104E-26	0.000	7	2	5	8	2	6	301
13545.1816	0	0.207E-26	0.000	7	3	5	8	3	6	301
13546.3439	7	0.107E-26	0.493	4	1	3	5	3	2	301
13546.9039	0	0.704E-27	0.000	2	1	2	3	0	3	320
13546.9784	0	0.540E-27	0.000	3	1	3	4	3	2	301
13548.3016	0	0.384E-26	0.000	2	2	0	3	2	1	221
13549.7047	30	0.706E-27	11.760	6	5	1	7	5	2	221
13550.2245	0	0.239E-26	0.000	2	1	2	3	1	3	221
13553.0362	10	0.155E-26	1.126	2	2	1	3	2	2	221
13555.2194	12	0.557E-27	4.622	4	1	4	5	2	3	400
13558.2580	0	0.227E-26	0.000	6	4	2	7	4	3	301
13560.4912	9	0.816E-27	0.564	6	4	3	7	4	4	301
13560.6782	6	0.122E-26	0.521	7	3	4	8	2	7	320
13562.3982	0	0.462E-27	0.000	4	2	3	5	3	2	400
13562.7720	0	0.112E-26	0.000	5	2	3	6	3	4	400
13563.0564	0	0.172E-26	0.000	1	1	0	2	1	1	221
13568.0268	0	0.690E-26	0.000	8	1	8	9	0	9	400
13568.1672	0	0.165E-26	0.000	7	1	6	8	2	7	400
13570.0311	0	0.252E-26	0.000	7	2	6	8	2	7	301
13570.0870	0	0.109E-26	0.000	7	1	6	8	1	7	301
13572.9941	1	0.577E-26	0.500	1	1	1	2	1	2	221
13576.2124	0	0.696E-26	0.000	6	2	4	7	2	5	301
13577.1986	4	0.146E-26	0.468	6	3	4	7	3	5	301
13577.5226	0	0.145E-26	0.000	3	1	3	3	1	2	221
13579.3285	0	0.439E-27	0.000	6	3	3	7	1	6	221
13584.1965	25	0.277E-27	4.615	4	2	2	5	3	3	400
13588.9553	0	0.453E-26	0.000	0	0	0	1	0	1	221
13591.6475	14	0.747E-27	5.386	6	1	5	7	2	6	400
13592.0680	0	0.129E-26	0.000	5	4	1	6	4	2	301

Table A.1: Continued.

wavenumber	$\Delta\nu$	intensity	ΔI	J′	K'_a	K'_c	J″	K''_a	K''_c	vib
13592.8761	0	0.386E-26	0.000	5	4	2	6	4	3	301
13596.0206	12	0.661E-27	5.686							
13597.0031	27	0.601E-27	12.684	2	1	2	2	1	1	221
13597.1979	0	0.111E-25	0.000	7	1	7	8	1	8	301
13597.2481	0	0.363E-26	0.000	7	0	7	8	0	8	301
13598.0567	0	0.584E-26	0.000	6	1	5	7	1	6	301
13598.4945	0	0.282E-26	0.000	6	2	5	7	2	6	301
13600.6690	23	0.257E-27	4.439	6	4	3	6	5	2	400
13600.8846	16	0.485E-27	5.362	2	1	1	3	3	0	301
13601.4696	0	0.294E-26	0.000	5	3	2	6	3	3	301
13602.0683	11	0.628E-27	4.672	4	2	3	4	2	2	221
13602.1624	1	0.543E-26	0.497	6	2	5	7	1	6	400
13602.3729	18	0.463E-27	5.027	8	1	8	8	2	7	400
13607.1921	0	0.492E-27	0.000	3	2	1	4	3	2	400
13607.9299	0	0.107E-26	0.000	6	3	4	7	2	5	400
13608.4154	0	0.880E-26	0.049	5	3	3	6	3	4	301
13608.5537	0	0.156E-27	0.000	5	4	2	5	5	1	400
13608.8958	1	0.540E-26	0.509	5	2	3	6	2	4	301
13609.9602	0	0.648E-26	0.000	1	1	1	1	1	0	221
13611.7037	0	0.414E-27	0.000	8	1	7	8	3	6	301
13614.9608	0	0.271E-26	0.000	5	1	4	6	2	5	400
13615.4288	1	0.463E-26	0.485	3	2	2	3	2	1	221
13616.5741	0	0.423E-27	0.000	8	7	1	8	7	2	301
13621.0961	0	0.214E-26	0.000	1	1	0	1	1	1	221
13623.0094	4	0.356E-26	1.021	2	2	1	2	2	0	221
13623.9813	0	0.438E-26	0.000	4	4	0	5	4	1	301
13624.1840	0	0.163E-26	0.000	4	4	1	5	4	2	301
13624.4485	3	0.189E-26	0.474	5	3	3	5	3	2	221
13624.7174	0	0.180E-25	0.049	6	0	6	7	0	7	301
13625.4278	0	0.677E-26	0.000	6	1	6	7	1	7	301
13625.6249	1	0.103E-25	0.099	2	2	0	2	2	1	221
13625.9553	1	0.557E-26	0.489	5	1	4	6	1	5	301
13627.2860	6	0.972E-27	0.446	7	7	1	7	7	0	301
13627.4398	0	0.162E-25	0.049	5	2	4	6	2	5	301
13627.5772	0	0.149E-26	0.000	3	2	1	3	2	2	221
13630.2905	2	0.290E-26	0.494	2	1	1	2	1	2	221
13631.5645	20	0.323E-27	4.548	7	0	7	7	2	6	301
13632.8671	4	0.162E-26	0.480	7	2	6	7	3	5	400
13633.9879	0	0.222E-26	0.000	4	2	2	4	2	3	221
13634.0608	0	0.753E-27	0.000	5	3	2	5	3	3	221
13634.2487	0	0.430E-27	0.000	7	4	4	7	4	3	221
13635.2004	0	0.184E-26	0.000	5	2	4	6	1	5	400
13635.4176	0	0.483E-26	0.000	4	3	1	4	3	2	221
13635.4751	4	0.175E-26	0.506	1	0	1	0	0	0	221
13635.9794	0	0.807E-27	0.000	4	1	3	5	2	4	400
13636.5021	0	0.116E-26	0.000	7	1	7	7	1	6	301
13637.6465	0	0.102E-25	0.049	3	0	3	3	3	0	400
13638.0864	2	0.353E-26	0.492	3	3	0	3	3	1	221

Table A.1: Continued.

wavenumber	$\Delta\nu$	intensity	ΔI	J′	K'_a	K'_c	J″	K''_a	K''_c	vib
13638.9428	1	0.438E-26	0.470	4	3	2	5	3	3	301
13640.9325	6	0.121E-26	0.545	4	2	2	5	2	3	301
13641.5912	0	0.256E-25	0.050	4	1	4	5	2	3	122
13642.9050	0	0.487E-27	0.000	6	4	3	6	4	2	221
13645.2939	0	0.139E-26	0.000	6	4	2	6	4	3	221
13645.3446	18	0.687E-27	7.360	5	2	3	5	2	4	221
13647.3799	0	0.370E-27	0.000	8	1	7	8	5	4	071
13648.4669	18	0.654E-27	6.921							
13649.5075	0	0.516E-26	0.000	5	0	5	6	1	6	400
13650.8893	15	0.474E-27	4.840	5	3	3	6	2	4	400
13651.9969	0	0.339E-25	0.148	5	1	5	6	1	6	301
13652.1691	0	0.119E-25	0.049	5	0	5	6	0	6	301
13653.3897	9	0.101E-26	0.606	5	3	2	5	4	1	400
13653.7102	0	0.328E-25	0.148	4	1	3	5	1	4	301
13654.3816	0	0.295E-26	0.000	6	1	5	6	3	4	301
13654.4414	0	0.824E-26	0.000	4	3	2	4	4	1	400
13654.5839	0	0.321E-27	0.000	3	0	3	2	1	2	320
13655.0427	0	0.204E-26	0.000	2	1	2	1	1	1	221
13655.0857	0	0.118E-26	0.000	7	5	3	7	5	2	301
13655.1617	18	0.132E-26	1.546	4	4	0	4	4	1	221
13655.6635	0	0.899E-26	0.000	4	2	3	5	2	4	301
13655.8044	0	0.894E-26	0.051	2	0	2	1	0	1	221
13655.9797	0	0.185E-26	0.000	3	1	2	4	2	3	400
13656.8084	0	0.283E-27	0.000	4	3	1	4	4	0	400
13658.0447	0	0.242E-26	0.000	6	0	6	6	2	5	301
13658.4838	3	0.257E-26	0.503	6	2	5	6	3	4	400
13659.4883	0	0.144E-26	0.000	2	1	2	1	0	1	320
13660.7922	0	0.821E-27	0.000	4	1	3	4	1	4	221
13662.9242	0	0.950E-27	0.000	6	5	2	6	5	1	301
13662.9850	0	0.298E-26	0.000	6	5	1	6	5	2	301
13667.2562	1	0.611E-26	0.491	2	1	1	1	1	0	221
13667.4988	0	0.438E-26	0.000	3	3	0	4	3	1	301
13668.2338	10	0.651E-27	4.588	6	1	6	6	1	5	301
13668.6374	0	0.145E-25	0.000	3	3	1	4	3	2	301
13669.3432	0	0.932E-26	0.048	5	5	1	5	5	0	221
13671.4175	0	0.830E-26	0.000	3	1	3	2	1	2	221
13671.4927	0	0.620E-27	0.000	7	2	6	7	2	5	301
13672.7767	0	0.995E-27	0.000	4	1	3	4	3	2	301
13673.9014	0	0.307E-26	0.000	3	0	3	2	0	2	221
13674.0067	0	0.121E-25	0.000	3	2	1	4	2	2	301
13674.2148	0	0.105E-26	0.000	4	0	4	5	1	5	400
13676.3332	1	0.479E-26	0.494	4	1	4	5	0	5	400
13677.7515	1	0.484E-25	0.349	4	0	4	5	0	5	301
13679.6049	0	0.214E-27	0.000	5	1	4	5	1	5	221
13681.8278	0	0.170E-25	0.049	3	1	2	4	1	3	301
13682.8448	0	0.174E-26	0.000	5	0	5	5	2	4	301
13683.2319	0	0.355E-25	0.149	3	2	2	4	2	3	301
13686.2042	2	0.318E-26	0.531	4	1	4	3	1	3	221

Table A.1: Continued.

wavenumber	$\Delta\nu$	intensity	ΔI	J′	K'_a	K'_c	J″	K''_a	K''_c	vib
13687.8664	0	0.979E-26	0.049	4	0	4	3	0	3	221
13689.8915	15	0.455E-27	4.561	3	2	2	3	0	3	221
13690.5767	0	0.296E-26	0.000	3	1	2	2	1	1	221
13692.6453	0	0.121E-26	0.000	4	4	0	5	2	3	221
13692.7526	0	0.495E-26	0.000	3	2	2	2	2	1	221
13696.1249	16	0.413E-27	4.985	6	2	4	6	3	3	400
13696.8145	1	0.479E-26	0.511	3	3	1	4	1	4	221
13697.1783	13	0.681E-27	6.181	5	4	1	6	3	4	400
13697.5512	4	0.168E-26	0.536	3	2	1	2	2	0	221
13698.9820	1	0.428E-26	0.496	5	1	5	5	1	4	301
13699.1383	0	0.753E-26	0.000	5	1	5	4	1	4	221
13700.0125	1	0.493E-26	0.525	5	0	5	4	0	4	221
13701.2384	0	0.134E-25	0.050	3	0	3	4	0	4	301
13702.2362	31	0.233E-27	4.659	6	1	6	5	0	5	320
13702.4386	1	0.627E-25	0.549	3	1	3	4	1	4	301
13703.1785	0	0.485E-26	0.000	4	0	4	4	2	3	301
13703.3757	0	0.830E-26	0.000	3	1	3	4	0	4	400
13703.8543	0	0.113E-26	0.000	6	2	5	6	2	4	301
13705.2030	0	0.103E-26	0.000	3	2	2	4	1	3	400
13705.5628	0	0.333E-25	0.100	2	2	0	3	2	1	301
13707.7341	12	0.993E-27	0.688	5	3	2	6	2	5	400
13710.1480	0	0.109E-25	0.049	2	2	1	3	2	2	301
13710.3079	1	0.628E-25	0.499	2	1	1	3	1	2	301
13710.4450	8	0.162E-26	0.902	6	1	6	5	1	5	221
13710.7120	1	0.576E-26	0.496	6	0	6	5	0	5	221
13711.7410	7	0.948E-26	0.344	4	1	3	3	1	2	221
13712.6042	8	0.808E-27	0.470	7	5	3	7	5	2	221
13717.2579	0	0.906E-27	0.000	2	0	2	3	1	3	400
13717.7092	9	0.130E-26	0.604	3	0	3	3	2	2	301
13718.1938	4	0.150E-26	0.489	7	4	4	7	4	3	301
13720.1377	6	0.126E-26	0.529	7	0	7	6	0	6	221
13720.2524	0	0.613E-27	0.000	5	1	4	5	2	3	400
13720.6614	16	0.430E-27	4.719	6	0	6	6	5	1	202
13720.8188	1	0.684E-26	0.533	7	1	7	6	1	6	221
13721.2530	0	0.374E-27	0.000	4	4	1	5	3	2	400
13721.8083	1	0.596E-26	0.507	4	2	2	3	2	1	221
13723.0944	7	0.969E-27	0.477	8	3	6	8	2	7	320
13723.5380	11	0.513E-27	4.467	8	4	4	8	4	5	301
13724.4815	1	0.725E-25	0.747	2	0	2	3	0	3	301
13725.3094	25	0.287E-27	4.662	4	3	1	5	2	4	400
13726.2380	0	0.234E-25	0.099	2	1	2	3	1	3	301
13727.1105	0	0.131E-26	0.000	5	3	2	4	2	3	042
13727.3423	3	0.207E-26	0.480	2	0	2	2	2	1	301
13727.7610	0	0.104E-25	0.048	5	5	1	5	5	0	301
13728.0367	0	0.280E-26	0.000	4	1	4	4	1	3	301
13729.0022	3	0.221E-26	0.501	8	0	8	7	0	7	221
13729.3329	0	0.392E-27	0.000	9	0	9	8	0	8	221
13729.5614	0	0.804E-26	0.000	2	1	2	3	0	3	400

Table A.1: Continued.

wavenumber	$\Delta\nu$	intensity	ΔI	J′	K'_a	K'_c	J″	K''_a	K''_c	vib
13730.0142	4	0.179E-26	0.511	5	1	4	4	1	3	221
13730.1989	4	0.157E-26	0.471	6	4	3	6	4	2	301
13731.1811	0	0.282E-26	0.000	5	4	2	4	2	3	141
13731.3501	0	0.151E-26	0.000	6	3	4	6	3	3	301
13731.4731	0	0.980E-27	0.000	4	3	2	3	3	1	221
13732.4060	0	0.419E-26	0.000	2	1	2	2	2	1	400
13732.7322	0	0.661E-26	0.000	5	2	4	5	2	3	301
13732.9254	0	0.470E-26	0.000	6	4	2	6	4	3	301
13733.7668	0	0.152E-26	0.000	9	1	9	8	1	8	221
13734.0223	30	0.221E-27	4.605	5	0	5	6	1	6	122
13735.6864	0	0.272E-27	0.000	4	1	3	4	2	2	400
13736.6119	8	0.105E-26	0.540	1	0	1	2	1	2	400
13737.8097	0	0.467E-27	0.000	10	0	10	9	0	9	221
13738.6603	0	0.174E-25	0.049	1	1	0	2	1	1	301
13739.1162	0	0.130E-25	0.049	5	4	2	5	4	1	301
13739.7109	1	0.441E-26	0.496	5	4	1	5	4	2	301
13740.0773	6	0.110E-26	0.486	2	2	1	3	1	2	400
13741.5342	7	0.120E-26	0.506	6	2	5	5	2	4	221
13743.8006	0	0.991E-27	0.000	3	1	2	3	2	1	400
13745.0163	0	0.274E-26	0.000	6	1	5	5	1	4	221
13745.0527	0	0.233E-26	0.000	5	2	3	4	2	2	221
13746.0554	1	0.103E-25	0.097	4	4	1	4	4	0	301
13746.1304	0	0.309E-25	0.098	4	4	0	4	4	1	301
13747.0677	0	0.496E-27	0.000	6	4	3	5	5	0	400
13747.7759	0	0.257E-25	0.050	1	0	1	2	0	2	301
13748.0691	0	0.118E-25	0.050	5	3	3	5	3	2	301
13749.3212	1	0.541E-25	0.351	1	1	1	2	1	2	301
13750.8841	2	0.453E-26	0.607	5	3	3	4	3	2	221
13753.3842	0	0.139E-25	0.049	3	1	3	3	1	2	301
13753.9547	7	0.126E-26	0.535	5	3	2	4	3	1	221
13755.0895	0	0.234E-26	0.000	7	2	6	6	2	5	221
13755.4273	0	0.894E-27	0.000	6	2	5	5	1	4	320
13756.3446	13	0.676E-27	5.006	0	0	0	1	1	1	400
13758.1641	0	0.721E-27	0.000	7	1	6	6	1	5	221
13758.8366	0	0.995E-26	0.050	4	3	2	4	3	1	301
13759.4839	0	0.378E-26	0.000	5	3	2	5	3	3	301
13760.1319	0	0.401E-26	0.000	6	3	3	6	3	4	301
13762.0305	0	0.303E-25	0.050	4	3	1	4	3	2	301
13763.3373	5	0.144E-26	0.495	6	0	6	5	2	3	301
13765.6220	1	0.660E-25	0.543	3	3	1	3	3	0	301
13766.1063	0	0.221E-25	0.049	3	3	0	3	3	1	301
13767.4194	0	0.183E-26	0.000	6	2	4	5	2	3	221
13768.7195	8	0.930E-27	0.492	6	3	4	5	3	3	221
13769.2315	0	0.132E-26	0.000	8	1	7	7	1	6	221
13771.0527	0	0.395E-25	0.199	3	2	2	3	2	1	301
13771.6433	1	0.497E-25	0.347	0	0	0	1	0	1	301
13771.7899	22	0.292E-27	4.591	8	3	5	8	3	6	301
13771.9084	0	0.531E-27	0.000	5	4	1	4	4	0	221

Table A.1: Continued.

wavenumber	$\Delta\nu$	intensity	ΔI	J′	K'_a	K'_c	J″	K''_a	K''_c	vib
13773.0175	0	0.928E-26	0.049	2	1	2	2	1	1	301
13775.5377	0	0.420E-27	0.000	5	3	2	4	4	1	400
13776.6955	9	0.777E-27	5.395	9	2	8	8	2	7	221
13777.3999	0	0.478E-27	0.000	3	0	3	4	1	4	122
13779.2258	0	0.170E-27	0.000	9	1	8	8	1	7	221
13779.9871	21	0.439E-27	5.024	3	3	0	2	2	1	320
13780.1206	0	0.296E-25	0.099	2	2	1	2	2	0	301
13782.8862	1	0.882E-25	0.090	2	2	0	2	2	1	301
13783.5905	0	0.657E-27	0.000	6	3	4	5	4	1	400
13783.7102	0	0.130E-25	0.000	3	2	1	3	2	2	301
13784.9317	0	0.149E-26	0.000	7	3	5	6	3	4	221
13785.8215	0	0.864E-27	0.000	4	2	3	3	3	0	400
13786.2864	1	0.652E-25	0.597	1	1	1	1	1	0	301
13787.4699	33	0.227E-27	4.753	4	2	2	4	2	3	301
13788.1296	0	0.163E-25	0.000	4	1	4	4	2	3	122
13789.8276	0	0.317E-27	0.000	3	1	3	2	2	0	400
13790.5474	14	0.533E-27	4.826	6	4	3	5	4	2	221
13790.8765	0	0.198E-27	0.000	4	3	1	4	1	4	221
13790.9971	5	0.222E-26	0.579	4	0	4	3	2	1	301
13791.5341	4	0.215E-26	0.553	6	4	2	5	4	1	221
13795.6787	0	0.571E-27	0.000	5	2	4	4	3	1	400
13795.9662	0	0.217E-26	0.000	5	2	3	5	2	4	301
13796.0866	22	0.295E-27	4.474	2	0	2	3	1	3	122
13796.7001	0	0.221E-25	0.100	1	1	0	1	1	1	301
13798.1287	14	0.148E-26	1.355	6	2	5	5	3	2	400
13804.2020	0	0.290E-25	0.100	2	1	1	2	1	2	301
13806.2140	0	0.263E-26	0.000	6	2	4	6	2	5	301
13808.9172	8	0.966E-27	0.482	7	4	4	6	4	3	221
13809.3740	5	0.153E-26	0.504	6	5	1	5	5	0	301
13810.0075	0	0.202E-27	0.000	7	6	1	7	5	2	400
13810.5289	16	0.407E-27	4.641	9	3	7	8	3	6	221
13810.8503	19	0.394E-27	5.134	7	4	3	6	4	2	221
13813.0204	32	0.262E-27	5.204	5	3	2	5	2	3	400
13815.0628	0	0.464E-26	0.000	3	1	2	3	1	3	301
13816.9103	12	0.745E-27	5.579	8	3	5	7	3	4	221
13817.7040	0	0.172E-25	0.000	1	0	1	0	0	0	301
13821.1244	0	0.139E-26	0.000	3	1	2	2	2	1	400
13822.0742	14	0.626E-27	4.928	2	0	2	1	1	1	400
13824.2967	12	0.763E-27	6.031	8	0	8	7	5	3	202
13824.6283	0	0.141E-27	0.000	8	4	5	7	4	4	221
13824.7996	32	0.274E-27	5.015	7	1	7	6	2	4	122
13826.2109	7	0.163E-26	0.704	7	5	3	6	5	2	301
13826.9428	22	0.311E-27	5.954	5	2	3	4	1	4	320
13827.0241	0	0.280E-27	0.000	8	2	6	8	2	7	301
13828.2425	1	0.714E-26	0.489	4	1	3	4	1	4	301
13828.8644	0	0.160E-26	0.000	5	2	3	4	3	2	400
13828.9288	0	0.647E-27	0.000	5	3	2	4	2	3	320
13829.4674	8	0.905E-27	0.476	7	4	4	7	3	5	400

Table A.1: Continued.

wavenumber	$\Delta\nu$	intensity	ΔI	J′	K'_a	K'_c	J″	K''_a	K''_c	vib
13829.9774	0	0.670E-27	0.000	8	4	4	7	4	3	221
13830.4438	0	0.234E-27	0.000	10	2	8	9	2	7	221
13831.0572	0	0.214E-25	0.100	2	1	2	1	1	1	301
13833.9687	0	0.353E-27	0.000	2	2	1	2	1	2	400
13835.3616	0	0.380E-27	0.000	6	4	3	6	3	4	400
13835.5822	9	0.798E-27	5.974	3	3	0	3	2	1	400
13836.8318	16	0.551E-27	5.017	5	4	1	5	3	2	400
13837.0634	1	0.827E-25	0.795	2	0	2	1	0	1	301
13837.9402	16	0.728E-27	5.563	5	3	3	5	2	4	400
13838.4260	0	0.289E-27	0.000	3	2	2	3	1	3	400
13838.9917	34	0.385E-27	5.833	9	4	6	8	4	5	221
13839.1860	0	0.849E-27	0.000	4	4	0	4	2	3	221
13841.1674	1	0.615E-25	0.496	2	1	1	1	1	0	301
13841.3579	16	0.504E-27	4.831	3	3	1	3	2	2	400
13841.6527	1	0.530E-26	0.521	3	3	1	2	1	2	221
13841.9196	0	0.111E-26	0.000	5	1	4	5	1	5	301
13842.1431	0	0.717E-26	0.000	2	1	2	1	0	1	400
13842.5475	0	0.689E-27	0.000	8	1	7	7	5	2	071
13844.2978	0	0.733E-27	0.000	4	2	3	4	1	4	400
13845.1910	0	0.553E-27	0.000	7	3	5	7	1	6	301
13845.3939	0	0.122E-26	0.000	4	1	3	3	2	2	400
13845.5149	0	0.437E-26	0.000	3	2	2	3	0	3	301
13846.3212	23	0.521E-27	22.784	4	4	0	4	3	1	400
13847.2785	1	0.881E-25	0.090	3	1	3	2	1	2	301
13847.6886	13	0.701E-27	5.542	4	4	1	4	3	2	400
13847.9011	29	0.299E-27	4.999	6	5	2	6	4	3	400
13848.3764	0	0.423E-25	0.254	3	2	2	2	2	1	301
13848.5984	11	0.138E-26	0.959	4	2	3	4	0	4	301
13848.7866	0	0.206E-27	0.000	6	3	4	6	1	5	301
13849.7011	12	0.944E-27	0.709	4	4	1	3	3	0	320
13851.3231	0	0.341E-26	0.000	1	0	1	1	1	0	122
13852.5450	0	0.212E-25	0.050	3	0	3	2	0	2	301
13853.6832	0	0.138E-25	0.000	3	2	1	2	2	0	301
13853.8441	2	0.304E-26	0.480	5	2	4	5	0	5	301
13854.4049	5	0.139E-26	0.501	6	1	5	6	1	6	301
13854.6822	1	0.111E-25	0.105	3	1	3	2	0	2	400
13855.4314	7	0.149E-26	0.569	5	3	3	5	1	4	301
13857.4446	1	0.661E-26	0.496	4	3	2	3	3	1	301
13857.8647	5	0.209E-26	0.619	4	0	4	3	1	3	400
13858.5081	9	0.975E-27	0.533	6	2	5	6	1	6	400
13859.0154	0	0.196E-25	0.049	4	3	1	3	3	0	301
13859.4204	0	0.379E-27	0.000	6	3	3	5	2	4	320
13860.2449	0	0.547E-27	0.000	6	2	5	6	0	6	301
13861.2709	0	0.366E-25	0.149	4	1	4	3	1	3	301
13861.5820	0	0.212E-26	0.000	5	4	1	4	4	0	301
13861.8423	0	0.266E-25	0.049	3	1	2	2	1	1	301
13864.0427	0	0.113E-25	0.000	4	1	4	3	0	3	400
13865.0758	0	0.169E-25	0.051	4	2	3	3	2	2	301

Table A.1: Continued.

wavenumber	$\Delta\nu$	intensity	ΔI	J′	K'_a	K'_c	J″	K''_a	K''_c	vib
13865.4615	1	0.863E-25	0.090	4	0	4	3	0	3	301
13866.3003	15	0.586E-27	6.406	7	1	6	7	0	7	400
13867.0966	0	0.189E-27	0.000	6	0	6	5	5	1	202
13867.2231	6	0.161E-26	0.630	6	5	1	5	5	0	221
13868.1640	0	0.439E-27	0.000	7	2	6	7	0	7	301
13870.5530	5	0.163E-26	0.509	5	4	1	4	3	2	320
13870.9353	6	0.124E-26	0.524	2	2	1	1	1	0	400
13871.0288	0	0.200E-26	0.000	5	0	5	4	1	4	400
13872.0001	0	0.417E-27	0.000	4	3	2	3	1	3	221
13872.4161	14	0.437E-27	4.719	8	1	7	8	1	8	301
13873.5146	1	0.783E-25	0.748	5	1	5	4	1	4	301
13874.5064	0	0.202E-25	0.050	5	3	3	4	3	2	301
13875.0495	0	0.442E-27	0.000	3	3	1	3	1	2	301
13875.2921	0	0.160E-26	0.000	4	2	2	3	2	1	301
13875.7811	0	0.280E-25	0.150	5	0	5	4	0	4	301
13875.9505	1	0.471E-25	0.298	4	1	4	3	2	1	122
13877.8432	0	0.207E-26	0.000	6	4	3	5	4	2	301
13879.1867	1	0.780E-25	0.680	4	1	3	3	1	2	301
13879.2706	2	0.377E-25	0.475	5	2	4	4	2	3	301
13879.3774	3	0.754E-26	1.617	5	3	2	4	3	1	301
13883.7293	9	0.793E-27	4.777	7	5	3	6	5	2	221
13884.1985	1	0.187E-25	0.146	6	1	6	5	1	5	301
13884.4484	0	0.487E-25	0.299	6	0	6	5	0	5	301
13885.2182	0	0.137E-26	0.000	3	2	2	2	1	1	400
13888.5317	0	0.109E-25	0.050	6	2	4	5	0	5	221
13889.3643	0	0.456E-26	0.000	6	3	4	5	3	3	301
13890.6584	10	0.768E-27	4.794	7	0	7	6	1	6	400
13890.9243	0	0.910E-26	0.049	6	2	5	5	2	4	301
13892.1424	0	0.374E-26	0.000	7	3	4	6	2	5	320
13892.2075	25	0.355E-27	4.985	1	1	0	1	0	1	122
13892.3323	0	0.154E-25	0.049	5	1	4	4	1	3	301
13892.8513	0	0.421E-25	0.248	7	1	7	6	1	6	301
13893.3140	0	0.132E-25	0.050	7	0	7	6	0	6	301
13893.6289	0	0.491E-27	0.000	8	2	6	7	3	5	400
13895.2442	1	0.723E-26	0.500	4	2	3	3	1	2	400
13895.6749	0	0.131E-25	0.000	5	2	3	4	2	2	301
13896.7159	6	0.120E-26	0.479	7	4	3	6	4	2	301
13899.6301	0	0.739E-26	0.000	7	1	6	6	2	5	400
13899.7860	0	0.144E-25	0.049	6	3	3	5	3	2	301
13900.0206	15	0.533E-27	5.684	6	4	3	6	1	6	042
13900.3274	1	0.741E-26	0.489	8	1	8	7	1	7	301
13901.3904	0	0.215E-25	0.098	6	1	5	5	1	4	301
13903.9674	15	0.508E-27	5.059	8	1	7	7	2	6	400
13904.4633	3	0.261E-26	0.505	7	2	6	6	1	5	400
13905.4961	0	0.144E-25	0.050	6	2	5	5	1	4	400
13905.8979	11	0.565E-27	4.486	8	4	5	7	4	4	301
13906.4439	6	0.165E-25	0.517	9	1	9	8	1	8	301
13907.2388	0	0.285E-26	0.000	8	2	7	7	2	6	301

Table A.1: Continued.

wavenumber	$\Delta\nu$	intensity	ΔI	J′	K'_a	K'_c	J″	K''_a	K''_c	vib
13907.4189	9	0.896E-27	0.541	9	2	7	8	3	6	400
13907.5013	9	0.114E-26	0.525	3	2	1	2	1	2	400
13908.4014	2	0.367E-26	0.527	7	1	6	6	1	5	301
13909.4893	12	0.762E-27	5.141	8	2	7	7	1	6	400
13911.1021	0	0.302E-26	0.000	8	3	6	7	3	5	301
13911.1461	0	0.583E-26	0.000	10	1	10	9	1	9	301
13911.5068	0	0.236E-25	0.050	6	2	4	5	2	3	301
13911.7169	0	0.100E-25	0.000	8	1	7	7	1	6	301
13912.6102	1	0.466E-26	0.492	9	2	8	8	2	7	301
13912.9055	7	0.123E-26	0.497	3	3	0	2	2	1	400
13914.4738	3	0.192E-26	0.473	8	4	4	7	4	3	301
13914.5165	0	0.325E-26	0.000	11	0	11	10	0	10	301
13915.7691	0	0.237E-27	0.000	5	5	0	4	4	1	320
13916.4048	0	0.205E-26	0.000	10	2	9	9	2	8	301
13916.9188	0	0.787E-27	0.000	9	4	6	8	4	5	301
13917.0432	0	0.405E-27	0.000	12	0	12	11	0	11	301
13917.5267	0	0.232E-26	0.000	10	1	9	9	1	8	301
13917.9336	0	0.155E-26	0.000	9	3	7	8	3	6	301
13918.5457	0	0.264E-26	0.000	3	2	1	2	0	2	301
13918.6719	0	0.257E-26	0.000	7	3	4	6	3	3	301
13919.5088	0	0.159E-27	0.000	12	1	11	11	1	10	301
13922.5211	2	0.380E-26	0.515	7	2	5	6	2	4	301
13926.2879	28	0.274E-27	4.792	4	3	2	3	2	1	400
13927.0056	0	0.237E-26	0.000	4	4	0	3	2	1	221
13930.4207	16	0.433E-27	4.736	9	2	7	8	2	6	301
13933.9477	0	0.362E-26	0.000	8	3	5	7	3	4	301
13934.2639	21	0.385E-27	4.883	6	5	2	5	4	1	320
13934.4763	10	0.741E-27	4.944	10	2	8	9	2	7	301
13937.6667	0	0.109E-26	0.000	5	3	3	4	2	2	400
13938.3227	17	0.478E-27	5.138	9	3	7	8	2	6	400
13939.0691	0	0.281E-27	0.000	2	1	1	3	1	2	023
13943.2249	0	0.372E-26	0.000	6	3	4	5	2	3	400
13944.6728	8	0.886E-27	0.469	4	4	1	3	3	0	400
13944.9326	0	0.299E-27	0.000	4	4	0	3	3	1	400
13946.7545	29	0.224E-27	4.622	10	4	6	9	4	5	301
13949.2767	22	0.308E-27	4.692	10	3	7	9	3	6	301
13949.4153	18	0.597E-27	6.522	7	5	2	6	4	3	320
13949.7547	0	0.668E-27	0.000	4	2	2	3	0	3	301
13950.4132	0	0.393E-26	0.000	4	1	4	3	0	3	122
13951.1694	0	0.629E-27	0.000	6	4	2	5	2	3	221
13953.4140	0	0.240E-27	0.000	3	3	0	2	1	1	301
13954.7722	26	0.434E-27	7.127	8	3	5	7	1	6	221
13959.5598	5	0.174E-26	0.530	5	3	2	4	2	3	400
13961.5181	0	0.435E-27	0.000	5	4	2	4	3	1	400
13963.2712	5	0.144E-26	0.483	5	4	1	4	3	2	400
13965.3828	21	0.410E-27	5.035	6	6	0	5	5	1	400
13968.4397	0	0.258E-26	0.000	4	3	1	3	1	2	301
13968.9457	13	0.757E-27	5.244	3	3	1	2	1	2	301

Table A.1: Continued.

wavenumber	$\Delta\nu$	intensity	ΔI	J′	K'_a	K'_c	J″	K''_a	K''_c	vib
13974.1724	0	0.412E-27	0.000	2	2	1	1	1	0	122
13974.5421	29	0.255E-27	4.651	1	1	1	2	1	2	023
13975.0156	0	0.157E-26	0.000	6	4	3	5	3	2	400
13975.2252	0	0.562E-27	0.000	8	4	4	7	2	5	221
13976.8812	0	0.455E-27	0.000	5	5	0	4	4	1	400
13981.1345	34	0.441E-27	6.037	7	6	1	6	5	2	400
13981.7446	0	0.462E-27	0.000	7	5	2	7	2	5	400
13983.6259	17	0.341E-27	4.430	7	4	4	6	3	3	400
13984.3244	13	0.552E-27	5.529	5	2	3	4	1	4	400
13985.2782	6	0.116E-26	0.493	5	3	2	4	1	3	301
13986.6178	12	0.701E-27	5.212	8	4	5	7	3	4	400
13988.6904	0	0.608E-27	0.000	7	0	7	8	1	8	202
13988.9027	0	0.103E-26	0.000	5	2	3	4	0	4	301
13990.1658	33	0.347E-27	6.030	10	0	10	11	0	11	103
13994.1337	22	0.633E-27	6.526	6	5	2	5	4	1	400
13995.2410	0	0.250E-27	0.000	8	6	3	7	5	2	400
13996.2951	0	0.226E-27	0.000	6	2	5	7	1	6	202
13997.9692	25	0.330E-27	4.883	4	3	2	3	1	3	301
14002.0051	0	0.458E-27	0.000	3	2	1	4	3	2	202
14002.9817	0	0.559E-27	0.000	6	3	4	6	5	1	103
14007.1544	2	0.304E-26	0.512	6	3	3	5	1	4	301
14007.5965	31	0.221E-27	4.644	6	5	1	7	5	2	103
14009.6495	0	0.417E-27	0.000	5	1	4	6	2	5	202
14011.1589	18	0.342E-27	4.941	7	5	2	6	4	3	400
14011.5069	26	0.269E-27	4.596	1	1	1	1	1	0	023
14017.3732	10	0.673E-27	4.703	6	1	6	7	0	7	202
14017.9757	16	0.358E-27	4.387	4	4	0	3	2	1	301
14019.2959	0	0.492E-27	0.000	7	4	3	8	3	6	202
14021.1423	0	0.561E-27	0.000	9	1	9	10	1	10	103
14021.2232	0	0.359E-27	0.000	8	1	7	9	1	8	103
14022.6635	0	0.302E-27	0.000	1	1	0	1	1	1	023
14023.8428	0	0.595E-27	0.000	2	2	0	2	2	1	023
14025.5787	10	0.871E-27	0.495	2	2	1	3	3	0	202
14028.8265	0	0.446E-27	0.000	6	4	2	7	4	3	103
14029.7997	0	0.284E-27	0.000	5	4	1	4	2	2	301
14029.9710	0	0.116E-26	0.000	5	3	3	4	1	4	301
14030.0206	0	0.561E-27	0.000	3	3	1	3	3	0	023
14030.2720	22	0.312E-27	4.663	6	4	3	7	3	4	202
14032.6183	0	0.140E-26	0.000	6	2	4	5	0	5	301
14036.1007	14	0.695E-27	5.576	7	3	4	6	1	5	301
14038.7999	0	0.100E-26	0.000	6	4	2	5	2	3	301
14039.3732	36	0.323E-27	6.251	4	4	0	4	4	1	023
14043.5793	6	0.113E-26	0.474	5	0	5	6	1	6	202
14044.7449	17	0.433E-27	4.805	5	1	5	6	0	6	202
14045.2892	10	0.782E-27	5.446	5	4	2	4	2	3	301
14046.2997	0	0.354E-27	0.000	3	3	0	2	2	1	122
14047.6647	0	0.244E-27	0.000	7	4	3	6	2	4	301
14049.5554	0	0.372E-27	0.000	4	3	2	4	4	1	202

Table A.1: Continued.

wavenumber	$\Delta\nu$	intensity	ΔI	J′	K'_a	K'_c	J″	K''_a	K''_c	vib
14049.6852	0	0.428E-27	0.000	2	1	2	3	2	1	202
14049.7611	0	0.858E-27	0.000	7	2	6	8	2	7	103
14050.9233	0	0.803E-27	0.000	3	1	2	4	2	3	202
14051.0115	0	0.108E-26	0.000	8	0	8	9	0	9	103
14051.6169	24	0.328E-27	4.922	7	1	6	8	1	7	103
14052.8406	0	0.796E-27	0.000	6	3	3	7	3	4	103
14059.7244	0	0.114E-26	0.000	8	4	4	7	2	5	301
14060.9036	22	0.304E-27	4.983	7	5	3	6	3	4	301
14061.9182	6	0.135E-26	0.492	6	2	4	7	2	5	103
14063.5016	0	0.739E-27	0.000	5	4	2	6	4	3	103
14064.3877	0	0.515E-27	0.000	4	2	3	5	1	4	202
14064.7483	0	0.262E-27	0.000	6	3	4	5	1	5	301
14068.5223	0	0.520E-27	0.000	4	0	4	5	1	5	202
14069.9275	0	0.442E-27	0.000	2	1	1	1	1	0	023
14071.3350	0	0.221E-26	0.000	4	1	4	5	0	5	202
14071.8033	0	0.636E-27	0.000	8	3	5	7	1	6	301
14074.4731	0	0.414E-27	0.000	3	1	3	2	1	2	023
14075.6915	30	0.348E-27	5.307	6	4	3	7	2	6	023
14078.6696	26	0.550E-27	7.669	7	2	5	7	3	4	202
14079.1356	0	0.930E-27	0.000	7	4	3	8	1	8	122
14079.8667	0	0.629E-27	0.000	7	0	7	8	0	8	103
14080.3247	8	0.111E-26	0.589	7	1	7	8	1	8	103
14080.6013	0	0.115E-26	0.000	5	4	1	6	3	4	202
14080.9737	3	0.195E-26	0.490	6	1	5	7	1	6	103
14083.4601	0	0.451E-27	0.000	4	2	3	4	3	2	202
14086.2354	29	0.346E-27	5.239	1	1	1	2	2	0	202
14090.5514	0	0.161E-27	0.000	5	0	5	5	1	4	202
14091.3277	0	0.191E-26	0.000	3	0	3	4	1	4	202
14092.0161	28	0.349E-27	5.250	6	2	4	6	3	3	202
14092.7318	7	0.124E-26	0.495	1	1	0	2	2	1	202
14093.2159	0	0.934E-27	0.000	5	2	3	6	2	4	103
14093.4413	19	0.397E-27	4.755	7	4	4	6	2	5	301
14095.3237	9	0.774E-27	4.689	4	4	0	5	4	1	103
14095.4788	26	0.370E-27	5.167	4	4	1	5	4	2	103
14096.7583	18	0.448E-27	4.885	4	1	4	4	2	3	202
14097.4657	0	0.524E-27	0.000	5	3	3	6	3	4	103
14097.5965	0	0.901E-27	0.000	3	1	3	4	0	4	202
14098.2941	0	0.578E-27	0.000	5	2	3	5	3	2	202
14098.8335	7	0.117E-26	0.504	5	3	2	6	2	5	202
14098.9943	22	0.357E-27	4.797	3	2	1	3	3	0	202
14101.5441	12	0.402E-27	4.174	7	3	5	6	1	6	301
14107.3246	0	0.101E-26	0.000	6	1	6	7	1	7	103
14107.4305	0	0.343E-26	0.000	6	0	6	7	0	7	103
14108.6859	0	0.159E-26	0.000	4	4	1	5	3	2	202
14109.2155	0	0.114E-26	0.000	5	1	4	6	1	5	103
14111.9142	0	0.633E-27	0.000	2	0	2	3	1	3	202
14112.3888	0	0.618E-27	0.000	4	4	0	5	3	3	202
14112.9557	0	0.198E-26	0.000	5	2	4	6	2	5	103

Table A.1: Continued.

wavenumber	$\Delta\nu$	intensity	ΔI	J′	K'_a	K'_c	J″	K''_a	K''_c	vib
14114.0777	0	0.281E-27	0.000	3	1	3	3	2	2	202
14114.9414	12	0.623E-27	4.955	5	1	4	5	2	3	202
14116.2749	20	0.279E-27	4.350	6	0	6	5	0	5	023
14116.9392	21	0.411E-27	4.975	4	1	3	3	1	2	023
14118.9307	44	0.162E-27	4.651	4	0	4	4	1	3	202
14120.1254	0	0.790E-27	0.000	4	3	1	5	3	2	103
14124.1474	5	0.168E-26	0.507	2	1	2	3	0	3	202
14124.2306	1	0.470E-26	0.514	4	2	2	5	2	3	103
14125.1674	28	0.275E-27	4.808	8	2	6	7	0	7	301
14127.9140	33	0.208E-27	4.583	4	3	1	3	3	0	023
14131.3353	5	0.158E-26	0.492	1	0	1	2	1	2	202
14133.4966	1	0.596E-26	0.525	5	1	5	6	1	6	103
14133.8566	0	0.193E-26	0.000	5	0	5	6	0	6	103
14136.6798	0	0.601E-26	0.000	4	1	3	5	1	4	103
14137.9063	5	0.147E-26	0.487	4	2	3	5	2	4	103
14138.7450	0	0.137E-26	0.000	3	1	2	3	2	1	202
14140.7600	0	0.509E-27	0.000	6	0	6	6	2	5	103
14141.2275	31	0.311E-27	5.159	2	1	1	2	2	0	202
14142.1791	0	0.312E-27	0.000	3	3	0	4	2	3	202
14142.2739	0	0.134E-26	0.000	3	0	3	3	1	2	202
14143.8906	10	0.815E-27	5.261	3	3	0	4	3	1	103
14144.9683	3	0.255E-26	0.513	3	3	1	4	3	2	103
14152.0748	11	0.658E-27	5.034	6	6	0	6	6	1	103
14153.1334	11	0.851E-27	0.639	4	2	2	5	1	5	202
14154.8994	4	0.204E-26	0.496	3	2	1	4	2	2	103
14158.6937	0	0.759E-27	0.000	2	0	2	2	1	1	202
14159.0855	0	0.871E-26	0.000	4	0	4	5	0	5	103
14160.8946	0	0.243E-26	0.000	4	1	4	5	1	5	103
14163.6818	0	0.597E-26	0.000	3	2	2	4	2	3	103
14164.0525	2	0.369E-26	0.595	3	1	2	4	1	3	103
14164.5316	39	0.418E-27	7.289	5	0	5	5	2	4	103
14168.3001	4	0.183E-26	0.499	1	0	1	1	1	0	202
14180.4813	9	0.981E-27	0.514	5	1	5	5	1	4	103
14181.4505	21	0.455E-27	5.415	7	3	5	6	4	2	202
14183.0749	2	0.388E-26	0.508	3	0	3	4	0	4	103
14183.8833	0	0.107E-25	0.050	3	1	3	4	1	4	103
14184.5082	8	0.117E-26	0.576	4	0	4	4	2	3	103
14184.7930	1	0.557E-26	0.506	2	2	0	3	2	1	103
14186.9367	3	0.274E-26	0.508	5	5	1	5	5	0	103
14187.7480	0	0.422E-27	0.000	7	4	4	7	4	3	103
14189.2118	4	0.194E-26	0.527	2	2	1	3	2	2	103
14191.6613	0	0.107E-25	0.052	2	1	1	3	1	2	103
14200.2546	0	0.328E-27	0.000	6	4	3	6	4	2	103
14202.4546	3	0.223E-26	0.526	1	1	0	1	0	1	202
14203.4915	0	0.103E-26	0.000	6	4	2	6	4	3	103
14203.5472	0	0.104E-26	0.000	4	2	2	4	1	3	202
14203.7044	0	0.349E-27	0.000	6	4	2	6	3	3	202
14204.1251	0	0.161E-26	0.000	5	3	2	5	2	3	202

Table A.1: Continued.

wavenumber	$\Delta\nu$	intensity	ΔI	J′	K'_a	K'_c	J″	K''_a	K''_c	vib
14206.0635	0	0.133E-25	0.050	2	0	2	3	0	3	103
14207.1441	0	0.402E-26	0.000	2	1	2	3	1	3	103
14208.4158	3	0.240E-26	0.511	3	2	1	3	1	2	202
14208.9241	0	0.534E-27	0.000	2	0	2	2	2	1	103
14209.7410	0	0.254E-26	0.000	5	4	2	5	4	1	103
14210.4646	33	0.804E-27	14.467	5	4	1	5	4	2	103
14213.2081	0	0.188E-26	0.000	3	1	2	3	0	3	202
14214.5366	19	0.696E-27	6.397	2	2	0	2	1	1	202
14217.3438	3	0.203E-26	0.513	4	4	1	4	4	0	103
14217.4716	1	0.536E-26	0.483	4	4	0	4	4	1	103
14218.4718	0	0.562E-27	0.000	4	3	1	4	2	2	202
14219.2934	2	0.293E-26	0.502	1	1	0	2	1	1	103
14220.2559	0	0.229E-26	0.000	5	4	1	5	3	2	202
14221.0213	0	0.508E-27	0.000	1	1	1	0	0	0	202
14223.8230	17	0.387E-27	4.528	4	1	3	4	0	4	202
14224.4412	11	0.705E-27	6.364	6	4	3	6	3	4	202
14228.8992	0	0.116E-26	0.000	2	2	1	2	1	2	202
14228.9841	0	0.414E-26	0.000	1	0	1	2	0	2	103
14229.3830	0	0.679E-27	0.000	5	4	2	5	3	3	202
14229.7977	0	0.891E-26	0.000	1	1	1	2	1	2	103
14230.0001	0	0.157E-26	0.000	3	3	0	3	2	1	202
14231.5584	14	0.472E-27	5.191	6	3	4	6	2	5	202
14232.2806	0	0.177E-26	0.000	4	4	0	4	3	1	202
14234.8295	0	0.192E-26	0.000	3	1	3	3	1	2	103
14235.1234	1	0.422E-26	0.493	4	4	1	4	3	2	202
14236.1664	5	0.158E-26	0.483	3	0	3	2	1	2	202
14236.7275	0	0.177E-26	0.000	2	1	2	1	0	1	202
14237.1226	33	0.219E-27	4.689	5	3	3	5	3	2	103
14237.6135	0	0.645E-27	0.000	4	2	3	4	2	2	103
14238.9220	10	0.100E-26	0.520	4	2	3	4	1	4	202
14241.9529	0	0.111E-25	0.000	3	3	1	3	3	0	103
14242.4989	2	0.384E-26	0.496	3	3	0	3	3	1	103
14244.4558	35	0.157E-27	4.278	4	3	2	4	3	1	103
14245.5915	0	0.223E-27	0.000	5	2	4	5	1	5	202
14246.5622	7	0.112E-26	0.494	4	3	1	4	3	2	103
14247.0022	26	0.314E-27	5.501	6	3	3	6	3	4	103
14248.9020	14	0.637E-27	5.040	3	1	3	2	0	2	202
14251.5031	0	0.575E-26	0.000	3	2	2	3	2	1	103
14252.1660	0	0.533E-27	0.000	4	0	4	3	1	3	202
14252.5809	0	0.761E-26	0.000	0	0	0	1	0	1	103
14253.9235	0	0.150E-26	0.000	2	1	2	2	1	1	103
14259.0423	0	0.189E-26	0.000	4	1	4	3	0	3	202
14259.1845	0	0.493E-26	0.000	2	2	1	2	2	0	103
14262.1167	0	0.145E-25	0.050	2	2	0	2	2	1	103
14264.6038	0	0.192E-26	0.000	3	2	1	3	2	2	103
14265.0960	0	0.151E-26	0.000	5	0	5	4	1	4	202
14265.8625	5	0.157E-26	0.488	2	2	1	1	1	0	202
14266.7630	0	0.107E-25	0.000	1	1	1	1	1	0	103

Table A.1: Continued.

wavenumber	$\Delta\nu$	intensity	ΔI	J′	K'_a	K'_c	J″	K''_a	K''_c	vib
14268.3617	16	0.603E-27	5.145	5	1	5	4	0	4	202
14270.7696	0	0.242E-26	0.000	4	2	2	4	2	3	103
14277.1034	7	0.112E-26	0.530	6	1	6	5	0	5	202
14277.3326	0	0.360E-26	0.000	1	1	0	1	1	1	103
14285.5551	1	0.458E-26	0.500	2	1	1	2	1	2	103
14289.8661	0	0.954E-27	0.000	4	2	3	3	1	2	202
14292.1775	0	0.215E-27	0.000	8	1	8	7	0	7	202
14297.2903	0	0.724E-27	0.000	3	1	2	3	1	3	103
14298.9117	0	0.298E-26	0.000	1	0	1	0	0	0	103
14299.6298	22	0.344E-27	4.720	6	2	5	5	1	4	202
14302.3171	25	0.404E-27	5.172	3	2	1	2	1	2	202
14305.9875	18	0.380E-27	4.563	3	3	1	2	2	0	202
14307.3248	11	0.855E-27	0.530	3	3	0	2	2	1	202
14311.2123	6	0.126E-26	0.504	4	1	3	4	1	4	103
14311.9631	0	0.372E-26	0.000	2	1	2	1	1	1	103
14318.6448	0	0.153E-25	0.051	2	0	2	1	0	1	103
14321.3920	0	0.547E-27	0.000	4	3	2	3	2	1	202
14322.5213	0	0.105E-25	0.049	2	1	1	1	1	0	103
14325.9659	13	0.805E-27	6.117	3	2	2	3	0	3	103
14328.7232	0	0.163E-25	0.050	3	1	3	2	1	2	103
14328.8263	1	0.858E-26	0.051	3	2	2	2	2	1	103
14331.8923	10	0.850E-27	0.542	5	4	2	4	4	1	103
14332.1066	0	0.385E-27	0.000	4	4	1	3	3	0	202
14334.3816	0	0.582E-26	0.000	3	0	3	2	0	2	103
14334.5770	0	0.278E-26	0.000	3	2	1	2	2	0	103
14343.0638	5	0.138E-26	0.486	4	3	2	3	3	1	103
14343.5470	1	0.460E-26	0.513	4	3	1	3	3	0	103
14344.0694	0	0.491E-26	0.000	3	1	2	2	1	1	103
14344.5424	1	0.514E-26	0.509	4	1	4	3	1	3	103
14346.6908	0	0.983E-27	0.000	5	4	1	4	3	2	202
14346.7957	0	0.169E-25	0.000	4	0	4	3	0	3	103
14347.8973	0	0.411E-27	0.000	6	4	3	5	4	2	103
14349.7317	11	0.775E-27	5.040	6	4	2	5	4	1	103
14350.6624	11	0.741E-27	5.131	5	3	2	4	2	3	202
14355.0145	0	0.135E-25	0.051	5	1	5	4	1	4	103
14357.4691	0	0.471E-26	0.000	5	0	5	4	0	4	103
14358.5909	0	0.967E-26	0.050	4	2	2	3	2	1	103
14362.1574	0	0.134E-25	0.051	4	1	3	3	1	2	103
14362.4106	15	0.477E-27	4.693	7	4	4	6	4	3	103
14363.5562	2	0.388E-26	0.492	5	3	3	4	3	2	103
14364.7865	1	0.805E-26	0.505	5	2	4	4	2	3	103
14365.3642	5	0.157E-26	0.518	5	3	2	4	3	1	103
14367.1619	0	0.105E-25	0.050	6	0	6	5	0	5	103
14368.1196	14	0.537E-27	4.734	6	4	3	5	2	4	023
14371.8363	19	0.439E-27	4.928	2	2	0	1	0	1	103
14374.7860	2	0.353E-26	0.518	7	4	3	6	1	6	122
14375.5981	2	0.434E-26	0.544	5	1	4	4	1	3	103
14375.9323	0	0.215E-26	0.000	7	0	7	6	0	6	103

Table A.1: Continued.

wavenumber	$\Delta\nu$	intensity	ΔI	J′	K'_a	K'_c	J″	K''_a	K''_c	vib
14375.9763	0	0.357E-26	0.000	7	1	7	6	1	6	103
14380.1974	10	0.894E-27	0.505	5	2	3	4	1	4	202
14381.2238	0	0.325E-26	0.000	7	2	6	6	2	5	103
14383.3219	0	0.141E-26	0.000	8	1	8	7	1	7	103
14383.4896	0	0.417E-26	0.000	8	0	8	7	0	7	103
14384.3058	1	0.734E-26	0.526	6	1	5	5	1	4	103
14387.9293	0	0.748E-27	0.000	6	3	3	5	2	4	202
14390.0254	0	0.657E-27	0.000	9	0	9	8	0	8	103
14394.2907	0	0.229E-26	0.000	8	1	7	7	1	6	103
14395.3544	0	0.189E-26	0.000	10	0	10	9	0	9	103
14397.2131	0	0.496E-26	0.000	6	2	4	5	2	3	103
14399.3226	11	0.749E-27	5.720							
14399.4311	0	0.394E-27	0.000	3	2	1	2	0	2	103
14400.5330	14	0.633E-27	5.010							
14402.1498	8	0.112E-26	0.676	7	3	5	6	3	4	103
14406.4879	10	0.700E-27	5.317	7	3	4	6	3	3	103
14408.9756	9	0.119E-26	0.564							
14414.9410	24	0.609E-27	6.779							
14416.3378	7	0.113E-26	0.489	8	2	6	7	2	5	103
14422.4276	0	0.674E-27	0.000	8	3	5	7	3	4	103
14494.0262	36	0.299E-27	5.611	6	3	3	5	1	4	103
14518.3138	56	0.415E-27	8.250	6	2	4	5	0	5	103

Table A.2: The line positions (cm^{-1}) and intensities (cm $molecule^{-1}$) of $H_2{}^{18}O$ observed in the range 16570 – 17120 cm^{-1}. The intensities are scaled to match the natural abundance of $H_2{}^{18}O$ and normalised at 296 K. Vibrational states are given in $v_1v_2v_3$ normal mode notation in column 9. The estimated uncertainty on the line position is 0.01 cm^{-1} and on the line intensity is about 15% (see section 7.1.1). Unlike the Fourier transform spectra, the uncertainty in line position and intensity cannot be obtained individually for each line in CRDS.

frequency	intensity	J′	K'_a	K'_c	J″	K''_a	K''_c	vib
16573.006	0.964E-28							
16573.726	0.791E-28							
16574.309	0.349E-27							
16576.343	0.340E-27							
16576.959	0.150E-27							
16582.506	0.110E-28							
16583.088	0.344E-28							
16586.780	0.150E-27	6	3	4	7	3	5	401
16591.441	0.305E-27	6	1	5	7	1	6	321
16598.170	0.147E-27	3	1	3	4	2	2	420
16599.987	0.688E-28							
16601.743	0.945E-28							
16603.306	0.120E-27							
16604.621	0.378E-27	3	2	1	4	3	2	420
16605.490	0.944E-28							
16606.257	0.272E-28							
16606.497	0.215E-27	5	2	3	6	2	4	321
16607.326	0.217E-28							
16607.626	0.935E-28							
16609.648	0.156E-27							
16611.020	0.752E-28	4	1	3	3	1	2	241
16611.756	0.428E-28							
16612.072	0.148E-27	5	3	3	6	4	2	142
16612.561	0.361E-27							
16614.039	0.197E-27	5	4	2	6	3	3	340
16614.576	0.258E-28							
16616.319	0.372E-28							
16616.739	0.219E-27	5	1	4	6	1	5	321
16619.024	0.583E-27	5	3	3	6	3	4	401
16622.008	0.570E-28	7	1	6	8	2	7	500
16622.628	0.110E-27	8	5	3	9	5	4	241
16623.297	0.198E-27	5	2	3	6	3	4	500
16624.777	0.590E-27	5	2	4	6	2	5	321
16627.815	0.195E-28							
16631.551	0.891E-28	6	2	4	7	2	5	401
16631.791	0.687E-27	5	1	5	6	1	6	321
16632.097	0.164E-27	6	3	3	7	3	4	321
16636.440	0.153E-27	6	4	2	7	2	5	241
16637.354	0.133E-28							
16637.554	0.494E-28							
16639.039	0.807E-27	4	2	2	5	2	3	321

Table A.2: Continued.

frequency	intensity	J′	K'_a	K'_c	J″	K''_a	K''_c	vib
16639.998	0.155E-28							
16642.176	0.780E-27	4	1	3	5	1	4	321
16642.945	0.236E-28							
16645.355	0.277E-28	6	3	4	7	3	5	321
16645.802	0.351E-27							
16646.091	0.221E-27	4	4	1	5	4	2	401
16646.532	0.289E-27	4	3	1	5	3	2	401
16647.525	0.604E-28							
16649.082	0.468E-27	4	4	1	5	3	2	340
16649.556	0.184E-27	7	3	4	7	4	3	500
16650.058	0.131E-27	3	1	2	4	2	3	420
16650.441	0.667E-27	7	1	7	8	1	8	401
16650.862	0.221E-27	4	3	2	5	3	3	401
16651.310	0.242E-28							
16653.224	0.337E-27	4	2	3	5	2	4	321
16653.783	0.384E-27	6	1	5	7	1	6	401
16654.498	0.116E-27							
16655.347	0.101E-27							
16656.825	0.112E-27	8	1	8	7	2	5	142
16657.307	0.928E-28	5	1	4	5	3	3	321
16659.110	0.979E-28	5	3	3	5	4	2	500
16659.512	0.204E-28	6	3	3	6	4	2	500
16661.399	0.258E-27							
16663.306	0.434E-28	6	4	3	6	4	2	241
16664.535	0.983E-28	5	3	2	5	4	1	500
16665.156	0.172E-27							
16665.878	0.510E-28	6	4	2	6	4	3	241
16666.643	0.136E-27	4	2	3	5	1	4	420
16667.189	0.225E-27	5	2	3	6	2	4	401
16668.173	0.149E-27	5	3	2	6	3	3	321
16668.668	0.608E-27	3	1	2	4	1	3	321
16670.848	0.399E-28							
16671.981	0.399E-27	3	2	1	4	2	2	321
16672.367	0.245E-27							
16673.255	0.255E-27	3	1	3	4	3	2	043
16675.408	0.553E-28							
16676.108	0.245E-27	5	3	3	6	3	4	321
16676.259	0.924E-28							
16676.428	0.483E-28							
16676.842	0.767E-28							
16677.142	0.236E-28							
16679.534	0.364E-27							
16680.171	0.276E-27	6	1	6	7	1	7	401
16680.880	0.145E-26	3	2	2	4	2	3	321
16682.120	0.672E-27	3	3	1	4	3	2	401
16682.435	0.361E-27	5	1	4	6	1	5	401
16683.266	0.461E-28	4	3	2	4	2	3	340
16683.746	0.333E-28	6	3	4	6	2	5	340

Table A.2: Continued.

frequency	intensity	J′	K'_a	K'_c	J″	K''_a	K''_c	vib
16685.683	0.108E-26							
16686.327	0.676E-27	5	2	4	6	2	5	401
16689.235	0.128E-28							
16689.746	0.631E-28	7	1	7	7	1	6	401
16690.561	0.101E-27	3	1	3	3	2	2	142
16696.057	0.111E-26	2	1	1	3	1	2	321
16696.738	0.519E-28							
16698.737	0.124E-27	5	2	3	5	3	2	420
16700.521	0.102E-26	4	2	2	5	2	3	401
16700.815	0.142E-27							
16701.424	0.111E-27							
16702.638	0.438E-27	4	3	1	5	3	2	321
16705.671	0.509E-28	4	3	2	5	2	3	500
16706.996	0.629E-28							
16708.331	0.116E-26	5	1	5	6	1	6	401
16709.109	0.215E-27	4	1	4	4	1	3	321
16709.475	0.198E-28							
16710.212	0.403E-27	2	1	2	3	1	3	321
16711.115	0.121E-26	4	1	3	5	1	4	401
16713.456	0.287E-27	6	5	2	6	5	1	401
16715.177	0.526E-27	4	2	3	5	2	4	401
16716.094	0.719E-28	3	1	2	4	2	3	500
16718.091	0.551E-28	5	4	1	6	3	4	500
16719.190	0.935E-28							
16721.523	0.604E-28	3	1	2	3	2	1	142
16721.755	0.109E-27							
16722.371	0.537E-28							
16723.738	0.422E-27							
16724.094	0.121E-27	5	1	4	5	2	3	420
16724.495	0.816E-28							
16729.757	0.132E-28	7	2	6	7	4	3	043
16730.049	0.178E-27							
16730.201	0.669E-28	4	1	3	4	3	2	401
16730.816	0.330E-28	6	1	6	5	2	3	142
16731.081	0.198E-27							
16732.298	0.933E-28	3	1	3	3	1	2	321
16732.950	0.231E-27	4	1	3	4	2	2	142
16733.319	0.398E-28							
16733.570	0.986E-28	1	1	1	2	1	2	321
16733.832	0.143E-26							
16735.193	0.725E-27	4	1	4	5	1	5	401
16735.681	0.494E-28							
16735.880	0.576E-27	3	3	1	4	3	2	321
16736.247	0.814E-27							
16736.262	0.773E-27	7	3	5	6	5	2	321
16736.621	0.485E-27	2	2	1	3	1	2	420
16737.206	0.147E-27	2	1	1	3	2	2	500
16737.847	0.122E-27							

Table A.2: Continued.

frequency	intensity	J′	K'_a	K'_c	J″	K''_a	K''_c	vib
16738.820	0.639E-28							
16740.176	0.943E-27	9	6	4	9	7	3	340
16740.913	0.142E-27	6	3	4	6	3	3	401
16741.217	0.417E-28	7	3	5	7	4	4	142
16743.347	0.119E-26	3	2	2	4	2	3	401
16745.341	0.614E-28							
16747.541	0.135E-27	6	4	3	6	4	2	401
16747.892	0.476E-28							
16750.188	0.574E-27	4	2	3	4	3	2	500
16752.460	0.187E-28							
16753.701	0.112E-28							
16755.314	0.123E-27	5	1	5	5	1	4	401
16755.605	0.100E-27							
16756.960	0.131E-27							
16758.762	0.121E-26	5	4	2	5	4	1	401
16759.720	0.389E-27	5	3	3	5	4	2	142
16759.845	0.361E-28	3	2	2	3	3	1	500
16760.093	0.365E-27	3	2	1	4	1	4	420
16760.558	0.416E-28	4	3	2	5	2	3	420
16761.004	0.155E-26	3	1	3	4	1	4	401
16762.379	0.111E-28	5	4	1	6	2	4	401
16762.694	0.274E-27	7	3	4	6	5	1	321
16763.528	0.698E-28	5	3	2	5	5	1	043
16764.966	0.903E-29	4	2	2	4	3	1	500
16767.930	0.130E-26	5	3	2	5	3	3	401
16768.696	0.923E-27	3	2	2	3	2	1	321
16769.398	0.167E-26	2	1	1	3	1	2	401
16770.482	0.190E-27	6	4	3	6	3	4	340
16770.777	0.133E-26	2	2	1	3	2	2	401
16770.777	0.135E-26	4	3	2	4	3	1	401
16772.040	0.873E-28	5	4	2	5	3	3	340
16772.209	0.445E-28							
16772.948	0.466E-27	4	3	1	4	3	2	401
16775.524	0.816E-27	4	4	1	4	3	2	340
16776.797	0.250E-28	7	3	5	7	3	4	321
16778.320	0.322E-27	4	1	4	3	3	1	401
16781.731	0.761E-27							
16785.435	0.952E-27	2	1	2	3	1	3	401
16785.598	0.669E-27	4	2	2	4	2	3	321
16786.721	0.781E-29							
16787.147	0.138E-28							
16789.968	0.507E-27	2	1	1	2	1	2	321
16790.790	0.653E-28							
16791.624	0.173E-27	5	2	4	5	2	3	401
16793.244	0.348E-27	2	1	2	2	2	1	500
16793.562	0.107E-27	5	2	3	5	2	4	321
16793.810	0.829E-28							
16794.149	0.108E-27							

Table A.2: Continued.

frequency	intensity	J′	K'_a	K'_c	J″	K''_a	K''_c	vib
16794.820	0.192E-27	7	3	4	7	2	5	500
16798.849	0.825E-28	3	1	2	2	2	1	142
16799.555	0.163E-27							
16799.879	0.358E-28	6	3	3	6	1	6	241
16801.893	0.132E-27	3	1	2	3	1	3	321
16803.908	0.431E-27	3	1	2	3	2	1	500
16805.931	0.439E-28							
16806.114	0.553E-28	5	2	3	5	1	4	420
16808.968	0.191E-26	1	1	1	2	1	2	401
16811.599	0.511E-28							
16811.956	0.631E-27	3	1	3	3	1	2	401
16814.888	0.299E-27	4	2	3	4	2	2	401
16815.013	0.222E-27	2	1	2	1	1	1	321
16815.751	0.238E-27	5	3	3	5	3	2	321
16816.131	0.748E-28							
16816.689	0.247E-27	4	1	3	4	1	4	321
16818.944	0.521E-28							
16819.254	0.536E-28							
16824.231	0.862E-28	7	3	4	6	4	3	500
16824.447	0.432E-28	6	3	3	5	2	4	340
16825.483	0.703E-28							
16826.196	0.822E-27	3	1	3	2	1	2	321
16826.897	0.869E-27	4	1	3	3	2	2	420
16829.097	0.718E-27							
16830.273	0.711E-28							
16830.522	0.929E-27	5	4	1	5	4	2	321
16832.196	0.324E-27	2	1	2	2	1	1	401
16835.597	0.154E-27							
16839.056	0.713E-28							
16840.774	0.738E-27							
16843.393	0.478E-27							
16843.578	0.117E-26	3	2	1	3	2	2	401
16845.041	0.216E-27							
16845.308	0.165E-27							
16845.549	0.905E-27	7	2	5	6	1	6	340
16845.965	0.130E-26							
16847.053	0.719E-27	4	2	2	4	2	3	401
16847.788	0.110E-27	6	1	5	6	1	6	321
16848.663	0.415E-27	6	3	4	6	2	5	500
16850.461	0.166E-28							
16852.343	0.836E-28							
16853.251	0.349E-27							
16854.286	0.157E-27	6	4	3	6	3	4	500
16854.736	0.321E-28							
16854.943	0.302E-28							
16855.200	0.589E-28	3	3	1	3	2	2	500
16855.455	0.263E-27	5	5	1	6	2	4	500
16858.334	0.412E-28	6	3	4	6	1	5	401

Table A.2: Continued.

frequency	intensity	J′	K'_a	K'_c	J″	K''_a	K''_c	vib
16858.832	0.820E-28							
16859.885	0.283E-27	6	5	2	5	5	1	401
16861.530	0.538E-28	6	2	4	6	2	5	401
16861.759	0.119E-27							
16862.612	0.339E-27							
16863.294	0.110E-26	2	1	1	2	1	2	401
16864.308	0.309E-27							
16865.498	0.259E-28							
16865.739	0.149E-28							
16866.025	0.955E-28	5	3	3	5	1	4	401
16866.420	0.385E-27							
16866.969	0.294E-28							
16867.284	0.220E-27							
16867.652	0.746E-27	4	1	3	3	1	2	321
16868.076	0.423E-27							
16869.366	0.614E-27	4	3	2	3	3	1	401
16870.049	0.258E-27							
16870.632	0.266E-27	5	1	4	4	2	3	420
16871.352	0.458E-28							
16873.434	0.101E-26	3	1	2	3	1	3	401
16874.583	0.104E-27							
16875.541	0.179E-27	6	1	5	5	2	4	420
16875.965	0.648E-28							
16876.629	0.786E-27	5	2	4	4	2	3	321
16877.857	0.114E-27							
16881.221	0.336E-27	3	1	2	2	2	1	500
16882.860	0.185E-27							
16883.089	0.353E-27	5	1	4	4	1	3	321
16883.321	0.546E-29							
16883.930	0.252E-28							
16884.392	0.349E-28							
16884.684	0.504E-28							
16885.104	0.417E-27	5	3	3	4	3	2	401
16885.398	0.202E-27							
16887.839	0.189E-27	5	3	2	4	3	1	401
16888.535	0.591E-28	3	3	1	3	1	2	401
16889.397	0.370E-27	5	2	3	4	3	2	500
16890.252	0.676E-27	2	1	2	1	1	1	401
16890.719	0.956E-28	9	4	5	8	5	4	420
16891.913	0.169E-27							
16892.121	0.565E-27	4	2	3	3	1	2	420
16892.641	0.301E-27	7	1	6	6	2	5	420
16893.278	0.317E-27	5	2	3	4	2	2	321
16894.783	0.452E-27	6	1	5	5	1	4	321
16895.179	0.135E-27	6	4	3	5	4	2	401
16896.059	0.523E-27							
16896.232	0.512E-27							
16896.436	0.412E-27	6	4	2	5	4	1	401

Table A.2: Continued.

frequency	intensity	J′	K'_a	K'_c	J″	K''_a	K''_c	vib
16896.650	0.402E-27	7	2	6	6	2	5	321
16898.142	0.200E-27							
16898.395	0.911E-28	5	1	4	5	1	5	401
16898.761	0.173E-27							
16898.933	0.146E-27	6	3	4	5	3	3	401
16901.511	0.528E-27							
16902.001	0.577E-28							
16902.471	0.469E-28							
16903.352	0.315E-27							
16904.484	0.357E-27	4	1	3	3	2	2	500
16904.945	0.295E-27	3	2	1	2	1	2	420
16905.304	0.336E-27							
16905.652	0.506E-27	4	2	3	4	1	4	500
16905.913	0.711E-27	6	3	4	6	2	5	420
16906.306	0.670E-28	5	3	3	5	2	4	420
16906.700	0.650E-28	9	2	8	8	1	7	420
16907.863	0.835E-28	7	3	5	7	2	6	420
16908.256	0.702E-28							
16908.487	0.980E-27	3	2	2	2	2	1	401
16908.805	0.698E-28							
16909.282	0.279E-27							
16909.603	0.445E-27							
16909.914	0.145E-27							
16910.132	0.301E-27	6	1	5	6	1	6	401
16910.910	0.143E-27	7	3	5	6	4	2	142
16912.437	0.950E-28	8	1	7	7	2	6	420
16916.931	0.696E-28	6	3	4	6	1	5	321
16920.214	0.587E-27	3	1	2	2	1	1	401
16924.018	0.255E-27							
16924.534	0.770E-27	4	3	2	3	3	1	321
16924.727	0.543E-27	5	1	4	4	2	3	500
16925.480	0.235E-27							
16926.637	0.107E-27							
16927.125	0.338E-27							
16928.795	0.139E-26							
16929.833	0.137E-26	5	1	5	4	1	4	401
16930.376	0.801E-28							
16934.860	0.133E-26	4	2	2	3	2	1	401
16935.594	0.268E-28	10	2	8	9	2	7	321
16936.618	0.148E-26	4	1	3	3	1	2	401
16938.172	0.723E-27	5	2	4	4	2	3	401
16938.340	0.443E-27	4	4	1	4	3	2	420
16938.961	0.508E-27	6	1	6	5	1	5	401
16940.017	0.392E-27	4	3	2	3	2	1	500
16941.285	0.261E-27	6	1	5	5	2	4	500
16941.457	0.123E-27							
16942.214	0.290E-27	5	3	3	4	3	2	321
16942.830	0.392E-28							

Table A.2: Continued.

frequency	intensity	J′	K'_a	K'_c	J″	K''_a	K''_c	vib
16945.466	0.399E-28							
16945.659	0.402E-27							
16946.091	0.142E-26	5	3	2	4	3	1	321
16947.154	0.239E-27	3	2	2	2	1	1	500
16947.654	0.151E-27	4	3	1	3	2	2	500
16948.179	0.310E-27	6	5	1	6	3	4	401
16948.801	0.453E-27	5	1	4	4	1	3	401
16949.212	0.462E-27	5	3	3	4	2	2	500
16949.524	0.159E-27	6	2	5	5	2	4	401
16952.754	0.410E-27	5	4	2	4	4	1	321
16953.459	0.929E-27	7	1	6	6	2	5	500
16953.588	0.123E-27							
16953.718	0.500E-27							
16953.965	0.730E-27	6	3	4	5	2	3	500
16954.105	0.540E-27							
16955.697	0.164E-27							
16956.569	0.655E-27							
16957.113	0.475E-27	6	1	5	5	1	4	401
16957.390	0.224E-27							
16957.531	0.602E-28	6	3	4	5	3	3	321
16957.997	0.625E-27							
16958.719	0.134E-27	5	4	1	4	2	2	241
16959.322	0.194E-27	9	2	7	8	1	8	340
16959.913	0.386E-28							
16961.093	0.246E-28							
16961.703	0.179E-27							
16962.317	0.294E-27	5	2	4	4	1	3	500
16965.120	0.916E-28	5	4	1	5	1	4	500
16965.296	0.118E-28							
16965.913	0.240E-27	6	3	3	5	3	2	321
16966.325	0.270E-27	6	2	5	5	1	4	500
16966.830	0.357E-27	6	2	4	5	2	3	401
16967.953	0.156E-27							
16969.289	0.262E-27	3	2	1	2	1	2	500
16970.719	0.252E-27	5	3	2	4	2	3	500
16970.859	0.126E-27	6	4	2	5	4	1	321
16971.739	0.292E-27	10	2	9	9	1	8	142
16974.844	0.664E-28							
16974.968	0.537E-28							
16978.470	0.133E-27							
16979.250	0.298E-27							
16981.955	0.249E-27	4	4	1	3	1	2	340
16982.447	0.281E-27	3	3	1	2	1	2	401
16984.185	0.557E-27	7	3	4	6	3	3	321
16984.825	0.384E-27							
16985.548	0.177E-27							
16987.883	0.313E-28							
16988.514	0.216E-27							

Table A.2: Continued.

frequency	intensity	J′	K'_a	K'_c	J″	K''_a	K''_c	vib
16988.818	0.840E-28	6	1	6	5	4	1	222
16991.334	0.529E-28							
16997.874	0.125E-27	6	5	1	7	2	6	420
17000.191	0.204E-27	9	6	4	10	3	7	340
17000.335	0.283E-28							
17001.776	0.144E-27							
17002.447	0.990E-28							
17002.904	0.116E-27							
17004.093	0.578E-28	4	2	2	3	1	3	500
17005.100	0.819E-29							
17005.665	0.127E-27							
17006.108	0.172E-28							
17007.412	0.444E-28							
17007.687	0.316E-28							
17008.575	0.705E-28							
17008.877	0.108E-27	8	5	4	7	4	3	340
17011.158	0.546E-28	6	3	3	5	1	4	401
17012.624	0.191E-27							
17014.089	0.104E-28							
17014.661	0.215E-28							
17017.508	0.410E-27	6	4	3	5	1	4	340
17025.072	0.186E-28							
17026.757	0.211E-27	5	3	2	4	2	3	420
17030.448	0.560E-28							
17030.718	0.130E-27							
17033.511	0.300E-28							
17035.238	0.311E-28							
17035.481	0.169E-27	4	3	1	3	1	2	321
17036.146	0.583E-28							
17038.154	0.296E-28	5	4	2	5	1	5	500
17040.049	0.225E-28	8	5	3	7	5	2	241
17040.580	0.146E-27	5	3	3	4	1	4	401
17045.823	0.325E-28							
17046.496	0.769E-29							
17047.380	0.306E-28							
17047.903	0.417E-28							
17048.725	0.284E-28	5	2	4	6	1	5	222
17049.783	0.451E-28	5	3	3	4	2	2	142
17050.509	0.120E-28							
17053.276	0.201E-28	5	4	2	4	3	1	420
17055.778	0.190E-28							
17056.081	0.180E-27	6	4	2	5	2	3	401
17059.225	0.322E-29							
17059.914	0.906E-29							
17061.892	0.467E-28							
17063.205	0.128E-28							
17064.066	0.471E-29							
17064.351	0.757E-29							

Table A.2: Continued.

frequency	intensity	J′	K'_a	K'_c	J″	K''_a	K''_c	vib
17064.933	0.132E-27	5	4	2	4	2	3	401
17065.287	0.290E-28							
17068.104	0.278E-28							
17068.531	0.186E-28	9	6	4	9	5	5	340
17071.873	0.763E-28	2	1	1	3	2	2	222
17072.280	0.153E-28							
17072.482	0.509E-29							
17073.286	0.131E-27	6	3	3	5	1	4	321
17074.120	0.179E-28							
17074.312	0.303E-28	6	3	4	5	1	5	401
17076.250	0.174E-28							
17076.836	0.771E-28	7	1	6	7	2	5	222
17077.360	0.220E-28							
17077.662	0.507E-28	5	5	1	4	3	2	401
17078.244	0.583E-29							
17080.609	0.459E-29							
17081.521	0.110E-28							
17082.965	0.831E-29							
17083.955	0.113E-28							
17087.831	0.123E-27	6	5	1	5	3	2	401
17090.802	0.980E-29							
17093.943	0.906E-29							
17094.265	0.211E-28							
17094.716	0.112E-28							
17096.983	0.154E-28	5	1	5	5	4	2	302
17097.660	0.578E-28	5	3	3	4	1	4	321
17101.697	0.263E-28							
17104.225	0.161E-29							
17105.030	0.271E-28							
17105.911	0.342E-28							
17106.670	0.151E-28							
17107.805	0.165E-28							
17112.551	0.138E-28							
17114.170	0.439E-28							
17114.720	0.169E-28							
17116.912	0.306E-28	4	2	2	4	3	1	222
17117.094	0.198E-28							
17118.013	0.325E-28							
17118.310	0.424E-28							
17122.932	0.390E-28							
17123.434	0.429E-28							

Table A.3: The observed line positions (cm^{-1}) and absolute intensities (cm $molecule^{-1}$) of $H_2{}^{17}O$ observed in the range 11365 – 14514 cm^{-1}. The absolute intensities are scaled to match the natural abundance of $H_2{}^{17}O$ and normalised at 296 K. Uncertainty in line position is given in 10^{-4} cm^{-1} ($\Delta\nu$ in column 2) and for intensity is given in 10^{-28} cm $molecule^{-1}$ (ΔI in column 4). Vibrational states are given in $v_1v_2v_3$ normal mode notation in column 11.

wavenumber	$\Delta\nu$	intensity	ΔI	J′	K'_a	K'_c	J″	K''_a	K''_c	vib
11365.4669	0	0.952E-28	0.000	8	2	6	7	0	7	003
11641.2035	0	0.121E-27	0.000	6	0	6	7	0	7	131
11643.9814	0	0.120E-27	0.000	6	1	5	7	1	6	131
11677.9047	0	0.112E-27	0.000	4	1	3	5	1	4	131
11685.1840	32	0.354E-27	7.233	4	0	4	5	0	5	131
11692.8648	38	0.177E-27	5.454	4	2	2	5	2	3	131
11699.9046	0	0.276E-27	0.000	3	1	2	4	1	3	131
11714.0811	21	0.372E-27	4.948	3	1	3	4	1	4	131
11718.4674	0	0.829E-28	0.000	5	3	3	6	3	4	131
11724.0625	19	0.250E-27	4.269	2	1	1	3	1	2	131
11724.7944	0	0.265E-27	0.000	2	0	2	3	0	3	131
11732.7940	0	0.123E-27	0.000	3	2	2	4	2	3	131
11752.1812	0	0.111E-27	0.000	2	2	0	3	2	1	131
11759.2148	23	0.159E-27	3.825	1	1	1	2	1	2	131
11769.0535	50	0.167E-27	4.984	0	0	0	1	0	1	131
11796.2545	23	0.305E-27	4.748	1	1	1	1	1	0	131
11804.1493	0	0.107E-27	0.000							
11816.0537	0	0.119E-27	0.000	1	0	1	0	0	0	131
11820.8003	0	0.171E-27	0.000	3	2	2	3	2	1	131
11827.0684	0	0.128E-27	0.000	2	2	1	2	2	0	131
11829.4684	0	0.564E-27	0.000	2	2	0	2	2	1	131
11833.1450	0	0.352E-27	0.000	3	1	2	3	1	3	131
11837.5608	0	0.271E-27	0.000	2	0	2	1	0	1	131
11837.8719	19	0.733E-28	27.773							
11854.9864	0	0.321E-27	0.000	2	1	1	1	1	0	131
11857.4987	0	0.258E-27	0.000	10	0	10	11	0	11	211
11859.1510	16	0.952E-27	0.800	3	1	3	2	1	2	131
11868.0632	12	0.477E-27	4.446	3	3	1	3	3	0	131
11868.3953	26	0.376E-27	6.786	3	3	0	3	3	1	131
11871.5921	0	0.184E-27	0.000	8	3	5	9	3	6	211
11873.3077	13	0.555E-27	5.063	4	0	4	3	0	3	131
11875.0140	48	0.309E-27	12.633	4	1	4	3	1	3	131
11875.6627	0	0.267E-27	0.000	9	2	8	10	2	9	211
11880.0732	12	0.137E-27	3.868	3	1	2	2	1	1	131
11883.8801	0	0.243E-27	0.000	8	2	6	9	2	7	211
11887.8198	10	0.559E-27	4.745	9	1	9	10	1	10	211
11898.0881	27	0.260E-27	4.780	3	2	2	2	2	1	131
11901.4704	23	0.266E-27	4.571	6	0	6	5	0	5	131
11903.0247	5	0.132E-26	0.499	8	1	7	9	1	8	211
11903.2353	11	0.297E-27	4.981	8	2	7	9	2	8	211
11903.6743	13	0.399E-27	4.857	4	1	3	3	1	2	131
11903.9468	22	0.267E-27	4.611	7	3	4	8	3	5	211

Table A.3: Continued.

wavenumber	$\Delta\nu$	intensity	ΔI	J′	K'_a	K'_c	J″	K''_a	K''_c	vib
11914.2299	26	0.227E-27	4.674	5	4	2	5	4	1	131
11916.1102	13	0.330E-27	4.262	8	1	8	9	1	9	211
11917.1836	10	0.142E-26	1.085	8	0	8	9	0	9	211
11917.5197	10	0.559E-27	5.478	4	4	0	4	4	1	131
11919.2934	22	0.486E-27	5.807	7	4	4	8	4	5	211
11920.8798	10	0.916E-27	0.696	7	3	5	8	3	6	211
11927.2162	17	0.498E-27	5.151	4	2	2	3	2	1	131
11928.1610	17	0.172E-27	4.726	7	3	5	8	1	8	131
11929.9139	4	0.108E-26	0.437	7	2	6	8	2	7	211
11930.7816	21	0.249E-27	4.394	7	1	6	8	1	7	211
11937.0910	3	0.192E-26	0.515	6	2	4	7	2	5	211
11937.1759	5	0.100E-26	0.440	6	3	3	7	3	4	211
11938.2591	12	0.759E-27	5.269	5	2	4	4	2	3	131
11944.2458	8	0.104E-26	0.523	7	0	7	8	0	8	211
11944.6967	2	0.234E-26	0.452	7	1	7	8	1	8	211
11947.4406	8	0.773E-27	0.594	6	4	2	7	4	3	211
11949.5545	0	0.312E-27	0.000	6	3	4	7	3	5	211
11950.2040	5	0.112E-26	0.445	6	2	5	7	1	6	310
11953.1343	0	0.109E-27	0.000	8	1	8	8	1	7	211
11954.0859	6	0.154E-26	0.571	6	2	5	7	2	6	211
11956.0550	4	0.142E-26	0.487	6	1	5	7	1	6	211
11956.8860	35	0.186E-27	5.346	6	2	5	5	2	4	131
11959.8077	38	0.238E-27	5.198	6	1	6	7	0	7	310
11960.3461	0	0.497E-27	0.000	6	4	3	7	2	6	131
11963.3395	0	0.241E-27	0.000	4	3	2	3	3	1	131
11965.6311	0	0.111E-26	0.000	5	2	3	6	2	4	211
11970.5837	1	0.520E-26	0.482	6	0	6	7	0	7	211
11970.8069	0	0.154E-26	0.000	6	1	6	7	1	7	211
11971.0539	51	0.162E-27	5.084	6	5	1	6	5	2	131
11972.6146	30	0.144E-27	4.050	2	2	1	3	3	0	310
11973.4495	19	0.281E-27	4.381	5	5	1	5	5	0	131
11975.8905	6	0.199E-26	0.960	5	1	4	6	1	5	211
11978.1063	2	0.223E-26	0.480	5	3	3	6	3	4	211
11979.0800	14	0.336E-27	4.255	5	4	1	6	4	2	211
11979.9207	0	0.102E-26	0.000	5	4	2	6	4	3	211
11983.7511	0	0.423E-26	0.000	5	2	4	6	2	5	211
11984.0313	0	0.180E-27	0.000	5	0	5	6	1	6	310
11984.2875	60	0.247E-27	6.153	7	1	7	7	1	6	211
11984.3829	0	0.154E-26	0.000	5	2	4	6	1	5	310
11984.8573	20	0.484E-27	5.892	3	1	3	3	3	0	211
11985.6791	61	0.290E-27	6.984	5	1	5	6	0	6	310
11989.3302	17	0.305E-27	4.329	2	0	2	3	2	1	211
11995.3864	1	0.617E-26	0.503	4	2	2	5	2	3	211
11995.7061	2	0.260E-26	0.473	5	0	5	6	0	6	211
11996.1776	0	0.790E-26	0.048	5	1	5	6	1	6	211
12000.6490	0	0.763E-26	0.476	4	1	3	5	1	4	211
12002.9755	0	0.311E-26	0.000	4	3	1	5	3	2	211
12003.9287	17	0.621E-27	5.545	6	0	6	6	2	5	211

Table A.3: Continued.

wavenumber	$\Delta\nu$	intensity	ΔI	J′	K'_a	K'_c	J″	K''_a	K''_c	vib
12006.4755	0	0.105E-26	0.000	4	3	2	5	3	3	211
12009.0203	5	0.105E-26	0.467	4	4	0	5	4	1	211
12009.1073	30	0.138E-27	4.083	6	3	3	5	3	2	131
12009.2410	25	0.704E-27	6.736	4	4	1	5	4	2	211
12009.4198	2	0.215E-26	0.466	4	2	3	5	2	4	211
12010.9103	0	0.449E-27	0.000	4	1	4	5	0	5	310
12011.8602	27	0.282E-27	4.945	6	1	5	6	3	4	211
12016.1706	21	0.185E-27	3.943	4	2	3	5	1	4	310
12019.5055	0	0.119E-25	0.000	4	0	4	5	0	5	211
12020.6318	0	0.380E-26	0.000	4	1	4	5	1	5	211
12023.5843	0	0.256E-27	0.000	7	3	5	6	3	4	131
12025.9077	2	0.258E-26	0.490	3	2	1	4	2	2	211
12026.2270	0	0.369E-26	0.000	3	1	2	4	1	3	211
12026.2962	0	0.348E-27	0.000	5	0	5	5	2	4	211
12032.1908	15	0.407E-27	4.633	7	2	6	7	2	5	211
12033.3106	6	0.104E-26	0.504	3	3	0	4	3	1	211
12034.2288	27	0.289E-27	4.982	4	2	3	4	3	2	310
12034.4561	0	0.330E-26	0.000	3	3	1	4	3	2	211
12035.1622	0	0.849E-26	0.049	3	2	2	4	2	3	211
12036.0710	18	0.430E-27	4.904	3	1	3	4	0	4	310
12042.0556	1	0.481E-26	0.491	3	0	3	4	0	4	211
12043.5447	7	0.790E-27	0.483	5	1	5	5	1	4	211
12044.3232	0	0.160E-25	0.051	3	1	3	4	1	4	211
12044.7298	7	0.109E-26	0.510	4	0	4	4	2	3	211
12056.2306	0	0.719E-26	0.496	2	2	0	3	2	1	211
12058.1975	0	0.366E-27	0.000	3	0	3	3	2	2	211
12060.8027	2	0.242E-26	0.493	2	2	1	3	2	2	211
12061.5036	1	0.577E-26	0.497	2	1	2	3	0	3	310
12064.2292	0	0.121E-25	0.050	2	0	2	3	0	3	211
12066.6227	10	0.453E-27	4.169	2	0	2	2	2	1	211
12067.4512	1	0.567E-26	0.501	2	1	2	3	1	3	211
12071.3811	14	0.464E-27	4.732	4	1	4	4	1	3	211
12076.6778	29	0.147E-27	4.199	7	7	1	7	7	0	211
12079.2892	0	0.430E-27	0.000	3	1	2	3	2	1	310
12079.9105	1	0.373E-26	0.497	1	1	0	2	1	1	211
12083.7954	14	0.296E-27	4.054	7	3	5	7	3	4	211
12088.9664	0	0.220E-27	0.000	1	1	1	2	0	2	310
12089.5665	0	0.148E-26	0.000	5	2	4	5	2	3	211
12090.1088	0	0.121E-25	0.050	1	1	1	2	1	2	211
12095.5168	2	0.310E-26	0.488	3	1	3	3	1	2	211
12102.7955	51	0.491E-27	9.451	1	0	1	1	1	0	310
12104.1748	23	0.467E-27	6.338	6	3	4	6	3	3	211
12109.2191	0	0.104E-25	0.000	0	0	0	1	0	1	211
12109.4693	0	0.124E-26	0.000	4	2	3	4	2	2	211
12110.4951	14	0.418E-27	4.586	7	4	4	7	4	3	211
12113.1174	21	0.278E-27	6.003	8	5	3	8	5	4	211
12114.3810	3	0.158E-26	0.447	2	1	2	2	1	1	211
12116.4994	49	0.219E-27	5.497	4	2	2	5	0	5	211

Table A.3: Continued.

wavenumber	$\Delta\nu$	intensity	ΔI	J′	K'_a	K'_c	J″	K''_a	K''_c	vib
12118.0146	3	0.502E-26	1.013	5	3	3	5	3	2	211
12119.4125	20	0.256E-27	4.385	7	5	3	7	5	2	211
12119.7122	9	0.714E-27	5.643	6	4	3	6	4	2	211
12122.0327	0	0.136E-26	0.000	6	4	2	6	4	3	211
12123.1662	0	0.829E-26	0.000	3	2	2	3	2	1	211
12125.8657	18	0.477E-27	5.692	6	5	2	6	5	1	211
12125.9379	5	0.120E-26	0.545	6	5	1	6	5	2	211
12126.2284	1	0.313E-26	0.467	5	4	2	5	4	1	211
12126.4798	2	0.229E-26	0.500	4	3	2	4	3	1	211
12126.7350	5	0.992E-27	0.451	5	4	1	5	4	2	211
12127.1493	0	0.140E-25	0.099	1	1	1	1	1	0	211
12128.4103	6	0.884E-27	0.445	5	3	2	5	3	3	211
12129.3431	0	0.655E-26	0.467	4	3	1	4	3	2	211
12130.1602	0	0.287E-27	0.000	7	6	2	7	6	1	211
12130.8535	0	0.632E-26	0.000	2	2	1	2	2	0	211
12130.9692	6	0.102E-26	0.461	6	3	3	6	3	4	211
12131.1483	2	0.267E-26	0.479	4	4	1	4	4	0	211
12131.2094	0	0.720E-26	0.469	4	4	0	4	4	1	211
12131.3174	1	0.336E-26	0.475	5	5	1	5	5	0	211
12131.4934	0	0.145E-25	0.000	3	3	1	3	3	0	211
12131.9253	0	0.481E-26	0.000	3	3	0	3	3	1	211
12133.5216	0	0.195E-25	0.049	2	2	0	2	2	1	211
12135.5044	2	0.286E-26	0.467	3	2	1	3	2	2	211
12135.6030	7	0.933E-27	0.519	6	6	0	6	6	1	211
12137.9505	1	0.507E-26	0.496	1	1	0	1	1	1	211
12141.7410	1	0.367E-26	0.452	4	2	2	4	2	3	211
12146.6995	1	0.685E-26	0.510	2	1	1	2	1	2	211
12152.4589	19	0.808E-27	1.000	5	2	3	5	2	4	211
12155.5984	2	0.315E-26	0.478	1	0	1	0	0	0	211
12158.9715	10	0.558E-27	4.381	1	1	1	0	0	0	310
12159.4568	5	0.117E-26	0.492	3	1	2	3	1	3	211
12166.8586	7	0.723E-27	4.614	6	2	4	6	2	5	211
12172.4221	0	0.468E-26	0.000	2	1	2	1	1	1	211
12173.2230	26	0.611E-27	13.037	3	0	3	2	1	2	310
12174.2678	1	0.372E-26	0.487	2	1	2	1	0	1	310
12175.2244	0	0.217E-26	0.000	4	1	3	4	1	4	211
12176.9936	0	0.158E-25	0.048	2	0	2	1	0	1	211
12183.7400	0	0.133E-25	0.049	2	1	1	1	1	0	211
12189.4000	0	0.193E-25	0.000	3	1	3	2	1	2	211
12192.0052	22	0.332E-27	4.849	5	1	4	5	1	5	211
12193.6720	0	0.776E-26	0.050	3	0	3	2	0	2	211
12198.0642	6	0.134E-26	0.537	3	2	2	3	0	3	211
12200.0190	22	0.358E-27	6.473	7	0	7	8	1	8	112
12200.4564	0	0.916E-26	0.000	3	2	2	2	2	1	211
12200.5045	0	0.325E-27	0.000	5	2	4	5	1	5	310
12202.9272	12	0.398E-27	4.257	4	2	3	4	0	4	211
12204.6097	1	0.668E-26	0.485	4	1	4	3	1	3	211
12205.5551	2	0.315E-26	0.507	3	2	1	2	2	0	211

Table A.3: Continued.

wavenumber	$\Delta\nu$	intensity	ΔI	J′	K'_a	K'_c	J″	K''_a	K''_c	vib
12206.3880	0	0.599E-26	0.000	3	1	2	2	1	1	211
12206.8479	17	0.465E-27	6.072	6	2	5	6	1	6	310
12207.6285	7	0.194E-25	1.009	4	0	4	3	0	3	211
12210.7006	7	0.946E-27	0.496	5	2	4	5	0	5	211
12212.6959	28	0.344E-27	6.841	6	1	5	6	1	6	211
12214.1850	15	0.490E-27	5.169	2	2	1	1	1	0	310
12218.1181	0	0.174E-25	0.049	5	1	5	4	1	4	211
12219.0663	1	0.393E-26	0.497	4	2	3	3	2	2	211
12219.8043	1	0.612E-26	0.504	5	0	5	4	0	4	211
12222.1841	18	0.300E-27	4.458	5	4	2	4	2	3	131
12225.0934	4	0.165E-26	0.520	4	3	2	3	3	1	211
12226.3823	7	0.476E-26	2.601	4	3	1	3	3	0	211
12226.4188	1	0.160E-25	0.196	4	1	3	3	1	2	211
12228.6258	0	0.367E-27	0.000	7	2	6	7	0	7	211
12229.7440	0	0.113E-25	0.049	4	2	2	3	2	1	211
12229.8716	30	0.268E-27	5.000	3	2	2	2	1	1	310
12230.0881	1	0.429E-26	0.482	6	1	6	5	1	5	211
12230.8615	1	0.131E-25	0.097	6	0	6	5	0	5	211
12235.9212	0	0.106E-25	0.049	5	2	4	4	2	3	211
12238.6195	18	0.394E-27	6.219	2	2	1	3	3	0	112
12240.9394	0	0.111E-25	0.050	7	1	7	6	1	6	211
12241.9314	4	0.133E-26	0.474	4	2	3	3	1	2	310
12242.7556	0	0.325E-26	0.000	5	1	4	4	1	3	211
12243.8906	0	0.433E-27	0.000	2	2	0	1	0	1	211
12244.3718	2	0.638E-26	1.026	5	3	3	4	3	2	211
12248.4154	3	0.334E-26	0.989	5	3	2	4	3	1	211
12248.6594	10	0.568E-27	5.836	5	4	1	4	4	0	211
12249.0882	9	0.147E-26	0.943	8	1	8	7	1	7	211
12250.3422	1	0.527E-26	0.481	8	0	8	7	0	7	211
12250.7543	12	0.607E-27	5.215	5	0	5	6	1	6	112
12251.2412	7	0.101E-26	0.497	5	2	4	4	1	3	310
12251.6532	0	0.280E-27	0.000	3	2	1	2	1	2	310
12252.5137	4	0.349E-26	1.031	5	2	3	4	2	2	211
12253.2414	4	0.198E-26	0.559	6	4	3	5	2	4	131
12254.2061	4	0.362E-26	1.067	6	2	5	5	1	4	310
12256.7323	0	0.991E-27	0.000	9	0	9	8	0	8	211
12257.3700	0	0.265E-26	0.000	9	1	9	8	1	8	211
12260.0606	1	0.551E-26	0.485	6	1	5	5	1	4	211
12261.9609	0	0.524E-26	0.000	7	2	6	6	2	5	211
12261.9923	0	0.118E-26	0.000	6	3	4	5	3	3	211
12263.4357	0	0.472E-27	0.000	10	1	10	9	1	9	211
12263.5198	4	0.119E-26	0.451	10	0	10	9	0	9	211
12263.9352	0	0.428E-27	0.000	7	2	6	6	1	5	310
12267.3531	0	0.591E-27	0.000	6	4	3	5	4	2	211
12268.3392	0	0.159E-26	0.000	6	4	2	5	4	1	211
12268.7948	0	0.809E-27	0.000	11	1	11	10	1	10	211
12269.8848	5	0.127E-26	0.486	7	1	6	6	1	5	211
12270.8662	1	0.411E-26	0.515	6	3	3	5	3	2	211

Table A.3: Continued.

wavenumber	$\Delta\nu$	intensity	ΔI	J′	K'_a	K'_c	J″	K''_a	K''_c	vib
12270.9802	23	0.235E-27	4.356	3	2	1	2	0	2	211
12272.3840	7	0.970E-27	0.488	6	5	1	5	5	0	211
12272.6761	0	0.623E-26	0.000	6	2	4	5	2	3	211
12272.8128	32	0.297E-27	5.463	12	0	12	11	0	11	211
12273.2401	7	0.745E-27	0.456	8	2	7	7	2	6	211
12274.5450	20	0.259E-27	4.545	4	0	4	5	1	5	112
12276.9524	0	0.245E-26	0.000	8	1	7	7	1	6	211
12277.5877	2	0.242E-26	0.491	7	3	5	6	3	4	211
12278.0052	0	0.863E-27	0.000	4	1	4	5	0	5	112
12281.4624	31	0.174E-27	4.539	7	4	4	6	2	5	131
12282.8052	4	0.127E-26	0.495	9	2	8	8	2	7	211
12285.0823	5	0.112E-26	0.470	7	4	4	6	4	3	211
12285.2918	13	0.657E-27	6.787	9	1	8	8	1	7	211
12288.3734	13	0.680E-27	6.455	4	3	2	3	2	1	310
12288.4112	0	0.298E-27	0.000	10	1	9	9	1	8	211
12289.5114	0	0.125E-26	0.000	7	2	5	6	2	4	211
12290.5944	19	0.572E-27	7.315	7	5	3	6	5	2	211
12290.7190	20	0.320E-27	5.608	10	2	9	9	2	8	211
12292.6253	9	0.826E-27	0.544	7	3	4	6	3	3	211
12295.2620	8	0.859E-27	0.489	3	0	3	4	1	4	112
12295.5271	23	0.188E-27	4.182	11	2	10	10	2	9	211
12296.7753	22	0.254E-27	4.400	1	1	0	2	2	1	112
12302.4664	4	0.138E-26	0.474	8	2	6	7	2	5	211
12303.1728	45	0.367E-27	12.976	3	1	3	4	0	4	112
12304.6437	9	0.740E-27	5.005	4	2	2	3	0	3	211
12307.6992	0	0.522E-28	0.000							
12307.8344	0	0.525E-27	0.000	8	4	4	7	4	3	211
12308.3756	0	0.198E-27	0.000	8	5	3	7	5	2	211
12309.8125	17	0.294E-27	4.325	6	3	4	5	2	3	310
12311.6971	38	0.130E-27	4.337	9	3	7	8	2	6	112
12312.0026	5	0.129E-26	0.529	8	3	5	7	3	4	211
12314.3520	0	0.119E-27	0.000	7	3	5	6	2	4	310
12315.7207	0	0.105E-27	0.000							
12315.7614	0	0.798E-28	0.000	3	2	2	4	1	3	112
12316.4085	19	0.218E-27	4.101	9	4	6	8	4	5	211
12317.2820	0	0.111E-27	0.000	5	2	3	5	3	2	112
12318.2428	18	0.354E-27	4.737	8	3	6	7	2	5	310
12319.3107	42	0.193E-27	5.835	3	1	3	3	2	2	112
12320.2883	0	0.963E-28	0.000							
12321.9949	31	0.271E-27	5.541	5	3	2	4	2	3	310
12324.1059	0	0.168E-27	0.000	6	4	2	6	2	5	211
12324.3169	24	0.430E-27	6.646	10	2	8	9	2	7	211
12325.2943	0	0.203E-27	0.000	4	0	4	4	1	3	112
12325.5375	0	0.820E-28	0.000	4	4	0	3	3	1	310
12327.6229	40	0.253E-27	5.958	9	3	6	8	3	5	211
12328.9027	10	0.723E-27	5.371	2	1	2	3	0	3	112
12329.7977	39	0.123E-27	4.209	5	1	4	5	2	3	112
12332.7054	18	0.433E-27	4.902	1	0	1	2	1	2	112

Table A.3: Continued.

wavenumber	$\Delta\nu$	intensity	ΔI	J′	K'_a	K'_c	J″	K''_a	K''_c	vib
12337.0388	16	0.335E-27	4.368	4	3	1	3	1	2	211
12337.6691	31	0.163E-27	4.441	10	3	7	9	3	6	211
12346.0419	0	0.235E-27	0.000	10	4	6	9	4	5	211
12346.3987	23	0.269E-27	4.541	3	1	2	3	2	1	112
12346.4581	22	0.324E-27	4.759	3	0	3	3	1	2	112
12349.2661	27	0.303E-27	5.006	2	2	1	3	1	2	112
12355.2879	24	0.162E-27	3.972	7	1	7	8	1	8	013
12361.1896	17	0.505E-27	5.054	2	0	2	2	1	1	112
12362.7080	0	0.870E-28	0.000	7	5	2	6	3	3	131
12364.2791	18	0.164E-27	3.574	6	1	5	7	1	6	013
12369.7484	0	0.468E-27	0.000	1	0	1	1	1	0	112
12375.6766	0	0.458E-28	0.000	5	5	1	4	4	0	310
12375.7475	0	0.142E-27	0.000	5	5	0	4	4	1	310
12379.1611	15	0.320E-27	4.284	6	3	3	5	1	4	211
12380.9356	23	0.485E-27	6.320	6	0	6	7	0	7	013
12381.9752	60	0.221E-27	5.943	5	3	3	6	3	4	013
12387.9129	0	0.174E-27	0.000	5	1	4	6	1	5	013
12391.7454	12	0.607E-27	5.219	5	2	4	6	2	5	013
12393.8012	0	0.197E-27	0.000	6	2	4	5	0	5	211
12394.3393	31	0.248E-27	6.033	6	5	2	5	4	1	310
12401.0950	45	0.133E-27	7.231	4	4	0	5	4	1	013
12403.8905	8	0.587E-27	5.585	4	2	2	5	2	3	013
12406.0917	15	0.386E-27	4.475	5	1	5	6	1	6	013
12407.1498	11	0.610E-27	4.708	1	1	0	1	0	1	112
12411.4094	7	0.129E-26	0.529	4	1	3	5	1	4	013
12421.2979	13	0.557E-27	4.873	3	1	2	3	0	3	112
12422.6545	0	0.148E-27	0.000	4	2	2	4	1	3	112
12424.1923	8	0.121E-26	0.535	3	2	1	3	1	2	112
12425.5527	0	0.354E-27	0.000	5	2	3	5	1	4	112
12428.7492	0	0.935E-27	0.000	4	0	4	5	0	5	013
12429.7996	0	0.237E-27	0.000	4	1	4	5	1	5	013
12429.9610	7	0.102E-26	0.494	6	4	2	5	2	3	211
12432.2287	12	0.550E-27	5.038	3	2	1	4	2	2	013
12433.8821	20	0.181E-27	3.854	3	3	1	4	3	2	013
12435.7494	28	0.383E-27	6.295	3	1	2	4	1	3	013
12440.3478	35	0.275E-27	5.252	3	0	3	2	1	2	112
12440.7392	14	0.501E-27	4.824	3	2	2	4	2	3	013
12441.6877	26	0.556E-27	12.399	2	1	2	1	0	1	112
12449.9610	41	0.194E-27	5.094	8	3	5	7	1	6	211
12451.2889	0	0.342E-27	0.000	3	0	3	4	0	4	013
12452.8168	0	0.121E-26	0.000	3	1	3	4	1	4	013
12453.4458	0	0.241E-27	0.000	5	1	5	5	1	4	013
12454.4756	0	0.175E-27	0.000							
12454.5266	0	0.363E-27	0.000							
12454.7722	0	0.103E-26	0.000	3	1	3	2	0	2	112
12456.7396	0	0.385E-27	0.000	4	2	3	4	1	4	112
12460.0824	0	0.422E-27	0.000	3	3	0	3	2	1	112
12460.8160	0	0.227E-26	0.000	2	2	0	3	2	1	013

Table A.3: Continued.

wavenumber	$\Delta\nu$	intensity	ΔI	J′	K'_a	K'_c	J″	K''_a	K''_c	vib
12461.1562	0	0.826E-27	0.000	2	1	1	3	1	2	013
12465.5803	0	0.204E-27	0.000	3	3	1	3	2	2	112
12466.1274	0	0.113E-26	0.000	4	1	4	3	0	3	112
12466.7556	0	0.200E-27	0.000	5	3	3	5	2	4	112
12469.8444	0	0.216E-27	0.000							
12470.1409	0	0.176E-27	0.000							
12472.4585	0	0.161E-26	0.000	2	0	2	3	0	3	013
12472.6872	0	0.239E-27	0.000	5	0	5	4	1	4	112
12475.2870	0	0.290E-27	0.000	2	1	2	3	1	3	013
12476.1434	0	0.196E-27	0.000	5	1	4	4	2	3	112
12480.1979	0	0.353E-27	0.000	2	2	1	1	1	0	112
12481.5930	0	0.189E-27	0.000	7	1	6	7	0	7	112
12483.2502	0	0.166E-27	0.000	6	4	3	6	3	4	112
12485.4483	0	0.179E-27	0.000	6	0	6	5	1	5	112
12495.9361	0	0.235E-27	0.000	3	2	2	2	1	1	112
12497.3965	0	0.923E-27	0.000	1	1	1	2	1	2	013
12497.5673	0	0.201E-27	0.000	5	2	4	5	2	3	013
12507.9321	0	0.314E-27	0.000	4	2	3	3	1	2	112
12508.2677	0	0.172E-27	0.000	6	5	1	6	5	2	013
12512.7094	0	0.198E-27	0.000	5	5	1	5	5	0	013
12516.2077	0	0.187E-27	0.000							
12517.4520	0	0.155E-26	0.000	0	0	0	1	0	1	013
12521.8732	0	0.195E-27	0.000	5	3	3	5	3	2	013
12523.2811	0	0.440E-27	0.000	4	4	0	4	4	1	013
12528.7384	0	0.854E-27	0.000	3	2	2	3	2	1	013
12530.9161	0	0.101E-26	0.000	3	3	1	3	3	0	013
12531.1975	0	0.284E-27	0.000	4	3	1	4	3	2	013
12531.4090	0	0.829E-27	0.000	3	3	0	3	3	1	013
12534.4396	0	0.121E-26	0.000	1	1	1	1	1	0	013
12535.2638	0	0.442E-27	0.000	2	2	1	2	2	0	013
12535.6216	0	0.443E-27	0.000	3	3	1	2	2	0	112
12537.3697	0	0.382E-27	0.000	3	3	0	2	2	1	112
12538.1156	0	0.135E-26	0.000	2	2	0	2	2	1	013
12541.8252	0	0.190E-27	0.000	3	2	1	3	2	2	013
12545.3938	0	0.223E-27	0.000	1	1	0	1	1	1	013
12553.6522	0	0.225E-27	0.000	4	3	2	3	2	1	112
12555.0352	0	0.613E-27	0.000	2	1	1	2	1	2	013
12564.3523	0	0.258E-27	0.000	1	0	1	0	0	0	013
12585.2257	0	0.127E-26	0.000	2	0	2	1	0	1	013
12592.0776	0	0.110E-26	0.000	2	1	1	1	1	0	013
12597.8973	0	0.121E-26	0.000	3	1	3	2	1	2	013
12602.8940	0	0.359E-27	0.000	3	0	3	2	0	2	013
12606.0291	0	0.112E-26	0.000	3	2	2	2	2	1	013
12613.7771	0	0.459E-27	0.000	4	1	4	3	1	3	013
12616.8707	0	0.120E-26	0.000	4	0	4	3	0	3	013
12628.0320	0	0.105E-26	0.000	5	1	5	4	1	4	013
12628.2325	0	0.670E-27	0.000	4	3	1	3	3	0	013
12629.5780	0	0.319E-27	0.000	5	0	5	4	0	4	013

Table A.3: Continued.

wavenumber	$\Delta\nu$	intensity	ΔI	J′	K'_a	K'_c	J″	K''_a	K''_c	vib
12637.1952	0	0.136E-26	0.000	4	1	3	3	1	2	013
12638.2493	0	0.883E-27	0.000	4	2	2	3	2	1	013
12641.2099	0	0.101E-26	0.000	6	0	6	5	0	5	013
12643.9086	0	0.552E-27	0.000	5	2	4	4	2	3	013
12646.1746	0	0.558E-27	0.000	5	4	2	4	4	1	013
12648.2358	0	0.381E-27	0.000	5	3	3	4	3	2	013
12651.5323	0	0.604E-27	0.000	7	1	7	6	1	6	013
12654.7863	0	0.349E-27	0.000	5	1	4	4	1	3	013
12661.8387	0	0.311E-27	0.000	8	0	8	7	0	7	013
12668.2852	0	0.126E-26	0.000	6	1	5	5	1	4	013
12674.8215	0	0.467E-27	0.000	7	2	6	6	2	5	013
12678.2916	0	0.478E-27	0.000							
12679.5373	0	0.432E-27	0.000	6	3	3	5	3	2	013
12685.4276	0	0.385E-27	0.000	6	2	4	5	2	3	013
12687.8784	0	0.604E-27	0.000	8	1	7	7	1	6	013
13145.7553	0	0.806E-28	0.000							
13396.5249	0	0.328E-27	0.000	4	1	3	5	3	2	221
13443.7912	34	0.195E-27	4.686	7	1	7	8	1	8	221
13450.5661	0	0.173E-27	0.000	6	2	4	7	2	5	221
13460.3853	0	0.131E-27	0.000	6	3	3	7	3	4	221
13460.6987	0	0.117E-27	0.000	6	1	5	7	1	6	221
13469.4502	0	0.443E-27	0.000	6	0	6	7	0	7	221
13470.1725	0	0.160E-27	0.000	6	1	6	7	1	7	221
13476.5122	0	0.192E-27	0.000	6	1	5	7	3	4	301
13477.1007	0	0.427E-27	0.000	5	2	3	6	2	4	221
13478.2975	0	0.158E-27	0.000	6	3	4	7	4	3	400
13482.0515	0	0.250E-27	0.000	5	1	4	6	1	5	221
13489.6585	0	0.129E-27	0.000	6	4	2	7	4	3	221
13490.0157	0	0.135E-27	0.000	10	1	9	11	1	10	301
13490.1366	0	0.459E-28	0.000							
13492.8281	22	0.295E-27	4.712	5	2	4	6	2	5	221
13494.9139	0	0.281E-27	0.000	5	0	5	6	0	6	221
13496.1477	17	0.979E-27	0.645	5	1	5	6	1	6	221
13497.5880	0	0.115E-27	0.000	5	3	2	6	2	5	042
13503.6731	0	0.431E-27	0.000	5	3	3	6	3	4	221
13504.8355	0	0.921E-27	0.000	4	1	3	5	1	4	221
13506.3510	0	0.571E-27	0.000	4	2	2	5	2	3	221
13510.1628	0	0.169E-27	0.000	6	5	1	7	5	2	301
13510.2964	0	0.185E-27	0.000	8	3	5	9	3	6	301
13518.7061	0	0.108E-26	0.000	4	0	4	5	0	5	221
13521.1382	39	0.339E-27	5.886	4	1	4	5	1	5	221
13522.0835	61	0.314E-27	8.862	10	0	10	11	0	11	301
13522.4592	0	0.116E-26	0.000	5	3	2	6	4	3	400
13522.9440	18	0.552E-27	5.622	9	1	8	10	1	9	301
13527.0888	0	0.211E-27	0.000	8	2	6	9	2	7	301
13528.0354	16	0.413E-27	4.717	4	3	1	5	3	2	221
13528.9715	0	0.157E-27	0.000	8	3	6	9	3	7	301
13529.2608	0	0.442E-27	0.000	3	1	2	4	1	3	221

Table A.3: Continued.

wavenumber	$\Delta\nu$	intensity	ΔI	J′	K'_a	K'_c	J″	K''_a	K''_c	vib
13531.9129	0	0.146E-27	0.000	4	3	2	5	3	3	221
13536.8083	28	0.256E-27	5.853	3	2	1	4	2	2	221
13539.4819	0	0.474E-27	0.000	6	3	3	6	5	2	301
13541.1341	21	0.399E-27	6.123	3	0	3	4	0	4	221
13543.5325	0	0.571E-27	0.000	5	1	5	5	1	4	221
13545.2442	0	0.129E-26	0.000	3	1	3	4	1	4	221
13546.4236	0	0.942E-27	0.000	3	2	2	4	2	3	221
13546.6374	74	0.186E-27	6.036	7	3	4	8	3	5	301
13551.3650	0	0.260E-27	0.000	4	4	0	5	4	1	221
13553.7944	47	0.142E-27	4.812	9	0	9	10	0	10	301
13553.8854	15	0.353E-27	4.453	9	1	9	10	1	10	301
13554.2280	0	0.148E-27	0.000	8	2	7	9	2	8	301
13554.9920	0	0.440E-27	0.000	8	1	7	9	1	8	301
13555.1743	0	0.110E-26	0.000	2	1	1	3	1	2	221
13558.5173	0	0.151E-27	0.000	3	3	0	4	3	1	221
13559.6199	0	0.465E-27	0.000	3	3	1	4	3	2	221
13559.9613	0	0.850E-28	0.000	7	2	5	8	2	6	301
13561.7082	0	0.356E-27	0.000	7	3	5	8	3	6	301
13561.7657	0	0.131E-26	0.000	2	0	2	3	0	3	221
13562.5409	0	0.183E-27	0.000	3	1	3	4	3	2	301
13564.9749	0	0.272E-27	0.000	2	1	2	3	0	3	320
13567.2399	0	0.740E-27	0.000	2	2	0	3	2	1	221
13567.8818	0	0.212E-27	0.000	6	5	1	7	5	2	221
13568.9769	0	0.516E-27	0.000	2	1	2	3	1	3	221
13571.9038	0	0.276E-27	0.000	2	2	1	3	2	2	221
13575.2416	0	0.471E-27	0.000	6	4	2	7	4	3	301
13577.2578	0	0.235E-27	0.000	7	1	6	8	2	7	400
13577.4093	0	0.852E-28	0.000	6	4	3	7	4	4	301
13578.0849	0	0.252E-27	0.000	5	2	3	6	3	4	400
13581.8735	0	0.304E-27	0.000	1	1	0	2	1	1	221
13582.6830	0	0.943E-27	0.000	6	3	3	7	3	4	301
13584.2607	38	0.914E-27	1.048	1	0	1	2	0	2	221
13584.2938	7	0.125E-26	0.519	8	0	8	9	0	9	301
13584.6305	0	0.593E-27	0.000	7	2	6	8	2	7	301
13586.4842	0	0.393E-27	0.000	7	1	6	8	1	7	301
13587.1741	22	0.782E-27	0.678	7	3	4	8	2	7	320
13591.7637	0	0.122E-26	0.000	1	1	1	2	1	2	221
13592.7249	6	0.125E-26	0.532	6	2	4	7	2	5	301
13593.6234	0	0.239E-27	0.000	6	3	4	7	3	5	301
13596.4310	41	0.621E-27	9.488	3	1	3	3	1	2	221
13599.3864	52	0.271E-27	7.920	5	5	1	6	5	2	301
13607.6367	0	0.116E-27	0.000	6	1	5	7	2	6	400
13607.7263	8	0.979E-27	0.555	0	0	0	1	0	1	221
13609.0067	0	0.205E-27	0.000	5	4	1	6	4	2	301
13609.7803	0	0.688E-27	0.000	5	4	2	6	4	3	301
13613.5256	3	0.207E-26	0.544	7	1	7	8	1	8	301
13613.6075	0	0.689E-27	0.000	7	0	7	8	0	8	301
13614.4988	0	0.111E-26	0.000	6	1	5	7	1	6	301

Table A.3: Continued.

wavenumber	$\Delta\nu$	intensity	ΔI	J′	K'_a	K'_c	J″	K''_a	K''_c	vib
13614.9011	0	0.696E-27	0.000	6	2	5	7	2	6	301
13615.9052	0	0.259E-27	0.000	2	1	2	2	1	1	221
13616.3206	0	0.140E-27	0.000	2	1	1	3	3	0	301
13617.8547	0	0.789E-28	0.000	6	6	0	6	6	1	221
13618.2161	0	0.628E-27	0.000	5	3	2	6	3	3	301
13618.6620	0	0.119E-26	0.000	6	2	5	7	1	6	400
13618.7270	0	0.384E-27	0.000	8	0	8	8	2	7	301
13621.3587	0	0.996E-28	0.000	4	2	3	4	2	2	221
13625.0164	0	0.147E-26	0.000	5	3	3	6	3	4	301
13625.2179	23	0.377E-27	5.161	6	3	4	7	2	5	400
13625.4902	0	0.798E-27	0.000	5	2	3	6	2	4	301
13628.0110	59	0.833E-28	4.271	8	1	7	8	3	6	301
13628.8009	3	0.185E-26	0.447	1	1	1	1	1	0	221
13630.8291	15	0.638E-27	6.634	5	1	4	6	2	5	400
13634.4275	9	0.813E-27	0.485	3	2	2	3	2	1	221
13639.9274	36	0.798E-27	0.793	1	1	0	1	1	1	221
13640.8820	0	0.709E-27	0.000	4	4	0	5	4	1	301
13641.0852	21	0.203E-27	4.334	4	4	1	5	4	2	301
13641.2742	2	0.368E-26	0.534	6	0	6	7	0	7	301
13641.8813	0	0.112E-26	0.000	6	1	6	7	1	7	301
13641.9562	0	0.792E-27	0.000	2	2	1	2	2	0	221
13642.3870	0	0.169E-26	0.000	5	1	4	6	1	5	301
13643.5774	0	0.310E-27	0.000	5	3	3	5	3	2	221
13643.9102	2	0.310E-26	0.533	5	2	4	6	2	5	301
13644.5345	4	0.228E-26	0.567	2	2	0	2	2	1	221
13646.4094	0	0.833E-27	0.000	3	2	1	3	2	2	221
13647.0020	0	0.344E-27	0.000	6	2	4	7	0	7	221
13649.0557	12	0.618E-27	5.473	2	1	1	2	1	2	221
13651.8244	21	0.552E-27	6.869	5	2	4	6	1	5	400
13651.9137	0	0.110E-27	0.000	4	3	2	4	3	1	221
13652.3335	3	0.258E-26	0.519	4	3	1	5	3	2	301
13652.7097	0	0.410E-27	0.000	4	2	2	4	2	3	221
13652.9004	0	0.163E-27	0.000	6	3	4	6	4	3	400
13652.9581	0	0.145E-27	0.000	7	1	6	7	3	5	301
13653.1304	21	0.228E-27	4.249	7	1	7	7	1	6	301
13654.1736	0	0.158E-27	0.000	6	3	3	6	3	4	221
13654.2630	16	0.354E-27	5.175	1	0	1	0	0	0	221
13655.6093	10	0.146E-26	0.792	4	3	2	5	3	3	301
13656.6571	0	0.201E-26	0.000	3	3	1	3	3	0	221
13657.1343	11	0.614E-27	4.704	3	3	0	3	3	1	221
13658.2193	0	0.475E-26	0.000	4	2	2	5	2	3	301
13664.2625	26	0.292E-27	5.025	6	4	2	6	4	3	221
13665.5671	0	0.232E-27	0.000	3	3	0	4	1	3	221
13665.6760	33	0.193E-27	4.678	5	0	5	6	1	6	400
13666.5130	63	0.275E-27	6.546	6	3	3	6	4	2	400
13668.4415	2	0.658E-26	1.081	5	1	5	6	1	6	301
13668.6355	0	0.938E-26	0.051	5	0	5	6	0	6	301
13668.7614	0	0.512E-27	0.000	5	3	2	5	4	1	400

Table A.3: Continued.

wavenumber	$\Delta\nu$	intensity	ΔI	J′	K'_a	K'_c	J″	K''_a	K''_c	vib
13669.0779	50	0.208E-27	5.458	5	4	1	5	4	2	221
13670.2266	0	0.583E-26	0.000	4	1	3	5	1	4	301
13671.8381	0	0.287E-27	0.000	3	1	2	4	2	3	400
13672.2049	4	0.155E-26	0.480	4	2	3	5	2	4	301
13673.2857	0	0.154E-27	0.000	7	5	3	7	5	2	301
13673.4949	0	0.490E-27	0.000	4	4	1	4	4	0	221
13673.5521	0	0.162E-26	0.000	4	4	0	4	4	1	221
13674.5299	5	0.182E-26	0.683	2	0	2	1	0	1	221
13674.6102	22	0.248E-27	4.381	6	0	6	6	2	5	301
13675.9433	32	0.210E-27	4.863	7	6	2	7	6	1	301
13679.4083	32	0.103E-27	3.681	4	1	3	4	1	4	221
13681.3532	12	0.702E-27	6.644	6	5	1	6	5	2	301
13684.2215	0	0.834E-27	0.000	3	3	0	4	3	1	301
13684.8356	8	0.823E-27	0.475	6	6	0	6	6	1	301
13685.3288	0	0.247E-26	0.000	3	3	1	4	3	2	301
13686.0955	6	0.137E-26	0.543	2	1	1	1	1	0	221
13686.5333	0	0.659E-27	0.000	4	2	3	5	1	4	400
13688.3079	0	0.260E-27	0.000	4	1	3	4	3	2	301
13690.3191	5	0.162E-26	0.554	3	1	3	2	1	2	221
13690.4064	0	0.946E-28	0.000	4	0	4	5	1	5	400
13690.7149	3	0.207E-26	0.491	3	2	1	4	2	2	301
13692.7520	0	0.291E-26	0.000	3	0	3	2	0	2	221
13694.1359	2	0.280E-26	0.489	4	1	4	5	1	5	301
13694.2864	0	0.869E-26	0.051	4	0	4	5	0	5	301
13698.4340	0	0.296E-26	0.000	3	1	2	4	1	3	301
13699.2185	0	0.184E-27	0.000	5	0	5	5	2	4	301
13699.8354	0	0.628E-26	0.000	3	2	2	4	2	3	301
13705.1277	0	0.560E-27	0.000	4	1	4	3	1	3	221
13706.8319	4	0.184E-26	0.527	4	0	4	3	0	3	221
13709.4309	16	0.422E-27	4.689	3	1	2	2	1	1	221
13710.0134	0	0.161E-27	0.000	4	3	2	5	2	3	400
13711.7377	6	0.582E-26	1.835	3	2	2	2	2	1	221
13715.8055	0	0.642E-27	0.000	5	1	5	5	1	4	301
13716.1336	20	0.522E-27	5.477	3	3	1	4	1	4	221
13716.4582	0	0.390E-27	0.000	3	2	1	2	2	0	221
13717.5408	3	0.276E-26	0.536	3	0	3	4	0	4	301
13718.0955	0	0.156E-26	0.000	5	1	5	4	1	4	221
13719.0433	1	0.117E-25	0.108	3	1	3	4	1	4	301
13719.5091	0	0.786E-27	0.000	4	0	4	4	2	3	301
13719.8458	4	0.229E-26	0.567	3	1	3	4	0	4	400
13722.0590	0	0.104E-27	0.000	3	2	2	4	1	3	400
13722.2830	0	0.575E-26	0.000	2	2	0	3	2	1	301
13724.6337	21	0.346E-27	4.928	7	3	5	7	3	4	301
13726.8006	4	0.195E-26	0.509	2	2	1	3	2	2	301
13726.9765	0	0.114E-25	0.052	2	1	1	3	1	2	301
13729.4550	0	0.251E-27	0.000	6	1	6	5	1	5	221
13729.7273	7	0.989E-27	0.486	6	0	6	5	0	5	221
13730.6011	0	0.132E-26	0.000	4	1	3	3	1	2	221

Table A.3: Continued.

wavenumber	$\Delta\nu$	intensity	ΔI	J′	K'_a	K'_c	J″	K''_a	K''_c	vib
13730.9583	23	0.187E-27	4.128	7	5	3	7	5	2	221
13733.4738	0	0.177E-27	0.000	2	0	2	3	1	3	400
13733.6792	0	0.159E-27	0.000	3	0	3	3	2	2	301
13735.3470	0	0.270E-27	0.000	7	4	4	7	4	3	301
13735.9871	0	0.296E-27	0.000	3	1	3	3	2	2	400
13740.0436	0	0.539E-27	0.000	7	1	7	6	1	6	221
13740.4836	0	0.489E-26	0.000	2	0	2	3	0	3	071
13740.7140	0	0.113E-26	0.000	4	2	2	3	2	1	221
13741.3737	0	0.801E-26	0.000	2	0	2	3	0	3	301
13742.8480	1	0.422E-26	0.517	2	1	2	3	1	3	301
13743.7881	15	0.656E-27	5.354	2	0	2	2	2	1	301
13744.8839	0	0.367E-27	0.000	4	1	4	4	1	3	301
13745.8345	60	0.236E-26	6.888	5	5	1	5	5	0	301
13746.0579	1	0.676E-26	0.491	2	1	2	3	0	3	400
13747.2481	0	0.138E-27	0.000	6	4	3	6	4	2	301
13748.2071	26	0.626E-27	6.396	8	0	8	7	0	7	221
13748.9137	25	0.346E-27	5.166	5	1	4	4	1	3	221
13749.7300	0	0.133E-26	0.000	5	2	4	5	2	3	301
13749.8407	0	0.256E-27	0.000	6	4	2	6	4	3	301
13750.5359	0	0.149E-27	0.000	4	3	2	3	3	1	221
13751.4423	0	0.476E-27	0.000	4	3	1	3	3	0	221
13752.8549	19	0.273E-27	4.259	1	0	1	2	1	2	400
13755.3678	1	0.595E-26	0.511	1	1	0	2	1	1	301
13756.0873	0	0.234E-26	0.000	5	4	2	5	4	1	301
13756.6545	10	0.618E-27	4.624	5	4	1	5	4	2	301
13756.9753	27	0.151E-27	3.976	2	2	1	3	1	2	400
13760.9955	34	0.141E-27	4.226	6	2	5	5	2	4	221
13763.0053	4	0.171E-26	0.505	4	4	1	4	4	0	301
13763.0721	2	0.574E-26	1.059	4	4	0	4	4	1	301
13763.9831	0	0.427E-27	0.000	5	2	3	4	2	2	221
13764.4824	1	0.436E-26	0.513	1	0	1	2	0	2	301
13764.9127	3	0.187E-26	0.487	5	3	3	5	3	2	301
13765.1076	0	0.169E-27	0.000	5	4	1	5	3	2	320
13765.9831	0	0.955E-26	0.000	1	1	1	2	1	2	301
13769.9448	12	0.568E-27	4.740	5	3	3	4	3	2	221
13770.2389	0	0.293E-26	0.000	3	1	3	3	1	2	301
13772.2531	8	0.925E-27	0.513	4	2	3	4	2	2	301
13774.3255	17	0.380E-27	4.749	7	2	6	6	2	5	221
13775.6093	8	0.207E-26	1.203	4	3	2	4	3	1	301
13776.0285	0	0.238E-26	0.000	5	3	2	5	3	3	301
13776.4753	0	0.893E-27	0.000	6	3	3	6	3	4	301
13778.7022	1	0.518E-26	0.506	4	3	1	4	3	2	301
13780.4215	32	0.296E-27	5.832	6	0	6	5	2	3	301
13782.3671	2	0.115E-25	0.149	3	3	1	3	3	0	301
13782.8392	10	0.400E-26	2.509	3	3	0	3	3	1	301
13784.4998	0	0.156E-27	0.000	0	0	0	1	0	1	071
13786.1439	15	0.450E-27	4.764	6	2	4	5	2	3	221
13787.8387	1	0.787E-26	0.055	3	2	2	3	2	1	301

Table A.3: Continued.

wavenumber	$\Delta\nu$	intensity	ΔI	J′	K'_a	K'_c	J″	K''_a	K''_c	vib
13788.3846	0	0.890E-26	0.000	0	0	0	1	0	1	301
13788.4969	0	0.229E-27	0.000	8	1	7	7	1	6	221
13789.7799	4	0.212E-26	0.633	2	1	2	2	1	1	301
13790.9600	22	0.824E-27	0.859	5	3	2	4	4	1	400
13794.0662	19	0.479E-27	5.663	6	3	3	5	3	2	221
13795.8761	41	0.317E-27	7.784	9	2	8	8	2	7	221
13796.5287	0	0.623E-28	0.000							
13796.8531	1	0.678E-26	0.553	2	2	1	2	2	0	301
13799.2015	0	0.212E-27	0.000	6	3	4	5	4	1	400
13799.5737	0	0.159E-25	0.000	2	2	0	2	2	1	301
13800.3104	0	0.258E-26	0.000	3	2	1	3	2	2	301
13803.0239	0	0.124E-25	0.052	1	1	1	1	1	0	301
13804.0199	29	0.317E-27	5.311	7	3	5	6	3	4	221
13804.5749	2	0.322E-26	0.560	4	2	2	4	2	3	301
13804.9963	0	0.549E-28	0.000							
13807.5167	0	0.395E-27	0.000	4	0	4	3	2	1	301
13810.5176	0	0.717E-28	0.000	10	1	9	9	1	8	221
13810.5527	0	0.384E-27	0.000	6	4	2	5	4	1	221
13812.3223	0	0.707E-27	0.000	5	2	3	5	2	4	301
13813.4027	0	0.409E-26	0.000	1	1	0	1	1	1	301
13814.3711	29	0.499E-27	7.101	6	2	5	5	3	2	400
13817.8657	0	0.137E-27	0.000	8	3	6	7	3	5	221
13820.8587	0	0.510E-26	0.000	2	1	1	2	1	2	301
13822.4903	19	0.643E-27	7.399	6	2	4	6	2	5	301
13827.8069	32	0.249E-27	5.601	6	5	1	5	5	0	301
13827.8731	0	0.250E-27	0.000	7	4	4	6	4	3	221
13831.6626	0	0.960E-27	0.000	3	1	2	3	1	3	301
13833.4478	0	0.205E-27	0.000	7	2	5	7	2	6	301
13834.4866	0	0.296E-26	0.000	1	0	1	0	0	0	301
13844.3612	0	0.346E-27	0.000	5	2	3	4	3	2	400
13844.4636	0	0.425E-27	0.000	7	5	3	6	5	2	301
13844.8023	6	0.141E-26	0.566	4	1	3	4	1	4	301
13847.8188	0	0.365E-26	0.000	2	1	2	1	1	1	301
13853.2396	3	0.189E-26	0.469	2	0	2	1	0	1	071
13854.1382	0	0.957E-26	0.000	2	0	2	1	0	1	301
13854.9820	0	0.261E-27	0.000	6	3	4	6	2	5	400
13856.3544	0	0.954E-27	0.000	4	3	2	4	2	3	400
13857.8992	0	0.112E-25	0.000	2	1	1	1	1	0	301
13858.0727	0	0.637E-27	0.000	3	0	3	2	1	2	400
13858.5019	12	0.709E-27	5.125	5	1	4	5	1	5	301
13858.8310	0	0.139E-26	0.000	2	1	2	1	0	1	400
13861.1958	21	0.701E-27	7.938	3	3	1	2	1	2	221
13861.4483	38	0.259E-27	5.360	4	1	3	3	2	2	400
13862.7392	9	0.854E-27	0.565	3	2	2	3	0	3	301
13864.1206	0	0.157E-25	0.052	3	1	3	2	1	2	301
13865.1291	0	0.721E-26	0.000	3	2	2	2	2	1	301
13865.7107	0	0.143E-27	0.000	4	2	3	4	0	4	301
13869.1574	1	0.430E-26	0.531	3	0	3	2	0	2	301

Table A.3: Continued.

wavenumber	$\Delta\nu$	intensity	ΔI	J′	K'_a	K'_c	J″	K''_a	K''_c	vib
13870.3611	3	0.237E-26	0.496	3	2	1	2	2	0	301
13870.8608	0	0.552E-27	0.000	5	2	4	5	0	5	301
13871.1434	0	0.249E-27	0.000	6	1	5	6	1	6	301
13871.4583	4	0.189E-26	0.489	3	1	3	2	0	2	400
13873.2091	0	0.236E-27	0.000	5	3	3	5	1	4	301
13874.2265	7	0.138E-26	0.633	4	3	2	3	3	1	301
13874.4046	0	0.694E-27	0.000	4	0	4	3	1	3	400
13875.2948	0	0.871E-27	0.000	6	2	5	6	1	6	400
13875.7424	0	0.405E-26	0.000	4	3	1	3	3	0	301
13877.2100	0	0.157E-26	0.000	6	2	5	6	0	6	301
13878.1135	0	0.560E-26	0.000	4	1	4	3	1	3	301
13878.2746	5	0.123E-26	0.482	5	4	2	4	4	1	301
13878.5928	1	0.521E-26	0.529	3	1	2	2	1	1	301
13880.7779	3	0.347E-26	0.581	4	1	4	3	0	3	400
13881.8499	0	0.266E-26	0.000	4	2	3	3	2	2	301
13882.4098	0	0.156E-25	0.052	4	0	4	3	0	3	301
13882.9989	16	0.841E-27	0.942	5	1	4	4	2	3	400
13887.6086	27	0.291E-27	4.966	5	0	5	4	1	4	400
13887.9024	24	0.159E-27	3.860	2	2	1	1	1	0	400
13888.3356	0	0.181E-27	0.000	5	5	1	4	3	2	141
13891.2820	0	0.317E-26	0.000	5	3	3	4	3	2	301
13891.4706	0	0.325E-27	0.000	5	4	1	4	3	2	320
13891.7953	0	0.232E-27	0.000	7	2	5	6	3	4	400
13892.5783	0	0.877E-26	0.000	4	2	2	3	2	1	301
13892.7256	1	0.472E-26	0.498	5	0	5	4	0	4	301
13894.8988	0	0.358E-27	0.000	6	4	3	5	4	2	301
13895.9971	1	0.121E-25	0.100	4	1	3	3	1	2	301
13896.0805	2	0.102E-25	0.138	5	2	4	4	2	3	301
13896.1448	22	0.274E-27	7.294	6	4	2	5	4	1	301
13899.1437	0	0.165E-27	0.000	6	0	6	5	1	5	400
13901.1622	2	0.314E-26	0.491	6	1	6	5	1	5	301
13901.5463	21	0.124E-25	1.332	6	0	6	5	0	5	301
13902.2225	23	0.305E-27	4.758	3	2	2	2	1	1	400
13906.0575	0	0.929E-27	0.000	6	3	4	5	3	3	301
13907.2808	0	0.119E-26	0.000	6	2	4	5	0	5	221
13907.7885	0	0.158E-26	0.000	6	2	5	5	2	4	301
13909.2514	24	0.249E-26	3.921	5	1	4	4	1	3	301
13909.7720	1	0.669E-26	0.492	7	1	7	6	1	6	301
13909.9641	3	0.414E-26	0.605	2	2	0	1	0	1	301
13910.2866	6	0.234E-26	1.049	7	0	7	6	0	6	301
13910.8857	37	0.138E-27	4.267							
13912.3045	6	0.207E-26	0.774	4	2	3	3	1	2	400
13912.3744	3	0.202E-26	0.470	5	2	3	4	2	2	301
13913.6138	17	0.539E-27	5.336	7	4	3	6	4	2	301
13916.3761	2	0.298E-26	0.512	6	3	3	5	3	2	301
13916.6675	3	0.249E-26	0.561	7	2	6	6	2	5	301
13917.2685	5	0.136E-26	0.516	8	1	8	7	1	7	301
13917.4596	0	0.400E-26	0.000	8	0	8	7	0	7	301

Table A.3: Continued.

wavenumber	$\Delta\nu$	intensity	ΔI	J′	K'_a	K'_c	J″	K''_a	K''_c	vib
13918.4170	5	0.138E-26	0.497	7	3	5	6	3	4	301
13918.5069	0	0.397E-26	0.000	6	1	5	5	1	4	301
13918.6779	5	0.220E-26	0.588	5	2	4	4	1	3	400
13919.1910	0	0.968E-27	0.000	7	3	4	6	2	5	320
13921.7084	0	0.397E-27	0.000	7	2	6	6	1	5	400
13922.6714	0	0.272E-26	0.000	6	2	5	5	1	4	400
13923.4350	2	0.340E-26	0.586	9	1	9	8	1	8	301
13924.2263	13	0.502E-27	4.826	8	2	7	7	2	6	301
13925.5859	13	0.915E-27	0.699	7	1	6	6	1	5	301
13927.9342	29	0.299E-27	6.424	8	3	6	7	3	5	301
13928.0560	0	0.517E-27	0.000	10	1	10	9	1	9	301
13928.1062	0	0.885E-27	0.000	10	0	10	9	0	9	301
13928.3025	0	0.271E-26	0.000	6	2	4	5	2	3	301
13928.9037	25	0.189E-26	3.018	8	1	7	7	1	6	301
13929.6746	0	0.691E-27	0.000	9	2	8	8	2	7	301
13931.4920	0	0.398E-27	0.000	8	4	4	7	4	3	301
13932.0878	0	0.280E-27	0.000	9	1	8	8	1	7	301
13932.4414	36	0.237E-27	6.506							
13933.5703	0	0.121E-27	0.000	10	2	9	9	2	8	301
13934.3083	0	0.137E-27	0.000	9	4	6	8	4	5	301
13934.7249	0	0.783E-27	0.000	10	1	9	9	1	8	301
13935.0412	15	0.456E-27	4.920	9	3	7	8	3	6	301
13935.2999	15	0.513E-27	5.056	7	3	4	6	3	3	301
13939.4996	11	0.619E-27	4.801	7	2	5	6	2	4	301
13944.3756	7	0.126E-26	0.525	4	3	2	3	2	1	400
13945.6626	0	0.643E-27	0.000	8	2	6	7	2	5	301
13950.6879	0	0.712E-27	0.000	8	3	5	7	3	4	301
13959.8533	18	0.328E-27	4.822	8	3	6	7	2	5	400
13960.8029	14	0.611E-27	5.188	6	3	4	5	2	3	400
13961.6596	0	0.228E-27	0.000	7	3	5	6	2	4	400
13962.4728	26	0.180E-27	5.453	4	4	1	3	3	0	400
13967.4757	7	0.112E-26	0.512	4	2	2	3	0	3	301
13976.7343	34	0.159E-27	4.436	5	3	2	4	2	3	400
13981.0732	0	0.426E-27	0.000	5	4	1	4	3	2	400
13986.4066	0	0.104E-26	0.000	4	3	1	3	1	2	301
13992.9877	0	0.226E-27	0.000	6	4	3	5	3	2	400
14003.0786	0	0.178E-27	0.000	5	3	2	4	1	3	301
14005.8330	37	0.154E-27	4.471	5	2	3	4	0	4	301
14024.6702	0	0.421E-27	0.000	6	3	3	5	1	4	301
14049.4360	0	0.225E-27	0.000	6	2	4	5	0	5	301
14062.8993	46	0.140E-27	4.751							
14064.0351	0	0.262E-27	0.000	5	4	2	4	2	3	301
14064.8518	0	0.153E-27	0.000	2	1	2	3	2	1	202
14081.6806	21	0.343E-27	4.910	6	2	4	7	2	5	103
14086.2525	36	0.390E-27	7.716	2	1	1	3	2	2	202
14086.7439	23	0.397E-27	6.808	4	1	4	5	0	5	202
14088.6727	0	0.188E-27	0.000	8	3	5	7	1	6	301
14099.0623	0	0.434E-27	0.000	7	1	7	8	1	8	103

Table A.3: Continued.

wavenumber	$\Delta\nu$	intensity	ΔI	J′	K'_a	K'_c	J″	K''_a	K''_c	vib
14100.5737	0	0.462E-27	0.000	6	1	5	7	1	6	103
14106.6213	0	0.299E-27	0.000	3	0	3	4	1	4	202
14127.0111	7	0.123E-26	0.569	6	0	6	7	0	7	103
14128.9052	28	0.270E-27	5.680	5	1	4	6	1	5	103
14131.8517	16	0.369E-27	4.543	5	2	4	6	2	5	103
14139.7443	0	0.265E-27	0.000	2	1	2	3	0	3	202
14144.0397	0	0.821E-27	0.000	4	2	2	5	2	3	103
14152.9994	8	0.953E-27	0.511	5	1	5	6	1	6	103
14153.5004	2	0.404E-26	0.527	5	0	5	6	0	6	103
14153.8804	0	0.243E-27	0.000	3	1	2	3	2	1	202
14156.4412	8	0.108E-26	0.523	4	1	3	5	1	4	103
14157.8158	0	0.232E-27	0.000	3	0	3	3	1	2	202
14164.6073	19	0.350E-27	4.669	3	3	1	4	3	2	103
14172.4938	61	0.785E-28	4.130							
14174.7198	0	0.406E-27	0.000	3	2	1	4	2	2	103
14180.0783	19	0.478E-27	5.230	4	1	4	5	1	5	103
14183.3545	0	0.115E-26	0.000	3	2	2	4	2	3	103
14183.7172	21	0.370E-27	5.975	1	0	1	1	1	0	202
14202.8309	0	0.626E-27	0.000	3	0	3	4	0	4	103
14203.6252	4	0.216E-26	0.582	3	1	3	4	1	4	103
14204.6260	0	0.105E-26	0.000	2	2	0	3	2	1	103
14208.9774	0	0.261E-27	0.000	2	2	1	3	2	2	103
14211.5357	4	0.174E-26	0.494	2	1	1	3	1	2	103
14218.1573	0	0.429E-27	0.000	1	1	0	1	0	1	202
14221.7379	55	0.130E-27	4.752	2	1	1	2	0	2	202
14224.3599	0	0.352E-27	0.000	3	2	1	3	1	2	202
14225.8891	4	0.221E-26	0.514	2	0	2	3	0	3	103
14226.9519	14	0.801E-27	0.630	2	1	2	3	1	3	103
14228.7743	25	0.369E-27	5.221	3	1	2	3	0	3	202
14237.0166	8	0.105E-26	0.565	4	4	0	4	4	1	103
14238.4406	0	0.322E-27	0.000	5	4	1	5	3	2	202
14239.1919	21	0.432E-27	5.177	1	1	0	2	1	1	103
14248.8793	13	0.107E-26	0.602	1	0	1	2	0	2	103
14249.6548	4	0.207E-26	0.518	1	1	1	2	1	2	103
14251.6895	0	0.283E-27	0.000	3	0	3	2	1	2	202
14253.1040	0	0.579E-27	0.000	4	4	1	4	3	2	202
14254.8145	23	0.704E-27	7.737	3	1	3	3	1	2	103
14261.6609	1	0.593E-26	0.574	3	3	1	3	3	0	103
14271.3396	1	0.710E-26	0.562	3	2	2	3	2	1	103
14272.5060	0	0.137E-26	0.000	0	0	0	1	0	1	103
14273.8881	0	0.355E-27	0.000	2	1	2	2	1	1	103
14274.8687	0	0.496E-27	0.000	4	1	4	3	0	3	202
14279.0298	9	0.984E-27	0.562	2	2	1	2	2	0	103
14281.9154	3	0.279E-26	0.514	2	2	0	2	2	1	103
14286.6918	4	0.185E-26	0.502	1	1	1	1	1	0	103
14290.3953	0	0.469E-27	0.000	4	2	2	4	2	3	103
14297.2287	0	0.777E-27	0.000	1	1	0	1	1	1	103
14300.5326	84	0.221E-28	29.911							

Table A.3: Continued.

wavenumber	$\Delta\nu$	intensity	ΔI	J′	K'_a	K'_c	J″	K''_a	K''_c	vib
14305.4155	9	0.852E-27	0.527	2	1	1	2	1	2	103
14318.8731	16	0.451E-27	4.796	1	0	1	0	0	0	103
14331.9308	0	0.692E-27	0.000	2	1	2	1	1	1	103
14338.6507	0	0.266E-26	0.000	2	0	2	1	0	1	103
14342.4597	0	0.193E-26	0.000	2	1	1	1	1	0	103
14348.6481	6	0.130E-26	0.495	3	2	2	2	2	1	103
14348.7002	0	0.313E-26	0.000	3	1	3	2	1	2	103
14354.3672	21	0.710E-27	7.665	3	2	1	2	2	0	103
14361.8380	0	0.781E-27	0.000	4	3	1	3	3	0	103
14364.0500	0	0.174E-26	0.000	4	1	4	3	1	3	103
14366.9065	2	0.323E-26	0.545	4	0	4	3	0	3	103
14367.0603	0	0.628E-27	0.000	4	2	3	3	2	2	103
14374.9417	3	0.222E-26	0.498	5	1	5	4	1	4	103
14377.5935	9	0.861E-27	0.506	5	0	5	4	0	4	103
14378.3982	0	0.166E-26	0.000	4	2	2	3	2	1	103
14381.7883	0	0.573E-27	0.000	5	3	3	4	3	2	103
14382.2107	0	0.234E-26	0.000	4	1	3	3	1	2	103
14384.0235	0	0.132E-26	0.000	5	2	4	4	2	3	103
14386.1732	0	0.499E-27	0.000	6	1	6	5	1	5	103
14387.2886	0	0.182E-26	0.000	6	0	6	5	0	5	103
14395.3094	0	0.819E-27	0.000	7	1	7	6	1	6	103
14395.7599	0	0.425E-27	0.000	5	1	4	4	1	3	103
14395.9773	0	0.431E-27	0.000	7	0	7	6	0	6	103
14396.0673	0	0.212E-27	0.000	5	2	3	4	1	4	202
14399.8959	0	0.312E-27	0.000	5	2	3	4	2	2	103
14401.0328	0	0.452E-27	0.000	7	2	6	6	2	5	103
14401.8340	0	0.375E-27	0.000	6	5	2	5	4	1	202
14403.6275	0	0.917E-27	0.000	8	0	8	7	0	7	103
14404.5816	0	0.711E-27	0.000	6	1	5	5	1	4	103
14404.9788	0	0.483E-27	0.000	6	3	3	5	2	4	202
14416.6215	0	0.317E-27	0.000							
14417.2531	0	0.703E-27	0.000	6	2	4	5	2	3	103
14429.2119	0	0.211E-27	0.000	7	2	5	6	2	4	103
14472.4829	0	0.186E-27	0.000	4	3	1	3	1	2	103
14514.5447	0	0.184E-27	0.000							

Table A.4: The line positions (cm^{-1}) and intensities (cm $molecule^{-1}$) of $H_2{}^{17}O$ observed in the range 16665 – 17125 cm^{-1}. The intensities are scaled to match the natural abundance of $H_2{}^{17}O$ and normalised at 296 K. Vibrational states are given in $v_1v_2v_3$ normal mode notation in column 9. The estimated uncertainty on the line position is 0.01 cm^{-1} and on the line intensity is about 15% (see section 7.1.1). Unlike the Fourier transform spectra, the uncertainty in line position and intensity cannot be obtained individually for each line in CRDS.

frequency	intensity	J′	K'_a	K'_c	J″	K''_a	K''_c	vib
16665.905	0.110E-27	4	4	1	5	4	2	401
16668.500	0.147E-27	4	3	1	5	3	2	401
16670.275	0.429E-28	7	1	7	8	0	8	500
16670.641	0.227E-28	7	0	7	8	0	8	401
16670.847	0.151E-27	7	1	7	8	1	8	401
16674.419	0.134E-27							
16674.563	0.632E-28	6	1	5	7	1	6	401
16674.912	0.455E-28	6	2	5	6	3	4	420
16677.915	0.160E-28	6	2	5	7	2	6	401
16678.123	0.294E-28	7	4	4	7	4	3	241
16678.678	0.102E-27	4	0	4	5	0	5	321
16678.810	0.432E-28	5	3	3	5	4	2	500
16679.166	0.555E-28							
16679.564	0.126E-27	5	3	3	6	1	6	241
16681.079	0.307E-28	8	1	7	8	3	6	401
16683.282	0.622E-28	6	2	5	7	1	6	500
16683.933	0.743E-28	5	0	5	5	1	4	142
16684.487	0.779E-28	4	3	2	5	1	5	241
16687.628	0.344E-28	4	1	4	5	0	5	420
16687.953	0.460E-28	4	3	2	4	4	1	500
16690.180	0.102E-27	2	1	1	3	2	2	420
16692.609	0.336E-28	5	2	4	5	3	3	420
16693.315	0.133E-27	1	1	0	2	2	1	142
16693.505	0.655E-28							
16694.492	0.377E-28	3	2	1	2	1	2	340
16697.613	0.806E-28	4	4	0	4	4	1	241
16699.926	0.287E-28							
16700.113	0.405E-28	5	1	5	5	1	4	321
16700.813	0.194E-27	6	1	6	7	1	7	401
16701.680	0.834E-28	3	3	0	4	3	1	401
16702.221	0.220E-27	3	0	3	4	1	4	420
16702.821	0.167E-27	3	0	3	4	0	4	321
16707.256	0.287E-27	5	4	1	6	4	2	321
16707.386	0.142E-27	5	2	4	6	2	5	401
16710.459	0.333E-28	7	1	7	7	1	6	401
16712.108	0.101E-27							
16712.844	0.260E-28	6	0	6	5	3	3	420
16716.902	0.295E-28	3	0	3	3	3	0	500
16717.695	0.286E-27							
16718.616	0.204E-28	2	0	2	3	1	3	420
16721.651	0.244E-27	4	2	2	5	2	3	401

Table A.4: Continued.

frequency	intensity	J′	K'_a	K'_c	J″	K''_a	K''_c	vib
16722.101	0.979E-29							
16724.464	0.153E-27							
16724.878	0.115E-27	4	3	1	5	3	2	321
16726.348	0.346E-27	2	0	2	2	2	1	321
16726.943	0.735E-29	6	3	3	7	2	6	500
16728.230	0.651E-28	5	1	5	6	0	6	500
16728.432	0.315E-28	5	1	4	5	2	3	142
16728.751	0.260E-27	5	1	5	6	1	6	401
16729.210	0.206E-27	3	0	3	3	1	2	142
16729.558	0.190E-28	4	0	4	4	1	3	420
16730.557	0.182E-28	3	1	3	3	2	2	420
16731.787	0.356E-27	4	1	3	5	1	4	401
16734.137	0.271E-28							
16736.197	0.174E-27	4	2	3	5	2	4	401
16737.635	0.468E-29	4	4	0	5	4	1	321
16738.943	0.158E-28							
16739.112	0.253E-28	6	2	5	6	3	4	500
16741.516	0.171E-28	1	0	1	2	1	2	420
16743.958	0.234E-27	5	5	0	5	5	1	401
16745.453	0.962E-28							
16745.766	0.484E-28							
16749.524	0.104E-27							
16751.241	0.316E-29	1	1	1	2	0	2	142
16752.668	0.343E-28	7	2	6	7	4	3	043
16754.132	0.343E-28							
16754.694	0.232E-27	4	0	4	5	0	5	401
16755.012	0.905E-28	1	1	1	2	1	2	321
16755.481	0.222E-27							
16755.652	0.141E-27	4	1	4	5	1	5	401
16756.715	0.136E-27							
16757.925	0.673E-28	3	3	1	4	3	2	321
16758.469	0.423E-28	2	2	1	3	1	2	420
16760.301	0.325E-28	3	1	2	3	2	1	420
16760.790	0.153E-27	3	1	2	4	1	3	401
16764.331	0.216E-27	3	2	2	4	2	3	401
16765.847	0.181E-28	6	4	3	6	4	2	401
16772.950	0.252E-28	0	0	0	1	0	1	321
16773.394	0.138E-27							
16774.461	0.249E-28							
16774.982	0.235E-28							
16776.348	0.827E-28	3	0	3	4	1	4	500
16779.436	0.290E-27	1	1	0	2	2	1	500
16781.110	0.209E-27	3	2	1	4	1	4	420
16781.794	0.218E-27	3	1	3	4	1	4	401
16785.249	0.279E-28							
16786.255	0.514E-28	3	2	1	3	3	0	500
16786.815	0.285E-28							
16787.155	0.184E-27							

Table A.4: Continued.

frequency	intensity	J′	K'_a	K'_c	J″	K''_a	K''_c	vib
16787.322	0.115E-27	5	5	1	5	5	0	321
16787.775	0.159E-27	4	4	0	4	4	1	401
16788.619	0.340E-28	8	1	7	7	3	4	321
16789.968	0.111E-27	2	1	1	3	1	2	401
16790.082	0.146E-27							
16790.228	0.135E-27	3	2	2	3	2	1	321
16791.746	0.110E-27	2	2	1	3	2	2	401
16792.009	0.891E-28	4	3	2	4	3	1	401
16792.536	0.205E-27							
16794.869	0.177E-27	4	3	1	4	3	2	401
16795.593	0.498E-28	3	0	3	3	2	2	401
16796.293	0.916E-29	5	3	2	5	0	5	340
16797.253	0.139E-28	5	3	2	6	2	5	420
16798.157	0.995E-29	3	3	1	3	3	0	401
16799.136	0.312E-28	2	2	1	2	2	0	321
16799.312	0.142E-27	2	2	0	3	0	3	321
16799.791	0.109E-27	4	4	1	4	3	2	340
16799.898	0.138E-27	3	1	3	3	2	2	500
16800.295	0.163E-27	3	3	0	3	3	1	401
16800.830	0.195E-29	4	1	4	3	2	1	420
16801.708	0.200E-27	2	2	0	2	2	1	321
16802.964	0.803E-28	1	1	0	1	1	1	321
16803.504	0.959E-28							
16804.147	0.159E-27							
16805.965	0.166E-27	2	1	2	3	1	3	401
16806.420	0.295E-28							
16806.746	0.113E-27	4	2	2	4	2	3	321
16811.604	0.131E-27							
16812.864	0.241E-29							
16814.823	0.226E-28	6	2	5	5	3	2	420
16818.875	0.135E-27	1	1	0	2	1	1	401
16819.443	0.627E-28	4	2	2	3	3	1	420
16820.620	0.158E-28	7	3	4	7	2	5	500
16821.077	0.208E-28	7	3	5	6	4	2	500
16821.520	0.601E-29	5	3	2	4	2	3	340
16822.357	0.114E-28	6	3	4	6	3	3	321
16822.481	0.188E-28	3	3	1	4	2	2	420
16824.162	0.921E-28	3	1	2	3	2	1	500
16824.947	0.370E-28							
16827.529	0.113E-27	2	1	1	2	2	0	500
16827.675	0.135E-27	1	0	1	2	0	2	401
16829.494	0.120E-27	1	1	1	2	1	2	401
16829.602	0.132E-27							
16832.988	0.118E-27	3	1	3	3	1	2	401
16836.270	0.934E-28	2	1	2	1	1	1	321
16836.813	0.976E-28	7	2	5	7	1	6	500
16837.620	0.324E-28	4	1	3	4	1	4	321
16838.138	0.126E-27	5	3	3	5	3	2	321

Table A.4: Continued.

frequency	intensity	J′	K'_a	K'_c	J″	K''_a	K''_c	vib
16839.131	0.199E-27							
16839.929	0.155E-28	6	0	6	5	2	3	401
16841.595	0.100E-28	4	4	0	5	3	3	420
16843.481	0.889E-28							
16845.251	0.615E-28	2	0	2	2	1	1	500
16845.712	0.221E-28	3	2	1	4	1	4	500
16845.962	0.141E-27	5	3	2	5	2	3	500
16847.363	0.189E-28	5	3	2	5	3	3	321
16847.995	0.976E-28							
16848.412	0.670E-28	2	1	1	1	1	0	321
16848.614	0.250E-27	4	1	3	3	2	2	420
16851.254	0.137E-27	4	3	1	4	3	2	321
16851.847	0.281E-27	0	0	0	1	0	1	401
16852.326	0.299E-27	3	2	2	3	2	1	401
16853.994	0.160E-28	5	1	4	5	1	5	321
16854.253	0.788E-28	5	4	2	5	4	1	321
16854.975	0.303E-27	3	3	1	3	3	0	321
16855.171	0.534E-28	1	0	1	1	1	0	500
16855.401	0.133E-27	3	3	0	3	3	1	321
16859.787	0.788E-28	4	3	1	4	2	2	500
16861.805	0.185E-27	2	2	1	2	2	0	401
16862.800	0.115E-28	4	0	4	3	1	3	420
16864.509	0.359E-28	2	2	0	2	2	1	401
16864.604	0.206E-27	4	1	4	3	1	3	321
16865.061	0.172E-27							
16866.259	0.554E-28	5	1	5	4	0	4	142
16866.537	0.193E-27	1	1	1	1	1	0	401
16866.688	0.889E-28							
16866.826	0.112E-27							
16867.518	0.314E-27	3	2	2	2	2	1	321
16867.709	0.177E-27	4	2	3	4	0	4	321
16868.007	0.210E-27	4	2	2	4	2	3	401
16869.788	0.235E-28	3	1	2	2	1	1	321
16870.355	0.155E-27							
16870.847	0.284E-28	5	3	3	5	2	4	500
16872.779	0.458E-28	3	2	1	2	2	0	321
16874.058	0.146E-28	5	5	0	5	4	1	500
16874.478	0.753E-28	6	1	6	5	0	5	142
16875.140	0.722E-28	5	2	3	5	2	4	401
16875.288	0.259E-28	6	4	3	6	3	4	500
16875.744	0.147E-27	6	2	5	6	1	6	420
16877.261	0.873E-28							
16878.415	0.169E-27	5	0	5	4	1	4	420
16879.006	0.312E-28	5	4	1	5	3	2	500
16879.759	0.991E-29	6	3	4	6	1	5	401
16880.276	0.249E-28	6	5	1	5	5	0	401
16883.898	0.239E-27	8	1	8	7	1	7	321
16884.063	0.121E-27	6	2	4	6	2	5	401

Table A.4: Continued.

frequency	intensity	J′	K'_a	K'_c	J″	K''_a	K''_c	vib
16884.282	0.797E-28	7	2	6	7	0	7	321
16886.277	0.161E-28							
16887.955	0.491E-28	5	3	3	5	1	4	401
16889.135	0.741E-28	6	0	6	5	1	5	420
16890.628	0.803E-28	4	3	2	3	3	1	401
16890.841	0.150E-28	4	4	0	4	3	1	500
16891.270	0.673E-28	6	1	6	5	0	5	420
16891.873	0.165E-27	4	4	1	4	3	2	500
16892.947	0.119E-27	2	1	1	2	0	2	500
16893.516	0.660E-29							
16893.751	0.359E-28	5	1	4	4	2	3	420
16894.024	0.419E-28	3	1	2	3	1	3	401
16894.503	0.587E-29	7	4	4	7	2	5	401
16894.756	0.172E-27	4	2	2	3	2	1	321
16895.278	0.630E-28	8	0	8	7	0	7	321
16896.160	0.873E-28	2	2	0	1	1	1	420
16897.718	0.164E-27	7	0	7	6	1	6	142
16898.021	0.147E-27	5	2	4	4	2	3	321
16900.938	0.773E-28							
16901.246	0.384E-28	5	4	2	4	4	1	401
16904.095	0.394E-28	8	5	3	7	5	2	401
16904.214	0.171E-28							
16904.746	0.739E-28	5	1	4	4	1	3	321
16906.038	0.129E-27	5	3	3	4	3	2	401
16906.373	0.110E-27	4	1	3	4	1	4	401
16906.627	0.420E-28	8	1	7	7	2	6	142
16909.174	0.469E-28	6	2	5	5	2	4	321
16910.019	0.138E-27	5	2	3	4	3	2	500
16910.447	0.983E-28	5	3	2	4	3	1	401
16910.710	0.329E-28							
16910.920	0.162E-27	2	1	2	1	1	1	401
16912.121	0.370E-29	8	2	7	7	1	6	420
16913.920	0.167E-27							
16914.184	0.363E-28	6	4	2	5	4	1	401
16916.797	0.993E-28	6	3	3	5	4	2	142
16916.932	0.178E-27	2	0	2	1	0	1	401
16917.955	0.802E-28							
16919.245	0.265E-28	5	1	4	5	1	5	401
16919.624	0.400E-28							
16919.777	0.451E-28							
16919.937	0.520E-28							
16920.911	0.175E-27	2	1	1	1	1	0	401
16921.034	0.119E-27							
16921.431	0.259E-27	3	0	3	2	1	2	500
16923.119	0.135E-27	6	2	5	5	1	4	420
16923.792	0.227E-27	2	1	2	1	0	1	500
16924.246	0.209E-28							
16924.897	0.123E-27	4	1	3	3	2	2	500

Table A.4: Continued.

frequency	intensity	J′	K'_a	K'_c	J″	K''_a	K''_c	vib
16926.167	0.263E-27	3	2	1	2	1	2	420
16926.610	0.122E-27	8	1	7	7	1	6	321
16926.903	0.236E-27							
16927.720	0.119E-27	6	3	3	5	3	2	401
16929.628	0.267E-27	3	2	2	2	2	1	401
16930.761	0.135E-27	7	4	3	6	4	2	401
16931.076	0.208E-27	3	0	3	2	0	2	401
16932.093	0.255E-28	3	3	1	3	2	2	420
16934.344	0.113E-27	5	2	4	5	0	5	401
16934.666	0.148E-27	3	0	3	2	2	0	043
16935.383	0.153E-27	3	1	3	2	0	2	500
16937.262	0.163E-27	4	0	4	3	1	3	500
16939.623	0.168E-27	4	1	4	3	1	3	401
16940.947	0.244E-27	3	1	2	2	1	1	401
16942.072	0.236E-28	7	1	6	7	0	7	500
16942.356	0.496E-29	8	1	7	8	1	8	401
16942.821	0.219E-27	4	0	4	3	0	3	401
16945.534	0.175E-27	5	1	4	4	2	3	500
16945.831	0.108E-27	4	2	3	3	2	2	401
16946.467	0.310E-28	7	2	6	7	0	7	401
16947.026	0.858E-28	4	3	2	3	3	1	321
16947.722	0.377E-28	8	2	6	7	2	5	321
16948.326	0.857E-28	4	4	0	5	0	5	401
16948.557	0.690E-28	3	3	0	2	2	1	500
16949.510	0.142E-27	5	0	5	4	1	4	500
16950.687	0.147E-27	5	1	5	4	1	4	401
16952.302	0.409E-28	8	1	8	7	4	3	222
16953.280	0.137E-27	5	0	5	4	0	4	401
16954.972	0.576E-28							
16955.341	0.216E-28							
16956.021	0.153E-27	4	2	2	3	2	1	401
16957.538	0.180E-27	4	1	3	3	1	2	401
16959.244	0.218E-27	8	3	5	7	3	4	401
16959.607	0.170E-27							
16960.444	0.711E-29	6	1	6	5	0	5	500
16961.052	0.126E-27	6	0	6	5	0	5	401
16961.165	0.492E-28							
16961.619	0.698E-28	4	4	0	4	3	1	420
16962.013	0.162E-28							
16966.951	0.988E-28	7	1	7	6	0	6	500
16967.107	0.299E-27	7	1	7	6	1	6	401
16969.082	0.260E-28	5	1	4	4	3	1	043
16969.439	0.462E-28							
16969.649	0.742E-28	4	2	2	3	0	3	321
16971.990	0.201E-28							
16972.608	0.123E-27	8	1	8	7	1	7	401
16974.890	0.173E-27	2	2	0	1	0	1	401
16975.407	0.188E-27	7	1	6	6	2	5	500

Table A.4: Continued.

frequency	intensity	J′	K'_a	K'_c	J″	K''_a	K''_c	vib
16975.567	0.739E-28							
16976.825	0.428E-28	5	4	1	4	4	0	321
16978.424	0.166E-27							
16978.592	0.138E-27							
16981.591	0.253E-28							
16983.404	0.172E-28							
16984.391	0.655E-28	5	2	4	4	1	3	500
16987.291	0.133E-27	6	2	5	5	1	4	500
16989.248	0.340E-28	6	3	3	6	0	6	500
16992.367	0.446E-28							
16993.695	0.260E-28	7	3	5	6	3	4	321
16996.115	0.467E-28	5	5	1	4	4	0	500
16997.329	0.265E-28	5	2	3	6	3	4	222
17003.483	0.728E-28	3	3	0	2	2	1	420
17005.223	0.556E-28							
17006.855	0.114E-28	7	3	4	6	3	3	321
17007.619	0.296E-28	6	6	1	5	5	0	500
17007.977	0.185E-28							
17008.378	0.419E-29	7	4	3	6	2	4	241
17010.284	0.542E-28	6	1	6	5	4	1	222
17010.616	0.294E-28	6	5	2	5	4	1	500
17011.367	0.881E-29	7	4	4	6	4	3	321
17012.985	0.572E-29							
17015.793	0.155E-28							
17016.604	0.394E-29							
17016.890	0.105E-28							
17017.794	0.594E-28	4	3	2	3	2	1	420
17018.607	0.403E-28							
17019.244	0.275E-28	8	3	5	7	3	4	321
17021.234	0.219E-28							
17021.904	0.128E-28	7	5	3	6	4	2	500
17023.318	0.307E-28							
17023.688	0.868E-29	3	3	0	4	4	1	222
17025.169	0.192E-28	4	3	1	3	2	2	420
17025.655	0.173E-28							
17028.760	0.254E-28							
17029.584	0.161E-28							
17032.255	0.480E-29	8	5	4	7	4	3	340
17034.887	0.558E-28							
17035.995	0.346E-28	3	2	1	4	3	2	222
17036.480	0.192E-28							
17036.909	0.146E-28							
17039.631	0.153E-28							
17040.426	0.345E-28							
17046.632	0.541E-29							
17049.441	0.392E-28	5	3	2	4	2	3	420
17050.069	0.123E-28	7	5	3	6	5	2	241
17051.885	0.298E-28							

Table A.4: Continued.

frequency	intensity	J′	K'_a	K'_c	J″	K''_a	K''_c	vib
17056.224	0.779E-29							
17056.495	0.310E-29							
17057.217	0.475E-29							
17058.934	0.270E-28	4	3	1	3	1	2	321
17059.484	0.119E-28							
17060.017	0.119E-28	4	4	1	3	3	0	420
17062.520	0.339E-28	5	3	3	4	1	4	401
17066.504	0.575E-29	5	2	3	4	1	4	500
17067.580	0.769E-29	4	4	1	3	2	2	401
17071.441	0.148E-28							
17078.520	0.282E-28							
17079.754	0.669E-29	7	3	4	7	0	7	420
17083.315	0.938E-29							
17086.717	0.252E-28							
17091.638	0.183E-28							
17095.521	0.160E-28							
17095.874	0.223E-29	6	3	4	5	1	5	401
17097.243	0.164E-28	8	3	5	7	1	6	401
17098.315	0.717E-29	7	1	6	7	2	5	222
17099.404	0.699E-29	5	5	0	4	3	1	401
17100.797	0.766E-29	5	5	1	4	3	2	401
17105.488	0.356E-29	5	3	3	5	4	2	222
17110.745	0.158E-28	6	5	1	5	3	2	401
17115.391	0.820E-29							
17115.706	0.422E-29	6	5	2	5	3	3	401
17117.634	0.898E-29	8	3	5	8	1	8	321
17121.005	0.143E-28	5	3	3	4	1	4	321
17124.807	0.595E-29							

Bibliography

[1] Houghton J.T., Ding Y., Griggs D.J., Noguer M., van der Linden P.J., Dai X., Maskell K., and Johnson C.A. (editors), *Climate Change 2001: The Scientific Basis* (Cambridge University Press, 2001).

[2] Wayne R.P., *Chemisty of Atmospheres, second edition* (Oxford University Press Inc., New York, 1991).

[3] Cheung A.C., Rank D.M., Townes C., and Welch W.J., *Nature* **221** (1969) 917.

[4] Allard F., Hauschildt P.H., Miller S., and Tennyson J., *The Astrophys. J.* **39** (1994) 426.

[5] Wallace L., Bernath P.F., Livingston W., Hinkle K., Busler J.R., Guo B., and Zhang K.Q., *Science* **268** (1995) 1155.

[6] Flaud J.M., Camy-Peyret C., and Maillard J.P., *Molec. Phys.* **32** (1976) 499.

[7] Worden H., Beer R., and Rinsland C.P., *J. Geophys. Res. D* **102** (1997) 1287.

[8] *NATO AGARD (Advisory Group for Aerospace Research and Development), 1993, Advisory Report No. 287, Terminology and Assessment Methods of Solid Propellant Rocket Exhaust Signatures, Propulsion and Energetics Panel, Working Group 21 (Brussels: NATO).*

[9] Ramanathan V., Subsilar B., Zhang G.J., Conant W., Cess R.D., Kiehl J.T., Grassl H., and Shi L., *Science* **267** (1995) 499.

[10] Wild M., Ohshima A., Gilgen H., and Roeckner E., *J. Climate* **8** (1995) 1309.

[11] Arking A., *Science* **273** (1996) 779.

[12] Li Z., Moreau L., and Arking A., *Bull. Amer. Meteor. Soc.* **78** (1997) 53.

[13] Ramanathan V. and Vogelmann A.M., *Ambio* **26** (1997) 38.

[14] Learner R.C.M., Zhong W., Haigh J.D., Belmiloud D., and Clarke J., *Geophys. Res. Lett.* **26** (1999) 3609.

[15] Bernath P.F., *Science* **297** (2002) 943.

[16] Naus H., Ubachs W., Levelt P.F., Polyansky O.L., Zobov N.F., and Tennyson J., *J. Mol. Spectr.* **205** (2001) 117.

[17] Kalmar B. and O'Brien J.J., *J. Mol. Spectrosc.* **192** (1998) 386.

[18] Wong N.C. and Hall J.L., *J. Opt. Soc. Am. B* **6** (1989) 2300.

[19] Carleer M., Jenouvreier A., Vandeele A.C., Bernath P.F., Méienne M.F., Colin R., Zobov N.F., Polyansky O.L., Tennyson J., and Savin V.A., *J. Chem. Phys.* **111** (1999) 2444.

[20] Coheur P.F., Fally S., Carleer M., Clerbaux C., Colin R., Jenouvrier A., Mérienne M.F., Hermans C., and Vandaele A.C., *J. Quant. Spectrosc. Radiat. Transfer* **74** (2002) 493.

[21] Schermaul R., Learner R.C.M., Canas A.A.D., Brault J.W., Polyansky O.L., Belmiloud D., and Tennyson J., *J. Mol. Spectrosc.* **211** (2002) 169.

[22] Tolchenov R.N., Tennyson J., Brault J.W., Canas A.A.D., and Schermaul R., *J. Mol. Spectrosc.* **215** (2002) 269.

[23] Chevillard J.P., Mandin J.Y., Flaud J.M., and Camy-Peyret C., *Can. J. Phys.* **63** (1985) 1112.

[24] Chevillard J.P., Mandin J.Y., Flaud J.M., and Camy-Peyret C., *Can. J. Phys.* **64** (1986) 746.

[25] Chevillard J.P., Mandin J.Y., Flaud J.M., and Camy-Peyret C., *Can. J. Phys.* **65** (1987) 777.

[26] Toth R.A., *J. Mol. Spectr.* **190** (1998) 379.

[27] Toth R.A., *J. Opt. Soc. Amer. B* **9** (1992) 462.

[28] Toth R.A., *J. Opt. Soc. Amer. B* **10** (1993) 1526.

[29] Toth R.A., *J. Mol. Spectr.* **166** (1994) 184.

[30] Toth R.A., *Appl. Opt.* **33** (1994) 4868.

[31] Bykov A., Naumenko O., Petrova T., Scherbakov A., Sinitsa L., Mandin J.Y., Camy-Peyret C., and Flaud J.M., *J. Mol. Spectr.* **172** (1995) 243.

[32] Camy-Peyret C., Flaud J.M., Mandin J.Y., Bykov A., Naumenko O., Sinista L., and Voronin B., *J. Quant. Spectrosc. Radiat. Transfer* **61** (1999) 795.

[33] Rothman L.S., Barbe A., Benner D.C., Brown L.R., Camy-Peyret C., Carleer M.R., Chance K., Clerbaux C., Dana V., Devi V.M., Fayt A., Flaud J.M., Gamache R.R., Goldman A., Jacquemart D., Jucks K.W., Lafferty W.J., Mandin J.Y., Massie S.T., Nemtchinov V., Newnham D.A., Perrin A., Rinsland C.P., Schroeder J., Smith K.M., Smith M.A.H., Tang K., Toth R.A., Auwera J.V., Varanasi P., and Yoshino K., *J. Quant. Spectrosc. Radiat. Transfer* **82** (2003) 5.

[34] Jacquinet-Husson N., Arié E., Ballard J., Barbe A., Bjoraker G., Bonnet B., Brown L.R., Camy-Peyret C., Champion J.P., Chédin A., Chursin A., Clerbaux C., Duxbury G., Flaud J.M., Fourrié N., Fayt A., Graner G., Gamache R., Goldman A., Golovko V., Guelachvili G., Hartmann J.M., Hillico J.C., Hillman J., Lefèvre G., Lellouch E., Mikhailenko S.N., Naumenko O.V., Nemtchinov V., Newnham D.A., Nikitin A., Orphal J., Perrin A., Reuter D.C., Rinsland C.P., Rosenmann L., Rothman L.S., Scott N.A., Selby J., Sinitsa L.N., Sirota J.M., Smith A.M., Smith K.M., Tyuterev V.G., Tipping R.H., Urban S., Varanasi P., and Weber M., *J. Quant. Spectrosc. Radiat. Transfer* **62** (1999) 205.

[35] Rothman L.S., *HITRAN 2000,* `www.hitran.com`.

[36] Belmiloud D., Schermaul R., Smith K., Zobov N.F., Brault J.W., Learner R.C.M., Newnham D.A., and Tennyson J., *Geophys. Res. Lett.* **27** (2000) 3703.

[37] Rothman L.S., Rinsland C.P., Goldman A., Massie S.T., Edwards D., Flaud J.M., Perrin A., Camy-Peyret C., Dana V., Mandin J.Y., Schroeder J., McCann A., Gamache R.R., Wattson R., Yoshino K., Chance K., Jucks K., Brown L., Nemtchinov V., and Varanasi P., *J. Quant. Spec. Radiative Transf.* **60** (1998) 665.

[38] Giver L.P., Chackarian C., and Varanasi P., *J. Quant. Spectrosc. Radiat. Transfer* **66** (2000) 101.

[39] Schermaul R., Learner R.C.M., Newnham D.A., Williams R.G., Ballard J., Zobov N.., Belmiloud D., and Tennyson J., *J. Mol. Spectrosc.* **208** (2001) 32.

[40] Schermaul R., Learner R.C.M., Newnham D.A., Ballard J., Zobov N.F., Belmiloud D., and Tennyson J., *J. Mol. Spectrosc.* **208** (2001) 43.

[41] Schermaul R., Zobov N.F., Learner R.C.M., Newnham D.A., Ballard J., and Tennyson J., *ESA-WVR,* `http://badc.nerc.ac.uk/data/esa-wv/`.

[42] Partridge H. and Schwenke D.W., *J. Chem. Phys.* **106** (1997) 4618.

[43] Callegari A., Theulé P., Muenter J.S., Tolchenov R.N., Zobov N.F., Polyansky O.L., Tennyson J., and Rizzo T.R., *Science* **297** (2002) 993.

[44] *Université de Bruxelles - Faculté des Sciences, Service de Chimie Quantique et Photophysique (Atomes, Molécules et Atmosphères) website,* `http://www.ulb.ac.be/cpm`.

[45] Zobov N.F., Belmiloud D., Polyansky O.L., Tennyson J., Shirin S.V., Carleer M., Jenouvrier A., Vandaele A.C., Bernath P.F., Mérienne M.F., and Colin R., *J. Chem. Phys.* **113** (2000) 1546.

[46] Mérienne M.F., Jenouvrier A., Hermans C., Vandaele A.C., Carleer M., Clerbaux C., Coheur P.F., Colin R., Fally S., and Bach M., *J. Quant. Spectrosc. Radiat. Transfer* **82** (2003) 99.

[47] Burrows J.P., Weber M., Buchwitz M., Rozanov V., Ladstätter-Weissenmayer A., Richter A., de Beek R., Hoogen R., Bramstedt K., Eichmann K.U., Eisinger M., and Perner D., *J. Atmos. Sci.* **56** (1999) 151.

[48] Bovensmann H., Burrows J.P., Buchwitz M., Frerick J., Noël S., Rozanov V.V., Chance K.V., and Goede A.P.H., *J. Atmos. Sci.* **56** (1999) 127.

[49] Lang R., Maurellis A.N., van der Zande W.J., Aben I., Landgraf J., and Ubachs W., *J. Geophys. Res.* **107(D16)** (2002) art. no. 4300.

[50] Maurellis A.N., Lang R., van der Zande W.J., Aben I., and Ubachs W., *Geophys. Res. Lett.* **27** (2000) 903.

[51] Maurellis A.N., Lang R., Williams J.E., van der Zande W.J., Smith K., Tennyson J., and Tolchenov R.N., *In: Weakly Interacting Molecular Pairs: Unconventional Absorbers of Radiation in the Atmosphere. NATO SCIENCE series IV. Dordrecht: Kluwer Academic Publishers* **27** (2003) 259.

[52] Born M. and Oppenheimer J., *Ann. Phys.* **84** (1927) 457.

[53] Watson J.K.G., *Molec. Phys.* **15** (1968) 479.

[54] Watson J.K.G., *J. Chem. Phys.* **46** (1967) 1935.

[55] Eckart C., *Phys. Rev.* **47** (1935) 552.

[56] Polyansky O.L., *J. Mol. Spectrosc.* **112** (1985) 79.

[57] Lord Rayleigh, *Theory of Sound*, vol. 1 (Macmillan, London, 1937).

[58] Ritz W., *Reine Angew Math.* **135** (1908) 1.

[59] Tennyson J., Kostin M.A., Barletta P., Harris G.J., Ramanlal J., Polyansky O.L., and Zobov N.F., *Comp. Phys. Commun.* (2004), in press.

[60] Light J.C., Hamilton I.P., and Lill J.V., *J. Chem. Phys.* **82** (1985) 1400.

[61] Harris D.O., Engerholm G.G., and Gwinn W., *J. Chem. Phys.* **43** (1965) 1515.

[62] Tennyson J., *J. Chem. Soc. Faraday Trans.* **88** (1992) 3271.

[63] Ho T.S., Rabitz T.H.H., Harding L.B., and Schatz G., *J. Chem. Phys.* **105** (1996) 10472.

[64] Császár A.G. and Mills I.M., *Spectrochimica Acta* **53A** (1997) 1101.

[65] Polyansky O.L., Jensen P., and Tennyson J., *J. Chem. Phys.* **105** (1996) 6490.

[66] Shirin S.V., Polyansky O.L., Zobov N.F., Barletta P., and Tennyson J., *J. Chem. Phys.* **118** (2003) 2124.

[67] Schwenke D.W., *J. Phys. Chem. A* **105** (2001) 2352.

[68] Zobov N.F., Polyansky O.L., LeSueur C.R., and Tennyson J., *Chem. Phys. Lett.* **260** (1996) 381.

[69] Bunker P.R. and Moss R.E., *J. Mol. Spectrosc.* **80** (1980) 217.

[70] Sakurai J.J., *Advanced Quantum Mechanics* (Addison-Wesley, 1967).

[71] Császár A.G., Allen W.D., and Schaefer III H.F., *J. Chem. Phys.* **108** (1998) 9751.

[72] Tarczay G., Császár A.G., Klopper W., Szalay V., Allen W.D., and Schaefer III H.F., *J. Chem. Phys.* **110** (1999) 11971.

[73] Császár A.G., Kain J.S., Polyansky O.L., Zobov N.F., and Tennyson J., *Chem. Phys. Lett.* **293** (1998) 317.

[74] Császár A.G., Kain J.S., Polyansky O.L., Zobov N.F., and Tennyson J., *Chem. Phys. Lett.* **312** (1999) 613.

[75] Tarczay G., Császár A.G., Klopper W., and Quiney H.M., *Molec. Phys.* **99** (2001) 1769.

[76] Quiney H.M., Barletta P., Tarczay G., Császár A.G., Polyansky O.L., and Tennyson J., *Chem. Phys. Lett.* **344** (2001) 413.

[77] Halkier A., Klopper W., Helgaker T., and Jorgensen P., *J. Chem. Phys.* **111** (1999) 4424.

[78] de Oliveire G. and Dykstra C.E., *Theo. Chem. Acc.* **11** (1999) 435.

[79] Kjaergaard H.G., Bezar K.J., and Brooking K.A., *Mol. Phys.* **96** (1999) 1125.

[80] Lynas-Gray A.E., Miller S., and Tennyson J., *J. Mol. Spectrosc.* **169** (1995) 458.

[81] Michael E.A., Keoshian C.J., Wagner D.R., Anderson S.K., and Saykally R.J., *Chem. Phys. Lett.* **338** (2001) 277.

[82] Michael E.A., Keoshian C.J., Anderson S.K., and Saykally R.J., *J. Mol. Spectrosc.* **208** (2001) 219.

[83] Tennyson J., Barletta P., Kostin M.A., Polyansky O.L., and Zobov N.F., *Spectrochimica Acta A* **58** (2002) 663.

[84] Schwenke D.W., *J. Chem. Phys.* **118** (2003) 6898.

[85] Barletta P., Ph.D. thesis, University of London (2002).

[86] Jensen P. and Bunker P.R. (editors), *Computational Molecular Spectroscopy* (John Wiley & Sons, Ltd, 2000).

[87] Hougen J.T., Bunker P.R., and Johns J.W.C., *J. Mol. Spectrosc.* **34** (1970) 136.

[88] Tennyson J. and Sutcliffe B.T., *J. Chem. Phys.* **77** (1982) 4061.

[89] Jensen P., *Comp. Phys. Commun.* **1** (1983) 1.

[90] Sutcliffe B. and Tennyson J., *Int. J. Quantum Chem.* **39** (1991) 183.

[91] Johnson B.R. and Reinhardt W.P., *J. Chem. Phys.* **85** (1986) 4538.

[92] Choi S.E. and Light J.C., *J. Chem. Phys.* **97** (1992) 7031.

[93] Radau R., *Ann. Sci. Ecole Normale Superior* **5** (1868) 311.

[94] Tennyson J. and Sutcliffe B.T., *Int. J. Quantum Chem.* **42** (1992) 941.

[95] Tennyson J., Zobov N.F., Williams R., Polyansky O.L., and Bernath P.F., *J. Phys. Chem. Ref. Data* **30** (2001).

[96] Toth R.A., *J. Mol. Spectrosc.* **166** (1994) 176.

[97] Toth R.A., *J. Mol. Spectrosc.* **190** (1998) 379.

[98] Halonen L., *Adv. Chem. Phys.* **104** (1998) 41.

[99] Zobov N.F., Belmiloud D., Polyansky O.L., and Tennyson. J., *J. Chem. Phys.* **133** (2000) 1546.

[100] Matsushima F., Odashima H., Iwasaki T., Tsunekawa S., and Takagi K., *J. Mol. Struct.* **352** (1995) 371.

[101] Matsushima F., Nagase H., Nakauchi T., Odashima H., and Takagi K., *J. Mol. Spectrosc.* **193** (1999) 217.

[102] Kain J.S., Polyansky O.L., and Tennyson J., *Chem. Phys. Lett.* **317** (2000) 365.

[103] MacDonald J.K.L., *Phys. Rev.* **43** (1933) 830.

[104] Stroud A.H. and Secrest D., *Gaussian Quadrature Formulas* (Prentice-Hall: London, 1996).

[105] Dickinson A.S. and Certain P.R., *J. Chem. Phys.* **49** (1968) 4204.

[106] Bačić Z. and Light J.C., *Annu. Rev. Phys. Chem.* **40** (1989) 469.

[107] Wei H., *J. Chem. Phys.* **106** (1997) 6885.

[108] Tennyson J., Henderson J.R., and Fulton N.G., *Comp. Phys. Commun.* **86** (1995) 175.

[109] Tennyson J., *Comp. Phys. Commun.* **42** (1986) 257.

[110] Tennyson J. and Miller S., *Comp. Phys. Commun.* **55** (1989) 149.

[111] Tennyson J., Miller S., and LeSueur C.R., *Comp. Phys. Commun.* **75** (1993) 339.

[112] Tennyson J. and Sutcliffe B.T., *Mol. Phys.* **58** (1986) 1067.

[113] Fulton N.G., Ph.D. thesis, University of London (1994).

[114] Condon E.U. and Shortley G.H., *The Theory of Atomic Spectra* (Cambridge University Press, Cambridge, 1935).

[115] Hoy A.R., Mills I.M., and Strey G., *Molec. Phys.* **24** (1972) 1265.

[116] Carter S. and Handy N.C., *J. Chem. Phys.* **87** (1987) 4294.

[117] Halonen L. and Carrington Jr. T., *J. Chem. Phys.* **88** (1988) 4171.

[118] Jensen P., *J. Mol. Spectrosc.* **133** (1989) 438.

[119] Polyansky O.L., Jensen P., and Tennyson J., *J. Chem. Phys.* **101** (1994) 7651.

[120] Dunning Jr. T.H., *J. Chem. Phys.* **90** (1989) 1007.

[121] Polyansky O.L., Császár A.G., Shirin S.V., Zobov N.F., Barletta P., Tennyson J., Schwenke D.W., and Knowles P.J., *Science* **299** (2003) 539.

[122] Schwenke D.W. and Partridge H., *J. Chem. Phys.* **113** (2000) 6592.

[123] Faires L.M., *Anal. Chem.* **58** (1986) 1023A.

[124] Thorne A.P., *Spectrophysics, Second Edition* (Champman and Hall, 1988).

[125] Thorne A.P., *Anal. Chem.* **63(2)** (1991) 57A.

[126] Duxbury G., *Infrared Vibration-Rotation Spectroscopy* (John Wiley & Sons, Ltd, 2000).

[127] Davis S.P., Abrams M.C., and Brault J.W., *Fourier Transform Spectrometry* (Academic Press, 2001).

[128] Brault J.W., in *Proceedings of the 15th Annual Advanced Course of the Swiss Society of Astrophysics and Astronomy* (Geneva Observatory; Sauverny, Switzerland, 1985) .

[129] *Rutherford Appelton Laboratory (RAL) website* `http://www.msf.rl.ac.uk`.

[130] O'Keefe A. and Deacon D.A.G., *Rev. Sci. Instrum.* **59** (1988) 2544.

[131] Wheeler M.D., Newman S.M., Orr-Ewing A.J., and Ashfold N.R., *J. Chem. Soc., Faraday Trans.* **94(3)** (1998) 337.

[132] Naus H., de Lange A., and Ubachs W., *Phys. Rev. A* **56** (1997) 4755.

[133] Naus H., van Stokkum I.H.M., Hogervorst W., and Ubachs W., *Appl. Opt.* **40(24)** (2001) 4416.

[134] Sneep M. and Ubachs W., *In: Weakly Interacting Molecular Pairs: Unconventional Absorbers of Radiation in the Atmosphere, NATO Science series: IV: Earth and Environmental sciences* **27** (2003).

[135] Hodges J.T., Looney J.P., and van Zee R.D., *Appl. Opt.* **35** (1996) 4112.

[136] *National Optical Astronomy Observatory website* `http://www.noao.edu`.

[137] Gamache R.R., Hartmann J.M., and Rosenmann L., *J. Quant. Spectrosc. Radiat. Transfer* **52** (1994) 481.

[138] Gamache R.R., Lynch R., and Brown L.R., *J. Quanr. Spectrosc. Radiat. Transfer* **56** (1996) 471.

[139] Bauer A., Duterage B., and Godon M., *J. Quant. Spectrosc. Radiat. Transfer* **36** (1986) 307.

[140] Bauer A., Godon M., and Duterage B., *J. Quant. Spectrosc. Radiat. Transfer* **33** (1985) 167.

[141] Bauer A., Godon M., Kheddar M., Hartmann J.M., Bonamy J., and Robert D., *J. Quant. Spectrosc. Radiat. Transfer* **37** (1987) 531.

[142] Bauer A., Godon M., Kheddar M., and Hartmann J.M., *J. Quant. Spectrosc. Radiat. Transfer* **41** (1989) 49.

[143] Godon M. and Bauer A., *Chem. Phys. Lett.* **147** (1988) 189.

[144] Goyette T.M. and DeLucia F.C., *J. Mol. Spectrosc.* **143** (1990) 346.

[145] Toth R.A., *J. Mol. Spectrosc.* **201** (2000) 218.

[146] Rinsland C.P., Goldman A., Smith M.A.H., and Devi V.M., *Appl. Opt.* **30** (1991) 1427.

[147] Yamada K.M.T., Harter M., and Giesen T., *J. Mol. Spectrosc.* **157** (1993) 84.

[148] Bykov A.D., Lavrentieva N.N., Saveliev V.N., Sinitsa L.N., Camy-Peyret C., Claveau C., and Valentin A., *J. Mol. Spectrosc.* **224** (2004) 164.

[149] Toth R., Brown L.R., and Plymate C., *J. Quant. Spectrosc. Radiat. Transfer* **59** (1998) 529.

[150] Toth R.A., *J. Quant. Spectrosc. Radiat. Transfer* (2004), to be published.

[151] Rothman L.S., Gamache R.R., Goldman A., Brown L.R., Toth R.A., Pickett H.M., Poynter R.L., Flaud J.M., Camy-Peyret C., Barbe A., Husson N., Rinsland C.P., and Smith M.A.H., *Appl. Opt.* **26** (19987) 4058.

[152] Toth R.A., *J. Mol. Spectrosc.* **162** (1993) 41.

[153] Ormsby P.S., Rao K.N., Winnewisser M., Winnewisser B.P., Naumenko O.V., Bykov A.D., and Sinitsa L.N., *J. Mol. Spectrosc.* **158** (1993) 109.

[154] Cohen Y., Bar I., and Rosenwaks S., *J. Mol. Spectrosc.* **180** (1996) 298.

[155] Ulenikov O.N., He S.G., Onopenko G.A., Bekhtereva E.S., Wang X.H., Hu S.M., Lin H., and Zhu Q.S., *J. Mol. Spectrosc.* **204** (2000) 216.

[156] Wang X.H., Ulenikov O.N., Onopenko G.A., Bekhtereva E.S., He S.H., Hu S.M., Lin H., and Zhu Q.S., *J. Mol. Spectrosc.* **200** (2000) 25.

[157] He S.G., Ulenikov O.N., Onopenko G.A., Bekhtereva E.S., Wang X.H., Hu S.M., Lin H., and Zhu Q.S., *J. Mol. Spectrosc.* **200** (2000) 34.

[158] Ulenikov O.N., Hu S.M., Bekhtereva E.S., Onopenko G.A., He S.G., Wang X.H., Zheng J.J., and Zhu Q.S., *J. Mol. Spectrosc.* **210** (2001) 18.

[159] Zheng J.J., Ulenikov O.N., Onopenko G.A., Bekhtereva E.S., He S.G., Wang X.H., Hu S.M., Lin H., and Zhu Q.S., *Mol. Phys.* **99** (2001) 931.

[160] Hu S.M., Ulenikov O.N., Bekhtereva E.S., Onopenko G.A., He S.G., Lin H., Cheng J.X., and Zhu Q.S., *J. Mol. Spectrosc.* **212** (2002) 89.

[161] Shirin S.V., Zobov N.F., Polyansky O.L., Tennyson J., Parekunnel T., and Bernath P.F., *J. Chem. Phys.* **120** (2004) 206.

[162] Bykov A.D., Naumenko O.V., Sinitsa L.N., Winnewisser B.P., Ormsby P.S., and Rao K.N., *J. Mol. Spectrosc.* **166** (1994) 169.

[163] Toth R.A., *J. Mol. Spectrosc.* **195** (1999) 98.

[164] Schwenke D.W., *J. Phys. Chem.* **100** (1996) 2867, erratum **100**, 18884-18884 (1996).

[165] Mandin J.Y., Chevillard J.P., Camy-Peyret C., and Flaud J.M., *J. Mol. Spectrosc.* **116** (1986) 167.

[166] Gerstenkorn S. and Luc P., *Atlas du Spectroscopie d'Absorption de la Molcule de l'Iode Entre 14,800–20,000 cm^{-1}* (Presses du CNRS).

[167] Shirin S.V., Polyansky O.L., Zobov N.F., Császár A.G., and Tennyson J. (2004), to be submitted.

[168] Vidler M. and Tennyson J., *J. Chem. Phys.* **113** (2000) 9766.

[169] Hewitt A.J., Doss N., Zobov N.F., Polyansky O., and Tennyson J., *Mon. Not. R. astr. Soc.* (2004), submitted.

[170] Naumenko O., Bertseva E., and Campargue A., *J. Mol. Spectrosc.* **197** (1999) 122.

[171] Naumenko O. and Campargue A., *J. Mol. Spectrosc.* **199** (2000) 59.

[172] Campargue A., Bertseva E., and Naumenko O., *J. Mol. Spectrosc.* **201** (2000) 94.

[173] Hu S.M., Ulenikov O.N., Bekhtereva E.S., He S.G., Wang X., Lin H., and Zhu Q.S., *J. Mol. Spectrosc.* **203** (2000) 228.

[174] Jenouvrier A., Merienne M.F., Carleer M., Colin R., Vandaele A.C., Bernath P.F., Polyansky O.L., and Tennyson J., *J. Mol. Spectrosc.* **209** (2001) 165.